

PhD. 28106

University of Cambridge
Department of Engineering



Concepts for Retractable Roof Structures

Dissertation submitted to the University of Cambridge
for the Degree of Doctor of Philosophy

by

Frank Vadstrup JENSEN



To Helle, Erik and Flemming

Declaration

The author declares that this dissertation is his own work and contains nothing which is the outcome of work done in collaboration with others, except for commonly understood and accepted ideas or as specified in the text and Acknowledgements.

This dissertation has not been previously submitted, in part or in whole, to any University or Institution for any degree, diploma or other qualification. This report is presented in 158 pages and contains approximately 43.000 words and 124 figures.



Frank Vadstrup Jensen

Acknowledgements

The research presented in this dissertation has its roots in many places, much like the roots of a tree, and similarly to the tree it branches out into many interesting areas and results. However, the main focus, or trunk if you like, is the pursuit of novel retractable roof systems for large sporting venues.

The first seed was planted by Dr *Tim Ibell* while I was an exchange student at the University of Bath and for this I am deeply grateful. Though the seed had been planted it needed nutrition to grow – this was to be provided by my supervisor Professor *Sergio Pellegrino* at the Deployable Structures Laboratory, University of Cambridge, Department of Engineering.

I would like to express my gratitude to Professor *Sergio Pellegrino* for his invaluable scientific guidance, encouragement and many ideas throughout the course of this research.

To my advisor Professor *C. R. Calladine, FRS*, I would like to extend my gratitude for his ideas, suggestions and scientific advice.

At the Department of Engineering I would also like to thank the following: All the members of the Deployable Structures Laboratory for their advice and kind friendship. A special thanks must go to the following members or former members of the group; *Tyge Schioler, Matthew Santer, Paul Ong, Dr Alan Watt, Jeffrey Yee, Dr Lin Tze Tan, Dr Wesley Wong, Dr Elizbar Kebabze, Dr Andrew Lennon* and *Richard Dietricht*. For excellent technical support I would like to thank *Alistair Ross, Steven Robinson, Jeremy Penfold, Roger Denston* and *Peter Knott*. Importantly, my warmest thanks to Dr *Lars Ekström*, Dr *Claus B. W. Pedersen* and Dr *Guido Morgenthal* for their kind help and lasting friendship.

I am also grateful for my fruitful collaboration with Dr *Thomas Buhl*, of the Technical University of Denmark, and for his continuing friendship.

I gratefully acknowledge the financial support extended to me by the Cambridge University Engineering Department and Darwin College, which enabled me to take up a fellowship at the Faculty of Civil Engineering and Geosciences, Technical University of Delft, The Netherlands. There I was treated in the best possible manner by Professor *Leo Wagemans*, his staff and his students, and for this I am very grateful.

I would also like to extend my thanks and gratitude to Dr *Chris Williams* at the University of Bath for allowing me to visit and for his very kind help and continuing

advice. The same goes to *Quintin Lake* for his help, advice and friendship. And to my friends and former colleagues Dr *Paul Shepherd* and Dipl.Ing. *Markus Balz* for their friendship as well as their continued interest in my research. Also a heart felt thanks to all my other friends for enduring support and encouragements.

I would also like to thank Mr *Paul Meredith* for his work cutting CFRP model parts at BNFL's test and rehearsal facility at Littlebrook.

Many thanks should also go to the Happold Trust for financing my position as Design Teaching Assistant at the Cambridge University Engineering Department, and to the CUED Structures Group teaching staff and Professor *Ian Liddell, CBE* of Buro Happold Consulting Engineers for their kind help and support on teaching issues.

I am grateful for the financial support provided by Søren Jensen Rådgivende Ingeniørfirma of Denmark and the interest and encouragements of those employed there.

Finally, to those dearest to me, my parents *Helle* and *Erik Jensen* and my brother *Flemming*, I wish to express my love and give my most sincere thanks for all your love and support. A few further words of gratitude has been earned by *Erik* whom as a fellow engineer has not only been my father but also my tutor; without your nourishment I would not have come this far.

Cambridge, October 2004

Frank Vadstrup Jensen

Abstract

Over the last decade there has been a worldwide increase in the use of retractable roofs for stadia. This increase has been based on the flexibility and better economic performance offered by venues featuring retractable roofs compared to those with traditional fixed roofs. With this increased interest an evolution in retractable roof systems has followed. This dissertation is concerned with the development of concepts for retractable roof systems.

A review is carried out to establish the current state-of-the-art of retractable roof design. A second review of deployable structures is used to identify a suitable retractable structure for further development.

The structure chosen is formed by a two-dimensional ring of pantographic bar elements interconnected through simple revolute hinges. A concept for retractable roofs is then proposed by covering the bar elements with rigid cover plates. To prevent the cover plates from inhibiting the motion of the structure a theorem governing the shape of these plate elements is developed through a geometrical study of the retractable mechanism. Applying the theorem it is found that retractable structures of any plan shape can be formed from plate elements only. To prove the concept a 1.3 meter diameter model is designed and built.

To increase the structural efficiency of the proposed retractable roof concept it is investigated if the original plan shape can be adapted to a spherical surface. The investigation reveals that it is not possible to adapt the mechanism but the shape of the rigid cover plates can be adapted to a spherical surface. Three novel retractable mechanisms are then developed to allow opening and closing of a structure formed by such spherical plate elements.

Two mechanisms are based on a spherical motion for the plate elements. It is shown that the spherical structure can be opened and closed by simply rotating the individual plates about fixed points. Hence a simple structure is proposed where each plate is rotated individually in a synchronous motion. To eliminate the need for mechanical synchronisation of the motion, a mechanism based on a reciprocal arrangement of the plates is developed. The plate elements are interconnected through sliding connections allowing them mutually to support each other, hence forming a self-supporting structure in which the motion of all plates is synchronised.

To simplify the structure further, an investigation into whether the plate elements can be interconnected solely through simple revolute joints is carried out. This is not found to be possible for a spherical motion. However, a spatial mechanism is

developed in which the plate elements are interconnected through bars and spherical joints. Geometrical optimisation of the motion path and connection points is used to eliminate the internal strains that occur in the initial design of this structure so a single degree-of-freedom mechanism is obtained.

The research presented in this dissertation has hence led to the development of a series of novel concepts for retractable roof systems.

Keywords: Deployable structure, design, linkage, pantograph, retractable roof, spatial mechanism, spherical mechanism, stadia.

Contents

Declaration	i
Acknowledgements	ii
Abstract	iv
List of Figures	ix
List of Symbols and Abbreviations	xiii
1 Introduction	1
1.1 Stadia	1
1.2 Retractable Roofs	3
1.3 Deployable Structures	4
1.4 Aims & Scope of Research	4
1.5 Outline of Thesis	5
2 Review of Literature and Previous Work	7
2.1 Introduction	7
2.2 Retractable Roofs for Stadia	7
2.2.1 Classification of Retractable Roofs	9
2.2.2 Built Examples of Retractable Roofs	10
2.2.3 Recent Proposals for Retractable Roofs	14
2.3 Deployable Structures	18
2.3.1 Space Applications	18
2.3.2 Architectural and Civil Engineering Applications	18
2.4 Retractable Pantographic Structures	21
2.4.1 Closed Loop Structures	23
2.4.2 Structures formed by Angulated Elements	24
2.4.3 Other Closed Loop Structures	27
2.4.4 Retractable Dome Structures	28
3 Retractable Bar and Plate Structures	31
3.1 Introduction	31
3.2 Retractable Bar Structures	32
3.2.1 Radial Motion	32
3.2.2 Rotating Motion	35
3.2.3 Non-circular Structures	39
3.2.4 Additional Rotational Limits	43

3.3	Retractable Plate Structures	46
3.3.1	Movement of Bar Linkage	46
3.3.2	Application to Closed Loop Structures	47
3.3.3	Plate-only Structures	51
3.3.4	Periodicity of Boundary	53
3.4	Computer Assisted Design	56
3.4.1	Optimisation of Plate Shapes	59
3.5	Assemblies	60
3.5.1	Planar Assemblies	60
3.5.2	Stack Assemblies	66
3.6	Discussion	68
4	Design and Construction of Retractable Plate Structure	70
4.1	Introduction	70
4.2	Parts of the Model	70
4.2.1	Plate Elements	71
4.2.2	Hinges	72
4.2.3	Actuator Assembly	72
4.2.4	Supports	74
4.3	Structural Analysis	75
4.3.1	Finite Element Models	75
4.3.2	Physical Model	81
4.4	Actuator Design	84
4.4.1	Virtual Work Analysis	85
4.4.2	Gear Ratio	88
4.5	Discussion	90
5	Spherical Retractable Structures: Preliminary Studies	91
5.1	Introduction	91
5.2	Spherical Geometry	92
5.2.1	Spherical Excess	93
5.2.2	Spherical Trigonometry	95
5.3	Pantographic Elements on a Spherical Surface	96
5.4	Plate Shape	100
5.4.1	Periodicity of Boundaries	103
5.4.2	Non-Symmetric Structures	105
5.4.3	Physical Models	105
5.5	Discussion	106
6	Spherical Retractable Structures: Spherical Mechanisms	108
6.1	Introduction	108
6.2	Euler Pole	109
6.2.1	Compound Rotations	110
6.2.2	Spherical Trigonometry	113
6.3	Varying the Location of the Euler Pole	114
6.3.1	Selection of Euler Pole	116
6.3.2	Physical Models	116
6.4	Relative Motion of Parts	118

6.5	Reciprocal Mechanism	121
6.5.1	Small Physical Model	123
6.5.2	Large Physical Model	123
6.6	Discussion	126
7	Spherical Retractable Structures: Spatial Mechanism	128
7.1	Introduction	128
7.2	Spatial Mechanism	129
7.2.1	Mobility Count	129
7.3	Optimisation	131
7.3.1	Element Orientation	132
7.3.2	Connection Points	134
7.4	Kinematic Model	138
7.5	Discussion	142
8	Conclusions	144
8.1	Planar Structures	144
8.2	Spherical Structures	145
8.3	Further Work	146
	Bibliography	148

List of Figures

1.1	Coliseum in Rome (Escrig, 1996)	2
1.2	Schematic of retractable roof over the Minute Maid Park, US (Post, 2000)	3
1.3	Concept for deployable canopy (Mollaert <i>et al.</i> , 2003)	4
2.1	Methods for opening and closing (Ishii, 2000)	10
2.2	Methods for opening and closing of membrane structures by the Institute for Lightweight Structures (1971)	11
2.3	Folding membrane roofs at (a) Montreal Olympic Stadium, and (b) Za- ragoza Arena (Schlaich, 2000). Views from inside the stadia	11
2.4	Folding membrane roofs at (a) Parken Stadium (Courtesy of CENO Tec), and (b) Toyota Stadium (Shibata, 2003)	12
2.5	Miller Park (Courtesy of NBBJ Architects)	13
2.6	Parallel retracting systems at (a) Ariake Colosseum (Ishii, 2000), and (b) Millennium Stadium (Courtesy of Atkins)	14
2.7	(a) Amsterdam Arena (Ishii, 2000), (b) Gelredome (Courtesy of ABT), and (c) Oita Stadium (Courtesy of Kisho Kurokawa Architects)	15
2.8	(a) Wembley Stadium (2004), and (b) Arizona Cardinals Stadium (Riberich, 2003)	15
2.9	Four proposals for 2008 Beijing Olympic Stadium (a) B02; (b) B07; (c) B11; (d) B12 (Beijing Municipal Commission of Urban Planning, 2003)	17
2.10	'HIMAT' retractable mast for space applications (Kitamura <i>et al.</i> , 1990)	19
2.11	Solid Surface Deployable Antenna (Guest & Pellegrino, 1996b)	19
2.12	(a) Umbrellas Medinah by Otto <i>et al.</i> (1995), and (b) Floating Concrete Pavilion by Calatrava (Tzonis, 1999)	21
2.13	Piñero with his movable theater (Gantes, 2001)	22
2.14	<i>Lazy-tong</i> formed by three pantograph elements	22
2.15	Pantographic element consisting of two straight bars	23
2.16	(a) Pantographic element consisting of two angulated elements, each formed by two bars, and (b) Multi-angulated element with three bars	24
2.17	Radial movement of structure	25
2.18	Retractable structure formed by multi-angulated elements	25
2.19	Rotating movement of structure	26
2.20	Cover elements by Kassabian <i>et al.</i> (1997)	26
2.21	Reciprocal Plate Structure proposed by Chilton <i>et al.</i>	27
2.22	Retractable systems formed by four-bar linkages (You, 2000)	27
2.23	Swivel Diaphragm by Rodrigues & Chilton	28
2.24	Double-Chain mechanism by Wohlhart (2000)	29
2.25	Reciprocal dome proposed by Piñero (Escrig, 1993)	29

2.26	Iris Dome by Hoberman (Kassabian <i>et al.</i> , 1999)	30
3.1	Circular structure with $n;k = 8;3$ (a) Closed Configuration, and (b) Open configuration	33
3.2	The opening ratio OR as a function of $n;k$	34
3.3	The stowage ratio SR as a function of $n;k$	34
3.4	The limits of rotation coincide with the intersections of two neighbouring circles of motion	35
3.5	Definition of angles β, γ, δ and ϵ	36
3.6	The rotation angle β^* as a function of $n;k$	38
3.7	Sum of angles at internal hinges for structure with $k = 3$	38
3.8	Structures formed from identical polygons and showing element with largest kink angle (a) An angulated element, (b) Similar rhombuses, and (c) Similar parallelograms	40
3.9	Non-circular structures consisting of multi-angulated elements with variable sum of kink angles	42
3.10	Location of the fixed centre of rotation in (a) Intermediate configuration, and (b) Open configuration	43
3.11	Rotational limits of structure with hinges of finite size in (a) Closed configuration, and (b) Open configuration	44
3.12	Additional limit ζ for the rotation angle β^* of circular structures	45
3.13	Movement of four-bar linkage with two plates	46
3.14	Determining the boundary angle θ	47
3.15	Boundary angle θ for multi-angulated elements in (a) Closed configuration, and (b) Open configuration	48
3.16	Wedge-shaped cover elements for circular structure	49
3.17	Cover elements for a structure formed by projection onto a sphere	51
3.18	Wedge-shaped cover elements that fully cover the angulated elements and their hinges (a) $k = 2$, (b) $k = 3$, and (c) $k = 4$	52
3.19	Plastic model of wedge-shaped plate structure with $n;k = 12;3$	52
3.20	Cardboard model of non-circular plate structure	53
3.21	Periodic pattern of non-straight boundary	53
3.22	Direction of initial movement and region defining possible boundary shapes	54
3.23	Non-periodic end features	55
3.24	Model of sixteen identical plates forming a perfect circular opening	55
3.25	Plastic model of plate structure formed from similar parallelograms	56
3.26	Top and bottom faces of model of non-circular structure where all plates and boundaries are unique	56
3.27	Schematic of GTD application	58
3.28	Shape of cover elements after minimising the gaps and overlap between cover elements and maximising the size of central opening in the open configuration (Buhl <i>et al.</i> , 2004)	59
3.29	Single degree of freedom assembly of two rigidly interconnected structures	61
3.30	(a) Two identical structures, (b) Single degree of freedom assembly of two structures with congruent rhombus, and (c) Branched pantographic elements	62
3.31	Single degree of freedom assembly covered by rigid elements	63

3.32	Movement in node structure and its linkages forming parts of three ring structures	64
3.33	Cardboard model of assembly with node structure	64
3.34	Two degree of freedom node structure (a) Intermediate configuration, (b) One linkage pair fully sheared, and (c) Both linkage pairs fully sheared	65
3.35	Model of node assembly with two degrees of freedom	65
3.36	Expandable circular plate structure.	66
3.37	Model of stacked assembly	67
3.38	Expandable free-form or “blob” structure (Jensen & Pellegrino, 2004)	67
3.39	Stack assembly of two structures with three rigid connections	68
3.40	Proposed use of plate structure to cover a sporting venue	69
4.1	Hinge with a single rotational degree of freedom, scale 2:1	72
4.2	Actuator assembly	73
4.3	Switch and pin for reversing motion of model	74
4.4	Details of support cables in (a) Horizontal, and (b) Vertical configurations, scale 1:1	74
4.5	Beam model, with $n = 8$, in its closed configuration	77
4.6	Single plate element under self-weight (a) Mesh for shell elements, (b) Deflections, and (c) Maximum principal stresses	78
4.7	Contours of deflections under self-weight for $n = 9$ plate model, held horizontal, with three support points	80
4.8	Contours of deflections under self-weight for $n = 9$ plate model, held horizontal, with nine support points	82
4.9	Contours of deflections under self-weight for $n = 8$ plate model, held horizontal, with eight support points	83
4.10	Physical model with $n = 8$, hung horizontally	84
4.11	Physical model with $n = 8$, hung vertically	84
4.12	Vertical motion of hinge A_i hung from the fixed point P	87
4.13	Vertical displacement and its derivative for $r_P = 400\text{mm}$	89
5.1	Spherical geometry (a) The sphere and its circles, and (b) Angle between great arcs and the angular length of these	92
5.2	Spherical geometry (a) A lune, and (b) A spherical triangle	93
5.3	Spherical geometry (a) Area of a triangle, and (b) Area of a polygon	94
5.4	Pantographic element on a spherical surface	97
5.5	Plots of $\angle BPE$ for different n and lengths of AB	99
5.6	Spherical structure formed by multi-angulated elements (Kokawa, 2000)	100
5.7	Spherical plates with straight boundaries in (a) Overlap free closed configuration, and (b) Overlapping open configuration	101
5.8	Spherical plates with kinked boundaries in (a) Overlap free open configuration, and (b) Overlap free closed configuration	102
5.9	Determining (a) Kink angle κ , and (b) Vertex angle α	103
5.10	Plate elements exhibiting periodicity	104
5.11	Plate elements with periodic boundary formed by a small circle	104
5.12	Plate elements with periodic boundary forming a perfect circular opening	105
5.13	Model made from plastic hemispheres	106
5.14	Model made using rapid prototyping techniques	107

6.1	Rotated plate element in (a) Two extreme configurations, labelled 0 and m , and (b) Intermediate configuration	109
6.2	The non-commutativity of vector rotations (a) $\theta_x, \theta_y, \theta_z$, and (b) $\theta_y, \theta_x, \theta_z$	111
6.3	Large three-dimensional rotation about OP	111
6.4	A single rotation θ_E about P_E moves the plate element from its closed to its open configuration	113
6.5	Determining the Euler pole P_E and rotation θ_E from $\triangle P_E B_0 B_m$	113
6.6	Determining P_E and θ_E from $\triangle P_E B_0 B_m$ and the initial position given by λ	115
6.7	Location of the Euler pole, P_E , for varying positions λ of the plate in the closed configuration	117
6.8	Compound rotations for $-\pi/2 \leq \lambda \leq \pi/2$ (a) Individual rotations, and (b) Solutions for \vec{e}_{12} and \vec{e}_{13}	118
6.9	Possible locations of P_E for structures with $n = 8$ plates and increasing opening size $\angle POB_m$	119
6.10	Physical model with fixed points of rotation	120
6.11	Computer generated images of how a retractable roof could be constructed from spherical plates with fixed points of rotation	120
6.12	Incremental rotations of apex A_I and A_{II} (a) Absolute, and (b) Relative	121
6.13	Reciprocal retractable structures (a) Beam grillage, and (b) Swivel Diaphragm	122
6.14	Smaller model interconnected by pins running along curved paths	123
6.15	Model parts (a) Excavation from printer, and (b) Before polishing	124
6.16	400 mm span model fabricated using 3D Ink-Jet printing	125
7.1	Spatial motion of $n = 8$ plate structure (a) Axes of rotation, and (b)–(f) Opening of structure	130
7.2	Simulation results for (a) Internal strains, and (b) Rotations	133
7.3	Defining the location of point C using point B and angle ϕ	134
7.4	Convergence of $\Delta(\phi_C, \phi_E, \phi_G)$ using (a) <i>fminsearch</i> , or (b) <i>fminunc</i>	135
7.5	Simulation results for optimised values of ϕ (a) Internal strains, and (b) Rotations	136
7.6	Convergence of Δ using (a) <i>fminsearch</i> , or (b) <i>fminunc</i>	137
7.7	Two designs with finite sized spherical joints	138
7.8	Simulation results with lowest achieved strains (a) Internal strains, and (b) Rotations	139
7.9	Simulation results for design with finite sized joints (a) Internal strains, and (b) Rotations	139
7.10	Simulation results with four peaks in the strain function Δ (a) Internal strains, and (b) Rotations	140
7.11	ProEngineer kinematic model	141
7.12	Motion revealing conflicts between bars	143
8.1	Rendering of novel concept retractable roof	147

List of Symbols and Abbreviations

Chapters 1–4

A_{cen}	Centre of rotation for element A , p. 36
A_i	Hinge i of element A , p. 35
A_j	Internal hinge number j of element A , p. 37
E	Young's Modulus, p. 77
G	Weight of model, p. 87
h	Height of period, p. 54
i	Integer $\leq k$, p. 35
j	Integer $1 \leq j \leq k - 1$, p. 37
k	Number of bars per element, p. 32
l	Length of bar, p. 32
l_P	Length of hanger, p. 86
L	Length of period, p. 47
n	Number of elements per layer, p. 32
O	Origin, p. 33
r	Inner radius, p. 32
r_j	Radius of joint, p. 43
r, z	Coordinates in vertical plane, p. 87
r_P, z_P	Coordinates of fixed point P , p. 87
R	Outer radius, p. 32
T_a	Actuator torque, p. 85
T_b	Ball-bearing friction, p. 86
W_a	Virtual work done by actuator, p. 85

W_b	Virtual work done by friction, p. 86
W_g	Virtual work done by gravity, p. 87
α	Kink angle, p. 32
β	Rotation angle, p. 36
β^*	Total rotation angle ($\beta_{\text{open}} - \beta_{\text{closed}}$), p. 35
β'	Alternative total rotation angle ($2\alpha - \zeta$), p. 62
γ	Inner angle, p. 36
δ	Element angle ($k\alpha$), p. 36
ϵ	Limit angle ($\pi - \alpha$), p. 36
ζ	Additional limit angle, p. 45
η	Angle, p. 46
θ	Boundary angle, p. 47
ν	Poisson's ratio, p. 77

Abbreviations

ABS	Acrylonitrile-Butadiene-Styrene, p. 52
AWJ	Abrasive Water Jet Machine, p. 55
CFC	Carbon Fibre reinforced Carbon, p. 16
CFRP	Carbon Fibre Reinforced Plastic, p. 71
EDM	Wire Electrical Discharge Machine, p. 56
FA	British Football Association, p. 14
FIFA	Fédération Internationale de Football Association, p. 8
GTD	Computer application, p. 56
<i>OR</i>	Opening ratio ($r_{\text{open}}/R_{\text{closed}}$), p. 33
<i>SR</i>	Stowage ratio ($R_{\text{open}}/r_{\text{open}}$), p. 33
UEFA	Union of European Football Associations, p. 8
UV	Ultra Violet, p. 11

Chapters 5–8

A	Area, p. 92
\vec{e}	Unit-vector, p. 110
E	Spherical excess, p. 95
i	Integer, p. 95
I	Identity matrix, p. 112
j	Number of joints per plate element, p. 129
L	Length of period, p. 103
m	Number of rotations between closed and open configurations, p. 109
M	Relative mobility, p. 129
n	Number of plate elements, p. 96
O	Centre of sphere, p. 92
P, P^*	Pole and antipodal, p. 92
P_E	Euler pole, p. 110
r	Radius of small circle, p. 92
R	Radius of great circle and sphere, p. 92
R	Rotation matrix, p. 112
S	Spin matrix, p. 112
u_i	Number of constraints imposed by joint i , p. 129
x, y, z	Coordinates, p. 110
α	Apex angle, p. 97
β	Vertex angle, p. 94
γ	Vertex angle, p. 93
δ	Angular defect, p. 95
Δ	Strain function $\left(\Delta = \sqrt{\varepsilon_{BC}^2 + \varepsilon_{DE}^2 + \varepsilon_{FG}^2} \right)$, p. 132
ε	Strain, p. 132
ζ	Internal angle of spherical angulated element, p. 97
η	External angle $(\pi - \beta)$, p. 94
$\vec{\theta}$	Pseudo-vector $(\theta\vec{e})$, p. 110
θ_i	Rotation angle about axis i , p. 110

θ_E	Rotation angle about Euler pole P_E , p. 110
κ	Kink angle, p. 102
λ	Initial position angle, p. 115
μ	Angle, p. 113
ξ	Angle, p. 115
ϕ	Connection angle, p. 134
$\vec{\omega}$	Modified pseudo-vector $(2 \tan(\theta/2)\vec{e})$, p. 110

Abbreviations

ABS	Acrylonitrile-Butadiene-Styrene, p. 106
FDM	Fused Deposition Modelling, p. 106
PTFE	Polytetrafluoroethylene, p. 126

Chapter 1

Introduction

1.1 Stadia

Throughout civilisation, mankind has assembled to view with awe the spectacular and heroic feats performed by their sporting fellows. The theatres for these performances have been known as *stadia* since the first were built together with western civilisation in ancient Greece. The Greek stadia were U-shaped foot racecourses and the 1 *stadium* (approximately 200 meters) length of the racecourse gave name to these venues (Geraint & Sheard, 2001). The design of these first stadia was based on traditional open air theatres, excavated out of hillsides to form low uncovered seating tiers along both sides of the racecourse. They were of great civic importance in Greek life and could host up to 45,000 spectators. The sporting games held at the stadium in Olympia started what is still celebrated as the Olympic tradition. Centuries later the Romans dedicated the same importance to their stadia, the amphitheatre, though it no longer hosted peaceful athletic meetings. Instead they were the scenes for gory battles of life and death. The most famous of these is the Flavian Amphitheatre in Rome, better known as the Coliseum. From this particular venue many later stadia would inherit its structural form, with its good sightlines, structural stability and appropriate volumes of circulation space.

With the fall of the Roman Empire, European societies concentrated their architectural efforts on religious buildings and no new stadia would be built in the world until the arrival of the industrial revolution fifteen centuries later. With the new social order that followed also came a renewed interest in mass spectator events. On June 23rd, 1894, the French Baron Pierre de Coubertin founded the International Olympic Committee with a ceremony held at the University of Sorbonne in Paris. Together, the revival of the Olympic tradition and the rapid growth in popular sports, like football and baseball, would form the catalyst and economic base for the construction of most stadia in the twentieth century and this is likely to continue in the twenty-first century also. Though present day society recognises the civic importance of the stadia and the events hosted there, it is increasingly unwilling to support financially the construction and running of these venues. Because of this, the long-term economic performance of the venues has now become the single most important planning and design issue for any new stadium.

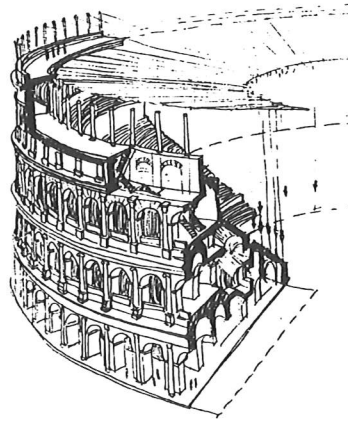


Figure 1.1: Coliseum in Rome (Escrig, 1996)

First generation modern stadia were not the grand monuments of the past. Instead they grew organically as attendance increased. First small shacks were erected for comfort, later cheaply built stands were built to improve sight-lines; both to attract the maximum number of spectators through the tills. To minimise the loss of revenue on rainy days many stands were fitted with simple corrugated steel sheet roofs to keep the rain out. The invention of TV and the broadcasting of live-sports from 1937 dramatically changed the existing economic situation. Now spectators had the possibility of watching sporting events in the comfort of their own living room. This started a steady continuing decrease in attendance resulting in venues having to find additional streams of revenue (Sheard, 1998).

This was mainly achieved by attaching a number of other facilities, such as shops, hotels, offices and fitness centres, to the venue itself (Roberts & Dickson, 1998). The stadia thus evolved from a simple sporting venue to a *multi-facility* complex aiming to secure constant revenues and long-term economic performance.

Despite the multi-facility approach, many venues still struggle economically as their largest space, the sporting theatre itself, is largely unused. The home team only plays at home approximately once per week and revenues are therefore only generated on these few game days. To overcome this problem many stadia are today *multi-purpose* venues able to host a small range of sporting and non-sporting events such as football, athletics and concerts. To increase the range of events that can be hosted, during the last 40 years some stadia, mainly in the USA, have been built as fully covered arenas (Geraint & Sheard, 2001; Lenczner, 1998). This has only been possible as their main sporting tenants are able to play on artificial surfaces. This attractive solution has not been available to the majority of venues throughout the rest of the world as the predominant sport, football, requires a natural turf that cannot be grown in a fully covered arena.

For these venues an alternative solution was also inspired by the Roman amphitheatre. Similarly to its structural section, its temporary roof formed by retractable canvas awnings, known as the *velum*, was to provide the inspiration for *retractable roofs* of modern day stadia (Escrig, 1996; Ishii, 2000; Sheard, 1998; Zablocki, 2002).

1.2 Retractable Roofs

A retractable roof is, unlike a demountable or temporary structure, a permanent structure capable of undergoing a geometric *transformation* or folding between two distinct configurations, usually referred to as the *open* and *closed* configurations. This ability to transform geometrically is what distinguishes retractable roofs from traditional static roofs. The transformation process of going from the open to the closed configuration is here referred to as *closing* or *retracting* and the reversed transformation as *opening* or *expanding*.

A retractable roof can provide a variable amount of cover for the space below and thus gives an increasing number of stadia the ability both to grow natural turf and fully enclose the venue temporarily hence increasing the range of events that can be hosted. Retractable roofs have not only found their use in sport venues but also at ship yards, exhibition and recreational spaces and in cars. Retractable roofs used for stadia are typically stable and thus able to carry loads throughout their transformation but some, such as folding membranes, are only stable and able to carry load in one or both of their extreme configurations.

Since large retractable roofs were first reintroduced in the 1950's a variety of retractable systems have been built and many more ideas and concepts have been proposed. The first systems were based on well-known crane technology, soon to be followed by folding membranes, inspired by umbrellas and tents, and telescopic systems. This evolution continues with various types of *deployable structures* being proposed as the next step in the evolution towards better structural and economical performance of retractable roofs (Ishii, 2000; Miura & Pellegrino, 2002).

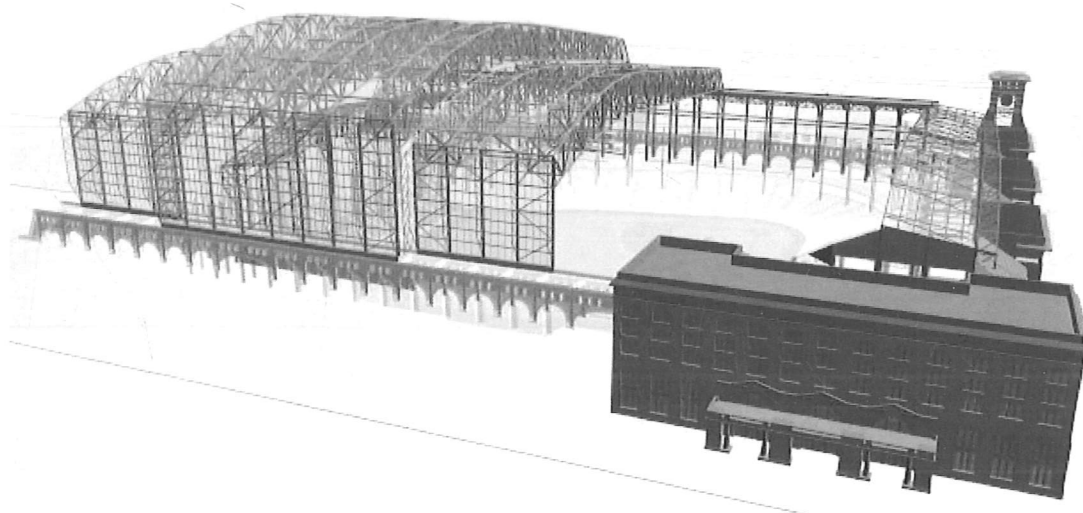


Figure 1.2: Schematic of retractable roof over the Minute Maid Park, US (Post, 2000)

1.3 Deployable Structures

A large group of structures have the ability to transform themselves from a small, closed or *stowed* configuration to a much larger, open or *deployed* configuration; these are generally referred to as deployable structures though they might also be known as erectable, expandable, extendible, developable or unfurlable structures. As retractable roofs can also transform from their open to a closed configuration they are sometimes also classified as a type of deployable structure.

The research subject of deployable structures is relatively young as it was pioneered only in the 1950s and '60s. Though the subject is young, many of its best known applications have been around for millennia, examples are the umbrella, the folding chair, and the velum of the Roman Coliseum, Figure 1.1. At present the two main applications areas of deployable structures are Aerospace and Architecture.

From the first man made satellite, Sputnik, launched on October 4th, 1957, the scientists and engineers behind space programs throughout the world have been faced with tight weight and space restrictions for their space structures. Because of these restrictions all spacecraft structures, or parts thereof, larger than the space available in the launch rocket must be stowed and later deployed in space. This is done for antennas, reflectors, masts, solar panels and so on. Each one having its own unique shape and characteristics often resulting in equally unique stowage and deployment techniques.

The Spanish architect Piñero was the first in modern times to explore systematically the possibilities and properties of deployable structures in architecture (during the middle ages prominent people such as Leonardo da Vinci had proposed deployable structures for trusses, bridges and machinery). Piñero proposed to use them for temporary coverings of exhibition spaces or swimming pools. The architectural uses of deployable structures were initially reserved for these temporary or mobile structures but they are now being applied to a wider range of structures, such as retractable roof systems.

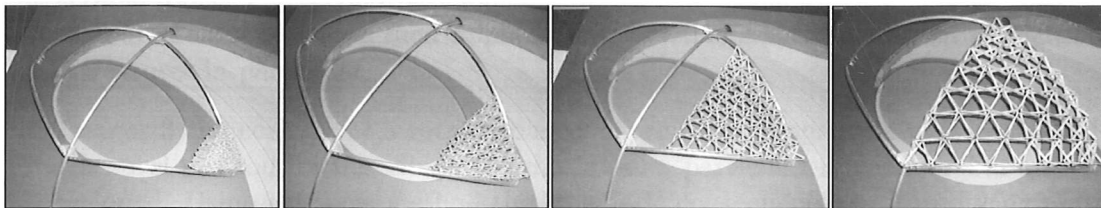


Figure 1.3: Concept for deployable canopy (Mollaert *et al.*, 2003)

1.4 Aims & Scope of Research

Though many different deployable structures have been proposed for retractable roofs, so far they have found limited use. This has often been caused by their many moving parts, complex hinges, discontinuous load paths or failure to provide adequate cover. In some of the structures that have been proposed, the sliding of different parts of the

structure against each other causes unwanted friction, in others the repeated folding and unfolding of membranes has caused material failure. Despite these problems there is an increasing interest in these structures as they promise to provide designers with visually unique and efficient structures.

This dissertation aims to provide designers with viable alternatives to the existing solutions for large span retractable roof structures. The design of a full scale structure is beyond the scope of the research undertaken. Hence the basis for the development has been the assumption that most of the problems limiting the use of deployable structures are caused by the geometry of the structure and its mechanism. The research has therefore been focussed on eliminating these problems mainly by means of geometric studies.

The problem has been approached by conducting a comprehensive review of the present state-of-the-art of large retractable roof structures and deployable structures proposed for retractable roofs. On the basis of this review it was decided to continue the development of a retractable mechanism based on hinged bars.

Through the development of this system a number of advances were made, notably a novel structure composed solely from plate elements forming a completely gap free roof surface in both open and closed configurations. However, a proof-of-concept model showed the potential structural stiffness limitations of flat two-dimensional systems. On the basis of this finding, three novel concepts with a spherical geometry have been developed.

1.5 Outline of Thesis

In Chapter 2, a review of existing retractable roof technologies and deployable structures is presented. The first part is concerned with the current state-of-the-art of retractable roofs. The second part focusses on current technologies within the field of deployable structures and on their applications in civil engineering, and for retractable roof structures in particular.

In Chapter 3 the concept of a retractable roof formed by hinged plates is developed. First a novel method for describing the motion of a particular retractable bar system is developed. Using this new method the kinematic consequences of introducing finite sized joints in the mechanism is investigated. A study of the motion of neighbouring elements within the overall structure reveals the possibility of replacing the bars of the structure with rigid plates, thus allowing the creation of retractable structures formed by plates. The method for designing such structures is then expanded to allow for a wide variety of possible shapes.

In Chapter 4, a 1.3 metre span physical model of such a retractable structure is presented. The first part of the chapter presents the model as built while the latter part presents the analysis carried out in order to produce the model. From this study it is then concluded that this particular retractable structure is not well suited for large scale applications such as stadia roofs. A number of alternative uses are then proposed.

In Chapter 5, a novel geometry for spherically shaped elements is revealed. Retractable

systems based on this new geometry seems better suited for applications on a large scale than geometries previously proposed by other authors. The derivation of the element shape is presented and linked to the geometry of the two-dimensional plate elements presented in Chapter 3.

In Chapter 6 the motion of such spherically shaped elements on the sphere itself is investigated. It is found that it is possible to create retractable structures in which the individual elements only undergo a rotation about a fixed axis. The position of this axis thus becomes important, and it is shown that it is possible to position this axis within the boundaries of the elements themselves thus greatly simplifying the structure. By investigating the relative motion between neighbouring elements it is not found possible to link two of these elements together using only cylindrical hinges. Instead, it is proposed to use a sliding mechanism to create a reciprocal system with only a single internal mechanism capable of supporting itself efficiently. A physical model is built to demonstrate the feasibility of the concept.

In Chapter 7 an alternative mechanism using the same spherical elements is proposed. The sliding mechanism and cylindrical hinges have been replaced by a series of bar linkages and spherical joints. Such a system is normally overconstrained and thus not capable of executing large motions without large strains occurring in the structure. However, it is shown that by carefully choosing the connection points it is possible to minimise the peak strains occurring in the structure, so they become very small, and thus allowing the structure to function as a mechanism.

Chapter 8 concludes the study by comparing the proposed structures and discussing their possible application as large retractable roofs. A number of ideas for the direction of future work are also provided.

Chapter 2

Review of Literature and Previous Work

2.1 Introduction

The beginning of this chapter discusses the drivers which over the last decade have resulted in a significant increase in the number of constructed and proposed stadia with retractable roofs. A classification of retractable roof systems is then presented and a number of commonly used systems are reviewed through built examples while state-of-the-art systems are reviewed through recently proposed stadia and the competition entries for the 2008 Beijing Olympic Stadium. The second part of the chapter presents a brief review of current deployable structures technologies, both for space and architectural applications. For architectural and civil engineering applications, deployable systems using pantograph elements have become quite popular. As they can be used to form closed loop structures which can retract towards their perimeter, they have been proposed for use as retractable roofs for stadia. Hence the third part of the chapter presents the research that has been carried out on the use of closed loop retractable roofs made from pantograph elements.

2.2 Retractable Roofs for Stadia

Though modern retractable roofing systems have been used throughout the world since the 1930's, in one form or another, it is only in recent decades that they have become commonly used in stadium design. At the start of the new millennium there were approximately 25 large-span retractable roofs in the world, of which around 15 of those were stadia roofs and approximately half of the total were located in Japan (Ishii, 2000; Zablocki, 2002). There was at the same time an equal number of roofs at various stages of planning or construction, thus marking a sharp increase in the construction of large retractable roofs.

Of the many factors contributing to this trend, economics is the main driving force, as demonstrated by Dean *et al.* (1998) using the retractable roof for the Victoria Dock-

lands Stadium, later renamed the Colonial Stadium, in Melbourne, Australia, as an example (Sheldon & Dean, 2002). As nearly all sporting facilities around the world have been privatised and have had their public subsidies considerably reduced it has become both more important and more difficult to operate these facilities profitably. This is especially true for the larger national or regional stadium venues, which have increased construction costs and limited possibilities of public access to the facilities, unlike swimming pools, arenas and training facilities, which can generate additional revenue through public use when no sporting events are hosted. This economic problem has led to most new stadia being built with a number of additional revenue generating facilities attached such as shops, hotels, cinemas and health clubs, turning them into what is known as *multi-facility* venues (Geraint & Sheard, 2001; Roberts & Dickson, 1998).

To improve their economic performance further many stadia have increased their hosting of non-sporting events, such as concerts and exhibitions, or sporting events for which the venue was not originally designed, such as boxing, tennis or speedway. These types of events are usually not as regular as the games played by the main tenant of the stadium. To achieve more regular use, an increasing number of stadia are home to more than one team and they are often from different sports. The best known example is the San Siro Stadium in Milan that hosts the city's two football teams Inter Milan and AC Milan. However, increasing the number of events hosted does cause a number of problems.

A large number of non-sporting events require an enclosed space and thus most stadia are not capable of hosting events such as conferences and exhibitions. This led to the construction of a generation of enclosed stadia in the USA, between the late 1960s and the 1980s. A fully enclosed venue also has the advantage that cancellations due to adverse weather conditions will not occur. This strategy has not been followed in other parts of the world, where football is the most popular sport, as its governing body, Fédération Internationale de Football Association (FIFA), still requires national and international games to be played "in the open-air" (Zablocki, 2002).

Another inherent problem with increased use is that the playing surface slowly deteriorates with the increased activity. Many non-sporting events also require some sort of temporary covering of the turf and thereby further aggravates the problem. In addition to this, in many of the newer stadia with higher stands and larger overhanging roofs, built to accommodate more spectators, it has been found that the playing surface deteriorates more rapidly, as sun light and air movement have been reduced considerably.

An often suggested solution to the above mentioned playing surface problems would be to install an artificial surface with synthetic grass. Such a surface would be able to withstand the use of both sports and pop concerts while eliminating many environmental problems inside the stadium. This has already been tried in the USA, where the introduction of artificial surfaces allowed the construction of fully enclosed stadia. In Europe and the rest of the world the installation of artificial grass in football stadia has been prevented by FIFA, which requires national and international games to be played on natural grass. In a recent development, the European football organisation Union of European Football Associations (UEFA) has announced it is running a number of trials with artificial grass which has now been installed in several stadia on a

trial basis (UEFA, 2003). Two of these are high-profile national stadia, namely the Finnair Stadium, Helsinki, and the Amsterdam Arena, Amsterdam (Bisson, 2003).

Another solution for the problem of poor conditions for natural grass has been implemented at Gelredome, Arnheim, and the 2001 Sapporo Dome, Hokkaido. Here the turf is planted in a large tray, which can then be transported outside the stadium when not in use. This provides the turf with good growth conditions while allowing the stadium the maximum flexibility. At the Sapporo Dome the tray is lifted using air pressure and rolled on wheels, while at Gelredome the tray is mounted on a series of low friction rails. The approach taken at Gelredome has later proven troublesome according to the design engineers Nijssen & van Vliet (2003).

In a 1995 British Sports Council publication on stadium design the problem of natural grass growth was said to be the limiting factor for further advances in stadium design in the United Kingdom. It was therefore found necessary either to find a method for growing turf beneath an enclosed roof, accept synthetic playing surfaces, or develop a cost-effective retracting roof system (Murray, 1995). The retractable roof solves the problem by reducing the size of the overhanging roof, thus allowing an increase in sun light and air movement and combining this with the flexibility of an enclosed venue.

2.2.1 Classification of Retractable Roofs

The first large retractable roof built for a sporting venue was the 1961 Pittsburgh Civic Arena, later renamed the Mellon Arena, USA (Ishii, 2001; Mellon Arena, 2004). It was a steel dome with four retractable steel truss panels making up half of the domed roof. In the open position these panels were then nested below the remaining fixed half of the roof in an overlapping arrangement. The dome was not self-supporting, rather it was hung from a large steel truss cantilevering over the dome. The dome was built using mechanical solutions borrowed from crane design. This is still the case for most large retractable roofs, as cranes provide tested and well-understood solutions for problems of tolerances, thermal expansion, and deflections – to name only a few among the many issues related to moving large and heavy structures along predefined paths.

Since then other stadia have been constructed with retractable roofs. To ensure that the lessons learned through these pioneering projects were not forgotten the International Association for Shell and Spatial Structures set up Working Group No. 16 in 1993. The aim of the group was “to develop a State-of-the-Art report and Guidelines for the design and construction of retractable structures” and their conclusions were presented in their resulting publication *Structural Design of Retractable Roof Structures* (Ishii, 2000). Two types of structures were reviewed by the group: rigid frame structures and folding membrane structures. The emerging group of structures utilising expandable frames, in general referred to as deployable structures, was not reviewed as this type had yet to be realised on a large scale.

Large retractable roofs are today an established building type and in Japan legal standards and design guidelines for new retractable roofs have been introduced through the Building Standard Law of Japan (Ishii, 2001).

In Figure 2.1 existing methods for opening and closing a large retractable roof are

shown. These methods can broadly be represented in a three-by-three matrix by classifying their movement as: (a) parallel, (b) circular or (c) vertical, and their method of stowing the retracted roof as: (i) overlapping, (ii) non-overlapping or (iii) folding, as shown in the figure. There are a number of systems that utilise a combination of these methods, as described below.

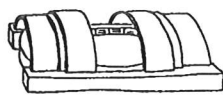
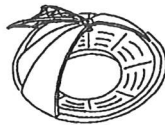


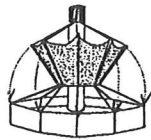

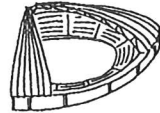

	(a) Parallel movement	(b) Circular movement	(c) Vertical movement
(i) Overlapping systems			
(ii) Non-overlapping systems			
(iii) Folding systems			

Figure 2.1: Methods for opening and closing (Ishii, 2000)

2.2.2 Built Examples of Retractable Roofs

Folding Membrane Systems

Since the 1950s research has been carried out into the use of folding membranes as retractable roofs. The pioneering work was led by Prof Frei Otto at the Institute for Lightweight Structures, Stuttgart, Germany. Many schemes were developed and some of those were realised as retractable or temporary coverings for skating rinks, exhibitions and open-air theatres (Institute for Lightweight Structures, 1971; Mollaert, 1996). A schematic representation of many possible schemes that were considered is shown in Figure 2.2.

The first application of a folding membrane roof to a stadium was the 1976 Montreal Olympic Stadium. The folding roof itself was however not completed until the mid-eighties and has later been replaced by a fixed roof due to wind-induced failures of the retractable membrane. The membrane could be lowered from a tower leaning over the stadium. The membrane was guided along a series of cables running from the tower to the boundary of the fixed roof over the stands. Other cables fixed to the membrane would provide the tensioning of the membrane once the boundary was held in place (Ishii, 2000; Schlaich, 2000).













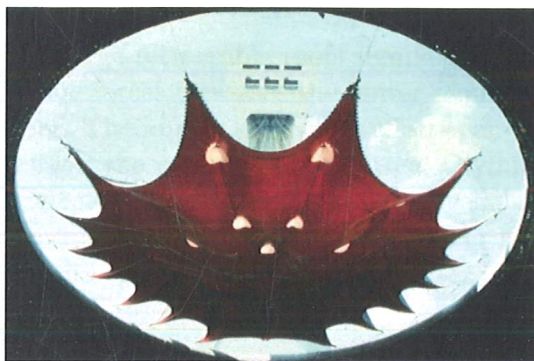
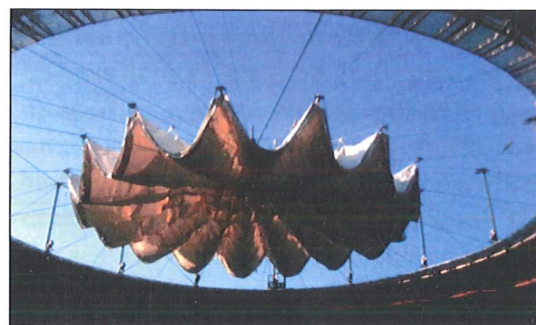
Construction system	Type of movement		Parallel	Central	Circular	Peripheral
Stationary supporting structure	Membrane	Bunching				
		Sliding				
Moveable supporting structure	Supporting structure	Rolling				
		Folding				
		Rotating				

Figure 2.2: Methods for opening and closing of membrane structures by the Institute for Light-weight Structures (1971)

The lessons learned from the very complicated Montreal roof were applied to another retractable membrane roof by the engineers Schlaich Bergermann and Partners. For the 1988 Zaragoza Arena, Spain, the existing bull fighting arena was covered with a partly retractable membrane roof. From a floating position at the centre of the opening in the fixed part of the roof, the folded membrane deploys along radial spokes, which also carry the load of the membrane (Ishii, 2000; Schlaich, 2000). The material of the folding membrane was replaced after ten years of use due to Ultra Violet (UV) degradation of the fabric and developing tears along the folding lines (Monjo *et al.*, 2002).



(a)



(b)

Figure 2.3: Folding membrane roofs at (a) Montreal Olympic Stadium, and (b) Zaragoza Arena (Schlaich, 2000). Views from inside the stadia

Two other stadia use folding membranes for their retractable roofs but unlike the

Montreal and Zaragoza roofs, the Toyota Stadium in Japan, built in 2001, and Parken Stadium in Denmark do not use a single large membrane to cover the pitch. Instead they are composed of air-inflateable membrane cushions attached between a number of large parallel trusses that run on two tracks either side of the opening in the fixed roof. In the open position the trusses are parked next to each other at one end of the pitch, with the cushions hanging deflated and folded between them. When the roof is closed the trusses move and the cushions are inflated and provide cover over the pitch. The system is simple in concept but in the case of the Toyota Stadium it was found necessary to also install smaller, folding trusses below the cushions to provide sufficient stiffness to the system (Shibata, 2003). In the case of the Parken Stadium, the retractable roof was fitted in 2001 to the existing 1992 stadium roof to provide a venue for the 2001 Eurovision Song Contest.



Figure 2.4: Folding membrane roofs at (a) Parken Stadium (Courtesy of CENO Tec), and (b) Toyota Stadium (Shibata, 2003)

Vertical Systems

For large retractable roofs significant vertical movement is usually avoided, as gravitational forces increases the power required by the mechanical systems that operates the roof. The impact of gravity effects can be minimised by constructing a very light roof, as was the case for the Montreal Olympic Stadium. A number of newer systems that are classified as having parallel movement do have gentle slopes in the path along which the roof is moved as it allows greater architectural freedom. Examples of this are the Toyota and Oita Stadia and Amsterdam Arena, see above and below in this section.

Circular Systems

The non-symmetrical layout of this type of retractable roof in its open configuration, and its ability to cover a triangular pitch has made it a popular choice for baseball venues in Japan and the USA. Figure 2.1(b) shows how the panels of the retractable roofs are pivoting about a fixed point allowing them to stowed by either overlapping or folding the panels. For stadia only overlapping systems using rigid panels have been constructed as the folding of large and non-symmetric panels is difficult (Geraint &

Sheard, 2001; Ishii, 2000, 2001). Examples of circular, overlapping systems are the 1993 Fukuoka Dome in Japan and the recent Miller Park, USA, and the Sendai Dome in Japan, both built in 2000 (Hewitt *et al.*, 1998; WG16 IASS, 2001).



Figure 2.5: Miller Park (Courtesy of NBBJ Architects)

Parallel Systems

The majority of large retractable roofs are based on parallel movement. The simplicity of this motion makes it an attractive option for most venues and many technical solutions can be taken directly from large cranes such as those used in container terminals. The simplest variation of the parallel system is simply to move the entire rigid roof off the venue itself and put it next to it to achieve the open configuration. This however does not reduce the plan area covered by the roof and thus additional space has to be allocated to this purpose; hence this form of retractable roof is thus rarely used. An example of this is the 1991 Ariake Colosseum (Ishii, 2000), Figure 2.6(a), where the roof is composed of two parts which both span the entire seating bowl of the stadium and thus can be rolled off completely.

Other variations of the parallel system have already been discussed above for the Toyota Stadium and Parken Stadium, in Section 2.2.2. Similarly, the 1989 Toronto Sky Dome retracts three large rigid space frame panels using a telescopic system. In the open configuration, these panels overlap the fixed structure at one end of the venue (Ishii, 2000). The most commonly used system, generally referred to as a bi-parting system, is also based on parallel movement (Griffins, 2003).

Bi-parting Systems

A retractable bi-parting roof is comprised of two large rigid panels, which when opened move in opposite directions. The panels are moved along two parallel rails mounted on two main trusses located along the edge of the fixed roof either along or perpendicular to the main axis of the venue, the first being the arrangement most frequently used. Hence this system covers only the large central opening between the fixed roof, that covers the seating areas on all four sides of the stadium. The two retractable panels can therefore be moved above or below the permanent roof when not in use. A typical example of this system is the 1999 Cardiff Millennium Stadium in Wales, shown in Figure 2.6(b).

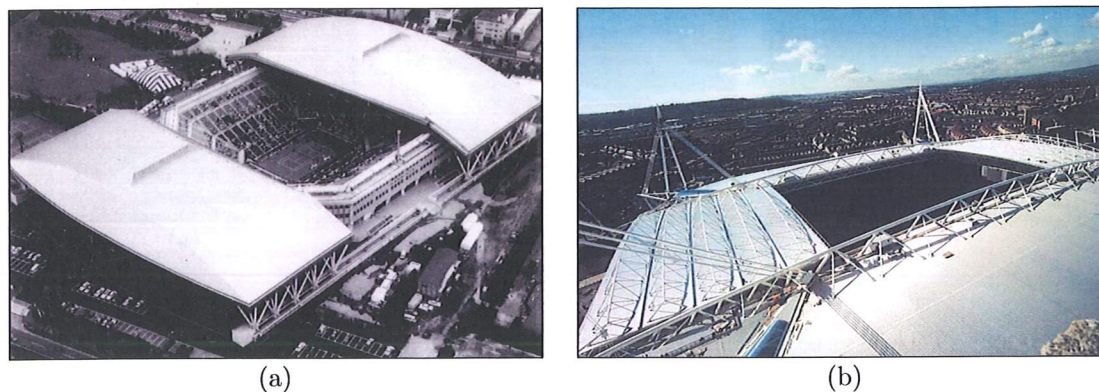


Figure 2.6: Parallel retracting systems at (a) Ariake Colosseum (Ishii, 2000), and (b) Millennium Stadium (Courtesy of Atkins)

Other interesting examples of this system and stadia design in general are the 2001 Oita Stadium, Japan, the 1996 Amsterdam Arena and the 1998 Gelredome, The Netherlands, all shown in Figure 2.7. The last two are interesting as they have retractable roof panels which span the longest direction of the opening, making them unusual. This solution has been found economical in both cases as it reduces the number of structural members. The Gelredome has two other interesting features: many retractable roofs are designed such that they cannot be moved when wind and/or snow loading surpasses a pre-determined level. This is not the case for the Gelredome as the designers found that the internal fire load imposed greater requirements on the roof structure than the ultimate wind and snow loads. Thus the roof can be opened under all load conditions as in case of fire this permits the ventilation of the enclosed space and prevents the heat from building up (Nijssse & van Vliet, 2003). It is also noteworthy that it was found economically viable to build a multi-purpose venue featuring both a retractable roof and a movable pitch. For the Amsterdam Arena it is interesting that the venue, as one of the few in Europe with a retractable roof, has decided to install an artificial playing surface, as mentioned in Section 2.2. The Oita Stadium is interesting as it uses a spherical cap, which provides a circular plan for a football stadium. The two roof panels are not supported on two rails running along the central opening, instead they are supported on seven arches of which five span across the oval opening in the roof. The movement of the panels is not purely horizontal, instead it follows the curved profile of the fixed roof and hence requires additional energy to overcome gravitational forces during closing. This is also the case for the roof of the Amsterdam Arena.

2.2.3 Recent Proposals for Retractable Roofs

The British Football Association (FA) has commissioned a new stadium to replace the old Wembley Stadium, in London. This new venue, currently under construction, will, when completed in 2006, have a retractable roof unlike any other in the world. Engineered for letting sunlight onto the famous grass turf the retractable roof will allow the entire pitch to be bathed in sunlight during the full length of the FA Cup final in

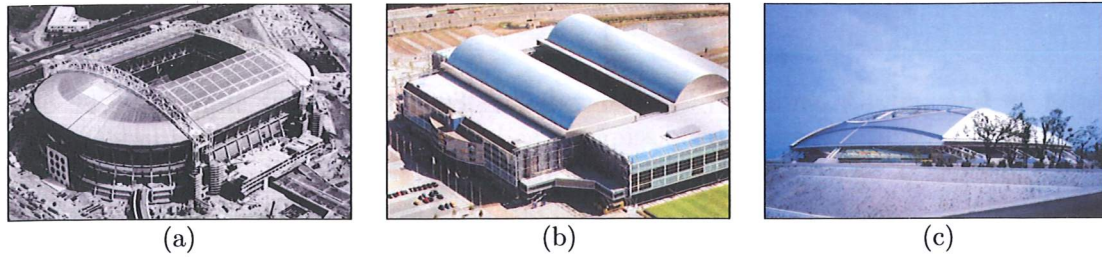


Figure 2.7: (a) Amsterdam Arena (Ishii, 2000), (b) Gelredome (Courtesy of ABT), and (c) Oita Stadium (Courtesy of Kisho Kurokawa Architects)

May. This was required by the FA as it avoids the presence of annoying contrasts between sunlit and shadow areas in TV pictures. Allowing the sunlight to reach all areas of the pitch could only be achieved by not covering the spectators on the South stand and hence a retractable roof system will be fitted over this. The retractable roof allows the stand to be covered when needed though it does not enclose the venue completely unlike other retractable roof systems (Barker, 2000; Manica, 2003).

In the USA an American football team, the Arizona Cardinals, is also building a new multi-purpose venue. The Arizona Cardinals Stadium will feature both a movable pitch and a bi-parting retractable roof, originally planned as a telescopic system (Gee, 2002). This is part of the trend in America where synthetic playing surfaces are being replaced with natural ones again, and combining a retractable roof with a movable pitch is found by some designers as the best way of providing full multi-use and achieving the best economic performance despite the additional construction and running costs (Riberich, 2003).

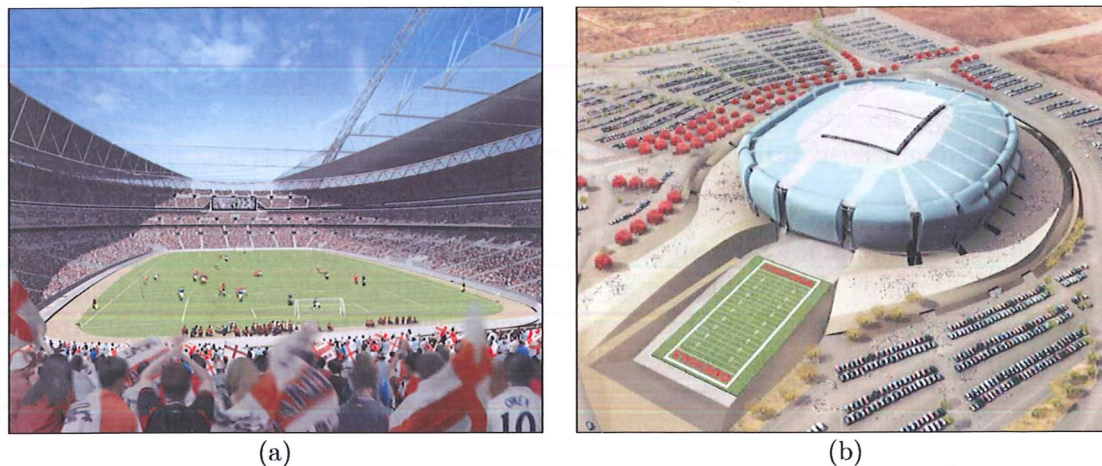


Figure 2.8: (a) Wembley Stadium (2004), and (b) Arizona Cardinals Stadium (Riberich, 2003)

2008 Beijing Olympic Stadium

The 29th Olympic Games, in 2008, will be hosted by Beijing, China, and as most other Olympic cities before it Beijing has commissioned a new stadium. The modern tradition for Olympic stadia is more than a hundred years old and nearly all stadia built for hosting the Games have been the pride and show piece of the host nation and thus often a state-of-the-art venue. It is therefore of particular interest to review the proposals for the architectural competition held for the 2008 Beijing Olympic Stadium by the Beijing Municipal Commission of Urban Planning (2003). Of the thirteen entries in the final round, all except one proposed a stadium with a retractable roof. Four schemes are presented below and shown in Figure 2.9: B02, B07, B11 and B12.

Scheme B02 was proposed by a team led by Gerkan, Marg and Partners, Germany. The engineers were Schlaich Bergermann and Partners of Germany. The scheme proposed a fixed tensegrity roof, see Section 2.3.2, covered with ETFE foil cushions. The retractable roof for the central circular opening was to consist of 16 cantilevering elements pivoting at the base about the edge of the fixed roof. Each element was to be fabricated as a single 63 meter long piece using Carbon Fibre reinforced Carbon (CFC). For opening and closing the roof, a system consisting of three synchronised, structural cable systems was to be used (Balz, 2003).

Scheme B07 by Hiroshi Hara + Atelier, Japan proposed to use an American patented retractable roof system, called the *Two Panel Spiral Rotating Shell Retractable Roof Geometry* (Allen & Robbie, 1994). This system uses two large curved shells, which run at ground level on two curved rails that form two overlapping circles. By running the two shells along the curved rails and thus rotating them, the roof is opened or closed as shown in Figure 2.9(b).

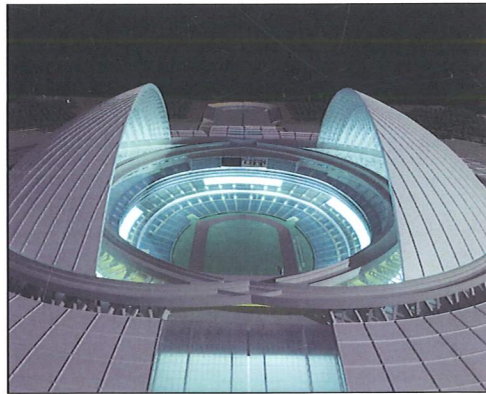
Led by the Swiss architects Herzog & de Meuron Architekten, scheme B11 won the competition and this design is currently being taken forward. This structure will be 67 meters high and made from steel box sections more than 10 meters deep, forming a structure that resembles the interwoven twigs of a birds' nest. On top of this birds' nest, a conventional bi-parting retractable roof, engineered by British engineers Arup, was proposed (Parrish, 2003). The retractable roof has later been removed from the project due to cost constraints.

Scheme B12 by Tianjin Architects & Consulting Engineers, China, put forward an often proposed concept — that of using a balloon as the retractable roof. Under normal conditions the roof would be hovering gently above the venue, ready to be hoisted down and fastened to the fixed roof should the weather change. This proposal came joint-second in the competition.

As can be seen from the examples above, there are many and varied design proposals for retractable stadium roofs. Current research within the field of deployable structures promises to deliver more structural concepts and solutions that in the future can be applied to large scale retractable roofs.



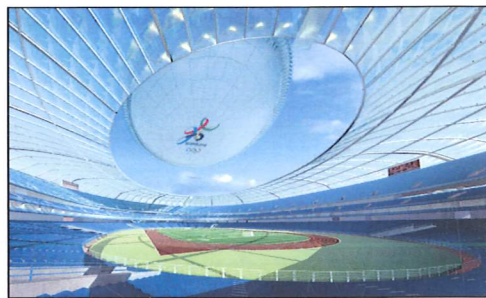
(a)



(b)



(c)



(d)

Figure 2.9: Four proposals for 2008 Beijing Olympic Stadium (a) B02; (b) B07; (c) B11; (d) B12 (Beijing Municipal Commission of Urban Planning, 2003)

2.3 Deployable Structures

Currently deployable structures have two very different main applications, space exploration and temporary, quick-to-erect earth-bound structures, each with its own particular requirements. Hence solutions developed and found applicable for one application are rarely directly transferrable to the other.

2.3.1 Space Applications

The development of deployable structures for space applications has been governed by the tight space and weight requirements for structures that are to be launched into space and the extreme, zero-gravity environment of space. Therefore these structures have been developed to minimise their weight and volume in the stowed configuration.

For space applications there are three main uses of deployable structures, according to Tibert (2002):

- Masts,
- Antennas, and
- Solar panels

Methods used for deploying these structures can be classified as

- Coiled rods,
- Flexible shells,
- Inflatable/folded membranes, and
- Structural mechanisms in the form of hinged, pinned, telescopic and sliding elements.

It is beyond the scope of this dissertation to go into details regarding the specific applications and deployment methods for the above mentioned applications. For further information refer to the latest reviews by Jensen & Pellegrino (2001), Tibert (2002) and Pellegrino (1995) for masts, antennas and solar panels respectively. Figures 2.10 and 2.11 show a few examples of deployable space structures.

2.3.2 Architectural and Civil Engineering Applications

The use of deployable structures for architectural applications has its roots in the ancient building types of tents, teepees and yurts. The architectural dream of temporary, adaptable and transportable structures has led to the development of this family of deployable structures though they have been found suitable for a number of other applications too. Hernandez *et al.* (1991) outlined, among other uses, seven suitable applications for deployable structures in architecture and civil engineering:

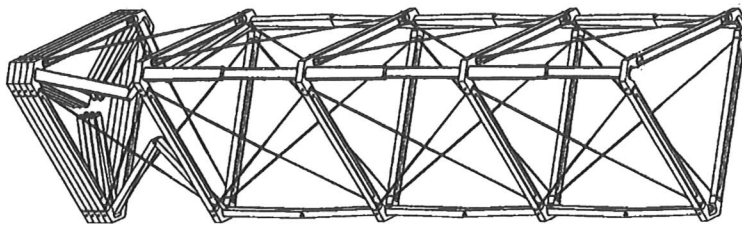


Figure 2.10: 'HIMAT' retractable mast for space applications (Kitamura *et al.*, 1990)

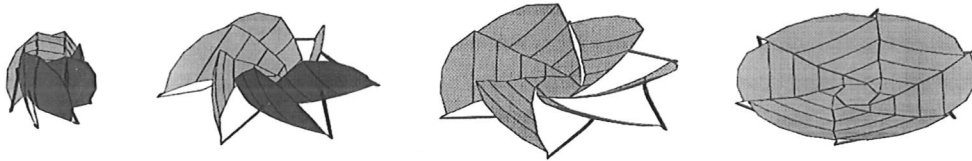


Figure 2.11: Solid Surface Deployable Antenna (Guest & Pellegrino, 1996b)

- Temporary shelters and enclosures suitable for storage,
- All types of structures for inaccessible regions,
- Large portable and rapidly erectable structures,
- Retractable roofs,
- Areas where there are high risks and labour costs involved with erection,
- Construction aids for traditional construction, and
- As a fundamentally new way to think about erection of permanent structures

A more exhaustive list is presented in Gantes (2001). Bulson (1991b), Hernandez *et al.* (1991), and more recently Miura & Pellegrino (2002) have proposed classification methodologies for deployable structures in general, which also include civil engineering applications. Escrig (1996) and Gantes (2001) have both proposed classification methods for deployable structures in architecture and civil engineering.

Retractable roofs are often classified as a separate group of structures as they can be constructed using any of the following systems:

- Tensegrity structures,
- Membrane structures without an underlying bar or panel structure,
- Plate structures consisting of hinged plates, and
- Bar structures consisting of hinged bars

Tensegrity Structures

This type of structure was invented by Fuller (1962). They consist solely of members either in tension or in compression, though many other interpretations of the phrase *tensegrity* have been put forward over the years (Motro, 1992). Despite the efficiency using members in pure tension or compression this system is not widely used. It has found a niche as a structural system for circular domes where a series of spoke and wheel rings are interconnected to form a stable and efficient fixed roof.

Membrane Structures

Unlike tensegrity structures, membrane, or tensile structures, have been widely adopted in both permanent and temporary architecture. The ability of the membrane to fold has made it the most widely used system for providing a deployable cover, either as an independent structure or as a cladding material for another deployable structural system. The best known deployable membrane structure is the umbrella. Frei Otto further developed the idea of the umbrella and created several retractable roofs based on this concept (Otto *et al.*, 1995), see Figure 2.12. Many other types of deployable membrane structures have been built, see Section 2.2.2. The use of inflatable membrane structures has also been researched and several small scale projects have been realised (Kronenburg, 2000).

Plate Structures

Larger deployable structures, consisting of hinged rigid plates are not common in architecture as these systems are not as light and compact as other systems. Also a limited number of folding methods are available for irregular structural shapes. The best known examples of this type of deployable structure are the pivoting plates and beams used by the Spanish architect and engineer Calatrava in his transformable architecture, see Figure 2.12 for an example.

Bar Structures

Bar structures are the most used and researched type of deployable structure in civil engineering. The first to research and build deployable structures for architectural use was the Spanish architect Piñero, during the 1960's. He proposed during his short life a number of novel structural systems for temporary enclosures, including retractable domes and travelling theatres and pavilions (Belda, 1996). One of his movable theatres is shown in Figure 2.13. Piñero's structures were based on bars hinged together at their midpoints as well as at their ends. Other designers, such as Calatrava, have used other methods of interconnecting the bars. However, the system used by Piñero, generally referred to as a *pantographic* element, has remained the most commonly used bar system.

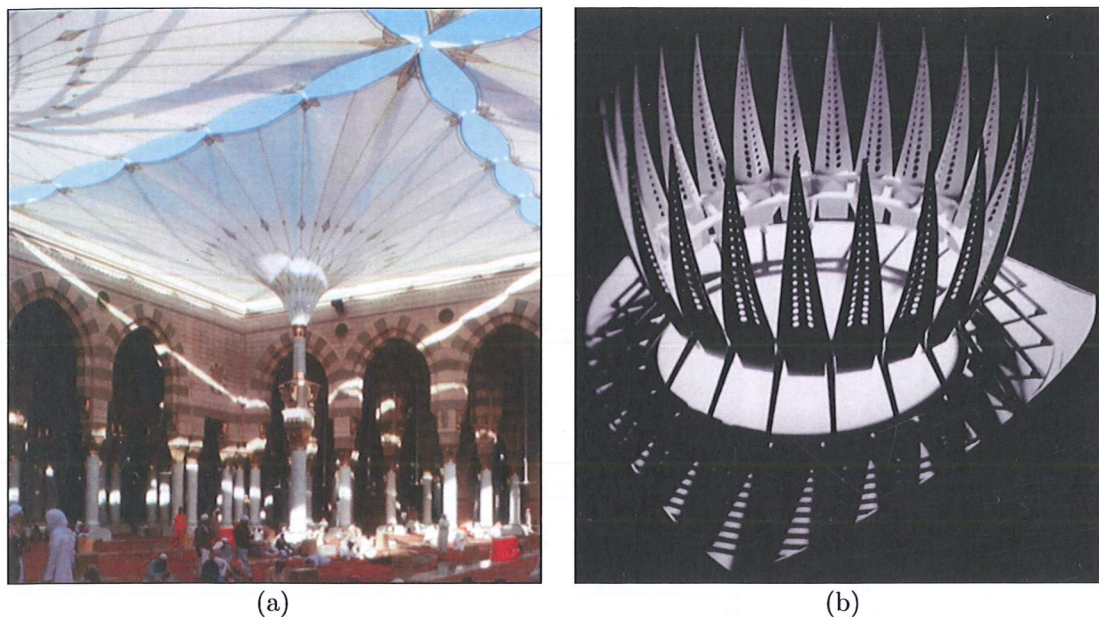


Figure 2.12: (a) Umbrellas Medinah by Otto *et al.* (1995), and (b) Floating Concrete Pavilion by Calatrava (Tzonis, 1999)

2.4 Retractable Pantographic Structures

A pantograph element consists of two identical straight bars in two separate *layers*, shown as red and blue in this dissertation, connected through a revolute joint, also called a *scissor hinge*, allowing the two bars to pivot about an axis perpendicular to the element itself. When a series of such pantographic elements are interconnected at the ends using revolute joints, a *two-dimensional transformable structure* is formed. This is often referred to as a *lazy-tong*, the principle of which has been known for millennia.

By arranging a series of such individually transformable structures in a grid, it was possible for Piñero to form structures that could be expanded and retracted again. These structures originally expanded only in the plane, but by varying the lengths the bars in the individual pantographic elements and adjusting the overall arrangement accordingly it became possible to create structures that could expand into cylindrical or spherical shapes from their original bundled configuration (Belda, 1996; Escrig, 1993; Gantes, 2001; Miura & Pellegrino, 2002).

As Piñero's systems of pantographic elements were unstressed throughout their transformation they had no stiffness in the directions of motion. Therefore, they formed unconstrained mechanisms and their hinges had to be locked, or the structure in some other way rigidified, once they had reached a configuration in which they were required to carry loads. During the transformation of the structure from one configuration to another, only a single point on the structure can remain in its original position. This prevents simple support conditions during the transformation, as is clearly visible in

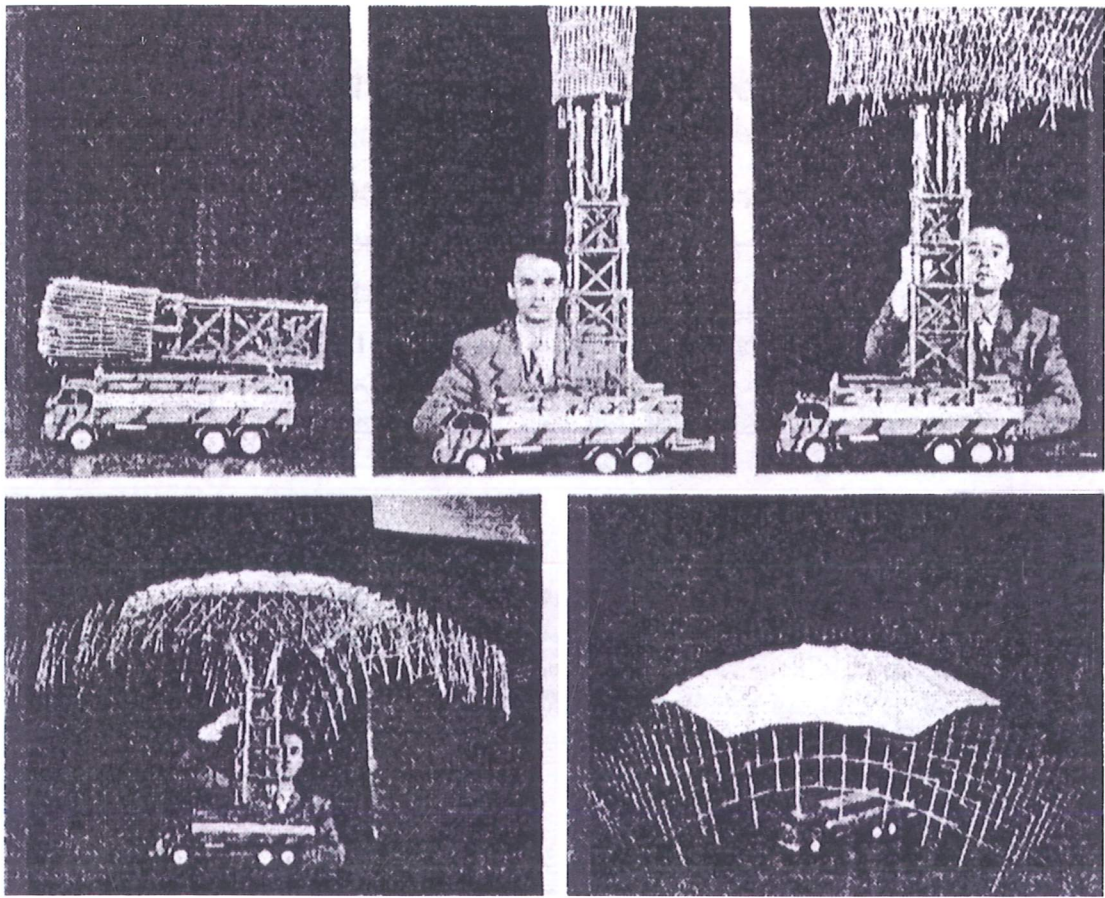


Figure 2.13: Piñero with his movable theater (Gantes, 2001)

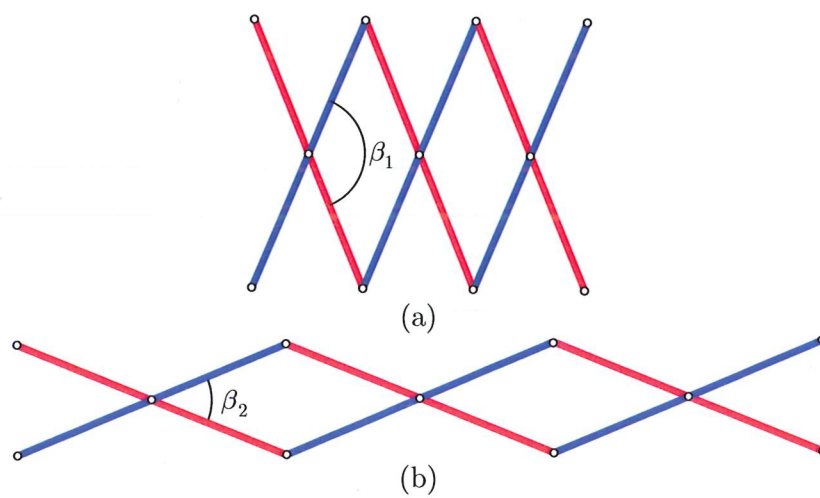
Figure 2.14: *Lazy-tong* formed by three pantograph elements

Figure 2.13. A distinct advantage for this system over others, however, is the simplicity of its joints.

After Piñero's early death in 1972 his work was carried forward by others and they have improved his original design. Zeigler (1981, 1984, 1987, 1993) patented a system in which some of the bars must deform during the transformation to provide a locking effect in the extreme configurations eliminating the need for additional locks to be added to the structure. Escrig from the School of Architecture in Seville, Spain, and his collaborators have also further developed systems formed by pantographic elements. Over the last two decades they have greatly advanced the understanding of these structures as well as promoting their use. Many new shapes have been identified and several larger structures have been realised (Escrig & Valcarcel, 1993; Gantes, 2001; Sanchez *et al.*, 1996; Valcárcel & Escrig, 1996). Others have also used pantographic elements.

2.4.1 Closed Loop Structures

It is possible to form a closed loop ring structure from n pantographic elements, each subtending an angle α ; the centre hinge has to be moved away from the mid-point of the bars, see Figure 2.15. Zanardo (1986) showed that such a pantographic ring is rigid and hence does not form a mechanism. You & Pellegrino (1997) illustrated this by deriving the relationship between the subtended angle α and the rotation angle β , see also Pellegrino & You (1993)

$$\tan \alpha/2 = \frac{\overline{CE} - \overline{AE}}{\overline{AC}} \tan \beta/2 \quad (2.1)$$

This relationship shows that any variation in the rotation angle β will result in change in the subtended angle α which is prohibited in a closed loop structure. Strictly, if $\overline{CE} = \overline{AE}$ then $\alpha = 0$ and independent of β .

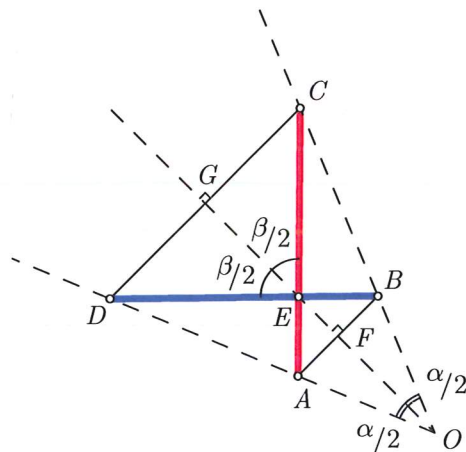


Figure 2.15: Pantographic element consisting of two straight bars

2.4.2 Structures formed by Angulated Elements

A considerable advance was made by Hoberman (1990), with his invention of the simple *angulated element*. Unlike the original pantograph element with its *straight* bars, this pantographic element consists of two identical *angulated* elements arranged in two separate layers as above. Each angulated element consists of two rigidly connected identical bars, each with the length l , that form a central kink of amplitude α . Connecting two such angulated elements through a scissor hinge at the centre, i.e. at node E in Figure 2.16(a), a pantographic element is formed that can be used for closed loop retractable structures. Writing the relationship between the subtended angle and the rotation angle (You & Pellegrino, 1997):

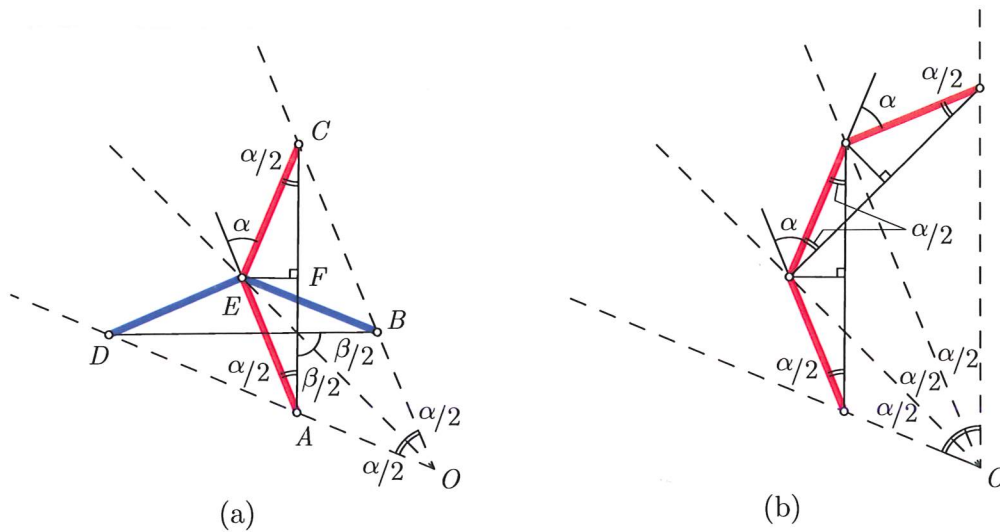


Figure 2.16: (a) Pantographic element consisting of two angulated elements, each formed by two bars, and (b) Multi-angulated element with three bars

$$\tan(\alpha/2) = \frac{\overline{CE} - \overline{AE}}{\overline{AC}} \tan(\beta/2) + 2\frac{\overline{EF}}{\overline{AC}} \tag{2.2}$$

If the conditions $\overline{AE} = \overline{CE}$ and $\alpha = 2 \arctan(\overline{EF}/\overline{AF})$ are met then α becomes (i) constant for all values of β , and so the pantographic element moves along fixed radial lines, and (ii) the angle between the radial lines has the required magnitude.

A simple flat circular pantographic structure can therefore be formed and it will be capable of retracting towards its own perimeter. Such a structure is formed by two identical layers of identical angulated elements, one layer formed by elements arranged in a clockwise sense, when the elements are traced from the innermost to the outermost end, shown in red in Figure 2.17 and the other formed by elements arranged in a counter-clockwise sense shown in blue.

As the structure expands along fixed radial lines each angulated element in the red layer also rotates *clockwise* as can be seen in Figure 2.17. The blue layer on the other hand rotates *counter-clockwise*. The rotations of the elements in the two layers are thus equal but opposite.

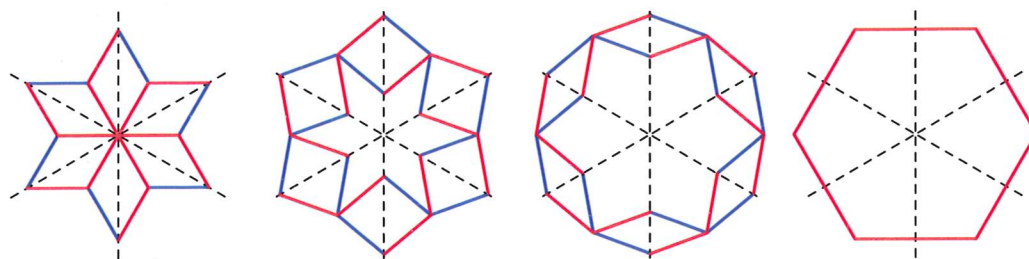


Figure 2.17: Radial movement of structure

You & Pellegrino (1996, 1997) found that two or more such retractable structures can be joined through the scissor hinges at the element ends. Two angulated elements from layers that turn in the same sense of two such interconnected structures, with a scissor hinge in common were found to maintain a constant angle during the transformation of the structure and hence could be *rigidly connected* to each other, thus forming a single *multi-angulated* elements with more than one kink as shown in Figure 2.16(b).

The retractable structure shown in Figure 2.18 consists of two layers each formed by 12 identical multi-angulated elements made from 4 rigidly connected bars. At each cross-over point, there is a scissor hinge. Note that the structure also forms a pattern of identical *rhombuses* or *four-bar linkages* which are “sheared” when the structure transforms.

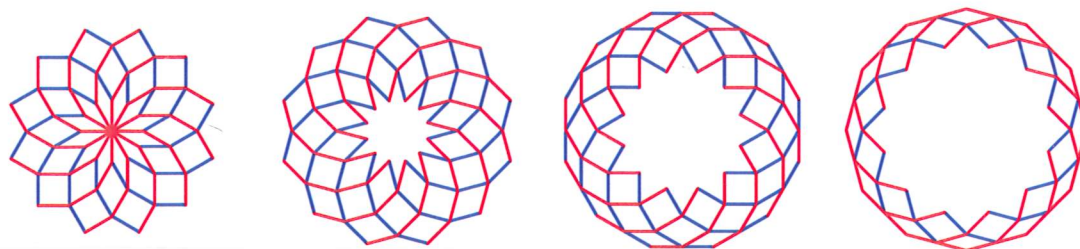


Figure 2.18: Retractable structure formed by multi-angulated elements

The same authors extended the proof based on in Equation 2.2 to include *generalised angulated elements* which allow for non-circular structures to be generated. Such structures form patterns of either rhombuses or parallelograms, as shown in Figure 3.8, depending on which type of generalised angulated elements was used for the structure (You & Pellegrino, 1996, 1997).

Teall (1996) explored the structural behaviour of two circular retractable structures. The structures had a dome like shape, following Hoberman (1991), see Section 2.4.4. As the perimeter of this type of structure varies during the transformation, the support conditions must be designed to allow for this. Teall proposed to overcome this problem by mounting the structure on pairs of hinged columns, each creating a four-bar linkage, such that the support points would be able to move radially with the structure.

A further investigations into the support conditions was carried out by Kassabian *et al.*

(1997). By studying the instantaneous centres of rotation for the elements, Kassabian found it was possible to find fixed points about which the elements rotate during their motion and thus can be fixed to. Such points, however, only exist for one layer of the structure. The solution requires a rigid body rotation to be imposed on the whole structure equal in magnitude to the original rotation of the elements which are to be fixed at a point. As the two layers rotate by equal but opposite amounts, imposing this rigid body rotation results in one layer of elements undergoing pure translations while the elements in the other layer undergo pure rotations about their own fixed point as shown in Figure 2.19 (Kassabian, 1997; Kassabian *et al.*, 1997). See also Sections 3.2.2 and 3.2.3.

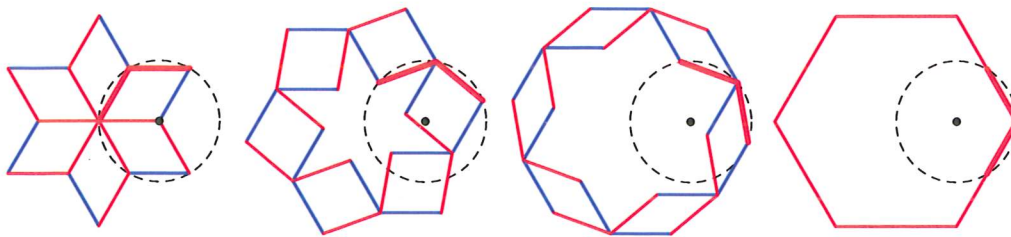


Figure 2.19: Rotating movement of structure

Kassabian *et al.* (1997) showed it to be possible to cover this type of structure using rigid cover elements. This allows the structure to perform as a retractable roof. To provide weatherproofing the cover elements creates a continuous, i.e. gap free, surface in both the open and closed configurations of the structure. Using a kinematic approach, two possible designs, shown in Figure 2.20, were developed.

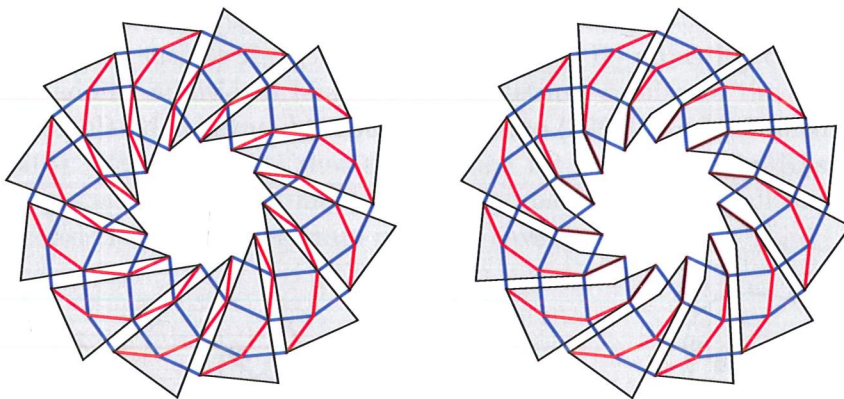


Figure 2.20: Cover elements by Kassabian *et al.* (1997)

Kassabian *et al.* (1999) presented an extensive review of retractable roof structures based on angulated, multi-angulated or cover elements and their possible uses.

2.4.3 Other Closed Loop Structures

Several authors (Chilton *et al.*, 1998; Escrig *et al.*, 1996; Rodriguez & Chilton, 2003; Wohlhart, 2000; You, 2000), have presented work on closed loop retractable structures. Chilton *et al.* (1998) have developed the *Retractable Reciprocal Plate Structure* shown in Figure 2.21. The structure shown consists of 6 triangular rigid plate elements that each slide against each other as the structure is opened hence providing a continuous surface throughout the opening. There are no fixed points for the particular structure shown though the authors have proposed several other variations of this system that have fixed points which can be supported, see Section 6.5.

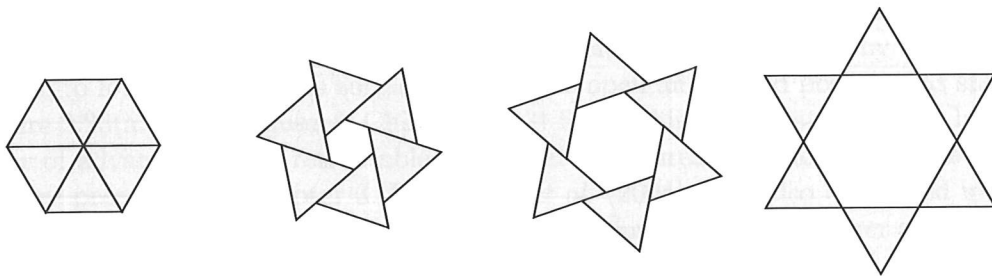


Figure 2.21: Reciprocal Plate Structure proposed by Chilton *et al.*

You (2000) expanded and simplified the method for generating pantographic retractable structures with fixed support points. Instead of starting with a fixed geometry for the angulated elements and then finding the fixed points as done by Kassabian *et al.* (1997), he prescribes the fixed points A_1 , B_1 and C_1 and connect these using three bars interconnected by scissor hinges, thereby creating a series of four linkages as shown in Figure 2.22(a). Rigidly connecting the bar pairs that share fix point creates angulated elements such as $A_0A_1A_2$ in Figure 2.22(b). By adjusting the lengths of the bars and by adding additional hinged bars, structures similar to the earlier work on generalised angulated elements by You & Pellegrino (1997) can be formed as shown in Figure 2.22(d). You concluded that the solution for fixed points by Kassabian *et al.* (1997) is a special case of this more general approach and that “all multi-angulated structures consisting of parallelogram modules have fixed points.”

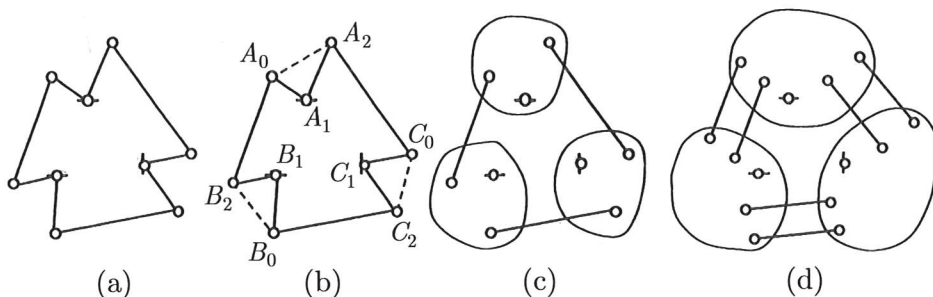


Figure 2.22: Retractable systems formed by four-bar linkages (You, 2000)

Extending this work, Rodriguez & Chilton (2003) proposed a novel retractable struc-

ture shown in Figure 2.23(a-d) called the *Swivel Diaphragm*. As proposed by You (2000) it uses the fixed points of the structure, together with straight bars, to form a concentric series of parallelograms between angulated elements. This can be clearly seen in Figure 2.23(e) where the structure has been opened beyond its normal extreme configuration shown in Figure 2.23(d).

By having the fixed points coincide with the scissor hinges it is guaranteed that the support points for the Swivel Diaphragm can be directly connected to its angulated elements. This is unlike the fixed points for the multi-angulated structures found by Kassabian *et al.*, which are always located away from to the angulated elements. Furthermore the authors have shown that any one of the three scissor hinges on an angulated element can be fixed if the remaining two points are connected to the neighbouring elements using bars. The angulated elements can be replaced by rigid plate elements, to form a continuous surface in both the open and closed positions as shown in Figure 2.23(a,d). Rodriguez & Chilton (2003) found this type of structure to have a number of advantages over retractable reciprocal structures and the retractable plate structures presented in Chapter 3. Rodriguez *et al.* (2004) have also developed methods for interconnecting several individual Swivel Diaphragms to form larger assemblies. Work on assemblies formed by retractable plate structures is presented in Section 3.5.

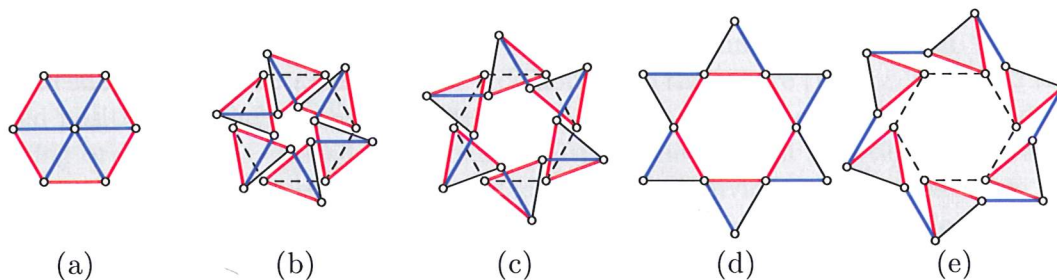


Figure 2.23: Swivel Diaphragm by Rodrigues & Chilton

Wohlhart (2000) presents another type of plane retractable structure, also based on the motion of parallel four-bar linkages. By connecting two concentric rings of triangular plate elements, each connected to its three neighbouring triangles through scissor hinges at their apexes, he achieves a structure with a single internal degree of freedom, a so-called *double-chain mechanism*. The structure is moved by rotating adjacent elements in opposite directions to one another. Interestingly, if the two rings are congruent the solutions found are those of Hoberman (1991) and You & Pellegrino (1997).

2.4.4 Retractable Dome Structures

Wohlhart (2000) expanded the solution of concentric rings to spherical structures that can expand along normals to the sphere. He also proposes spherical and conical chains but these are beyond the scope of this dissertation. Similar structures have been proposed by Kovács & Tarnai (2000) and Verheyen (1993). Several authors have proposed dome shaped structures that can retract towards their perimeter.

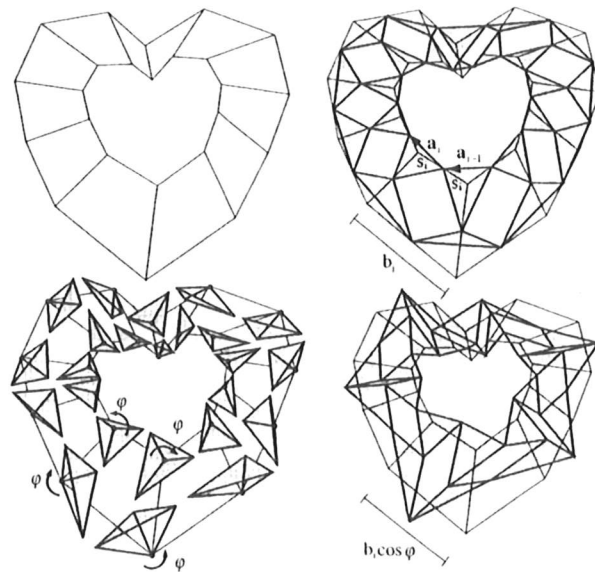


Figure 2.24: Double-Chain mechanism by Wohlhart (2000)

Piñero proposed a diaphragm retractable dome where a number of spherical “wedge” shaped shells are each rotated about an axis normal to the sphere (Escrig, 1993). In the closed position the shells form a gap free spherical cap. When the shells are rotated an opening or aperture is created at the centre of the dome through a motion comparable to that of the shutter mechanism in a camera. The individual shells overlap in all positions other than the closed position. To create a mechanism with a single degree of freedom, pairs of adjacent shells are connected to each other through a revolute joint at the apex of one shell. This joint is then run along a path on the other shell as illustrated in Figure 2.25.

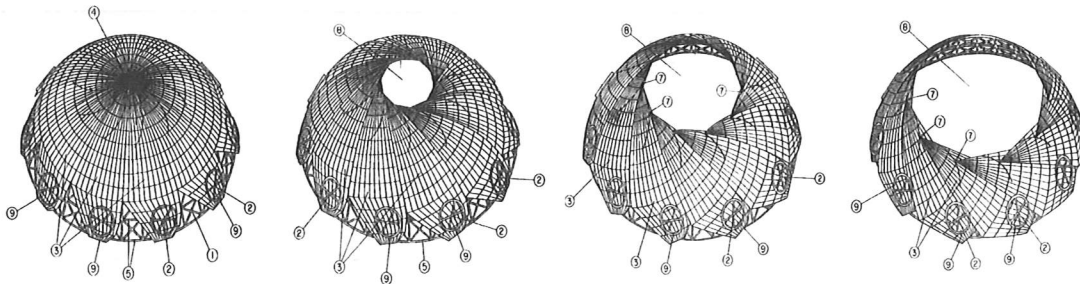


Figure 2.25: Reciprocal dome proposed by Piñero (Escrig, 1993)

Hoberman (1991) found that angulated elements connected using scissor hinges will not only subtend a constant angle on a plan surface, but also on a conical surface. Hoberman proposed to use five concentric rings of angulated elements, each on a different conical surface. By connecting these rings to each other through scissor hinges with axes of rotation tangential to the circular plan of the rings, a retractable dome is formed. The resulting *Iris Dome* is shown in Figure 2.26. As seen from the figure the

dome can be clad by rigid plates attached to the individual angulated elements. When the dome is closed, a continuous surface is formed while in the open configuration the plates are stacked on top of each other. The Iris Dome uses considerably more elements and hinges than that proposed by Piñero but as there are no sliding mechanisms the connections are simpler.

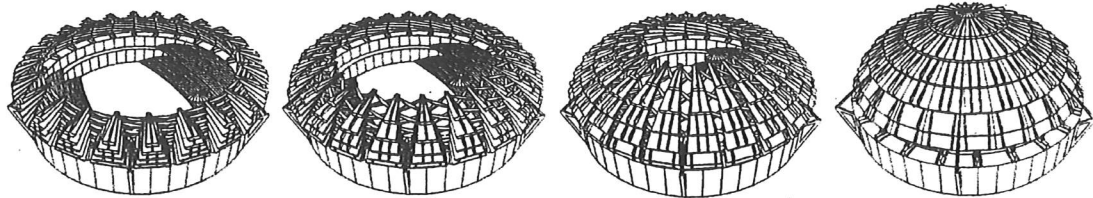


Figure 2.26: Iris Dome by Hoberman (Kassabian *et al.*, 1999)

A dome structure constructed from pantograph elements which retracts towards its perimeter was presented by Escrig *et al.* (1996). This structure is different from that proposed by Hoberman, as the pantographic elements are normal to the surface of the dome rather than parallel to the surface, as in the Iris Dome.

You & Pellegrino (1997) found that the two-dimensional solution for the multi-angulated elements could be projected onto any three-dimensional surface if the axes of rotation for the scissor hinges remains perpendicular to the plane of the original two-dimensional solution. This significantly decreased the number of elements required, compared to the Iris Dome. The work of Teall (1996) was based on this finding. Rigid cover elements for such a projected structure will be presented in Section 3.3.2.

The motion of the projected structure is purely horizontal, as all axes of rotation are vertical. The structure, therefore does not move on the surface of a sphere or dome; this is not because of the type of joints but because of the angular defect as will be shown in Section 5.3. Kokawa (2000, 2001) and Farrugia (2002) have proposed to overcome this problem by building additional freedoms into the joints. Figure 5.6 shows a spherical retractable dome proposed by Kokawa (2000). Kovács (2000) has been successful in creating a bar structure that moves on the sphere using simple revolute joints with their axes normal to the sphere. However, this solution only covers part of the sphere and to form a retractable dome structure additional bars have been introduced — all connected through revolute joints to allow the angles between adjacent bars to change effectively creating a series of spherical four-bar linkages. This creates a large number of bars that must be connected through their joints, making this structure as complicated as that proposed by Hoberman (1991).

Chapter 3

Retractable Bar and Plate Structures

3.1 Introduction

This chapter extends the work of Kassabian *et al.* (1999) on covering bar structures with rigid cover elements. The first part is concerned with circular structures with n -fold symmetry. Expressions are obtained for the inner and outer radii for such retractable structures, in the open and closed configurations. Using these expressions, design charts are determined, for which general conclusions are drawn regarding the radial displacements.

The rotation undergone by the individual elements of these structures is then used to provide a simpler approach for describing their motion. This method provides a uniform approach, suitable for both circular and non-circular structures, which is easily adapted to take into account the limits associated with models with finite sized members and hinges.

Using this new approach, the shape and properties of cover elements that do not affect the range of motion of the structure are determined. With this it becomes possible to cover the basic bar structure such that a continuous, gap free surface is generated in both the open and closed configurations of the structure. Furthermore, it is shown to be possible to construct structures comprised of two layer of plates, both of which form continuous surfaces in the extreme configurations of the structure. The positions of the scissor hinges are identical to those of an equivalent bar structure and their kinematical behaviour is therefore also identical.

It is shown that it is possible to vary the shape of the individual plates, within certain constraints, without affecting the movement of the structure. This approach can be used to optimise, for example, the range of motion which such plate structures can undergo. The chapter concludes by showing methods for rigidly interconnecting such plate structures so they can form stacked or planar arrays.

3.2 Retractable Bar Structures

In the following geometric studies the bars are considered to be lines of zero thickness and similarly the hinges are considered as having no finite size.

A general retractable circular bar structure, such as that shown in Figure 3.1, consists of $2 \times n$ identical angular or multi-angulated elements. Each layer, shown as red and blue, consists of n elements. The individual multi-angulated elements are comprised of k rigidly connected bars, hence the simple angular element, shown in Figure 2.16, can be seen as a special multi-angulated element with $k = 2$. Such a structure is therefore fully defined by the parameters $n;k$ plus the length l of all the bars, which defines the overall size of the structure.

The *kink angle* α between two consecutive bars in a simple angulated element is identical to the angle subtended by the element as shown in Figure 2.16(a). The kink angle can hence be found for circular structures using the n -fold symmetry of the structure (Hoberman, 1990) and You & Pellegrino (1997):

$$\alpha = \frac{2\pi}{n} \quad (3.1)$$

3.2.1 Radial Motion

Consider a general configuration of the bar structure. We denote by r and R its inner and outer radii, respectively. We use the subscripts *open* and *closed* for the two extreme configurations of the structure. The extreme closed configuration is reached when all the innermost hinges coincide at the centre of the structure, hence $r_{\text{closed}} = 0$. The extreme open configuration is reached when the outermost rhombuses formed by the angulated elements have been sheared so two diagonally opposite scissor hinges coincide and further motion is inhibited. The two extreme configurations are shown in Figure 3.1.

Using the maximum outer radius R_{open} to define the size of the structure

$$l = R_{\text{open}} \sin \frac{\alpha}{2} \quad (3.2)$$

The following expressions for the radial positions can be derived using simple trigonometry (Jensen, 2001)

$$R_{\text{closed}} = R_{\text{open}} \sin \left(k \frac{\alpha}{2} \right) \quad (3.3)$$

$$r_{\text{open}} = R_{\text{open}} \cos \left((k-1) \frac{\alpha}{2} \right) \quad (3.4)$$

To compare the effects of varying the parameters $n;k$ two ratios are introduced. The *opening ratio*, OR , is defined as the radius of the central opening in the open position,

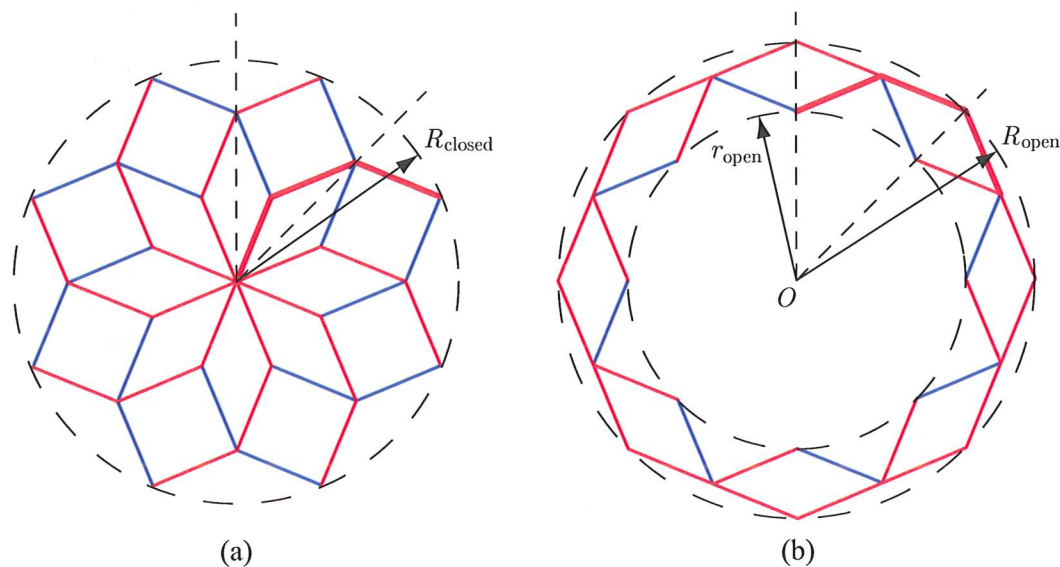


Figure 3.1: Circular structure with $n;k = 8;3$ (a) Closed Configuration, and (b) Open configuration

r_{open} , divided by the outer radius of the structure in the closed position, R_{closed} .

$$OR = \frac{r_{\text{open}}}{R_{\text{closed}}} = \frac{\cos\left((k-1)\frac{\alpha}{2}\right)}{\sin\left(k\frac{\alpha}{2}\right)} \quad (3.5)$$

Equation 3.5 is plotted as a function of $n;k$ in Figure 3.2. $OR < 1$ indicates that there is an overlap between the two positions, which can be used when considering different methods for supporting the structure. Note that continuous lines have been plotted in Figures 3.2, 3.3, 3.6, and 3.12 though only whole numbers of n creates closed loop structures.

The second ratio is the *stowage ratio*, SR . This is defined for the open position only and is defined as the radius of the opening, r_{open} , divided by the outer radius in the open position, R_{open} . It indicates the size of the central opening compared with the maximum, outer size of the structure.

The expression of SR is

$$SR = \frac{r_{\text{open}}}{R_{\text{open}}} = \cos\left((k-1)\frac{\alpha}{2}\right) \quad (3.6)$$

and is plotted for $n;k$ in Figure 3.3.

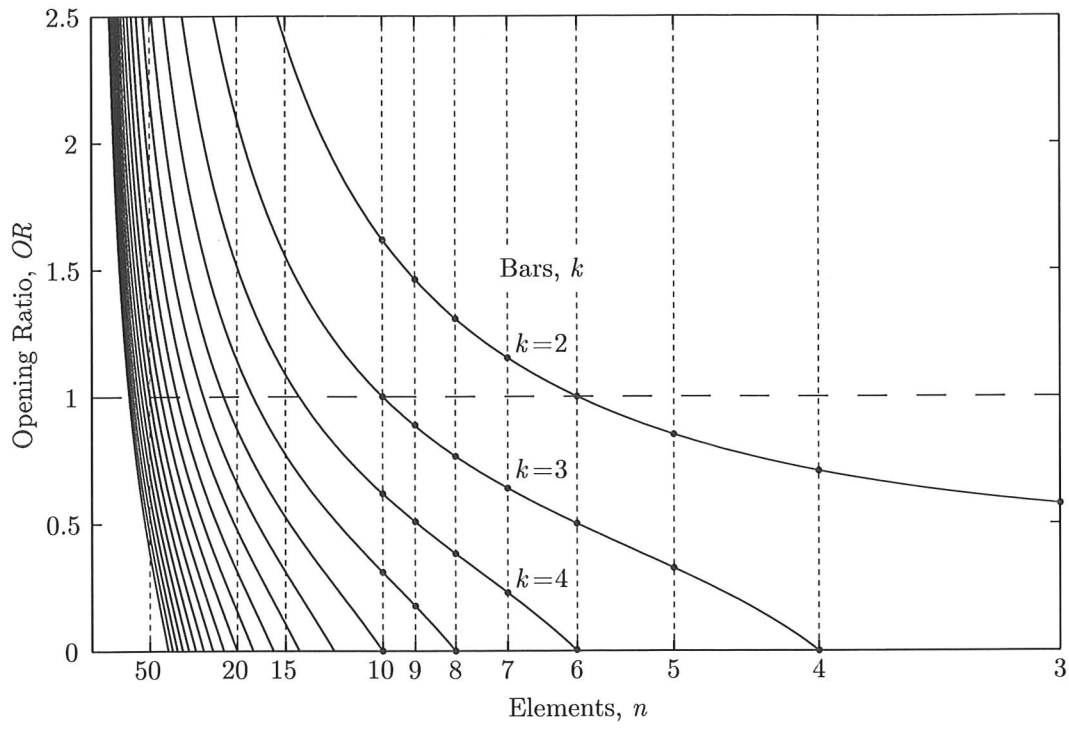


Figure 3.2: The opening ratio OR as a function of $n;k$

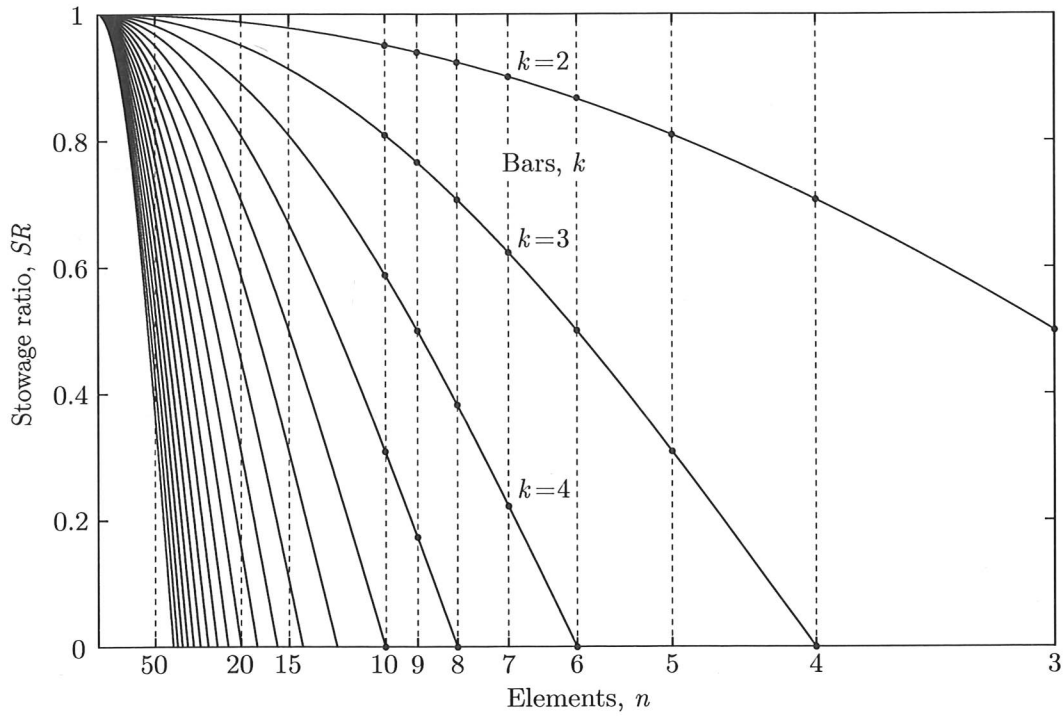


Figure 3.3: The stowage ratio SR as a function of $n;k$

3.2.2 Rotating Motion

As described in Section 2.4.2, Kassabian *et al.* (1999) found that if the structure is allowed to rotate while it opens and closes, i.e. the scissor hinges are not required to move on radial lines, the motion of one layer of elements could be described as a pure rotation and the motion of the other layer as a pure translation. As the positions of the scissor hinges for the two layers coincide, of course, the motion and positions of both layers can be determined by only considering the rotation undergone by the elements of the layer that undergo a pure rotation. Hence, the motion of each element can be described by a circle with its centre at a fixed point, the location of which is described in Section 3.2.3. Note, the *total rotation angle* undergone by all elements in the red layer from the fully-closed to the fully-open configuration is denoted by β^* as shown in Figure 3.4. The radius r^* of the circle describing the motion of the hinges, i.e. the kink points in the angulated elements, is

$$r^* = \frac{R_{\text{open}}}{2} \quad (3.7)$$

Rewriting the bar length l with Equations 3.2 and 3.7

$$l = 2r^* \sin \frac{\alpha}{2} \quad (3.8)$$

Figure 3.4(a) show that the circles of motion for two adjacent angulated elements intersect at the centre of the structure, O , as all the angulated elements have their innermost joint at O . Thus this intersection point represents the *closed limit* for the motion. Similarly the intersection point, P , represents the fully-open configuration, as shown in Figure 3.4(c). Thus P is the *open limit* for the rotation.

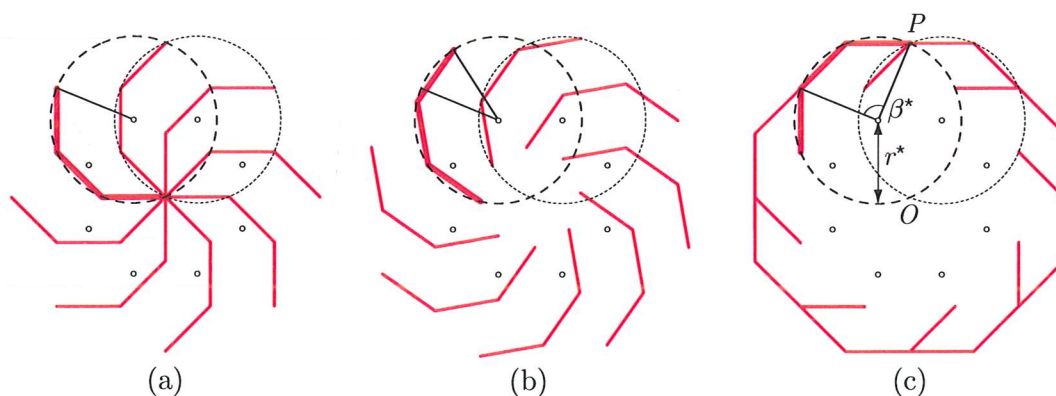


Figure 3.4: The limits of rotation coincide with the intersections of two neighbouring circles of motion

Figure 3.5 shows the same angulated element as that emphasised in Figure 3.4. The angulated element consists of k bars and its hinges, A_i , are numbered such that starting with the innermost hinge they have the numbers $0, 1, 2, \dots, k-1, k$. To describe the

rotation of the angulated element about its fixed point A_{cen} the four angles, β, γ, δ and ϵ are defined in Figure 3.5. Note that $\beta + \gamma + \delta + \epsilon = 2\pi$. The outer angle or *rotation angle*, β , is the angle between the open limit P and the outermost hinge on the element, A_k . Similarly, the inner angle, γ , is defined as the angle between the closed limit, i.e. the origin O and the innermost hinge A_0 . At the extreme configurations, open and closed, we denote the values of β and γ by, β_{open} and γ_{open} , β_{closed} and γ_{closed} respectively.

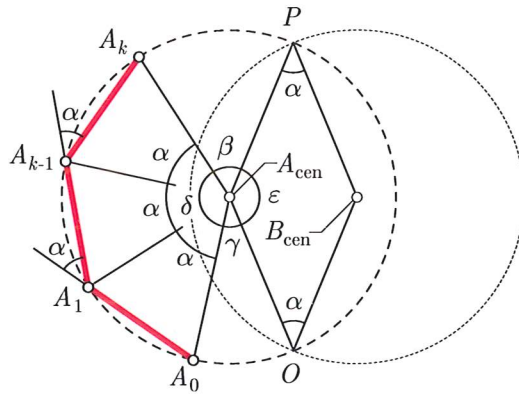


Figure 3.5: Definition of angles β, γ, δ and ϵ

From Equation 3.8 the angle subtended by a single bar on the circle is equal to α , as

$$\sin(\alpha/2) = l/2r^* \quad (3.9)$$

thus the *element angle*, δ , subtended by the multi-angulated element is

$$\delta = k\alpha \quad (3.10)$$

In Section 3.2.3 it will be shown that for non-circular structures the kink angles are not identical for all kinks in the angulated element and it will therefore be useful if all angles are determined using summation. The element angle, δ , is then

$$\delta = \sum_{i=1}^k \alpha_i \quad (3.11)$$

The *limit angle*, ϵ , subtended by the intersection points of the two neighbouring circles of motion, O and P , is found by noting that $\angle A_{\text{cen}}OB_{\text{cen}} = \alpha$ and that the triangles $\triangle A_{\text{cen}}OB_{\text{cen}}$ and $\triangle A_{\text{cen}}PB_{\text{cen}}$ are identical, hence

$$\epsilon = \pi - \alpha \quad (3.12)$$

The total rotation of the angulated element between the open and closed configurations is $\beta^* = \beta_{\text{closed}} - \beta_{\text{open}}$. Clearly $\beta_{\text{open}} = 0$ and, since $\gamma_{\text{closed}} = 0$

$$\beta_{\text{closed}} = 2\pi - \gamma_{\text{closed}} - \delta - \epsilon = 2\pi - \sum_{i=1}^k \alpha_i - (\pi - \alpha) = \pi - \sum_{i=1}^{k-1} \alpha_i \quad (3.13)$$

Hence, the rotation from the closed to the open configuration is

$$\beta^* = \beta_{\text{closed}} - \beta_{\text{open}} = \pi - \sum_{i=1}^{k-1} \alpha_i \quad (3.14)$$

The above equation clearly shows how the motion of the structure is governed by k and n , as α is solely a function of n . This simple expression is therefore an important tool for determining the motion of the circular retractable bar structure. In the Sections 3.2.3 and 3.2.4 it is extended to cover non-circular structures and structures which have their motion limited by for example hinges of finite size.

A plot of the rotation angle, β^* , for parameters $n;k$ is shown in Figure 3.6. Note that a number of structures with different $n;k$ parameters have identical rotations, in Figure 3.6 $\beta^* = 60^\circ$ is emphasised as an example. Structures with identical rotation angles also have identical radial displacements as can be seen in Figures 3.2 and 3.3.

Above the rotation angle β^* was derived by considering the rotation of the angulated element as whole. The rotation angle can also be derived by considering the rotations at a single hinge.

Consider the angulated elements in Figure 3.7(a). The hinges are numbered $0, 1, 2, \dots, k-1, k$, as in Figure 3.5. Hence the internal hinges, and hence the kinks of the elements are numbered $j = 1, \dots, k-1$. For each internal hinge the angles α, β and γ are labelled with a subscript, see Figure 3.7(a), and so for $j = 1$ the sum of the angles is $\pi = \alpha_1 + \beta_1 + \gamma_1$, for $j = 2$ the sum is $\pi = \alpha_1 + \alpha_2 + \beta_2 + \gamma_2$ and more generally for hinge number j

$$\pi = \alpha_1 + \alpha_2 + \dots + \alpha_j + \beta_j + \gamma_j = \sum_{i=1}^j \alpha_i + \beta_j + \gamma_j \quad (3.15)$$

Using this formulation the angle γ_j is identical for all internal hinges and thus will just be referred to as γ , while the angle β_j will always be the internal angle of a rhombus. This will prove useful in Section 3.3.

Figure 3.7(b) shows the angulated element when it has reached its closing limit. Since $\gamma_{\text{closed}} = 0$, $\beta_{j,\text{closed}}$ is then found from Equation 3.15

$$\pi = \sum_{i=1}^j \alpha_i + \beta_{j,\text{closed}} + \gamma_{\text{closed}} \Rightarrow \beta_{j,\text{closed}} = \pi - \sum_{i=1}^j \alpha_i \quad (3.16)$$

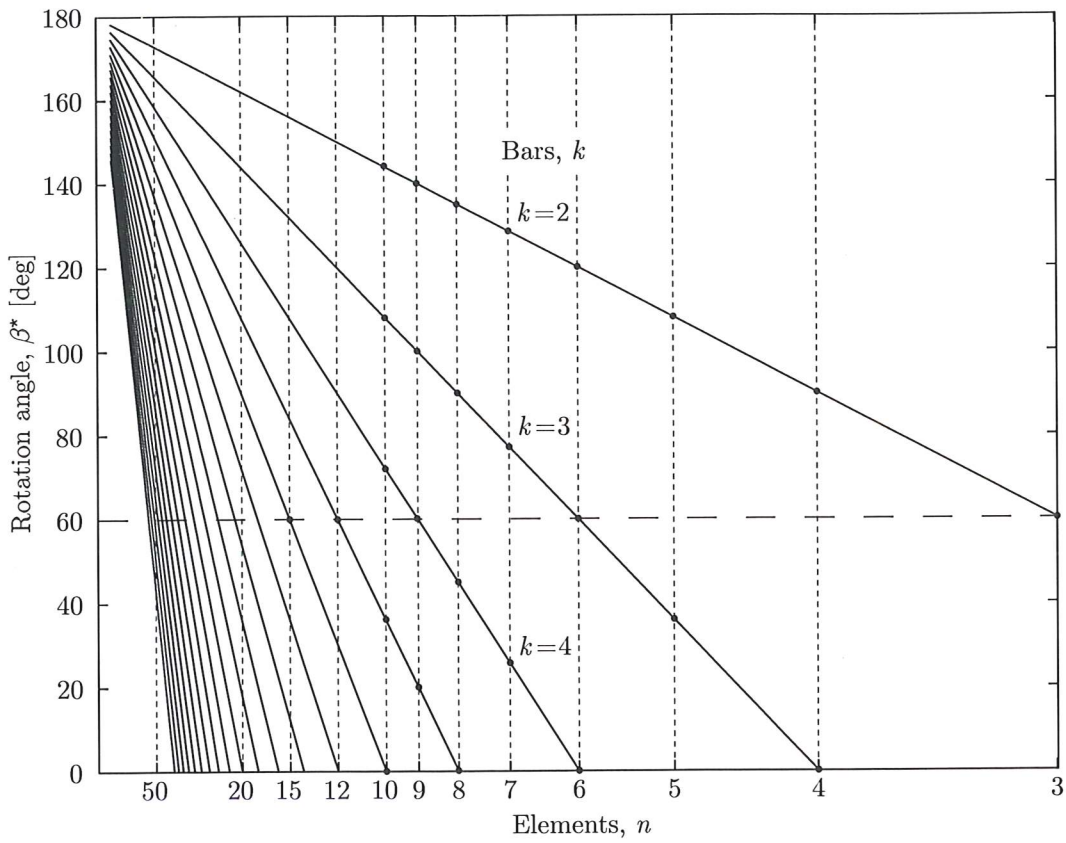


Figure 3.6: The rotation angle β^* as a function of $n;k$

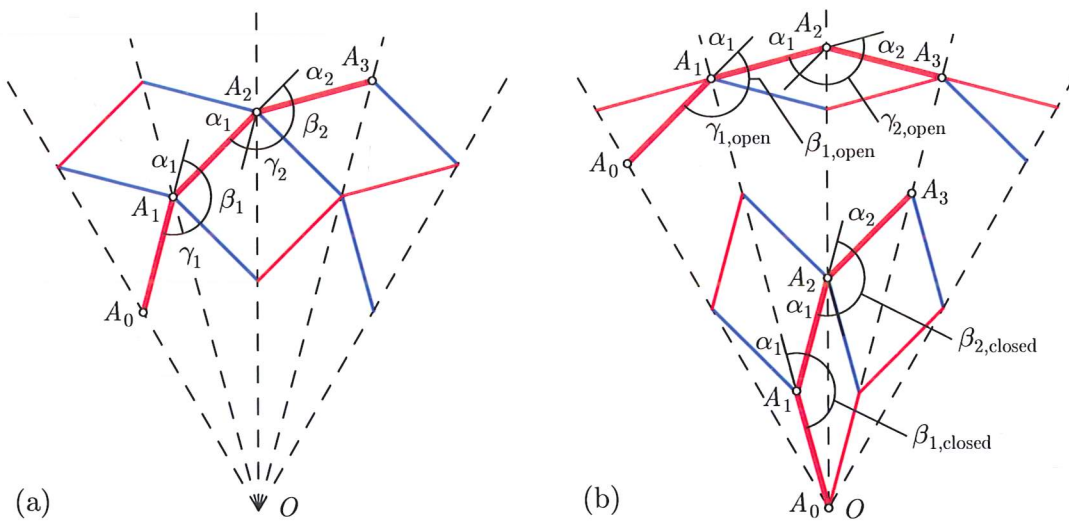


Figure 3.7: Sum of angles at internal hinges for structure with $k = 3$

Figure 3.7(b) shows also the same element when it has reached the opening limit. It can be seen that $\beta_{k-1,\text{open}} = 0$ at this limit. Using Equation 3.16 the limiting closing angle, $\beta_{k-1,\text{closed}}$, is determined for the same hinge

$$\beta_{k-1,\text{closed}} = \pi - \sum_{i=1}^{k-1} \alpha_i \quad (3.17)$$

The rotation angle for the angulated element can now be determined using the limits found for hinge $j = k - 1$

$$\beta^* = \beta_{k-1,\text{closed}} - \beta_{k-1,\text{open}} = \pi - \sum_{i=1}^{k-1} \alpha_i \quad (3.18)$$

Note that Equations 3.17 and 3.18 are identical to the previously derived Equations 3.13 and 3.14.

From Equation 3.16 the angle $\beta_{j,\text{closed}}$ can be found for any internal hinges and then, using Equation 3.18, the angle $\beta_{j,\text{open}}$ can be derived for any hinge

$$\beta_{j,\text{open}} = \beta_{j,\text{closed}} - \beta^* = \sum_{i=1}^{k-1} \alpha_i - \sum_{i=1}^j \alpha_i = \alpha_{j+1} + \alpha_{j+2} + \cdots + \alpha_{k-1} \quad (3.19)$$

Note that, because all elements undergo the same rotation β^* , any single element can be considered when determining the rotation angle.

3.2.3 Non-circular Structures

The above derived equations can be applied to non-circular structures with variable kink angles; note that for non-circular structures $\alpha \neq 2\pi/n$. A simple technique proposed by Hoberman (1990) for creating non-circular closed loop structures made from angulated elements, is to use a general polygon to define the open configuration of the structure. Hoberman's original technique made use of a series of similar rhombuses. This was later expanded by You & Pellegrino (1997) to multi-angulated elements and to allow the creation of retractable structures formed by similar parallelograms.

Structures Consisting of Similar Rhombuses

The simplest non-circular structure is formed using a general, n -sided polygon. A set of angulated elements, hence $k = 2$, is then formed by letting their single internal scissor hinge, i.e. $j = k - 1$, coincide with the vertices of the polygon, see Figure 3.8(a). The lengths of the individual bars are then equal to half the length of adjacent polygon sides. The two rigidly connected bars of an angulated element form a kink equal to the internal angle of the polygon vertex. The kink angle α of each angulated element is thus π minus the internal angle of the polygon. In this fully open configuration

the angulated elements coincide with the polygon and all n similar rhombuses have therefore an identical opening limit, $\beta_{\text{open}} = 0$.

The chain of rhombuses formed by the angulated elements, see Figure 3.8(b), remains *similar* throughout the motion of the structure as their diagonals are reduced in length by proportional amounts and their diagonals remain at constant angles (You & Pellegrino, 1997). The rotation undergone by all angulated elements in a layer is therefore also identical.

For circular structures the closing limit is reached when the innermost hinges all coincide with the origin of the structure. At this limit the innermost bars also coincide. For non-circular structures the closing limit is reached when the bars of a *single* pantographic element coincide, i.e. the angle γ is equal to *zero* for this particular, limiting pantographic element. As the movements of all elements are linked, all other elements are then inhibited from reaching their own closing limit because the limiting pantographic element cannot move any further.

From Equations 3.16 and 3.18 it then follows that the limiting pantographic element must be that with the largest kink angle, i.e. the angulated elements coinciding with the smallest internal angle of the polygon, see Figure 3.8(a)

$$\beta^* = \pi - [\alpha_1]_{\text{max}} \quad (3.20)$$

Interestingly, the above equation shows that the rotation limits, and thus the structure's radial displacements are directly influenced by the smallest internal angle of the polygon used to form the structure. Therefore a structure formed from a regular polygon, where the internal angles are identical, can execute the largest motion. Also, as previously shown by Figures 3.2 and 3.3, the more internal angles there are in a polygon, the smaller their magnitude and thus structures with larger number of elements, n , are capable of executing larger rotations.

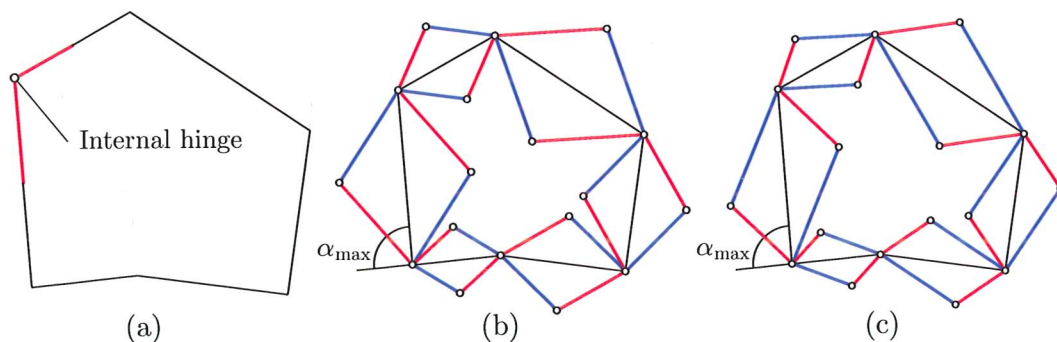


Figure 3.8: Structures formed from identical polygons and showing element with largest kink angle (a) An angulated element, (b) Similar rhombuses, and (c) Similar parallelograms

Structures Consisting of Similar Parallelograms

The same arguments can be repeated for structures formed by similar parallelograms, see Figure 3.8(c), where both angulated elements of a pantographic element have identical kink angles. They, however, do not have the same bar lengths as the angulated elements in one layer are proportionally larger than the elements in the other layer. In the open configuration all similar parallelograms have $\beta_{\text{open}} = 0$ as the parallelograms coincide with the defining polygon and hence are fully collapsed. Similarly to structures formed from similar rhombuses, the closing limit is governed by the two inner bars of a particular pantographic element coinciding. The two angulated elements will have $\gamma_{\text{closed}} = 0$ when their bars coincide. Therefore it is also found using Equations 3.16 and 3.18 that the movement of structures formed by similar parallelograms is limited by the angulated element with the largest kink angle, as already found in Equation 3.20.

Note that for structures made from similar parallelograms the two layers of the structure do not rotate by equal amounts when the internal hinges are forced to move radially. Depending on the ratio between the longer and the shorter bar lengths in the parallelogram one will rotate more than the other. However, the relative rotation between elements in different layers is not influenced and hence not the ability of either layer to rotate about fixed points.

Structures Consisting of Multi-Angulated Elements

For circular structures consisting of identical angulated or multi-angulated elements the rotation angle β^* can be found from Equation 3.18 by considering any of the identical elements. Considering the rotation angle for all the non-identical angulated elements composing a non-circular structure it was above found from Equation 3.18 that the limiting angulated element was that with the largest kink angle α .

From Equation 3.18 it also follows that for a non-circular structure composed of non-identical multi-angulated elements the motion of such a structure is not limited by the angulated element with the largest individual kink angle. Rather it is limited by the element with the largest sum of kink angles

$$\beta^* = \pi - \left[\sum_{i=1}^{k-1} \alpha_i \right]_{\text{max}} \quad (3.21)$$

If the number of bars in the individual multi-angulated elements is not identical throughout the structure the motion of the structure is still limited by the particular element the largest sum of kink angles. This is shown in Figure 3.9 where four elements in the red layer, one of which only have two bars, all have a sum of kink angles equal to 60 degrees. As all other elements have a lower sum of kink angles these four elements limits the motion of the structure as shown.

Equation 3.14 has thus been extended to cover not only circular bar structures but also non-circular structures formed by non-identical multi-angulated elements.

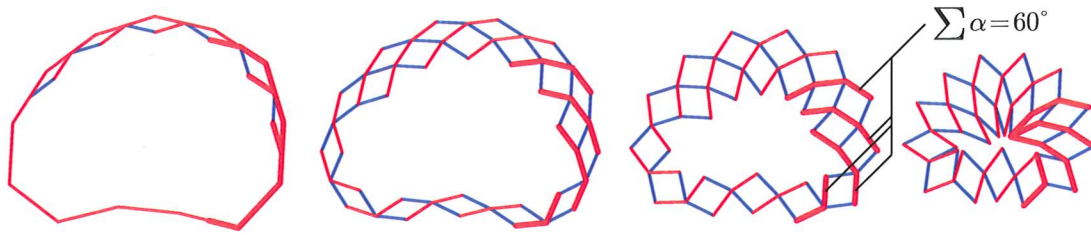


Figure 3.9: Non-circular structures consisting of multi-angled elements with variable sum of kink angles

Location of Fixed Centres of Rotation

As described in Section 2.4.2, Kassabian *et al.* (1997) found that if the structure is allowed to rotate while it opens and closes, i.e. the hinges are not required to move on radial lines, the motion of one layer of elements could be described as a pure rotation about fixed points. For a structure, of any plan shape, moving radially Kassabian found that the location of instantaneous centre of rotation A_{cen} for the angulated element A_0 – A_k can be obtained from the angle β_{k-1} and the distance between the origin O and hinge A_{k-1} . As shown in Figure 3.10(a) the centre is rotated by $\beta_{k-1}/2$ about the origin compared to the hinge A_{k-1} and the radial distance is given by

$$OA_{\text{cen}} = \frac{OA_{k-1}}{2 \cos(\beta_{k-1}/2)} \quad (3.22)$$

Hence, in the open configuration, where $\beta = 0$, the centre is located on the radial line OA_{k-1} and at exactly the half distance between the origin and the polygon vertex defining hinge A_{k-1} . Thus, all the fixed centres of rotation are given at the vertices of a polygon that is half the size of that defining the angulated elements themselves, as shown in Figure 3.10(b). Note that the origin need not be at the centre of the polygon.

Combining the polygon method for obtaining both the open configuration and the fixed centres of rotation with Equation 3.21, a simple method for determining the closed and any intermediate configurations is obtained. The shape of the individual angulated elements is given by the polygon and the closed configuration can easily be found by rotating the individual elements of a single layer by β^* about their individual fixed centres of rotation. The position of the elements of the second layer is then given by the connecting hinges on the rotated layer. Intermediate configurations for the structure can be found by rotating the elements by less than β^* .

For non-circular structures, in particular where calculating the radial position of the elements during the motion of the structure is not straight forward, this method provides a much easier and simpler approach for finding various configurations for the structure.

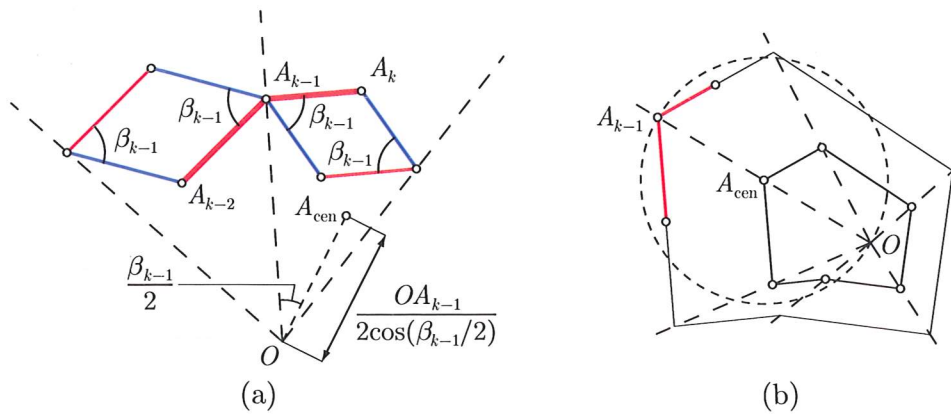


Figure 3.10: Location of the fixed centre of rotation in (a) Intermediate configuration, and (b) Open configuration

3.2.4 Additional Rotational Limits

As the bar structure is composed of two distinct layers, the only possible interferences to its movement are: between elements of the same layer, between elements and hinges, and between hinges. For structures generated from identical rhombuses, when all bars have the same length but different kink angles, interference will only occur between hinges.

Assuming that the hinges are all circular in shape, with a radius of r_j , then it can be seen from Figure 3.11 that such hinges will impose additional limits on the motion of the structure. Hence both the open and closed limits will be reached before the limits determined earlier, $\beta_{k-1,open} = 0$ and $\gamma_{closed} = 0$. The new limits are obtained by considering the minimum angle between two bars of length l attached to hinges of radius r_j . Therefore,

$$\beta_{k-1,open} = \gamma_{closed} = 2 \arcsin \left(\frac{r_j}{l} \right) \quad (3.23)$$

The reduce rotation angle is obtained by rewriting Equations 3.16, 3.18 and 3.19 for $\beta_{k-1,open} = \gamma_{closed} \neq 0$

$$\pi = \sum_{i=1}^j \alpha_i + \beta_{j,closed} + \gamma_{closed} \Rightarrow \beta_{j,closed} = \pi - \sum_{i=1}^j \alpha_i - \gamma_{closed} \quad (3.24)$$

The rotation angle β^* is then, following Equation 3.21

$$\beta^* = \beta_{k-1,closed} - \beta_{k-1,open} = \pi - \left[\sum_{i=1}^{k-1} \alpha_i \right]_{\max} - \beta_{k-1,open} - \gamma_{closed} \quad (3.25)$$

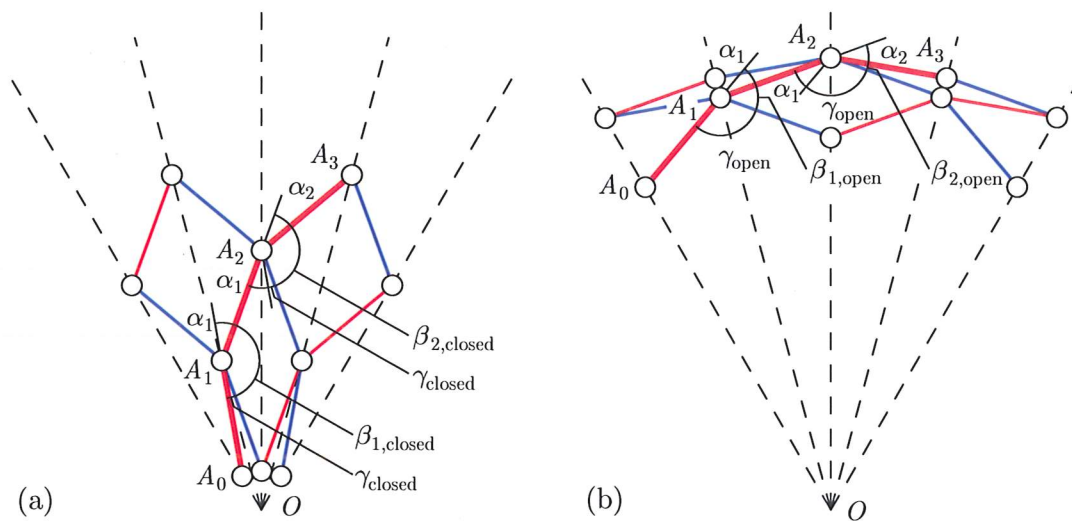


Figure 3.11: Rotational limits of structure with hinges of finite size in (a) Closed configuration, and (b) Open configuration

and so

$$\beta_{j,\text{open}} = \beta_{j,\text{closed}} - \beta^* = \alpha_{j+1} + \alpha_{j+2} + \cdots + \alpha_{k-1} + \beta_{k-1,\text{open}} \quad (3.26)$$

Note that for $j = k - 1$, $\beta_{j,\text{open}} = \beta_{k-1,\text{open}}$ as $j + 1 > k - 1$.

By expressing any limits imposed on the motion of the structure in terms of a rotational limit, as done in Equation 3.23, it is hence possible to subtract these from the uninhibited motion given by Equation 3.21. This allows the possible motion for almost all practical structures to be found using the resulting Equation 3.25.

In structures not made from identical rhombuses often it is not two hinges that interfere but rather a hinge and an element as seen in Figure 3.8(b,c) at the bottom-left angulated elements of the structures shown. This, however, only occurs when the structure is near the fully-open or fully-closed configurations. Conservatively, the limits for β_{open} and γ_{closed} for such structures can be estimated using Equation 3.23 with the shortest bar length in the structure. To find the exact limits of a complex shape one needs to identify the points of interference before any calculation is carried out.

If a circular structure is considered, such as those considered in Section 3.2.1, then defining the *additional limit angle* ζ as $\zeta = \beta_{\text{open}} + \gamma_{\text{closed}}$ Equations 3.23 and 3.25 can be simplified to

$$\beta^* = \pi - \sum_{i=1}^{k-1} \alpha_i - \zeta \quad (3.27)$$

and

$$\zeta = 4 \arcsin \left(\frac{r_j}{R_{\text{open}}} \frac{1}{\sin \left(\frac{\alpha}{2} \right)} \right) \quad (3.28)$$

where R_{open} is the maximum outer radius for hinge $k - 1$ for $\beta_{\text{open}} = \gamma_{\text{closed}} = 0$ as defined in Section 3.2.1.

The additional limits for the rotation have the effect of changing the radial distances found in Section 3.2.1, further details can be found in Jensen & Pellegrino (2002). Plotting Equations 3.14 and 3.28 the rotation angle for structures with finite sized hinges can be readily found from Figure 3.12. In the figure the additional limit ζ is plotted for different relative hinge sizes, given by the ratio r_j/R_{open} . The reduced rotation angle is found by subtracting ζ from the unreduced rotation angle given by Equation 3.14.

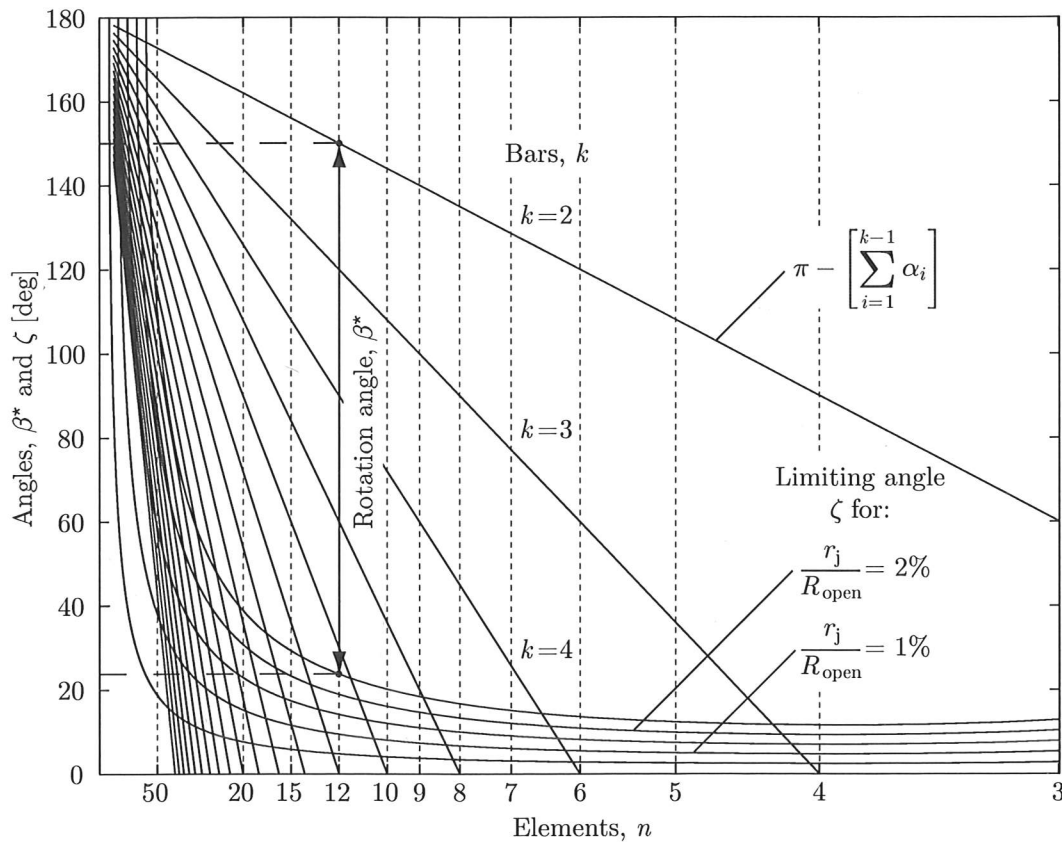


Figure 3.12: Additional limit ζ for the rotation angle β^* of circular structures

3.3 Retractable Plate Structures

By considering a retractable bar structure as a concentric ring of identical rhombuses or more generally as a ring of similar parallelograms it becomes possible to design plates that can be attached to the bar structure and provide a gap-free cover in both its open and closed configurations. This is done by considering what limitations are imposed on the movement of only a small part of the bar structure when covering plates are attached to it.

3.3.1 Movement of Bar Linkage

Consider the four bar linkage, consisting of two parallel bars $A_k A_{k-1}$ and $B_{k-1} B_{k-2}$ and a pair of parallel linking bars, shown in Figure 3.13. Bar $B_{k-1} B_{k-2}$ is assumed to be fixed, so no rigid body motions are allowed and this leaves *one* internal mechanism which allows the linking bars to rotate and bar $A_k A_{k-1}$ to translate, i.e. to shear the parallelogram $A_k A_{k-1} B_{k-2} B_{k-1}$. The bottom-left bars define the angle, β , as shown in Figure 3.13. Note that β can be defined at both A_{k-1} and B_{k-1} .

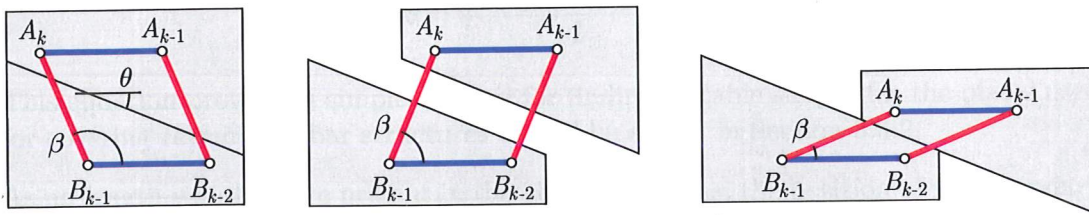
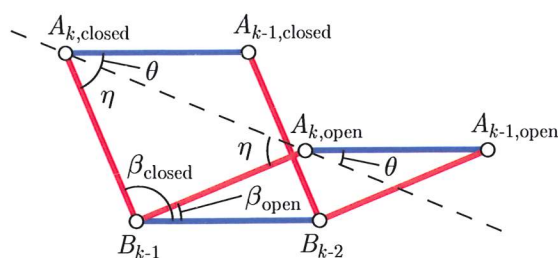


Figure 3.13: Movement of four-bar linkage with two plates

Consider attaching a rigid plate to bars $A_k A_{k-1}$ and $B_{k-1} B_{k-2}$ only. This rigid body eliminates the mechanism of the parallelogram. If a straight cut is made in the plate, at an angle θ to the bars $A_k A_{k-1}$ and $B_{k-1} B_{k-2}$, as shown in Figure 3.13, then the mechanism is restored. The line of the cut is called the *boundary line* and θ the *boundary angle*. So, now there are – in effect – two plates attached to the linkage and by not allowing these to overlap β is restricted to either increase or decrease depending on the boundary angle θ . In the case illustrated in Figure 3.13 β decreases until the gap between the two plates has closed again and the movement of the linkage has reached its other limit.

The two limits on the rotation angle are denoted by β_{closed} and β_{open} and, once they are known, θ can be found from Figure 3.14 by considering the sum of the internal angles in $\triangle A_{k,\text{closed}} B_{k-1} A_{k,\text{open}}$

$$\pi = 2\eta + (\beta_{\text{closed}} - \beta_{\text{open}}) \Rightarrow \eta = \frac{\pi - \beta_{\text{closed}} + \beta_{\text{open}}}{2} \quad (3.29)$$

Figure 3.14: Determining the boundary angle θ

In addition, by considering the parallel bars $A_{k,closed}A_{k-1,closed}$ and $B_{k-1}B_{k-2}$

$$\pi = \theta + \eta + \beta_{\text{closed}} \Rightarrow \eta = \pi - \theta - \beta_{\text{closed}} \quad (3.30)$$

The boundary angle is thus related to the limiting β 's by

$$\theta = \frac{\pi - \beta_{\text{closed}} - \beta_{\text{open}}}{2} \quad (3.31)$$

This equation provides a simple method for finding suitable shapes for the plates used for covering retractable bar structures as will be shown in Section 3.3.2.

As no length variables are present in the above equations, the position of the boundary line relative to the linkage does not affect the limits of the motion. The distance translated by bar A_kA_{k-1} , and its attached plate, parallel to the boundary line is

$$L = 2l \sin\left(\frac{\beta_{\text{closed}} - \beta_{\text{open}}}{2}\right) \quad (3.32)$$

where l is the length of the linking bars, i.e. A_kB_{k-1} and $A_{k-1}B_{k-2}$.

3.3.2 Application to Closed Loop Structures

Consider two adjacent multi-angulated elements, A_0-A_3 and B_0-B_3 , which are part of a circular retractable structure with $k = 3$, as shown in Figure 3.15. Together with bars A_1B_0 , A_2B_1 and A_3B_2 these multi-angulated elements form two interconnected linkages, I, $A_1A_2B_1B_0$, and II, $A_2A_3B_2B_1$, which are free to shear within the limits of motion for hinges A_1 and A_2 , respectively.

Consider attaching a rigid plate to the multi-angulated elements, A_0-A_3 and B_0-B_3 . This eliminates the single mechanism of the two interconnected linkages. To restore the mechanism the plate must be cut in two as was done for the four-bar linkage above. However, as there are now two linkages involved, any single straight cut must have a boundary angle θ that satisfies Equation 3.31 for both linkages in order to not interfere with the motion of the bar structure. With β defined at hinge A_j , with $j = 1$ and $j = 2$

for linkages I and II respectively, the limits β_{closed} and β_{open} are replaced by $\beta_{j,\text{closed}}$ and $\beta_{j,\text{open}}$ respectively,

$$\theta_j = \frac{\pi - \beta_{j,\text{closed}} - \beta_{j,\text{open}}}{2} \quad (3.33)$$

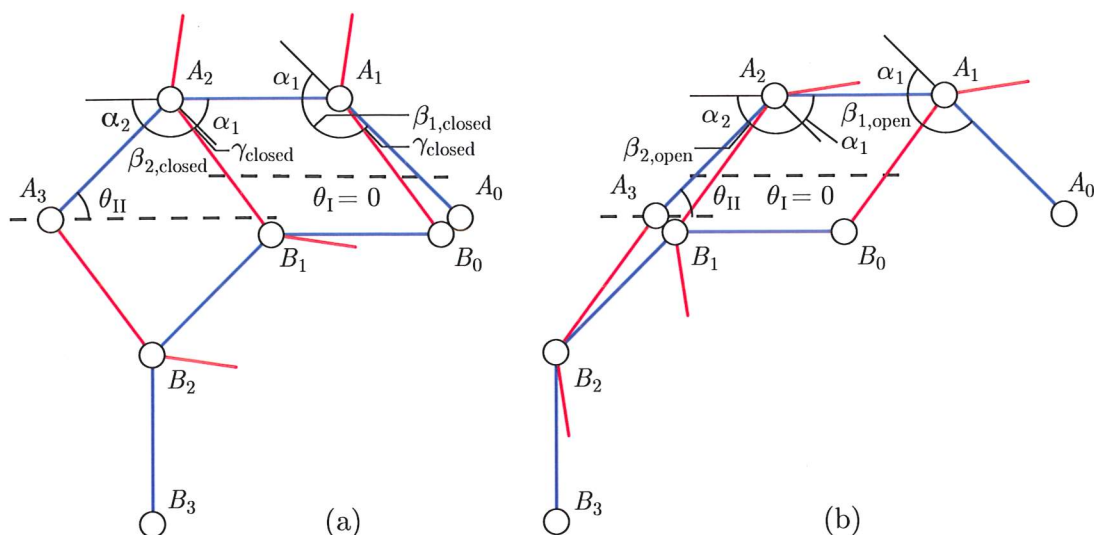


Figure 3.15: Boundary angle θ for multi-angled elements in (a) Closed configuration, and (b) Open configuration

Figure 3.15 shows the angles at A_j , at the limits of the motion for the bar structure. As the hinges are all of identical size the two limits γ_{closed} and $\beta_{k-1,\text{open}}$ are also identical following Equation 3.23.

The boundary angle θ_I that satisfies Equation 3.33 for I is found by considering the movement at A_1 . Equations 3.24, 3.26 and 3.33, noting that for a circular structure $\alpha_1 = \alpha_2$ and using $\gamma_{\text{closed}} = \beta_{2,\text{open}}$, give

$$\begin{aligned} \theta_I &= \frac{\pi - (\pi - \alpha_1 - \gamma_{\text{closed}}) - (\alpha_2 + \beta_{2,\text{open}})}{2} \\ &= \frac{\alpha_1 - \alpha_2 + \gamma_{\text{closed}} - \beta_{2,\text{open}}}{2} \\ &= 0 \end{aligned} \quad (3.34)$$

The boundary line, given by θ_I , is hence parallel to bars B_0B_1 and A_1A_2 as shown in Figure 3.15. The boundary angle θ_{II} that satisfies Equation 3.33 for II is similarly found by considering the movement at A_2 ,

$$\begin{aligned}
 \theta_{II} &= \frac{\pi - (\pi - \alpha_1 - \alpha_2 - \gamma_{\text{closed}}) - \beta_{2,\text{open}}}{2} \\
 &= \frac{\alpha_1 + \alpha_2 + \gamma_{\text{closed}} - \beta_{2,\text{open}}}{2} \\
 &= \alpha
 \end{aligned} \tag{3.35}$$

The boundary line, given by θ_{II} , is hence parallel to the boundary line given by θ_I as shown in Figure 3.15. It has been found that the two boundary lines are always parallel and hence a single straight, continuous boundary line can be defined without the motion of the interconnected linkages being inhibited and as a result a rigid plate attached to the multi-angulated elements can be cut by a single line, as for the simple angulated element.

For the complete structure, n straight boundary lines can be determined. They will define n identical wedge-shaped covering elements, each subtending the angle α at the tip and their tips coinciding at the centre of the structure, as shown in Figure 3.16. The same result was first obtained by Kassabian *et al.* (1997), but through a different approach.

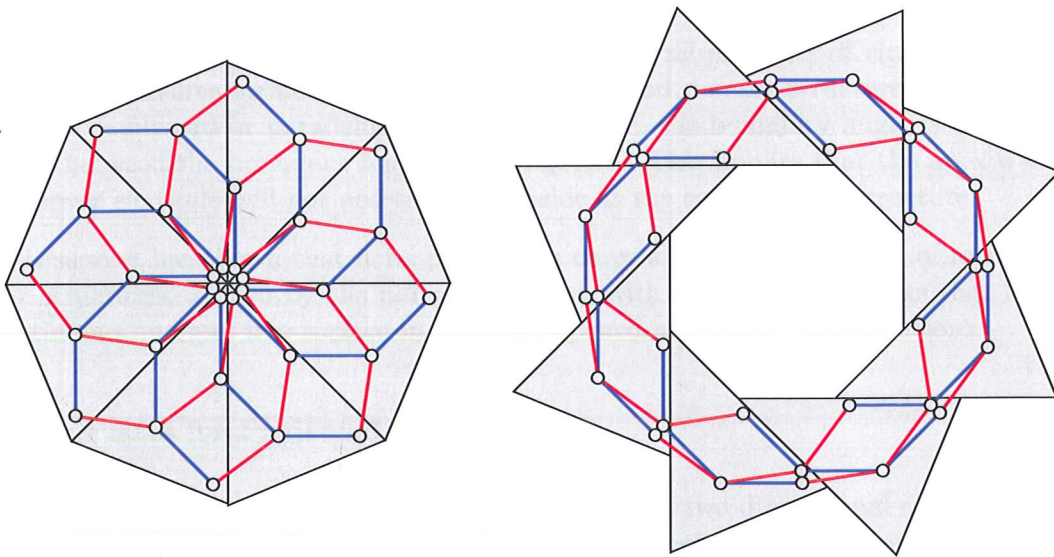


Figure 3.16: Wedge-shaped cover elements for circular structure

As the straight boundary line can be defined from any single linkage, it is possible to simplify the equations above. Equations 3.23 and 3.24 provides sufficient information to readily find the two limit angles for the parallelogram $A_k A_{k-1} B_{k-1} B_{k-2}$, and therefore, defining the boundary angle for A_{k-1} and using Equation 3.33, we obtain

$$\theta_{k-1} = \frac{\pi - \beta_{k-1,\text{closed}} - \beta_{k-1,\text{open}}}{2} = \frac{1}{2} \sum_{i=1}^{k-1} \alpha_i + \frac{\gamma_{\text{closed}}}{2} - \frac{\beta_{k-1,\text{open}}}{2} \tag{3.36}$$

$$\begin{aligned}
\theta_{II} &= \frac{\pi - (\pi - \alpha_1 - \alpha_2 - \gamma_{\text{closed}}) - \beta_{2,\text{open}}}{2} \\
&= \frac{\alpha_1 + \alpha_2 + \gamma_{\text{closed}} - \beta_{2,\text{open}}}{2} \\
&= \alpha
\end{aligned} \tag{3.35}$$

The boundary line, given by θ_{II} , is hence parallel to the boundary line given by θ_I as shown in Figure 3.15. It has been found that the two boundary lines are always parallel and hence a single straight, continuous boundary line can be defined without the motion of the interconnected linkages being inhibited and as a result a rigid plate attached to the multi-angulated elements can be cut by a single line, as for the simple angulated element.

For the complete structure, n straight boundary lines can be determined. They will define n identical wedge-shaped covering elements, each subtending the angle α at the tip and their tips coinciding at the centre of the structure, as shown in Figure 3.16. The same result was first obtained by Kassabian *et al.* (1997), but through a different approach.

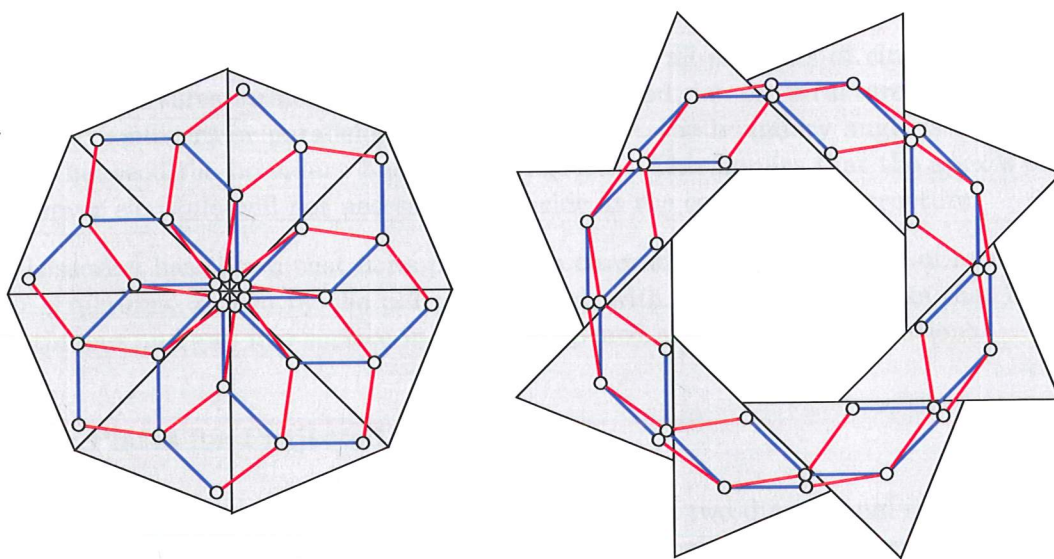


Figure 3.16: Wedge-shaped cover elements for circular structure

As the straight boundary line can be defined from any single linkage, it is possible to simplify the equations above. Equations 3.23 and 3.24 provides sufficient information to readily find the two limit angles for the parallelogram $A_k A_{k-1} B_{k-1} B_{k-2}$, and therefore, defining the boundary angle for A_{k-1} and using Equation 3.33, we obtain

$$\theta_{k-1} = \frac{\pi - \beta_{k-1,\text{closed}} - \beta_{k-1,\text{open}}}{2} = \frac{1}{2} \sum_{i=1}^{k-1} \alpha_i + \frac{\gamma_{\text{closed}}}{2} - \frac{\beta_{k-1,\text{open}}}{2} \tag{3.36}$$

For identical motion limits, $\gamma_{\text{closed}} = \beta_{k-1,\text{open}}$, Equation 3.36 gives simply

$$\theta_{k-1} = \frac{1}{2} \sum_{i=1}^{k-1} \alpha_i \quad (3.37)$$

Hence, in circular structures the boundary line is always parallel to a line from A_k to A_0 .

This is not the case for non-circular structures where one particular angulated or multi-angulated element governs the motion limit of the whole structure. As β^* and $\beta_{k-1,\text{open}}$ are identical for all elements, θ must also be identical for all elements, following Equations 3.25 and 3.33,

$$\theta_{k-1} = \frac{\pi - \beta_{k-1,\text{closed}} - \beta_{k-1,\text{open}}}{2} = \frac{\pi - \beta^*}{2} - \beta_{k-1,\text{open}} \quad (3.38)$$

If $\beta_{k-1,\text{open}} = \gamma_{\text{closed}} = 0$,

$$\theta_{k-1} = \frac{\pi - \beta^*}{2} \quad (3.39)$$

This shows that the boundary angle is identical for all elements of circular and non-circular structures formed using the polygon method, i.e. for structures consisting of similar rhombuses or parallelograms. Furthermore, the boundary angle is always the angle between the boundary line and bar $A_k A_{k-1}$. This implies that the apexes of all the cover elements will not necessarily coincide at the centre of the structure.

This section has shown that it is possible to cover all types and shapes of retractable bar structures, formed by the polygon method, with rigid cover elements that form a continuous and gap free surface in both the opened and closed configurations.

Cover Plates for Projected Structures

As described in Section 2.4.4 it is possible to project a two-dimensional retractable bar structure onto a three-dimensional surface. It is also possible to cover such a structure with wedge shaped cover elements, as the two-dimensional and three-dimensional structures are kinematically identical. However, as the motion of the projected structure is purely horizontal, the determined boundaries of the cover elements must remain horizontal in order to form a continuous surface in both the open and closed configurations. Between the boundaries, each cover element can have any three-dimensional shape, as long as interference with the motion of the underlying bar structure is prevented. An example of cover plates for a projected structure is shown in Figure 3.17.

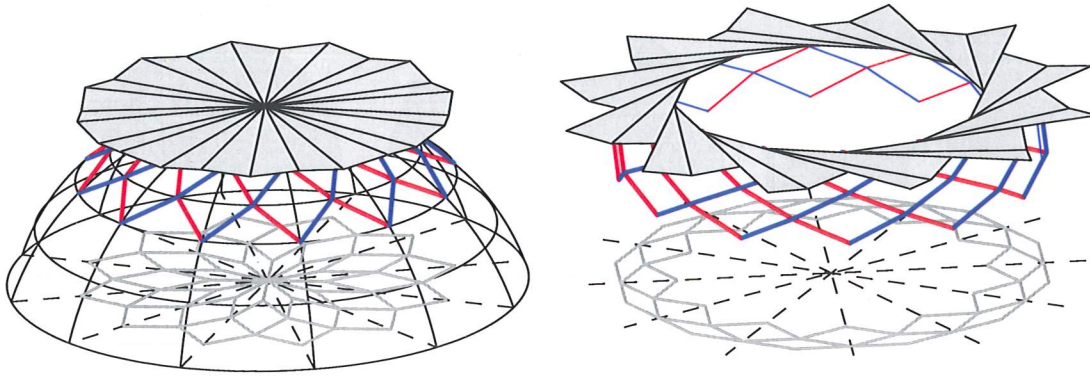


Figure 3.17: Cover elements for a structure formed by projection onto a sphere

3.3.3 Plate-only Structures

The shape of the covering elements shown in Figure 3.16 is such that they do not fully cover the multi-angulated elements to which they are attached. In this section it is shown that it is possible to construct a retractable plate structure by connecting, through hinges, two layers of rigid plate elements.

In Section 3.3.1 it was shown that the boundary angle is independent of the position of the boundary line and it is therefore possible to perform a translation of the boundary line relative to the bar structure. By performing such a translation, the cover elements can be made to cover fully both the multi-angulated elements and their hinges, as shown in Figure 3.18.

To allow the boundary line to pass between neighbouring elements it is often necessary to impose additional rotational limits. This is shown in Figure 3.15(b) where the boundary line for rhombus $A_2A_3B_2B_1$ cannot be arranged such that both the hinges A_3 and B_1 are fully covered. It is therefore necessary to increase either or both of the limits β_{open} and γ_{closed} ; giving additional clearance between the hinges. If the limits are increased identically the boundary angle will remain unchanged, following Equation 3.36.

As the boundary lines have been translated perpendicularly to themselves, they no longer meet at the centre, thus the cover elements will leave a small aperture at the centre of the structure in the closed configuration, as seen in Figure 3.18.

For circular structures each wedge-shaped cover element subtends an angle α and it therefore becomes increasingly difficult to cover multi-angulated elements as k increases. No solutions have been found for $k > 4$ as the central aperture becomes disproportionately large. Figure 3.18 shows solutions for $k \leq 4$. The problem is treated in greater detail in Jensen (2001).

For structures with $k \leq 4$ both the multi-angulated element and its hinges can be fully covered by the cover elements and hence a rigid cover element or a *plate* can be used to replace the multi-angulated element in the retractable structure. A plate structure

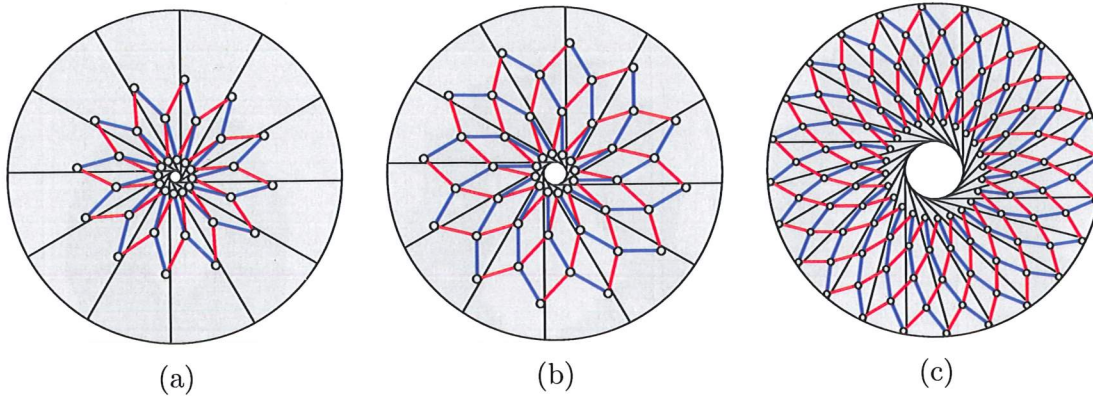


Figure 3.18: Wedge-shaped cover elements that fully cover the angulated elements and their hinges (a) $k = 2$, (b) $k = 3$, and (c) $k = 4$

without bar elements can thus be constructed from two layers of n plates each, where the hinges connecting the plates coincide with the layout of the hinges in the equivalent n -element bar structure.

Physical Models

Models of plate structures have been constructed from identical wedge-shaped Acrylonitrile-Butadiene-Styrene (ABS) plastic plates and more complex structures from cardboard. The connections were made using plastic snap rivets. Figure 3.19 shows an early circular model formed by plastic plates and Figure 3.20 shows a non-circular structure formed from cardboard plates.

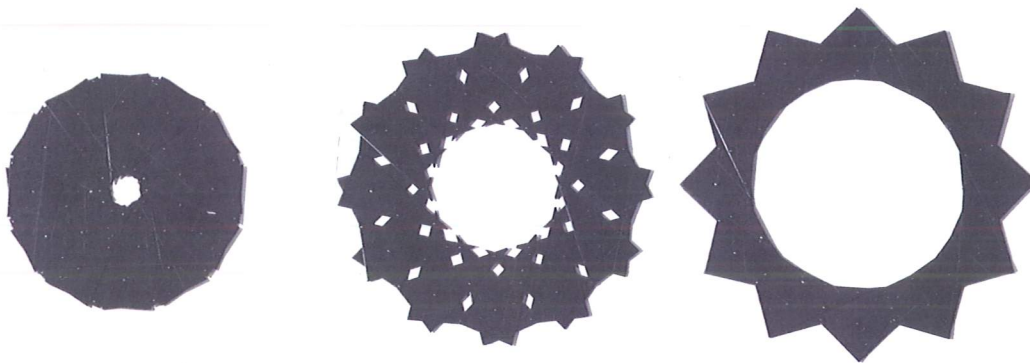


Figure 3.19: Plastic model of wedge-shaped plate structure with $n; k = 12; 3$

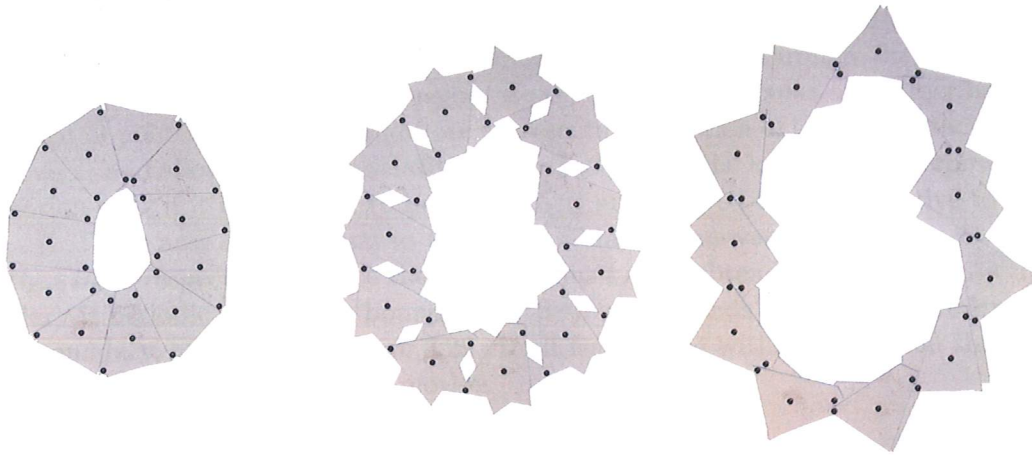


Figure 3.20: Cardboard model of non-circular plate structure

3.3.4 Periodicity of Boundary

So far, only straight-edged cover elements have been considered, but non-straight shapes are also possible. Consider the linkage shown in Figure 3.21; for the cover plates to fit together without any gaps or overlaps in both extreme configurations, the boundaries of the two plates must fit together in both configurations. Hence, if the boundaries are shaped such that no gaps or overlaps occur in either extreme configuration, non-straight features are allowed. These features must, however, repeat with period L , as shown in Figure 3.21. In general, common boundaries of neighbouring cover elements must be shaped such that all features have a periodic pattern.

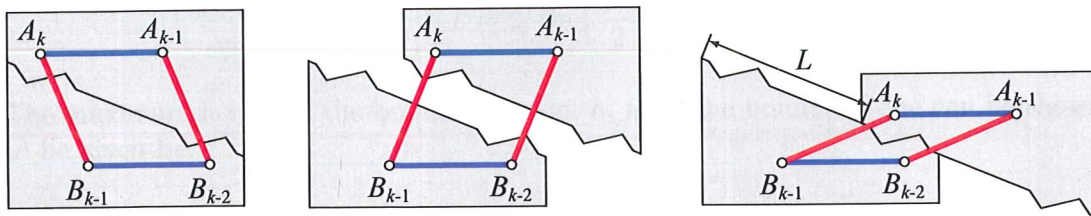


Figure 3.21: Periodic pattern of non-straight boundary

There are two important restrictions to this general periodicity rule, as obviously a boundary that deviates significantly from the original straight line would inhibit the movement of the linkage.

First, the movement at any time and of any point on either boundary is always perpendicular to the linking bars and this limits the maximum slope of any feature of the boundary. This condition is most severe in the two extreme configurations, where there is no gap between the plates. Hence, if the slope is at any point greater than the initial direction of movement of the boundary, all movement is inhibited.

Second, any features of the boundary shape deviating from the original straight line need to lie within a region bounded by circular arcs passing through the points O , P and Q , shown in Figure 3.22. Consider a point O . Two circular arcs describe the movement of point O ; the upper-right arc represents the motion of O if it is attached to bar $A_k A_{k-1}$ and allowed to move relative to bar $B_{k-1} B_{k-2}$; the lower-left arc represents the motion of O if it is attached to bar $B_{k-1} B_{k-2}$ and allowed to move relative to bar $A_k A_{k-1}$. These arcs are identical to those describing the movements of bars $A_k A_{k-1}$ and $B_{k-1} B_{k-2}$ respectively, hence they have radius l and subtend the angle β^* . As the boundary is periodic, the region bounded by these arcs extends along the entire length of the boundary, as shown in Figure 3.22. If all features lie within this region the two plates will not interfere during the motion.

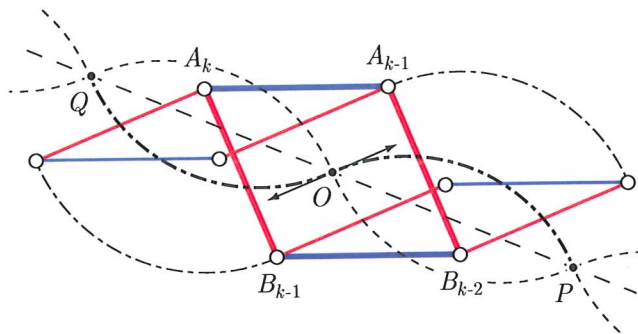


Figure 3.22: Direction of initial movement and region defining possible boundary shapes

The length of the period L was found in Equation 3.32 and, since $\beta^* = \beta_{\text{closed}} - \beta_{\text{open}}$, it can be written as

$$L = 2l \sin\left(\frac{\beta^*}{2}\right) \quad (3.40)$$

The maximum height of the bounded region, h , from the boundary line can be shown to be given by:

$$h = l - l \cos\left(\frac{\beta^*}{2}\right) \quad (3.41)$$

As already found for the position of the boundary line, there are no conditions on the positioning of the features along a straight boundary line. Thus, the region defining the limits for the features can be moved along the boundary line.

At either end of the periodic boundary it is possible to break the periodicity, as shown in Figure 3.23. This is because the movement of the four-bar linkage only allows the plates to translate by a single period and, importantly, always in the same direction. Therefore both ends of the boundary line need not be periodic at all, though they must not interfere with the motion. This feature can be applied to close the central aperture occurring in some structures and was first done by Kassabian *et al.* (1997), as shown in Figure 2.20.

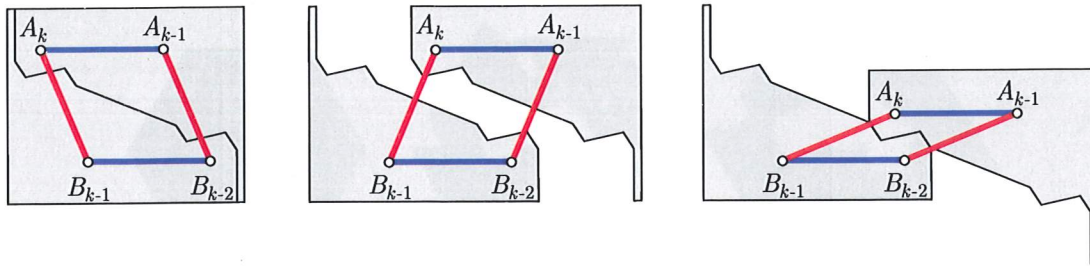


Figure 3.23: Non-periodic end features

Physical Models

A number of retractable plate structure models with non-straight boundaries have been built. Here only three will be presented though many others have been constructed.

The first model consists of sixteen identical plates. It is based on an equivalent circular bar structure with $n;k = 8;3$ and the boundaries have been formed by circular arcs with a radius equal to the radius of the opening in the open configuration. Thus the model forms a perfect circular opening in the open configuration as shown in Figure 3.24. As all the plates are identical, they can all be cast using the same mould, from which thermoplastic plate elements were injection moulded. The plates were connected with plastic snap rivets. Figure 3.36 show the layers of the structure in red and blue colours.

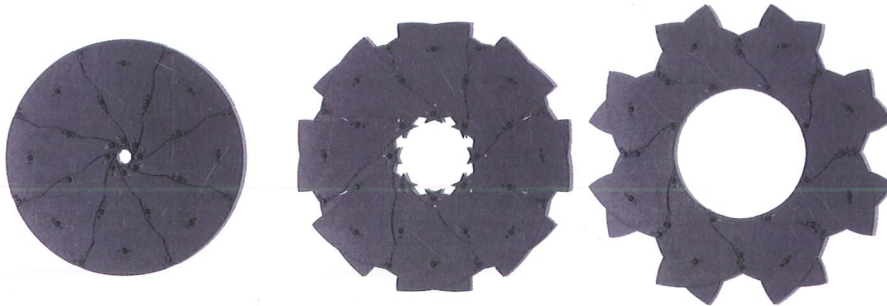


Figure 3.24: Model of sixteen identical plates forming a perfect circular opening

The second model is based on the bar structure formed by similar parallelograms shown in Figure 3.8(c). One layer is formed by angulated elements and the other from plate elements, both cut in ABS plastic using an Abrasive Water Jet Machine (AWJ) and connected through plastic snap rivets. From the model it can be seen how the period of each boundary is different as each set of linking bars has a different length l .

The third and final model presented is based on the non-circular bar structure shown in Figure 3.9. To show the wide range of possible boundary shapes, here all *twenty-six* plate elements are unique, and thus the two layers are also different as seen in Figure 3.26. The periodic boundaries have been generated using a wide variety of shapes; straight lines, circular arcs, parabolic curves, sinusoidal curves and splines.

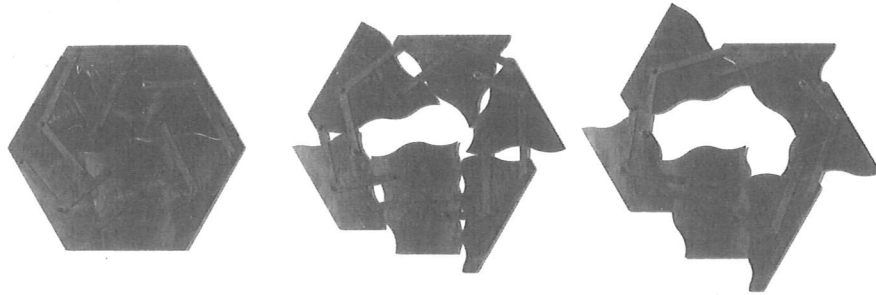


Figure 3.25: Plastic model of plate structure formed from similar parallelograms

All the boundaries are periodic except for the end features, which have been used to cover the central aperture in the closed configuration. Using a computer controlled Wire Electrical Discharge Machine (EDM) the plate elements were cut from aluminium-alloy plate and assembled with plastic snap rivets.

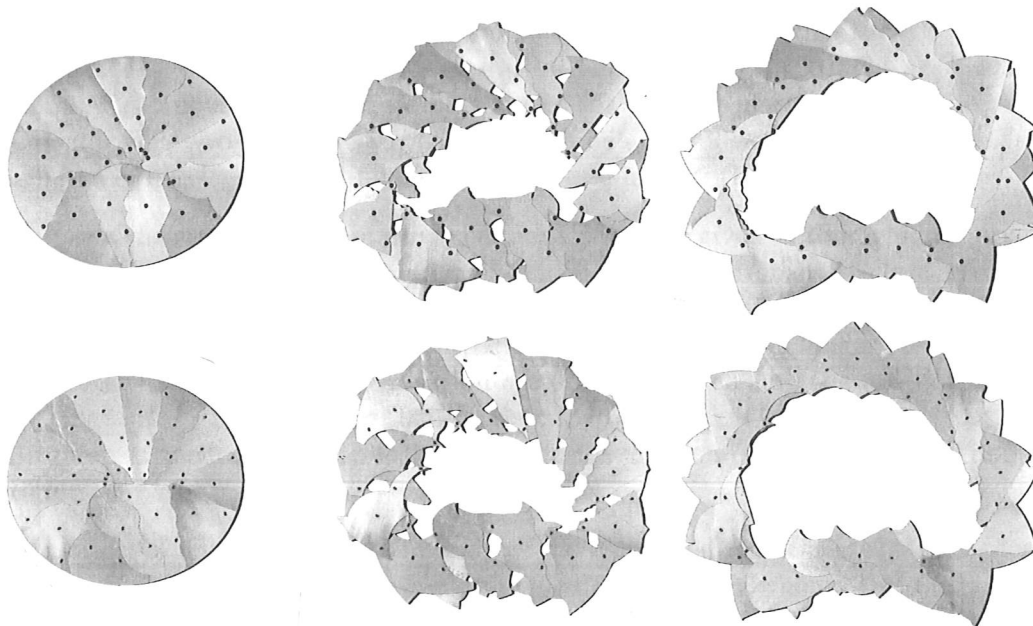


Figure 3.26: Top and bottom faces of model of non-circular structure where all plates and boundaries are unique

3.4 Computer Assisted Design

The model shown in Figure 3.26 was designed using a computer application written by the author in the programming language C++. The application has been called *GTD* after its functions of Generating, Transforming and Drawing bar and plate structures. *GTD* has been compiled for running on the MacOS 10.2 operating system. Figure 3.27

shows the flow of the application from the input-file to the resulting drawings and output-files.

The input-file contains the following information:

- Number of sides in the polygon, n (in Figure 3.27 denoted A, B, \dots, n),
- Number of bars, k , for each element and coordinates for the polygon vertices,
- Coordinates of the origin, $\{x_{\text{origin}}, y_{\text{origin}}\}$,
- Radii of hinges, r_j ,
- Additional rotational limits, β_{open} and γ_{closed} ,
- Number of retraction steps to be drawn, S , and
- Choice of radial or rotating motion, T ,

From the input-file GTD generates a hinge definition matrix containing the coordinates for all hinges in the structure in the configuration defined by $\beta_{\text{open}} = 0$. The application forms similar rhombuses, as they are best suited for forming plate structures because the elements of the two layers are equal in size. If similar parallelograms were used, then the elements in one layer would be larger than those in the other layer, see Figure 3.8.

GTD retracts the structure by rotating the hinge positions given in the definition matrix about fixed points. It then draws bars and boundaries from a constant element definition matrix. The rotation β is identical for all elements and hence the transformation matrix is constant. However, each particular element and its hinges have its own centre of rotation. The centres of rotation are obtained by scaling the polygon defining the hinges A_{k-1} by a factor of 0.5, as described in Section 3.2.3. If specified, the radial motion is generated by imposing an opposite rotation of magnitude $\beta/2$ about the origin.

As the motion of the structure is limited by the angulated element with the largest sum of kink angles, the sum of kink angles is calculated for all elements and the largest sum obtained.

The extreme configurations β_{open} and β_{closed} are found from Equations 3.23–3.25 by considering only hinge $k - 1$ of the limiting angulated element. The limits for the motion, β_{open} and γ_{closed} , is set to be the higher of (i) a value specified in the input-file or (ii) the limit imposed by the hinges, found from Equation 3.23.

Intermediate configurations are found by rotating the elements about their centres stepwise.

Straight boundaries for plate elements can also be drawn. This is done by drawing a line from hinge k to $k - 1$ for each element. These lines are then all rotated by θ about hinge k of the elements, hence creating the boundary lines for a plate structure. These are then scaled by L/l so they obtain a length of a single period. Translating the boundary lines by a distance equal to r_j , perpendicularly to themselves, the hinges k becomes positioned fully within the boundary of the plates.

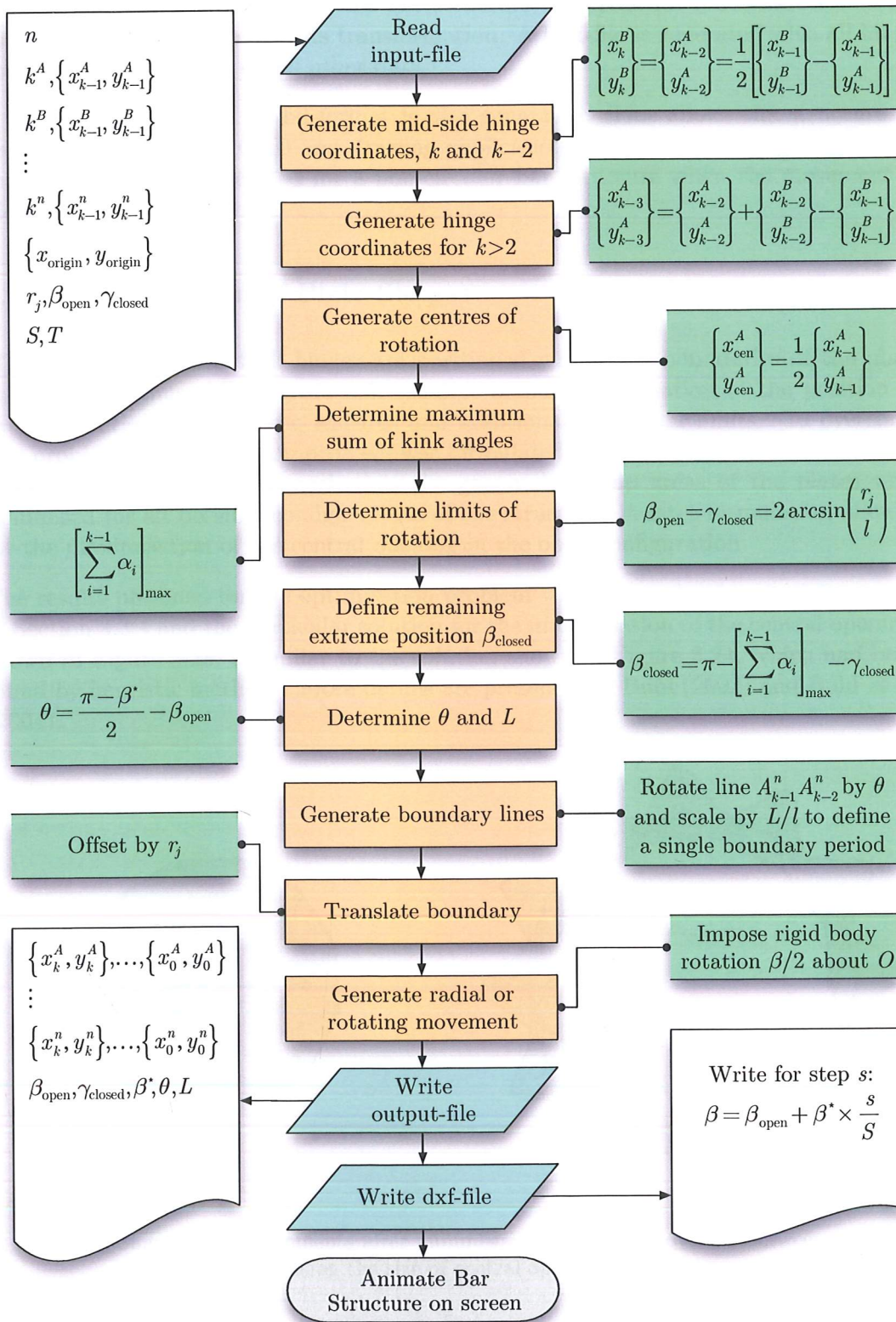


Figure 3.27: Schematic of GTD application

GTD generates an animation of the bar structure on screen for immediate visual inspection of the structure and its transformation. A text-file is generated with all hinge coordinates for $\beta_{open} = 0$ and other data.

A graphical output-file in dxf-format is also generated. This allows the structure to be imported into most CAD and drawing applications for post-processing. Figure 3.9 shows the drawing generated for a non-circular bar structure when the movement is plotted in four steps.

3.4.1 Optimisation of Plate Shapes

GTD does not detect if all hinges are positioned within the boundaries of the plate elements and thus the program still requires manual optimisation of the position of the boundaries, any periodic features and additional rotational limits. To overcome this problem an optimisation problem was formulated for cover elements by Buhl *et al.* (2004). It was formulated such that the gap and overlap areas of the plates were minimised for all possible configurations of the structure. A later formulation allowed for the maximisation of the central opening in the open configuration.

The results obtained for the optimisation problem verify the rule of periodicity stated in Section 3.3.4 and the particular solution for the maximisation of the central opening, shown in Figure 3.28, is similar to the solution shown in Figure 3.24, which had been found by heuristic methods. More details are presented in Buhl (2002) and Buhl *et al.* (2004).

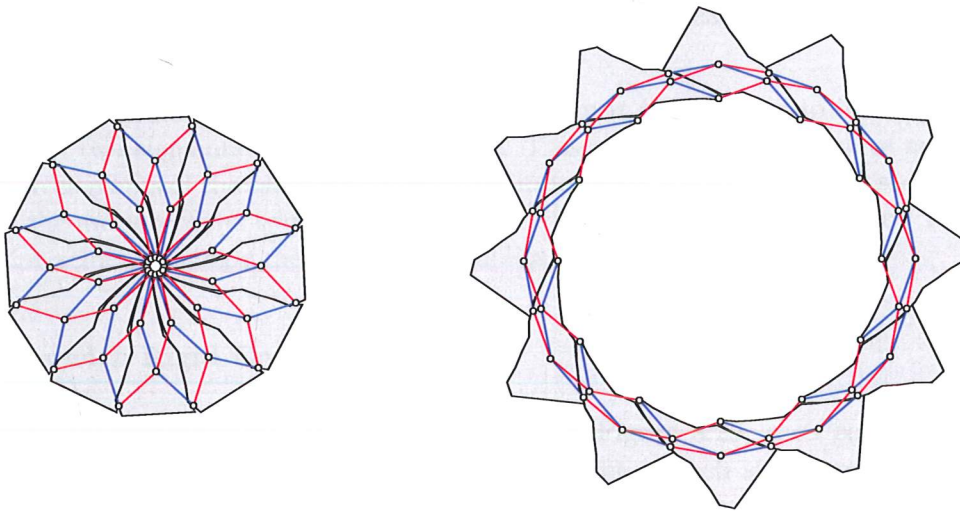


Figure 3.28: Shape of cover elements after minimising the gaps and overlap between cover elements and maximising the size of central opening in the open configuration (Buhl *et al.*, 2004)

3.5 Assemblies

For applications other than retractable roofs it is of interest that retractable bar and plate structures can be interconnected so they form larger assemblies. Such larger structures can be formed either by interconnecting the individual structures in their own flat plane, hence forming a two-dimensional *planar* assembly, or the structures can be rigidly connected to form a *stack* of such retractable structures. Assemblies of either type can be constructed so they possess only one internal degree of freedom and the motion of all individual structures in the assembly is hence synchronised.

3.5.1 Planar Assemblies

In Section 2.4.2 it was explained that the movement of a single layer in a bar structure can be a pure translation, and this was extended to structures formed by hinged plates in Section 3.3.3. If a single element in this layer is fixed, then no rigid body motions are allowed and all other plates in the structure will move in relation to this one element as the structure expands and retracts.

For an identical neighbouring structure, the above is also true and hence a single element in this second structure can also be fixed without inhibiting its movement. The two neighbouring structures now both have a single element fixed and thus no relative motion occurs between these two elements during the motion of either structure. Hence these two elements can be rigidly connected to each other without interfering with the motion of either of the two individual structures. This, however, does not provide an assembly with a single degree of freedom. Instead two independent mechanisms are present in this assembly.

To generate an assembly with only a single mechanism it is necessary to interconnect a minimum of two elements from each structure. This would allow the relative motion between two elements of the same structure to be imposed on the neighbouring structure and hence the motion of the two individual structures will become synchronised. Three methods for achieving single mechanism assemblies are presented below.

Assemblies with Rigid Connections

Consider the two identical bar structures I and II in Figure 3.29, each consisting of sixteen angulated elements. Say, the bottom, blue layer of each structure translates during the motion of each structure while the elements in the top, red layer undergo rigid body rotations about fixed points, as described in Section 2.4.2. The two structures are identical and the motion of element A_I in structure I is therefore identical to that of A_{II} in structure II and similarly for elements B_I, B_{II} . Hence the angulated elements A_I and A_{II} can be rigidly connected to each other without inhibiting the motion of either structure if the connection is physically made in a way such that it does not interfere with any of the angulated elements. This is also possible for angulated elements B_I and B_{II} . The bars connecting elements A_I and B_I form four-bar linkages, as described in Section 3.3.1, and they are parallel and of identical length to the bars connecting

elements A_{II} and B_{II} . Hence $A_I A_{II}$ and $B_I B_{II}$ can be considered to be two rigid bodies interconnected by four parallel bars and forming a single degree of freedom mechanism. Therefore, a relative movement between elements A_I and B_I results in an identical relative movement between elements A_{II} and B_{II} and hence the assembly is now a single degree of freedom system. Additional connections can be made between other element pairs without changing this property. It is possible to use this method also for non-identical structures.

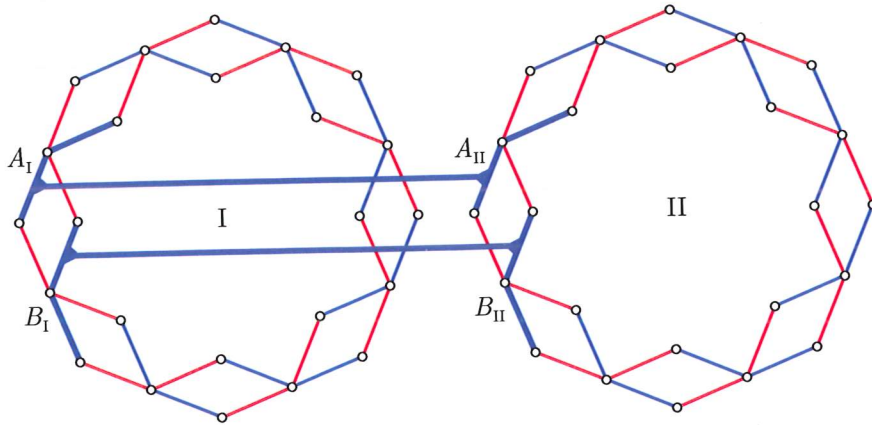


Figure 3.29: Single degree of freedom assembly of two rigidly interconnected structures

Assemblies with Congruent Linkages

The method proposed above requires a third layer of elements to make the connections and it is therefore not ideal for some applications. However, by considering each of the two bar structures as rings of identical linkages a simpler method of interconnecting the structures is proposed. From Figure 3.30(a) it can be seen that if both bar structures are in identical configurations, then rhombuses I and II are identical and their four bars in the top, red layer are parallel to each other, as are the four bars in the bottom, blue layer. By positioning the two structures such that I and II are coinciding, the shared rhombus $A_0 A_1 C_0 B_1$ is created in Figure 3.30(b). Noting linkage $A_0 A_1 C_0 B_1$ is able to shear identically to both I and II, the internal mechanisms of both ring structures have been preserved. However, their movement is now synchronous as all linkages are identical to $A_0 A_1 C_0 B_1$. This is illustrated in Figure 3.31.

Around hinges A_0 and C_0 , in Figure 3.30(b), a number of bars are found to be overlapping. Note A_0 coincides with B_0 in Figure 3.30(b). Bar $A_0 A_1$ from the angulated element $A_2 A_0 A_1$ overlaps with bar $A_0 A_1$ from element $A_3 A_0 A_1$ and similarly there are three other overlaps at $B_0 B_1$, $C_0 A_1$ and $C_0 B_1$. The angle $A_2 A_0 A_3$ is constant throughout the motion as elements $A_2 A_0 A_1$ and $A_3 A_0 A_1$ are rigid. It is therefore possible to connect rigidly bars $A_0 A_1$, $A_0 A_2$ and $A_0 A_3$ to form the *branched* element, A , shown in Figure 3.30(c).

Following Figure 3.30(c) it can be seen that it is now possible for the rotation about hinge A_0 to be inhibited by B_1 coinciding with A_1 or A_2 , B_2 coinciding with A_2 or A_3 or B_3 coinciding with A_1 or A_3 . The limits for the motion of B_1 and B_3 are identical

elements A_{II} and B_{II} . Hence $A_I A_{II}$ and $B_I B_{II}$ can be considered to be two rigid bodies interconnected by four parallel bars and forming a single degree of freedom mechanism. Therefore, a relative movement between elements A_I and B_I results in an identical relative movement between elements A_{II} and B_{II} and hence the assembly is now a single degree of freedom system. Additional connections can be made between other element pairs without changing this property. It is possible to use this method also for non-identical structures.

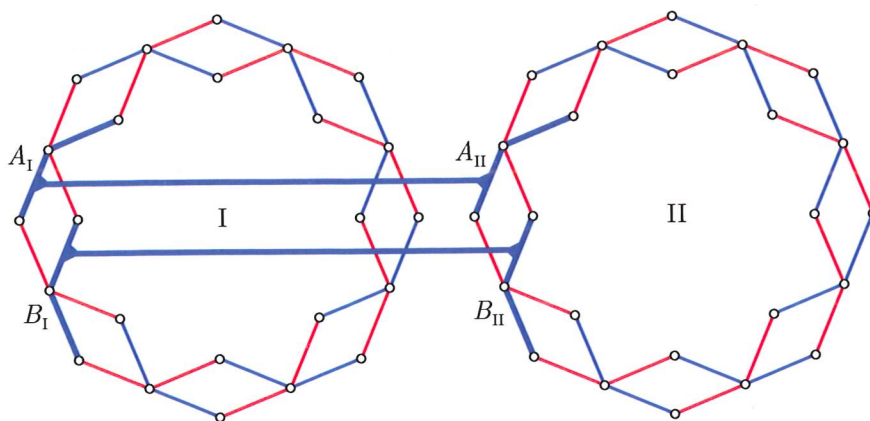


Figure 3.29: Single degree of freedom assembly of two rigidly interconnected structures

Assemblies with Congruent Linkages

The method proposed above requires a third layer of elements to make the connections and it is therefore not ideal for some applications. However, by considering each of the two bar structures as rings of identical linkages a simpler method of interconnecting the structures is proposed. From Figure 3.30(a) it can be seen that if both bar structures are in identical configurations, then rhombuses I and II are identical and their four bars in the top, red layer are parallel to each other, as are the four bars in the bottom, blue layer. By positioning the two structures such that I and II are coinciding, the shared rhombus $A_0 A_1 C_0 B_1$ is created in Figure 3.30(b). Noting linkage $A_0 A_1 C_0 B_1$ is able to shear identically to both I and II, the internal mechanisms of both ring structures have been preserved. However, their movement is now synchronous as all linkages are identical to $A_0 A_1 C_0 B_1$. This is illustrated in Figure 3.31.

Around hinges A_0 and C_0 , in Figure 3.30(b), a number of bars are found to be overlapping. Note A_0 coincides with B_0 in Figure 3.30(b). Bar $A_0 A_1$ from the angulated element $A_2 A_0 A_1$ overlaps with bar $A_0 A_1$ from element $A_3 A_0 A_1$ and similarly there are three other overlaps at $B_0 B_1$, $C_0 A_1$ and $C_0 B_1$. The angle $A_2 A_0 A_3$ is constant throughout the motion as elements $A_2 A_0 A_1$ and $A_3 A_0 A_1$ are rigid. It is therefore possible to connect rigidly bars $A_0 A_1$, $A_0 A_2$ and $A_0 A_3$ to form the *branched* element, A , shown in Figure 3.30(c).

Following Figure 3.30(c) it can be seen that it is now possible for the rotation about hinge A_0 to be inhibited by B_1 coinciding with A_1 or A_2 , B_2 coinciding with A_2 or A_3 or B_3 coinciding with A_1 or A_3 . The limits for the motion of B_1 and B_3 are identical

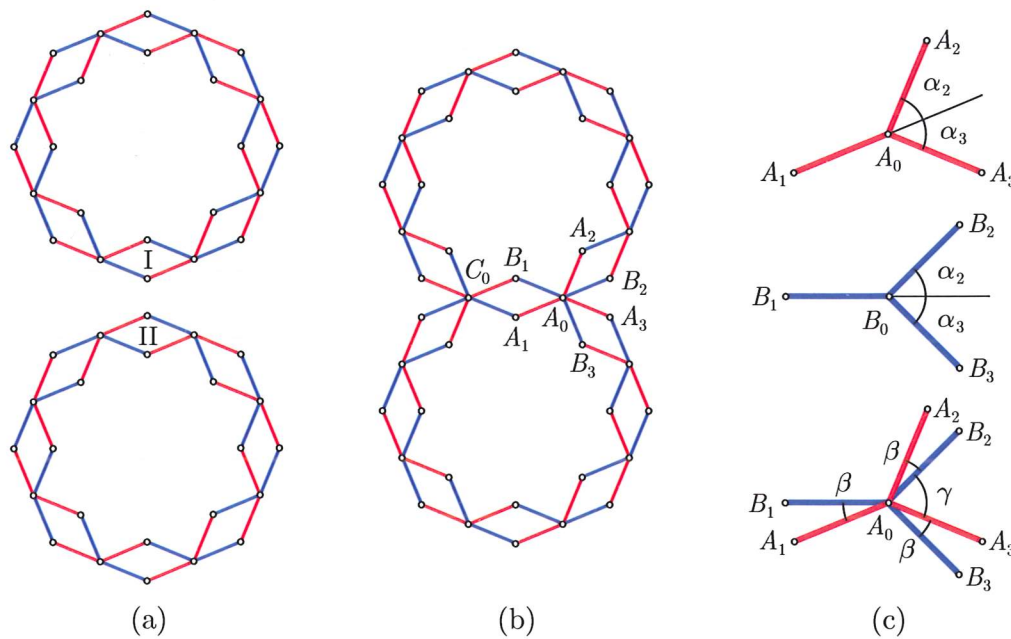


Figure 3.30: (a) Two identical structures, (b) Single degree of freedom assembly of two structures with congruent rhombus, and (c) Branched pantographic elements

and can be found to be identical to those derived for the simple angulated element in Section 3.2.2. For B_2 the limit is found from $2\alpha = \beta + \gamma$ giving an *alternative total rotation angle*, denoted β' , and found for circular structures similarly to Equation 3.25

$$\beta' = 2\alpha - \zeta \quad (3.42)$$

where the limit ζ is determined from Equation 3.28. The possible motion for the assembly is then the lower value of either β^* or β' . If $n/2 = k + 1$ for all structures in the assembly, then $\beta^* = \beta'$ as illustrated by the assembly shown in Figure 3.31 where both rings have $n; k = 8; 3$. Using the methods presented in Section 3.3.2 the assembly has been covered with rigid cover elements and can be constructed as a plate structure, as shown in Figure 3.31. The assembly shown can be further expanded by adding additional ring structures with one or more linkages congruent with the assembly.

Non-identical structures formed by similar rhombuses or parallelograms can also be assembled using this method if they have a single identical linkage through which the structures can be joined. This, however, complicates the process of establishing the rotation angle β' as the two kink angles at A_0 and at C_0 are no longer required to be identical. The rotation angle β' , for non-circular structures formed by similar rhombuses, is then determined by the smallest sum of the kinks at either A_0 or C_0 ,

$$\beta'_A = \alpha_2 + \alpha_3 - \zeta \quad (3.43)$$

and β'_C can be found similarly.

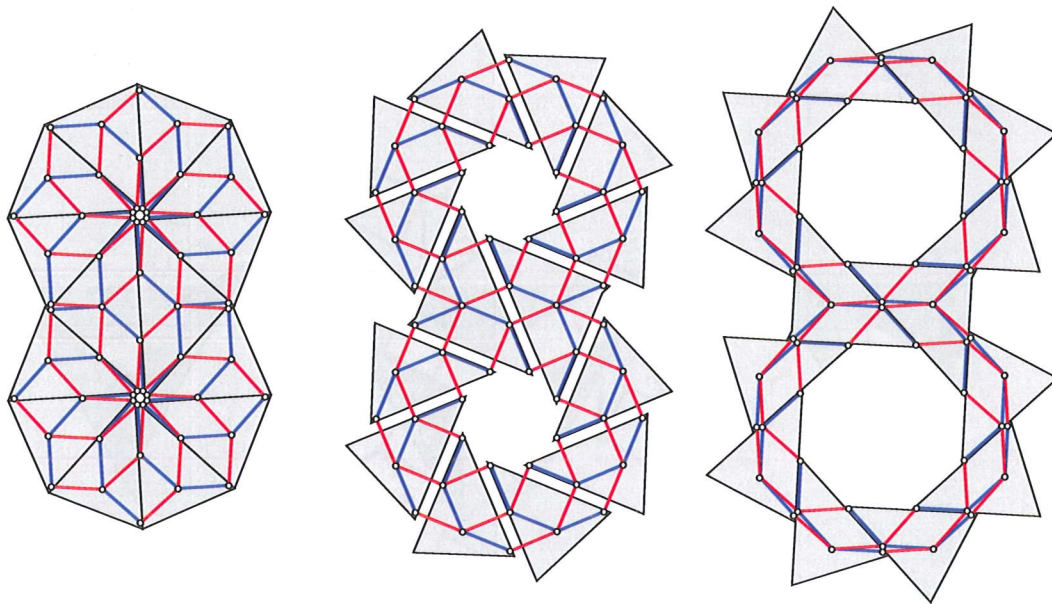


Figure 3.31: Single degree of freedom assembly covered by rigid elements

Assemblies with Node Structures

Another method for generating planar assemblies also uses the idea of a congruent linkage, i.e. a linkage that is part of two structures each with a single internal mechanism. Above, only structures formed by rings of angulated or multi-angulated elements were considered. However, other types of closed loop structures based on four-bar linkages exist and can be assembled using the method of congruent linkages. You (2000) proposed a novel type of closed loop expandable structures, as described in Section 2.4.1, formed both by linkages and rigid elements as shown in Figures 2.22. You showed that such a structure has a single internal degree of freedom and it is possible to design such structures so that the linkages are formed by three identical rhombuses, Figure 3.32. Each of these three linkages can form part of a ring structure. This is illustrated in Figure 3.32(b). The original three-linkage structure is called the *node* structure as it has the function of a central node for the ring structures.

As all of the *four* individual closed loop structures are single degree of freedom mechanisms, the motion of the assembly is synchronised. The limit for the shearing of the linkages forming parts of the node structure is determined by the shape of the rigid element boundaries and, following Equation 3.39, $\beta^* = \pi$ for $\beta_{\text{open}} = \gamma_{\text{closed}} = 0$ and $\theta = 0$. Figure 3.32 shows $\beta^* \approx \pi$. Hence, the rotation angle for the assembly is governed by the ring structures. A model of an assembly using a node structure is shown in Figure 3.33. The model is based on a three-linkage node structure and three bar structures with $n; k = 6; 2$ and is similar to that shown in Figure 3.32.

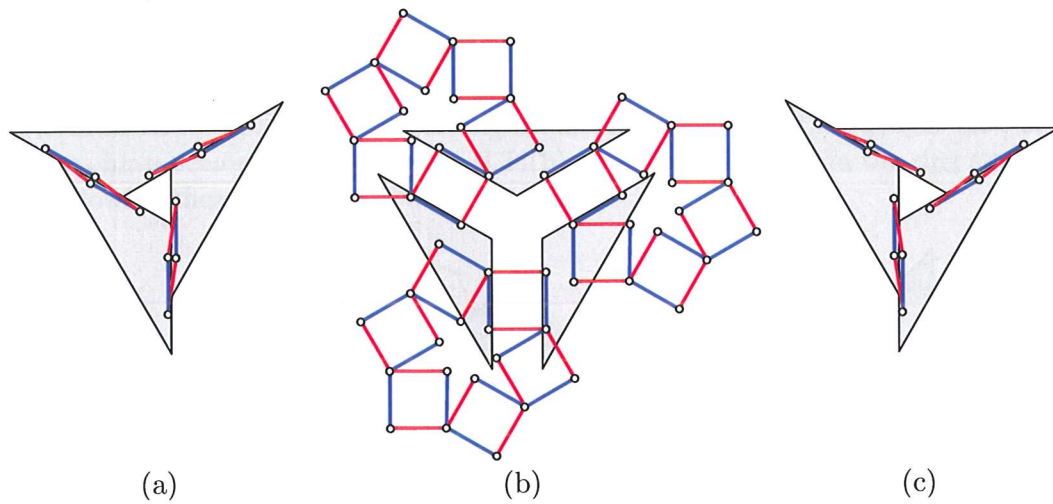


Figure 3.32: Movement in node structure and its linkages forming parts of three ring structures

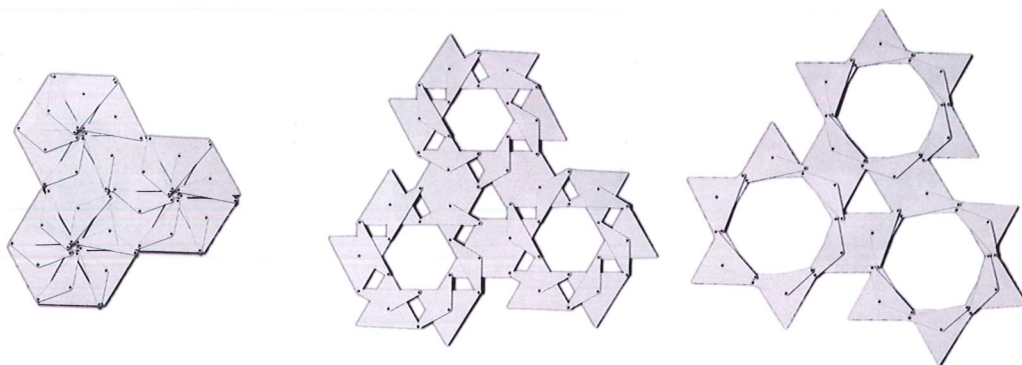


Figure 3.33: Cardboard model of assembly with node structure

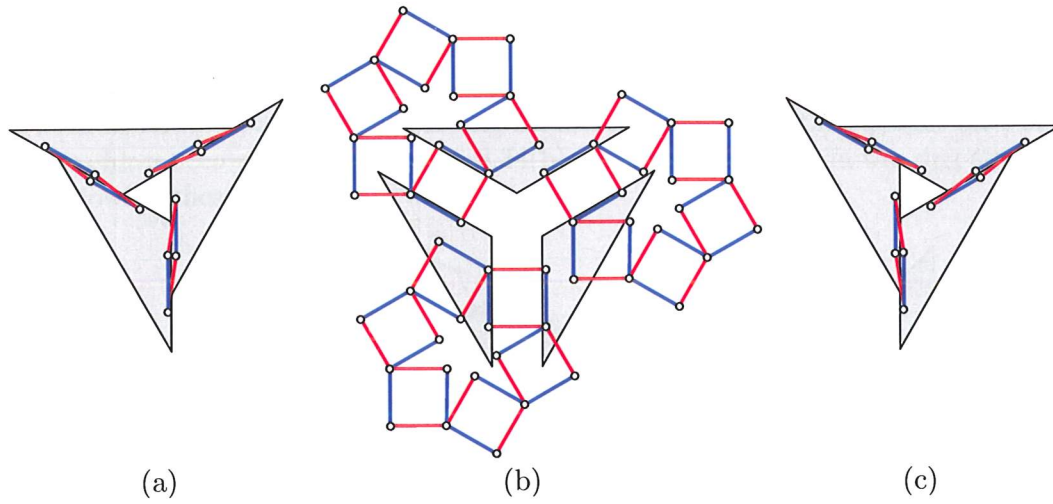


Figure 3.32: Movement in node structure and its linkages forming parts of three ring structures

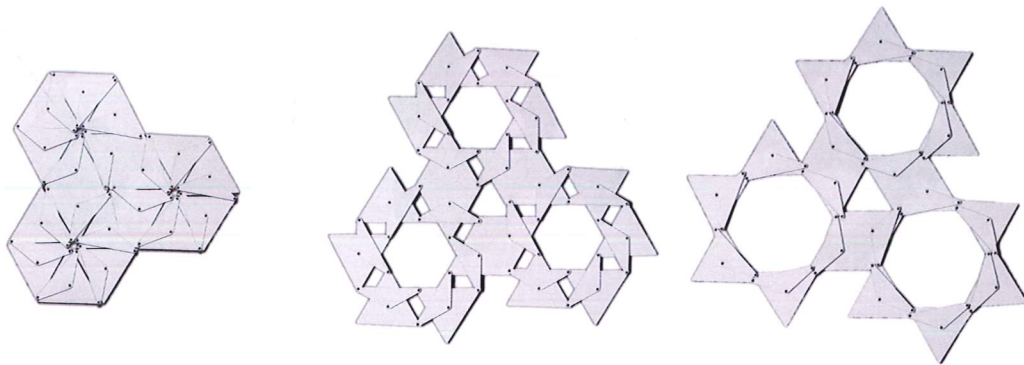


Figure 3.33: Cardboard model of assembly with node structure

Two Degree of Freedom Assemblies

If a node structure is formed by *four* four-bar linkages at right angles it is possible to design an assembly with two distinct internal degrees of freedom. With the rigid node elements at right angles to each other, the linkages become collinear pairwise and hence each pair can be sheared without motion occurring in the other pair of linkages. This is shown in Figure 3.34 and it can be seen it is also possible for this type of structure to perform as nodes in an assembly of ring structures. Note that the straight bars in the linkages have been replaced in Figure 3.34(b) by kinked elements in the ring structure, thus allowing these to have $n = 8$.

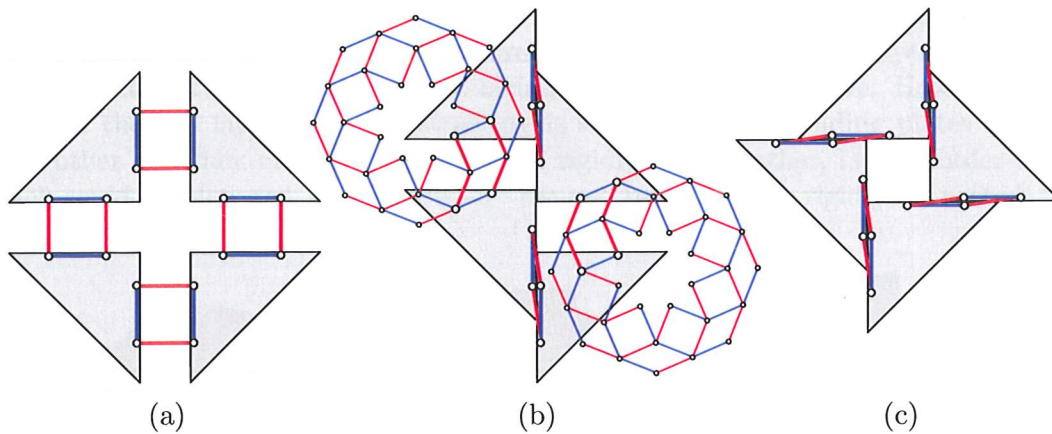


Figure 3.34: Two degree of freedom node structure (a) Intermediate configuration, (b) One linkage pair fully sheared, and (c) Both linkage pairs fully sheared

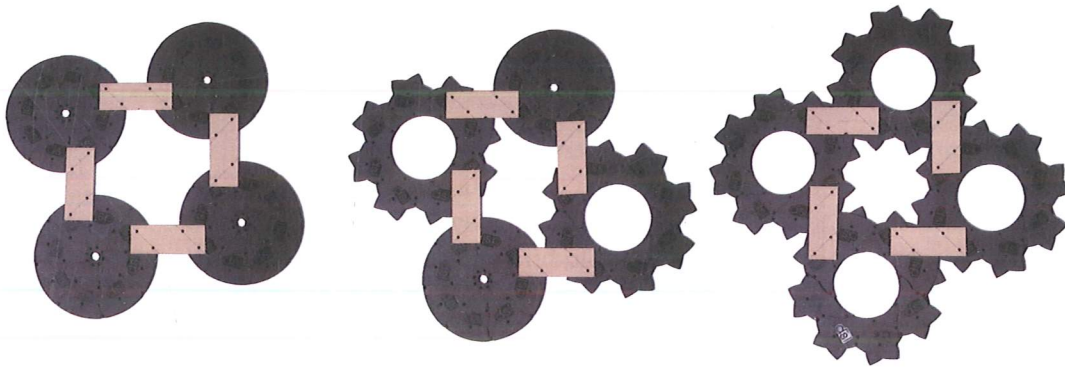


Figure 3.35: Model of node assembly with two degrees of freedom

The model shown in Figure 3.35 consists of four plastic structures identical to that shown in Figure 3.24. The node structure is formed by cardboard fixed to the structures.

3.5.2 Stack Assemblies

It is possible to generate assemblies by vertically stacking and connecting individually expandable structures. It will be shown that this can be done for non-identical structures of almost any plan shape.

Initially consider the circular plate structure, consisting of sixteen identical plate elements, shown in Figure 3.36. Expanding the structure in a radial motion the hinges move along radial lines and the two layers of plates translate and rotate. The rotations of the two layers of plates are equal but opposite, i.e. the top, red layer rotates *clockwise* as the structure expands while the bottom, blue layer rotates *counter-clockwise*. Because of the opposite rotation, it is not possible to connect rigidly two identical structures stacked one above the other as the top, red, layer of the lower structure cannot be connected to the facing lower, blue, layer above. However, if the order of the two layers in either structure is swapped, corresponding plates will face each other and they can then be connected rigidly to each other, i.e. the order of the stack could be blue, red, red, blue where the two red layers are rigidly connected.

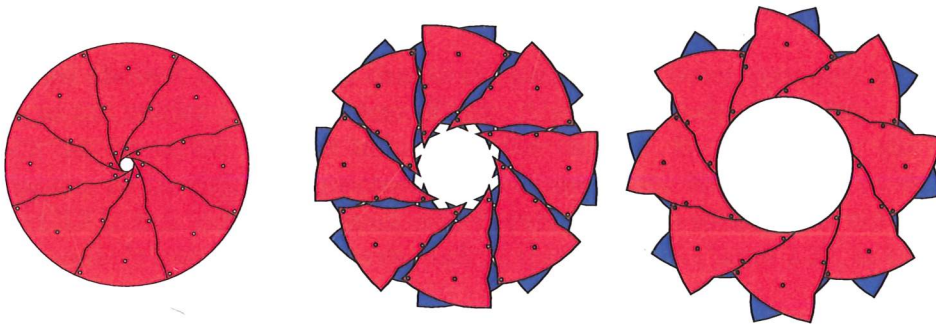


Figure 3.36: Expandable circular plate structure.

It is therefore possible to construct stacked assemblies of identical structures if the order of the layers is arranged such that layers that are to be connected have identical rotations, i.e. blue to blue and red to red. As the plates of the facing layers are identical the connections between the layers can be solid blocks with boundaries identical to those of the plates or any parts of such a solid, i.e. rods or walls.

Physical Model

The individual structures used for stacked assemblies do not have to be identical as long as they have an identical movement. An example of this is shown in Figure 3.37 where three plastic structures identical to that shown in Figure 3.36 have been connected to each other using foam board. To allow the structure to have a spherical profile in the closed configuration two of the plastic structures have had their outer boundaries trimmed so the outer diameter of these structures has been reduced and hence the outermost hinges have also been removed. Their motion remains unchanged as it is controlled by the boundary angle θ which is unchanged. The connecting blocks of foam

board have been cut using an AWJ machine such that their boundaries are identical to the boundaries of the plastic plates, including the periodic circular arcs along the boundary clearly visible in Figure 3.37.



Figure 3.37: Model of stacked assembly

Stacking Non-identical Structures

As described above it is possible to change the shape of the outer boundary of the plate elements as the motion is independent of this. Also the periodic deviations along each boundary can be varied without influencing the motion. By considering the motion of two layers, to be rigidly connected, as rotations about fixed points, as described in Section 3.2.2, it is possible to stack non-circular and non-identical structures. This allows expandable free-form structures, such as that shown in Figure 3.38, to be formed.

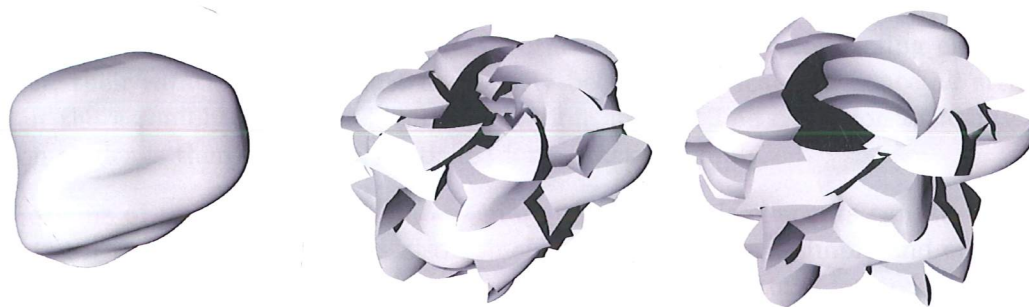


Figure 3.38: Expandable free-form or “blob” structure (Jensen & Pellegrino, 2004)

One such assembly is shown in Figure 3.39. The assembly consists of the two structures I and II, structure I is shown with dashed lines. They consist of angulated elements formed using the polygon method. The polygons used for forming the elements are not congruent and the origins O_I and O_{II} do not coincide. Let the red elements, which are to be rigidly connected, rotate about fixed points and the blue elements translate. By scaling each polygon to half its original size about its origin the centres of rotation are found, as previously discussed in Section 3.2.3. Note the design is such that three centres of rotation for structure I coincide with three centres of rotation for structure II.

These coinciding centres of rotation are denoted A_{cen} , B_{cen} and C_{cen} . Let the rotation angle for both structures β^* be governed by the largest kink angle in the assembly at hinge D_{II} . Hence all red elements will undergo identical rotations about their respective centres of rotation. The two angulated elements with internal hinges A_I and A_{II} both rotate about A_{cen} and the rotations they undergo are identical. Hence there is no relative movement between the two elements and they can be rigidly connected to each other. This is illustrated by the rigid plate $\triangle A_I A_{II} A_{cen}$ in Figure 3.39. Similarly, elements B_I and B_{II} , with the coinciding centre of rotation B_{cen} and C_I , C_{II} with the centre C_{cen} , can be rigidly connected.

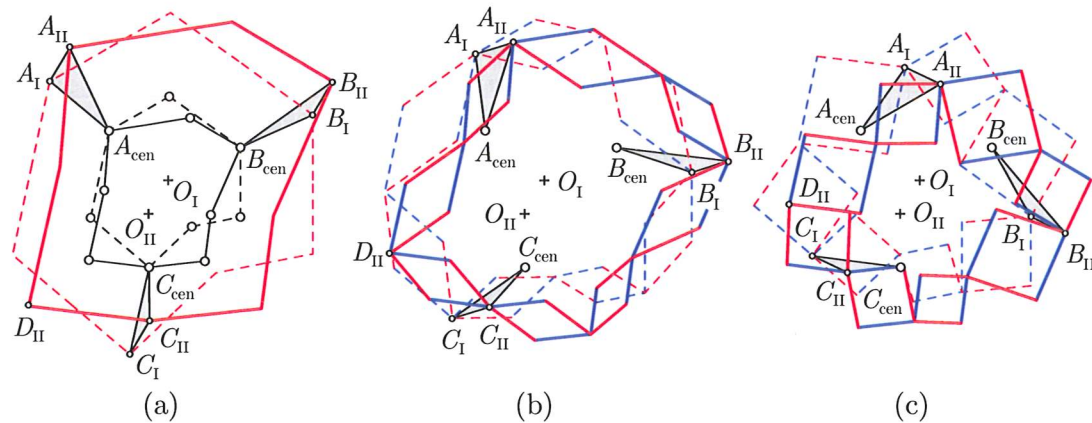


Figure 3.39: Stack assembly of two structures with three rigid connections

More generally, an element can be connected rigidly to another if their centres of rotation coincide and they undergo identical rotations. By rigidly connecting elements together, their rotation angles must necessarily become identical and hence all structures in the assembly will have identical rotation angles. The condition of identical rotation angles is therefore always satisfied for a stack assembly.

If the origins of two structures in an assembly coincide, their elements can be rigidly connected if their polygon vertices also coincide. This provides a simple and effective method for generating stack assemblies from non-circular structures formed using the polygon method, i.e. both structures of similar rhombuses and parallelograms can be assembled, see also Jensen & Pellegrino (2004) for further details.

3.6 Discussion

Extending the findings of Hoberman (1990), You & Pellegrino (1997) and Kassabian *et al.* (1999) a new uniform approach to describing the transformation of retractable bar structures has been developed. This new approach is based on the possibility of describing the motion of all parts of such structures by means of simple rotations. This allows the governing equations to be greatly simplified, and hence it has been possible to put forward simple design methods for previously unknown types of structures such as assemblies and plate structures.

In Section 3.2.2 an expression for the rotation undergone through the transformation of the structure, Equation 3.14, has been obtained by considering the overall circular motion of the element. This expression was then shown to be identical to Equation 3.18, obtained by considering the relative rotations undergone at each of the scissor hinges. Hence, as shown in Section 3.2.4, it has been possible to link the local limits on the motion of the structure, due to physical properties such as finite hinge sizes, to the overall ability of both circular and non-circular structures to transform.

Considering the shearing deformation of a four-bar linkage, a general condition, Equation 3.31, on the shape of the boundary between two rigid covering elements has been formulated. This equation guarantees that the plates do not restrict the motion of the linkage while resulting in a gap and overlap free surface in either extreme position of the linkage. As any bar structure is formed by a series of interconnected four-bar linkages it has thus been shown that it is possible to cover such bar structures with plates without inhibiting the motion of the structure.

In fact, instead of covering a bar structure with plates, it has been found to be possible to remove the angulated elements and connect the plates directly, by means of scissor hinges at exactly the same locations as in the original bar structure. Thus, the kinematic behaviour of the expandable structure remains unchanged. In Section 3.3.4 it was shown that, as long as the plate boundaries have a certain periodic shape, they need not be straight.

General methods for connecting expandable structures of any plan shape have been developed, leading to the possibility of creating plan or stacked assemblies composed of individual expandable structures when certain conditions are satisfied.

Figure 3.40 shows a novel concept for retractable stadium roof formed by hinged plates. The next step in the development is to investigate the structural and mechanical properties of such a roof.

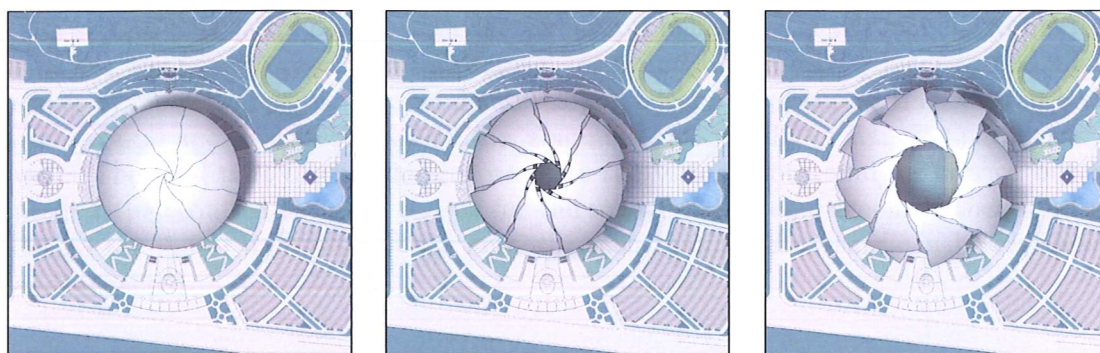


Figure 3.40: Proposed use of plate structure to cover a sporting venue

Chapter 4

Design and Construction of Retractable Plate Structure

4.1 Introduction

In the previous chapter a method for constructing retractable roof structures formed by hinged plates was proposed. This chapter presents the design and analysis carried out to construct a 1.3 meter diameter model of such a retractable plate structure.

The first part of the chapter presents the model, its individual parts in their final form and overall design considerations while the second and third parts are concerned with various aspects of the design process. This order of contents has been chosen as it reflects the design process for this model, where initial choices of material and design were subsequently verified and improved through analysis.

The second part is concerned with the structural behaviour of the model. Numerical analysis was used to predict the structural behaviour under gravity loading, and allow sizing of the model parts. The model developed is capable of supporting itself in both a horizontal and a vertical position, i.e. spanning horizontally or hanging parallel to a wall. The final part of this chapter presents the virtual work analysis carried out to predict the required actuator torque for the model. This requirement is then used to design the motor and gears of the actuator such that the structure can be expanded and retracted.

4.2 Parts of the Model

The model was designed and constructed with the aim of gaining an increased understanding of the structural behaviour of hinged plate structures and to provide a mechanical concept model of exhibition standard, for demonstration purposes. It was decided to pursue a model that would be capable of supporting itself when arranged in both a horizontal and a vertical position. It was later found practical to only exhibit the model hanging in its vertical position as this would result in a simpler and more

elegant demonstration of the proposed new concept.

The model is supported using thin steel cables, as a hanging system provides the simplest and least visually intrusive means of supporting the model. The overall size of the model was determined so that it can be transported in a small van in its assembled state, hence simplifying the hinges as they are not required to allow the model to be disassembled.

The geometry of the model is similar to the plastic model presented in Figure 3.24 with its perfect circular opening in the extreme open configuration. Its main dimensions are listed in Table 4.1. Each layer contains eight identical plate elements, and each plate is connected through four hinges, hence $n;k = 8;3$.

	Radius:	Diameter:
Maximum open size, R_{open}	857 mm	1714 mm
Minimum closed size, R_{closed}	652 mm	1304 mm
Maximum opening, r_{open}	368 mm	736 mm
Minimum opening, r_{closed}	42 mm	84 mm
Hinge radius, r_j	16 mm	
r^*	368 mm	

Table 4.1: Main dimensions of physical model

4.2.1 Plate Elements

The model was designed to only carry its own weight; to limit self-weight deflections a light, stiff material was to be used for the plate elements. However, the visual appearance was also taken into account in the material selection process. Carbon Fibre Reinforced Plastic (CFRP) was chosen, after considering materials such as wood, perspex and aluminium plates or honeycomb sandwich panels. The selection was made on the basis of its high stiffness-to-weight ratio, accurate machineability, low complexity of hinge connections and aesthetics.

The individual plate elements were machined in pairs from 800×600 mm sheets of 3 mm thick CFRP using diamond tipped tools. This was carried out at the BNFL's rehearsal and test facility at Littlebrook, UK, on a vacuum table and was computer controlled allowing for very high precision.

As the retractable plate structures presented in Section 3.3.3 are overdetermined, i.e. a number of hinges could be removed without introducing any additional degrees of freedom, stresses can be introduced in the structure if the hinges are out of position. Hence, high precision in the manufacturing process was needed to limit the built-in stresses of the model. During final assembly limited stresses were introduced by hand to overcome the approximate 0.5 mm error at the last 2 connections assembled.

The thickness of 3 mm for the plate elements was determined using numerical analysis as described in Section 4.3.1. The weight of the plate elements and hence the overall model weight is approximately 13.5 kg. The overall weight influences the torque requirement for the actuator, as will be discussed in Section 4.4.

4.2.2 Hinges

During the retraction of the structure, the plates in the two layers rotate relative to each other, as described in Section 3.2.2, and hence the connections made between the layers must allow this rotation. However, for the structure to carry its own weight in both its horizontal and vertical positions the same connections must be able to transfer both in-plane and out-of-plane shear and out-of-plane bending between the connected plates, Section 4.3.1. The hinges were thus designed such that an aluminium pin is fully restrained in the lower of the two plates and connected through a ball-bearing to the upper plate. This permits rotation about the axis of the pin, while all other degrees of freedom are constrained. The use of ball bearings nearly eliminates the friction in the hinges and hence the required actuator torque is reduced, as described in Section 4.4.1.

As shown in Figure 4.1 all three interfaces between plates, pin and ball-bearing were glued using DP490, an epoxy based structural adhesive from 3M. To provide extra contact surface for the adhesive and for ease of assembly, flanged bearings were used. The pin was shaped so it would act as a spacer between the layers and fit into holes in the plates identical to those used for the bearings, thus allowing all plates to be identical, see Figure 4.1.

A minimum edge distance between the hinges and the boundary of the plates was included in the design, by using a hinge radius of $r_j = 16$ mm instead of the physical size of $r = 5$ mm when determining the limits for the movement of the structure and the plate boundaries as described in Chapter 3.2.4.

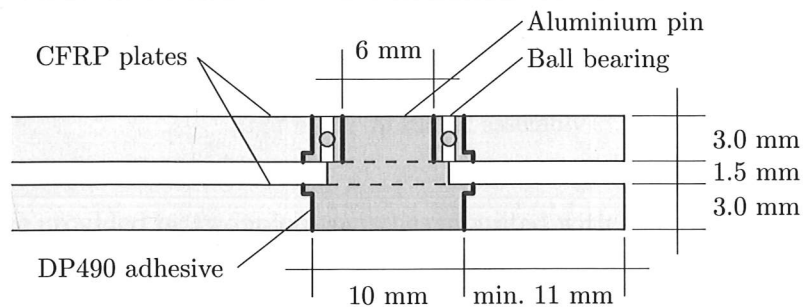


Figure 4.1: Hinge with a single rotational degree of freedom, scale 2:1

4.2.3 Actuator Assembly

An earlier model of a circular bar structure formed by multi-angulated beam elements had been retracted and expanded using a system of cables and springs (Kassabian,

1997), to demonstrate a solution that could be employed at large scale. A simpler actuation system was developed for the current plate model. Rather than imposing a change in the diagonal length of one or more of the rhombuses formed by the hinged elements of the structure, the new solution directly imposes a relative rotation between two elements in different layers, and by reversing the relative rotation it opens or closes the structure. Further details are given in Section 4.4.

The relative rotation is imposed by a Maxon 12V electrical motor, (a) in Figure 4.2, through two gearing units and a friction clutch (b), all housed in the actuator assembly shown in Figure 4.2. The entire assembly is rigidly attached to the upper plate of the structure with four screws while the shaft for the wheel gear (c), which can rotate relative to the rest of the assembly, is rigidly attached to the lower plate using adhesive and mechanical keys. The rotation of the worm gear (d) causes the assembly to rotate relative to the wheel gear (c) and hence a relative rotation between the upper and lower plates is imposed, driving the motion of the structure.

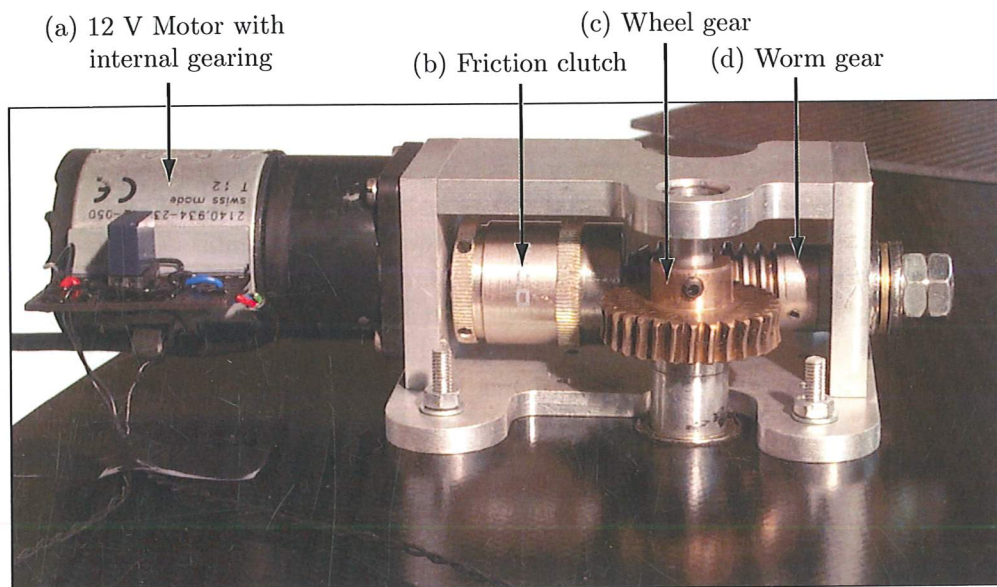


Figure 4.2: Actuator assembly

End stops are provided by two micro switches mounted with a spacing of a single period L along the boundary of the plate to which the actuator is attached. An adjustable pin mounted on the neighbouring plate is then able to activate one of the switches when the motion reaches either extreme, as shown in Figure 4.3. This reverses the current provided to the motor and the motion is hence also reversed. This simple control system provides the model with an autonomous actuation system. As a safeguard, an adjustable friction clutch, (b) in Figure 4.2, provides a slip mechanism preventing damage to both actuator and the structure in the event of failure of a switch or an object jamming the motion of the structure.

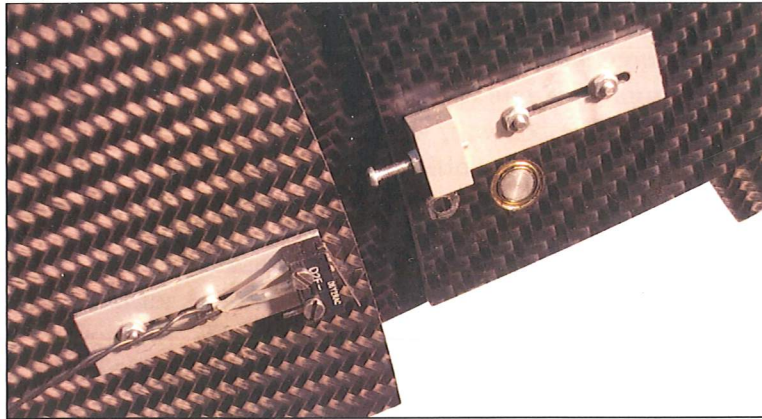


Figure 4.3: Switch and pin for reversing motion of model

4.2.4 Supports

Supports for the structure, when hung both vertically and horizontally, are provided by 2 mm diameter cables, as shown in Figures 4.10 and 4.11. These cables are attached to the enlarged hinges shown in Figure 4.4. By supporting the structure at the hinges both layers of plates can be supported at the same point. The choice of the number of supports and locations of these supports is treated in Sections 4.3.1 and 4.4.1. Using cables to support the model was preferred to other, more rigid support methods as it allows the supported hinges to move radially without the need for additional pivots, unlike the rigid pinned columns as used by Hoberman (1990) and Teall (1996). Of course, this type of solution is only possible where it is feasible to provide fixed attachment points for the cable hangers.

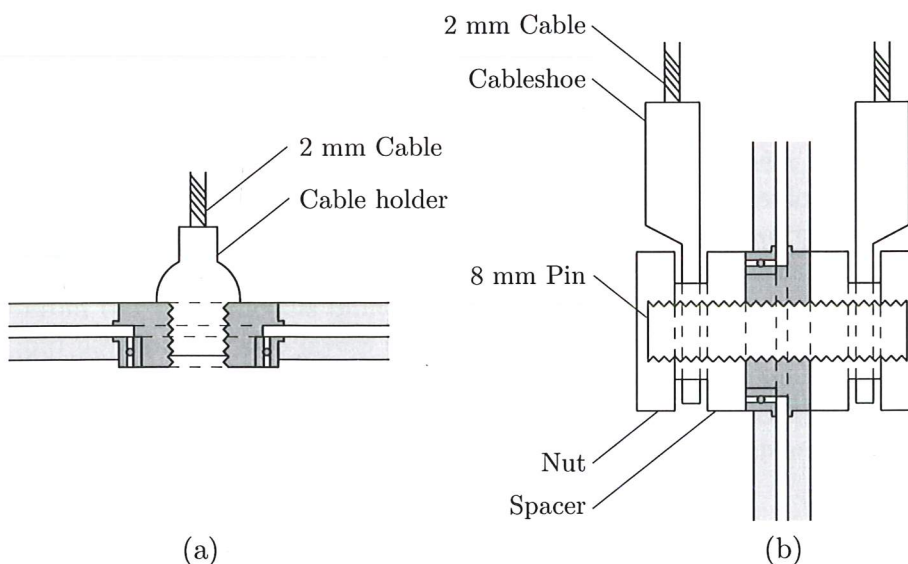


Figure 4.4: Details of support cables in (a) Horizontal, and (b) Vertical configurations, scale 1:1

Hanging in the horizontal plane the model is supported at eight points, as shown in Figure 4.4(a). When hung in the vertical configuration the model is only supported at the two mid-height support points, Figures 4.4(b) and 4.11, and hence near the centre of gravity. Therefore only limited stability is provided to the model by gravitational forces. To increase stability in the vertical position the actuator has been placed as low as possible to increase the stability of the model.

Above the model, the cables are attached to a ring which provides spacing between the attachment points for the cables and can be used both when hanging the model vertically and horizontally. The spacing between the attachment points for the cables is described in detail in Section 4.4.1. The ring can be supported by a tripod structure or hung from a suitable point in the exhibition space.

4.3 Structural Analysis

A finite element model was used to predict the internal forces in the model and its deformation when held both horizontal and vertical. The results were used for sizing the various parts of the model. To limit the scope of the analysis it was decided that only plates of constant thickness would be investigated.

A previous study by Teall (1996) investigated the structural behaviour of a projected, dome shaped, three layer retractable bar structure with a span of 2 m. The third layer, identical to the bottom layer, was required to provide additional stiffness and reduce bending in the hinges. The study was based on comparing the structural behaviour of a physical model with that of a numerical model simulated in a finite element package. The main finding was that inaccuracies in manufacturing and assembly, particularly in the hinges, would allow the structure to deflect up to *five* times the value predicted under self-weight. When additional loads were imposed on this model, the observed deflections were twice those predicted and Teall suggested the likely cause to be that the stiffness of the hinges has been overestimated by the numerical model, partly due to slip in the hinges.

Without substantially increasing the complexity of the finite element model, it seemed likely that similar difficulties in predicting the deformation behaviour would be encountered for the present model. Nonetheless, it did not seem worthwhile to pursue a complex study of the non-linear stiffness behaviour of the hinges for this concept model. From the small models built previously, it had been found necessary to introduce a gap between the two layers of plates that make up the structure, in order to eliminate contact and friction between the plates. Hence, the main reason for estimating the deformations of the structure was to establish the size of the gap needed to prevent such contacts and not the magnitude of the deflections themselves, though it was desirable that these should be kept visually small.

4.3.1 Finite Element Models

A finite element analysis was carried out in a number of stages. For each stage the complexity of the model was increased to allow more detailed and accurate modelling.

The analysis was performed using Pro/Engineer and its structural analysis package Pro/Mechanica (Parametric Technology Corporation, 2001). This application would allow the same numerical model to be analysed in a number of different configurations as the mechanism of the plate structure could also be kinematically modelled and hence the structure expanded or retracted as required. By defining two support and loading conditions, a single numerical model could hence be used for all configurations – hung both vertically and horizontally – resulting in a reduced modelling time. To limit the scope of the analysis the structure should only be analysed in the three configurations, open, half-deployed and closed.

Initially, a structure with 9 plates in each layer and four hinges in each layer, i.e. $n;k = 9;3$, was chosen for the analysis. A structure with 9 plates in each layer would allow the structure to be supported symmetrically by three supports while using 4 hinges for each plate would demonstrate the possibility of replacing multi-angulated elements with plates.

As a first step in modelling the full plate structure, a simple beam model of an equivalent bar structure with $n;k = 9;3$ was used to determine suitable supports and investigate methods for modelling the gap between the two layers of the structure. The next step was to model a single plate element supported at the position of its hinges. Thereby could meshing and local effects arising from concentrated loads at the support points, later to be connection points, be investigated.

The full model consisting of 18 plates and their connections was then modelled with 3 supports. This model displayed large deformations and the need for a large gap between the two layers to eliminate contact between plates of the two layers. Therefore, when the size of the model was increased by 40%, the number of supports was increased to 9 in the model. To reduce the actuator torque required for the model to open and close, a final design with 8 plates in each layer and 8 supports was adopted and analysed.

Bar Structure

A first analysis was carried out on a simple beam model, similar to that shown in Figure 4.5. This was done to find the best methods for modelling hinges and supports, as well as providing an easy-to-understand structural model of the complex load paths.

It was decided to model the hinges as short beam elements rigidly connected to the lower layer; these short beams are connected at the upper end by a revolute joint to the upper layer, as shown in Figure 4.5. This is identical to the method used by Teall (1996).

The supports were modelled as translational restraints in a polar coordinate system. For example, in Figure 4.5 each support prevents both vertical translation and changes in the polar angle, i.e. the support acts as a pinned, radial roller support with four degrees of freedom. As the internal mechanism of the structure has been removed – by removing the rotational freedom at a single hinge – these support conditions provide a statically determinate structure with six restraints in space.

A clear advantage was found in supporting the structure through the hinges as both

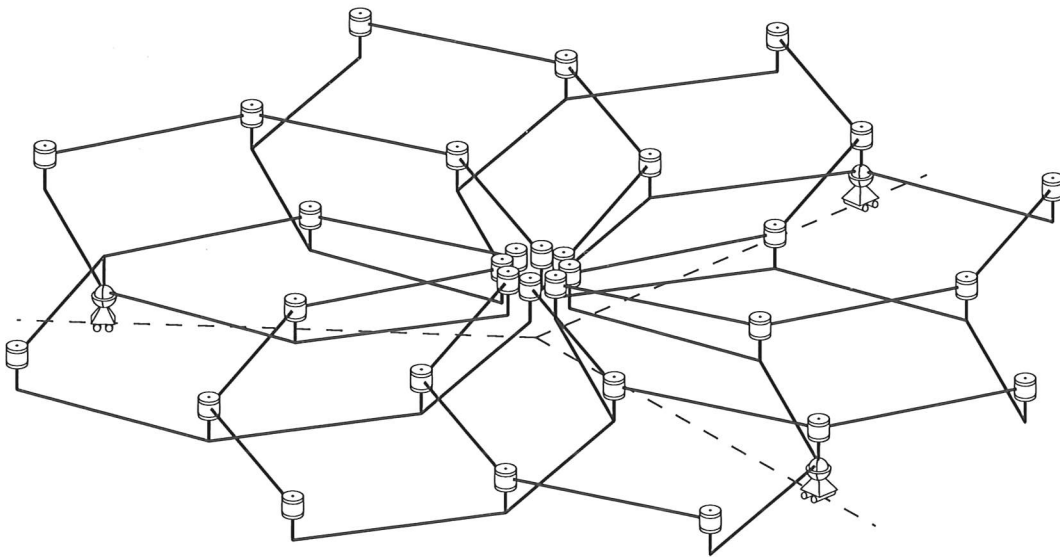


Figure 4.5: Beam model, with $n = 8$, in its closed configuration

layers can be supported at the same point reducing the deformation and internal forces in the structure.

Teall (1996) had supported his structure at the outermost hinges, to provide the maximum span. Using the beam model it was found that deflections and forces in the hinges would be substantially reduced if the structure was supported further toward the centre, as shown in Figure 4.5. As this result is also valid for the case of a plate structure, all models were supported similarly, at the third hinge from the centre.

Single Plate Element

A single plate element under self-weight was analysed to investigate the convergence of the finite element analysis when supported at four individual points. Any problems arising from this type of support would likely also occur when modelling connections between individual plates using short beam elements.

The plate was fully restrained at the four locations shown in Figure 4.6 and modelled using thin shell elements. A mesh of triangular and quadrilateral elements was generated by Pro/Mechanica and further subdivided by the application to obtain satisfactory convergence of the linear analysis performed. The unrefined mesh is shown in Figure 4.6(a). The thickness of the plate was initially set at 3 mm, and the quasi-isotropic CFRP laminate was modelled as isotropic with a Young's Modulus $E = 38,000 \text{ N/mm}^2$ and a Poisson's ratio $\nu = 0.4$.

The results exhibited, as expected, localised peak stresses and distortions at the supports. The stresses were small, though, with maximum principal stresses of 2 N/mm^2 . As can be seen from Figure 4.6(c) the extent of the local stresses is very limited and contained within the physical size of the hinges. Hence, in reality, the physical model

would not experience these peak stresses as they would be distributed within the size of the hinges.

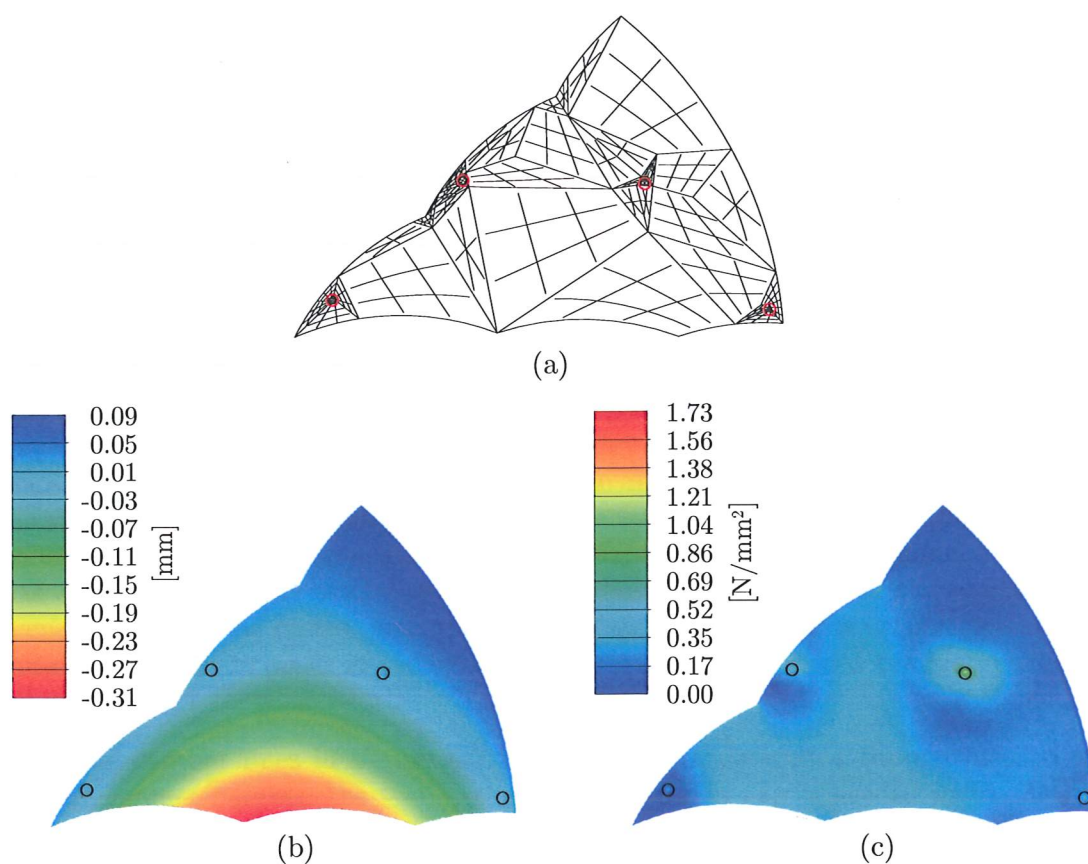


Figure 4.6: Single plate element under self-weight (a) Mesh for shell elements, (b) Deflections, and (c) Maximum principal stresses

Model with 9 Plates and 3 Supports

Models of the complete structure were set up from plate models identical to that used for the single plate analysis. Plates in different layers were interconnected using beam elements, as in the beam model. Problems were not encountered with stability or convergence for any of the following models.

Comparing early results for the structure held vertically and horizontally, it was found that the horizontal configuration would be governing the design, as the gravitational loading acts in the plane of the structure when it is held vertical and hence induces much smaller bending stresses. Therefore, only results from the horizontal configuration are presented below.

For a plate model with a thickness of 3 mm and a gap between the two layers of 0.5 mm the deflection contours are shown in Figure 4.7. From the contours it is clear that the two distinct layers of the model do not act as a single continuous plate. Instead

the behaviour is that of a series of interconnected plates. This results in large bending moments having to be transferred between the individual plates, through the hinges. The largest bending moments in the hinges, 1700 Nmm, were found at the second hinge from the centre. At this connection the largest principal stresses of 118 N/mm^2 were also found for the plates.

As seen in Figure 4.7, the maximum downward deflection is approximately 16 mm in both the closed and half-deployed configurations. The structure is hence most effective when open, where it acts like a continuous ring beam due to the hinges of the plates being closer to a circle. This is unlike the closed configuration, where the behaviour is more like three cantilevering assemblies of plates.

Increasing the thickness of the plates from 3 mm to 4 mm reduced the maximum deflection from 16 mm to 9 mm. However, importantly the paths of the contours were only changed marginally and hence it was concluded that there was little change in the way the structure carried the load, i.e. the relative stiffness between the hinges and the plates was largely unchanged. Changing the size of the gap between the two layers and the stiffness of the short beam elements used for modelling the hinges, within practical limits, had little influence on the overall structural behaviour of the model. Hence it was concluded that the most significant rotations and distortions at the hinges were occurring within the plates, near the joints. This lack of stiffness around the hinges cause three kinks to occur in the surface of the model in the closed configuration, see (a) in Figure 4.7.

From the contour lines in Figure 4.7 it is possible to determine the gap needed to prevent contact between the two layers. The maximum gap is needed in the closed configuration and between the two plates at the supported hinges. At (b) in Figure 4.7 it can be seen how the contour line for 5.0 mm upward deflection of the lower plate intersects with the contour line for 2.4 mm upwards deflection of the upper plate. Hence at the point of intersection a gap of minimum 2.6 mm between the two layers of plates is needed to avoid contact. For the entire structure a minimum gap of 3.0 mm was determined to be necessary.

Model with 9 Plates and 9 Supports

At this stage in it was decided to increase the size of the model by approximately 40%, to achieve a closed diameter of 1.3 m. This would not pose any problems for the model when exhibited vertically. However, in the horizontal configuration the deflections would be increased substantially and it was therefore decided to investigate the effect of increasing the number of supports.

Supporting the structure at *nine* hinges, all plates were directly supported at one location. This resulted, for a thickness of 3 mm, in a reduction of the maximum deflections from 16 mm to 11 mm, despite the increased size. As can be seen from Figure 4.8 the deflections are more uniformly distributed than in the model with only three supports. As a result the minimum gap between the two layers of plates could be reduced to less than 1 mm. Note that the required gap between the layers is now governed by the open position.

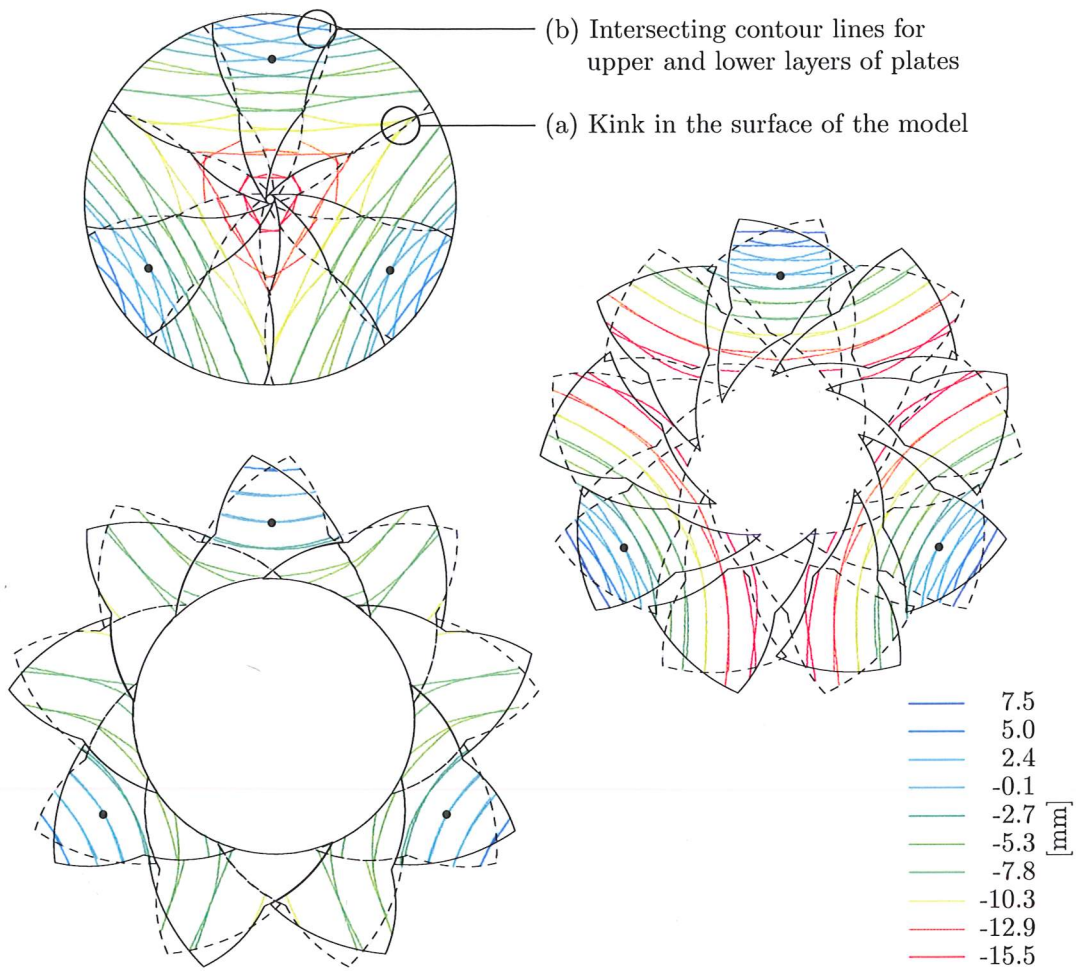


Figure 4.7: Contours of deflections under self-weight for $n = 9$ plate model, held horizontal, with three support points

It can also be seen that the hinge connections are now sufficiently stiff to ensure that at the connection points the slopes of the connected plates are nearly identical, unlike the previous model. It can hence be concluded that for any large span structure the stiffness requirements for the hinges are substantially lowered if all plates are directly supported.

Model with 8 Plates and 8 Supports

Based on the work carried out on the actuator assembly, presented in Section 4.4, it was decided to change the design to one with *eight* plates in each layer. An analysis was hence carried out on this updated but identically sized geometry.

Figure 4.9 shows that using fewer and wider plates further reduces the expected deflections. The maximum downward deflections are 8.3 mm, 7.4 mm and 5.2 mm for the closed, half-deployed and open configurations, respectively. Equally, the necessary gap between the layers was also reduced to about 0.6 mm. However, because of the known issues with predicting the stiffness of the hinges both this final numerical model and the physical model presented in Section 4.3.2 were built with a gap of 1.5 mm and hence a factor of 2.5 larger than necessary.

The maximum principal stress was found to be 32 N/mm^2 , at the connections; the stresses were much lower in regions without connections. Based on the maximum out-of-plane bending moment in the connecting beam elements of 600 Nmm, a diameter of 6 mm was found suitable for the Aluminium pin.

4.3.2 Physical Model

Based on the above results it was decided to build the $n = 8$ plate model using 3 mm thick CFRP as this would provide sufficient stiffness for the model. As no suitable miniature cylindrical bearings or double row ball-bearings were found, the model was built using single row ball-bearings as described in Section 4.2.2 resulting in a more flexible connection.

After assembly the model was hung horizontally, as shown in Figure 4.10. Measuring the vertical positions of the supported hinges and the boundaries of the plates it was found that deflections were four to six times those predicted by the numerical model, hence exceeding the factor of 2.5 introduced in the design of the gap amplitude. This was partly due to the additional bending introduced in the model by the inclined supports, which induces in-plane compression of the model and hence additional bending in the connections. However, the main cause was out-of-plane rotation in the bearings.

It was attempted to limit the deflections by attaching washers as spacers in the regions where contact or near-contact between the two layers was observed. It was also attempted to adjust the length of the support cables to redistribute the internal forces and deflections in the structure. However, the effects of these improvements were limited.

Despite the contact and resulting friction between the two layers of plates the actuator was found capable of opening and closing the model when hung horizontally.

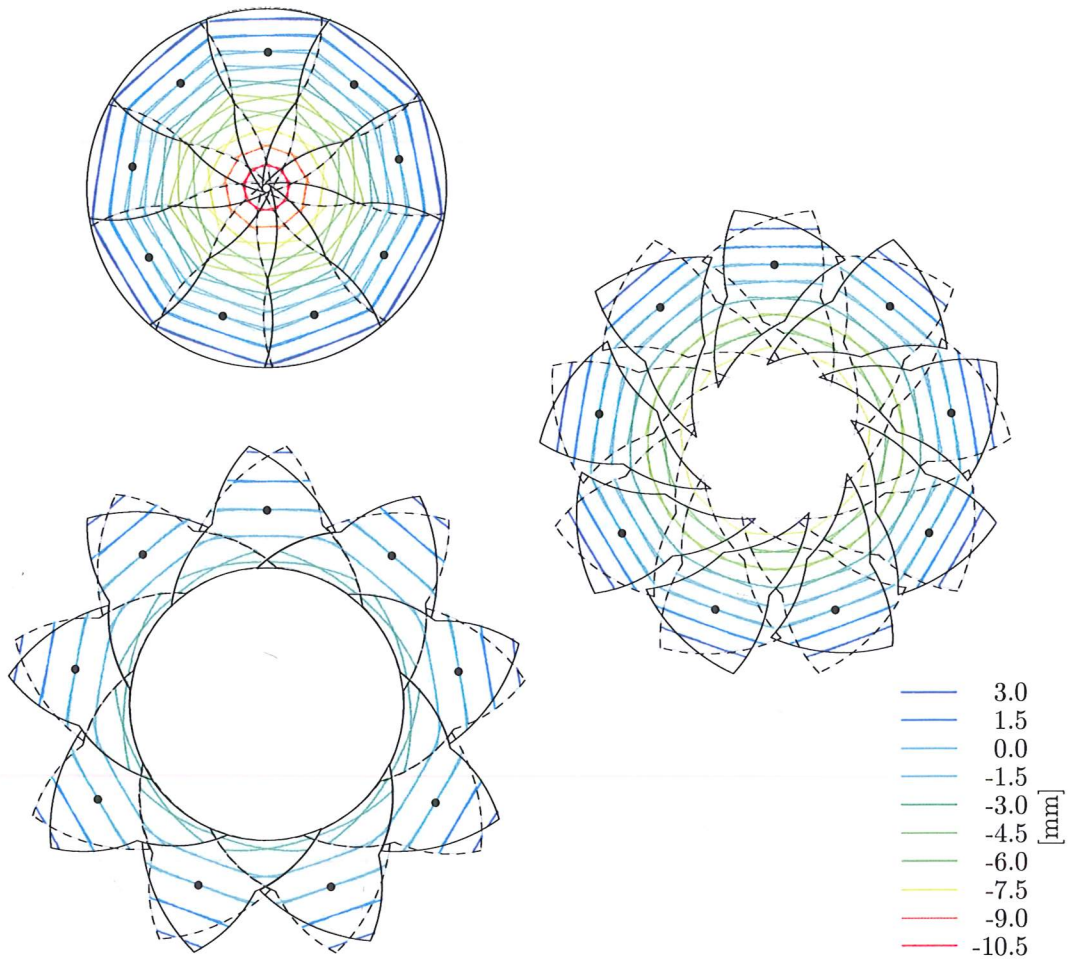


Figure 4.8: Contours of deflections under self-weight for $n = 9$ plate model, held horizontal, with nine support points

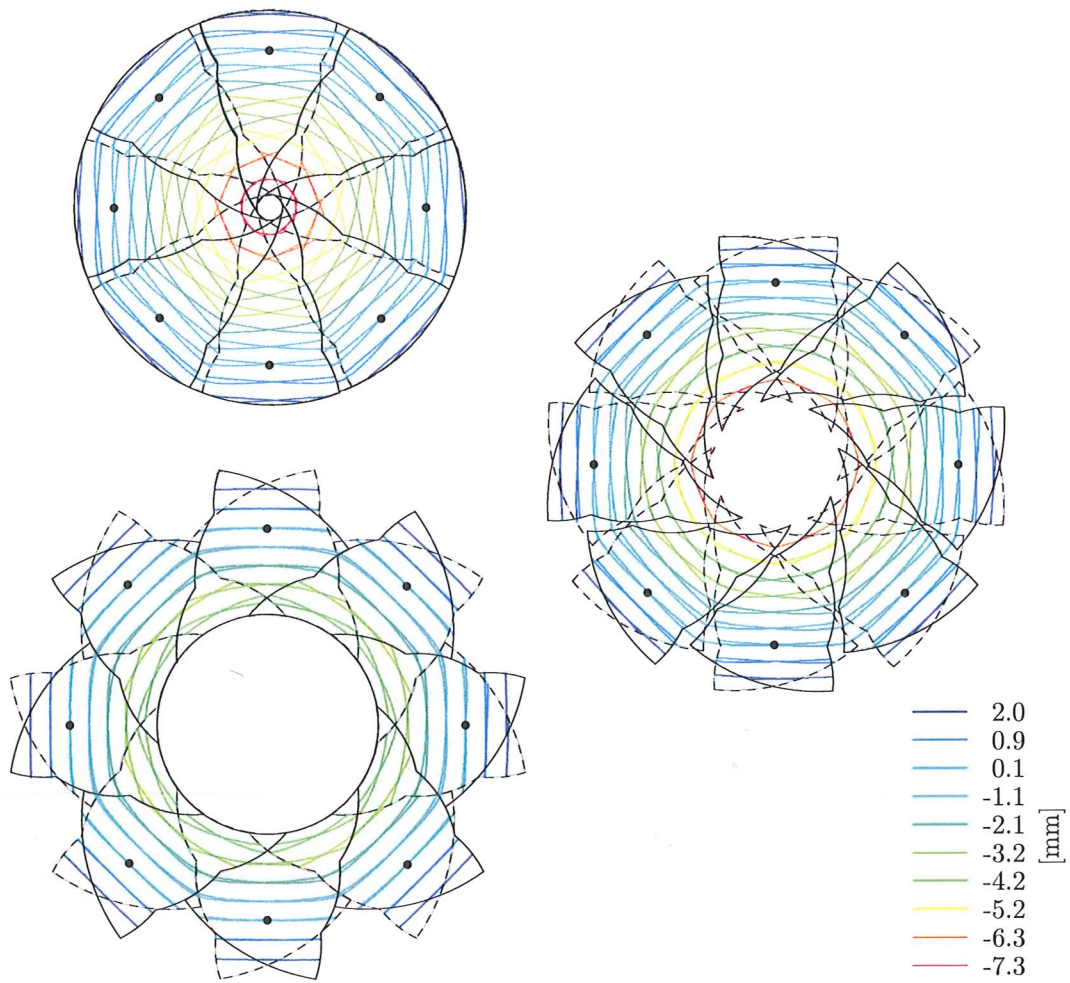


Figure 4.9: Contours of deflections under self-weight for $n = 8$ plate model, held horizontal, with eight support points

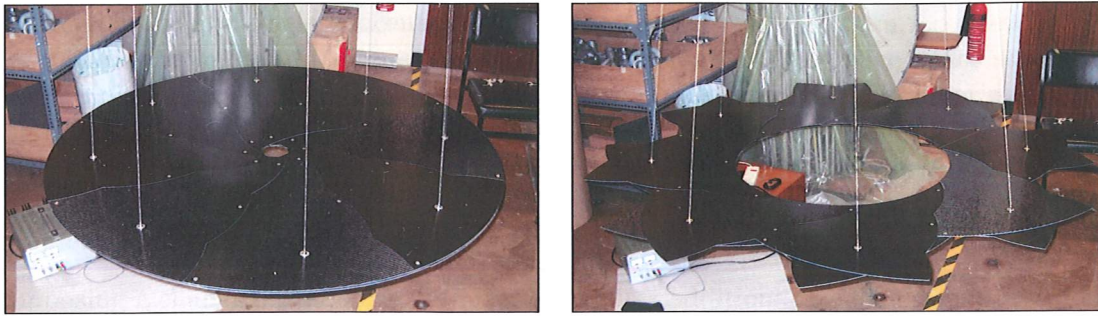


Figure 4.10: Physical model with $n = 8$, hung horizontally

Having concluded that the structure was capable of carrying its own weight, but the resulting deformations were too large, the model was rotated and hung vertically, supported by four cables at two hinges, as described in Section 4.4.

In this configuration, shown in Figure 4.11, the inclined supports were also imposing compression forces on the model and therefore a small-displacement snap-through buckling in the out-of-plane direction was observed. Hence the model was not completely flush when hanging vertically as the central out-of-plane displacement was approximately 10 mm. There was, however, no contact between the two layers of plates.

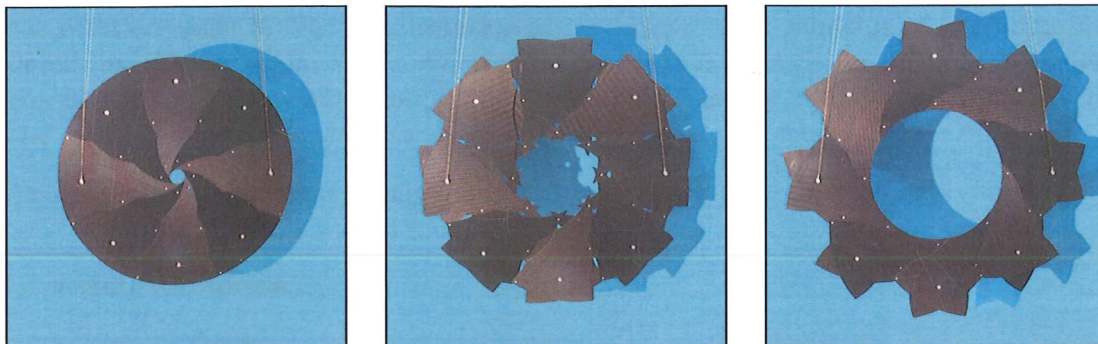


Figure 4.11: Physical model with $n = 8$, hung vertically

4.4 Actuator Design

In a previous study Kassabian (1997) had developed an actuation system for the 2 m span retractable model developed by Teall (1996). The actuation system was based on the concept of imposing a change in the diagonal length of one or more rhombus-shaped four-bar linkages that composed the structure. Such a change in length can be imposed using rigid bars, cables or – as in the Kassabian study – cables and springs.

Kassabian used a single, continuous cable loop to retract the model, by shortening

all diagonals in a single concentric ring of rhombuses. Springs were mounted in the perpendicular, radial direction of another ring of rhombuses and were hence stretched as the model was retracted. Elegantly, the stored elastic energy of the springs could then be used to close the structure when the tension in the cable loop was relaxed. Using virtual work analysis the position of the cable loop was optimised such that the tension and hence the torque in the motor used for shortening the cable loop was minimised. The same analysis was also used to position the springs optimally.

Imposing a change on the diagonal lengths requires additional diagonal members to be introduced in the structure. Such members were believed to be visually intrusive, and they would also increase the complexity of the model, hence it was decided to pursue an alternate actuation method. Noting that plates of different layers rotate relatively to one another, as described in Section 3.2.2, it was found that the model could also be actuated by simply imposing this relative rotation. As all plates rotate simultaneously, actuation is only required at a single connection point; both the expanding and retracting motions can be driven with a single rotational actuator.

Using virtual work, the actuator torque required to move the structure slowly through a series of equilibrium configurations was investigated.

4.4.1 Virtual Work Analysis

The relative rotation of the two connected plates was defined, as in Section 3.2.2, by the rotation angle β . The total rotation at the hinges of the model is $\beta^* = 60$ deg. To determine the maximum torque required for the retraction and expansion of the model, consider a general configuration of the structure defined by β and a small change in the rotation angle $d\beta$ and its associate virtual work.

The following forces were considered in the analysis:

- Actuator torque,
- Friction forces,
- Gravity

Due to symmetry and low accelerations in the structure all inertia forces were neglected.

Actuator Torque

The relative rotation between any two connected plates is identical and instantaneous for all hinges and hence the actual position of the actuator has no effect. The position of the actuator was hence governed by stability considerations, Section 4.2.4. Defining the actuator torque as T_a , the virtual work done by the actuator is then

$$W_a = T_a \times d\beta \quad (4.1)$$

Friction Forces

As explained in Section 4.3 the model was designed such that friction between the two layers of plates is avoided and hence the work done by friction between plates was assumed to be *zero*.

Friction in the individual hinges is limited to the friction in the ball-bearings and was given by $T_b = 470 \times 10^{-6}$ Nm (SMB Bearings Ltd., 2002). Hence the total work done by friction is

$$W_b = 4 \times 8 \times T_b \times d\beta \quad (4.2)$$

Gravity

The arrangement of the supports governs the motion of the centre of mass of the structure and hence the imposed gravitational forces.

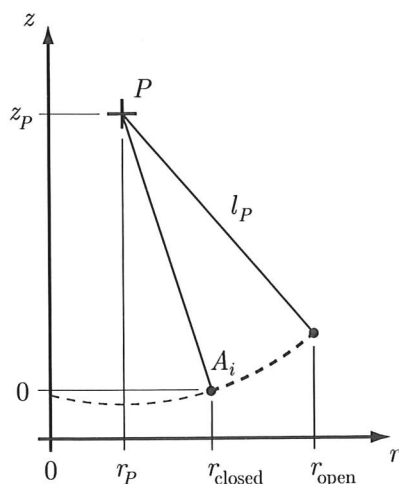
It is possible to support the model such that the supported hinges, which moves radially as the structure opens and closes, do not move in a horizontal plane perpendicular to the gravitational forces. An example of this is letting the supported hinges move along inclined paths as the structure opens and closes. As such inclined paths would lift and lower the entire structure, and hence its centre of mass, as it opens and closes, gravitational forces are imposed on the structure as it moves. Avoiding gravitational forces arising from the lifting of the entire model, a design with $n = 8$ was chosen as this would allow the supported hinges to move in a horizontal plane when hung both vertically and horizontally. In the vertical configuration the four mid-height hinges, of which two are supported, all move on a horizontal plane while when hung horizontally all hinges of the structure move in the horizontal plane of the structure.

However, by hanging the supported hinges from fixed points using cables the hinges must still vary their height z by a small amount when moving radially outwards in a vertical plane, as shown in Figure 4.12, independently of whether the structure hangs horizontally or vertically. Consider a hinge A_i of the plate structure that is connected by a hanger of length l_P to a fixed support point P , as shown in Figure 4.12, of coordinates r_P and z_P . The radial coordinate r for the hinge is found by rewriting Equation 3.3 using Figure 3.4

$$r(\beta) = 2r^* \sin \left(\frac{1}{2} \left(\gamma_{\text{closed}} + \sum_{i=1}^j \alpha_i + \beta \right) \right) = 2r^* \sin \left(\frac{\lambda + \beta}{2} \right) \quad (4.3)$$

where $\lambda = \gamma_{\text{closed}} + 2\alpha = 105^\circ$ when the structure is supported at the third hinge, i.e. $j = 2$, and $\gamma_{\text{closed}} = 15^\circ$.

From Figure 4.12 the height for the hinge A_i , and as the motion of all supported hinges

Figure 4.12: Vertical motion of hinge A_i hung from the fixed point P

are identical the height of the structure's centre of mass, is

$$z(r) = z_P - \sqrt{l_P^2 - (r - r_P)^2} \quad (4.4)$$

using Equation 4.3 to determine the radial coordinate r Equation 4.4 becomes

$$z(\beta) = z_P - \sqrt{l_P^2 - \left(2r^* \sin\left(\frac{\lambda + \beta}{2}\right) - r_P\right)^2} \quad (4.5)$$

The virtual work done by gravity is given by

$$W_g = G \times \frac{dz(\beta)}{d\beta} \times d\beta \quad (4.6)$$

where G is the total weight of the model and $dz(\beta)/d\beta$ is the derivative of Equation 4.5

$$\frac{dz(\beta)}{d\beta} = \frac{\left(2r^* \sin\left(\frac{\lambda + \beta}{2}\right) - r_P\right) \times r^* \cos\left(\frac{\lambda + \beta}{2}\right)}{\sqrt{4(r^*)^2 \sin^2\left(\frac{\lambda + \beta}{2}\right) + 4r_P r^* \sin\left(\frac{\lambda + \beta}{2}\right) - r_P^2 + l_P^2}} \quad (4.7)$$

In conclusion, the torque T_a required to impose a small change in the rotation angle β can be found by equating W_a to $W_b + W_g$.

Results

Determining the maximum torque required at any point during the motion, $T_{a,\max}$, it was found that the friction in the bearings was negligible in comparison to the gravity-induced forces and hence W_b was set to *zero*.

With the maximum length of the supporting cables set at $l_P = 1500$ mm, constrained by the height of the envisioned exhibition space, the required torque could be calculated as a function of the radial position, r_P , of the fixed point. Table 4.2 shows the maximum required torque for closing and opening the model when $G = 135$ N. A single fixed point at the centre of the structure corresponds to $r_P = 0$ mm while larger values corresponds to a ring of fixed points. The position $r_P = 557$ mm is right above the mid-point of the path taken by A_i and the resulting symmetric pendulum motion produce the lowest possible value of $T_{a,\max}$. A radial position of $r_P = 400$ mm was chosen for the design of the structure. Equations 4.5 and 4.7 are plotted for $r_P = 400$ mm in Figure 4.13.

Radial position, r_P	0 mm	400 mm	557 mm
Required torque, $T_{a,\max}$	9.88 Nm	2.50 Nm	0.63 Nm

Table 4.2: Maximum torque required for varying points of support

4.4.2 Gear Ratio

The gear ratio for the actuator was determined by the required maximum torque output, $T_{a,\max}$, and the required duration of an opening and closing cycle. This was set at 1 min. With a total rotation $2\beta^* = 120^\circ$ per cycle the required rate of rotation for the actuator was found from

$$\frac{120^\circ}{360^\circ} \times 1 \text{ min} = \frac{1}{3} \text{ r.p.m.} \quad (4.8)$$

No small electrical motor was found capable of delivering the required torque at this speed, and therefore gear units had to be included in the design. A motor with a built-in 200:1 gear was chosen. This is capable of producing a continuous torque of 0.6 Nm at 12 V with a speed of 8 r.p.m. An additional gear was therefore required. A worm and wheel gear was chosen for the second gear unit as this would allow the motor to be attached parallel to the plates, rather than perpendicular to them, and hence substantially reducing the visual impact of the actuator assembly. A 30:1 worm gear reduced the speed to approximately 1/4 r.p.m. thus providing the required rate of opening and closing. The efficiency of the worm gear is 39% (HPC Gears Ltd., 2002), and hence the maximum torque of the actuator assembly is

$$0.6 \text{ Nm} \times 0.39 \times 30 = 7.0 \text{ Nm} > 2.5 \text{ Nm} \quad (4.9)$$

hence exceeding the required torque $T_{a,\max}$ by a factor of almost 3. The actuator has been found to be capable of retracting and expanding the constructed model when hung both vertically and horizontally. The complete actuator assembly is shown mounted on the model in Figure 4.2.

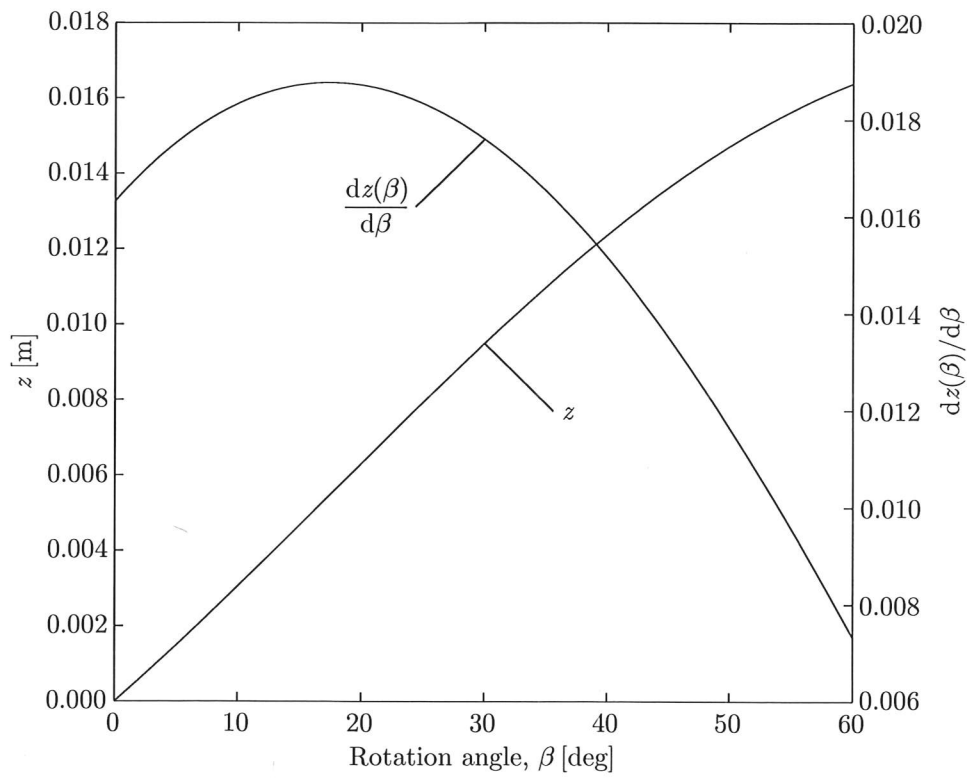


Figure 4.13: Vertical displacement and its derivative for $r_P = 400\text{mm}$

4.5 Discussion

A 1.3 metre diameter retractable plate structure has been constructed. It has been shown that such a structure, formed by hinged CFRP plates is capable of supporting its own weight in both a horizontal and a vertical configuration. A simple, effective method of autonomous actuation has also been developed.

Several important issues were encountered during the design and construction process. Using finite element modelling it was shown that such plate structures are capable of spanning horizontally if sufficient bending strength and stiffness are provided at the connections between the plates. It was found that, due to the discontinuity of the two layers, it was necessary to provide support for all plates as this significantly reduced the required strength and stiffness of the hinges. The analysis showed that forces in the plates were concentrated around the hinges and it is therefore possible to reduce the thickness of the plates if they are reinforced around the hinges. This would reduce the overall weight and hence the resulting gravity loads on the structure.

For the actuation of the model a new and innovative approach was taken. By using the relative rotation between plates of different layers it was found possible to design and construct a simple actuator with a minimum of moving parts and simple autonomous controls.

When hung in its vertical position the model is an elegant verification of the concept of hinged plate structures. Its simple supports and actuation method allow the model to be easily transported and erected.

Hanging the model horizontally large deflections were found. These were substantially larger than expected and were caused by the use of single row ball bearings, instead of double row or cylindrical bearings, in the hinges. However, the model did show that the structure is capable of both carrying itself and expanding and retracting when held horizontally.

Thus it has been proven that such plate structures can be used for retractable roof structures, though they would necessarily have to be designed with greater structural stiffness, particularly in the hinge elements. The structural efficiency of such a stiff structure remains to be proven.

Chapter 5

Spherical Retractable Structures: Preliminary Studies

5.1 Introduction

This chapter presents the background for two novel concepts for retractable structures that are presented in Chapters 6 and 7. Both structures are formed from interconnected curved, i.e. *three*-dimensional plate elements, unlike the structures presented in Chapters 3 and 4 which were based on flat, *two*-dimensional plate elements. Forming retractable structures in three-dimensions will allow these to take advantage of in-plane forces, unlike planar structures that rely on bending strength, and hence such structures have the potential for spanning greater distances efficiently. This work has been focused on spherical shapes.

The chapter begins by introducing some key concepts of spherical geometry and some relevant differences between the well-known Euclidean, two-dimensional geometry and the non-Euclidean, three-dimensional spherical geometry. Using these geometric tools it is shown that a ring structure formed by Hoberman's angulated elements is not mobile in non-Euclidean space, i.e. on the surface of a sphere.

Though the basic mechanism of the plate structures presented in Chapter 3 cannot be adopted for non-Euclidean geometry, it is investigated if the wedge-shaped plates that were derived in Section 3.3.2 are capable of forming a gap and overlap free spherical surface in both an open and a closed configuration. This geometric study proves that the shape of wedge-shaped *spherical plates* must be modified in order to be capable of forming an overlap-free open configuration. The basic geometric shape for such modified spherical plate elements is then derived and extended to allow greater variation of the shapes of the elements.

5.2 Spherical Geometry

This introduction to Spherical Geometry and Spherical Trigonometry contains a brief review of the concepts and tools used by the author to investigate the geometric properties of spherical structures. The review provides all necessary information for the reader to follow the arguments presented later in this chapter and is based on Carne (2002); Clough-Smith (1978); Lénárt (1996) and Wolfram Research (2004).

The sphere in Figure 5.1(a) can be defined as the surface on which all points are at an identical distance from a single point, the centre of the sphere O . A line from the centre of the sphere to the surface of the sphere is said to be *normal* to the surface. The length of this line is referred to as the *radius* of the sphere, R . The surface area of a sphere is $A(\text{sphere}) = 4\pi R^2$ and hence a unit sphere has the surface area 4π . Two *poles* of a sphere are always located diametrically opposite, i.e. a line drawn between the two poles P and P^* passes through the centre of the sphere. P^* is called the antipodal of P .

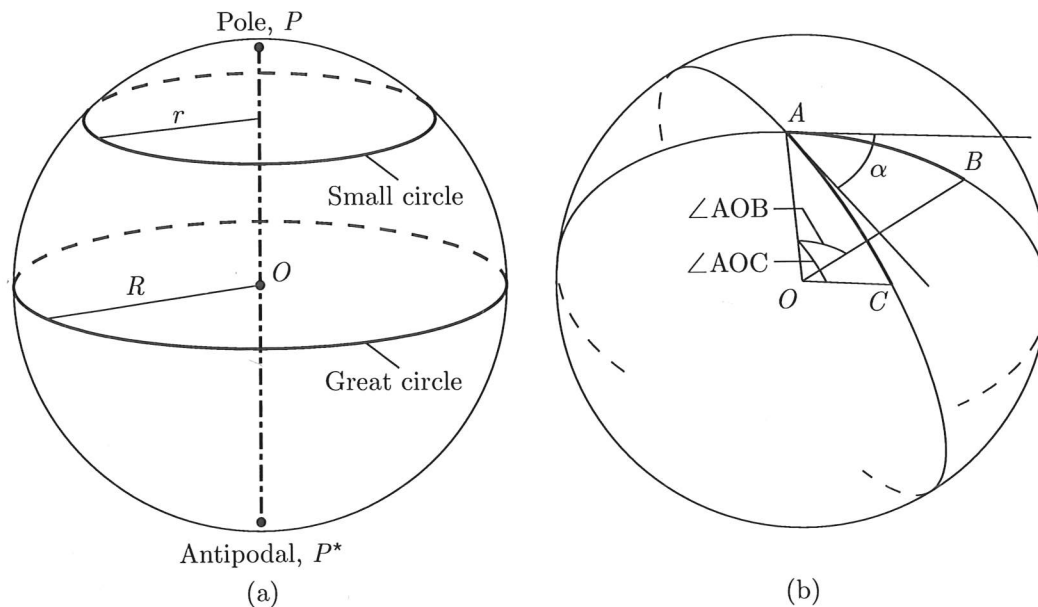


Figure 5.1: Spherical geometry (a) The sphere and its circles, and (b) Angle between great arcs and the angular length of these

A *great circle* is a circle on the sphere with the same radius as the sphere, i.e. the Equator and all meridians are great circles. Furthermore, the plane defined by a great circle will always pass through the centre of the sphere. Circles with a smaller radius are known as *small circles*. The plane defined by a small circle does not pass through the centre of the sphere. Figure 5.1(a) illustrates the concepts of poles, great and small circles.

Let a great circle pass through two points A and B on the sphere. This great circle consists of two segments or two *great arcs* from A to B . The shorter of these two great arcs defines the shortest distance between the two points, also known as a geodesic,

which is the spherical equivalent to a straight line. The angle between two great arcs or circles is defined as the angle between their tangents at the point of intersection. In Figure 5.1(b) the angle $\angle BAC$ between the arcs AB and AC , at their point of intersection A , is equal to α .

The *angular* length of a great arc is defined as the angle subtended by that arc at the centre of the sphere and hence the angular length of AB is $\angle AOB$. The *actual* length of the arc is equal to the angular length times the radius R . Unless stated otherwise the angular length is always assumed in the following.

A *lune* is a part of the surface bounded by two great arcs, which intersect at A and its antipodal A^* . From Figure 5.2(a) it can be seen that the angles subtended at the poles or *vertices* of the lune are identical. The spherical triangle $\triangle(ABC)$ in Figure 5.2(b) is similarly bounded by three great arcs, AB , AC and BC . The arcs intersect at the three vertices A , B and C . The angles between intersecting arcs, α , β and γ , are referred to as *vertex angles*.

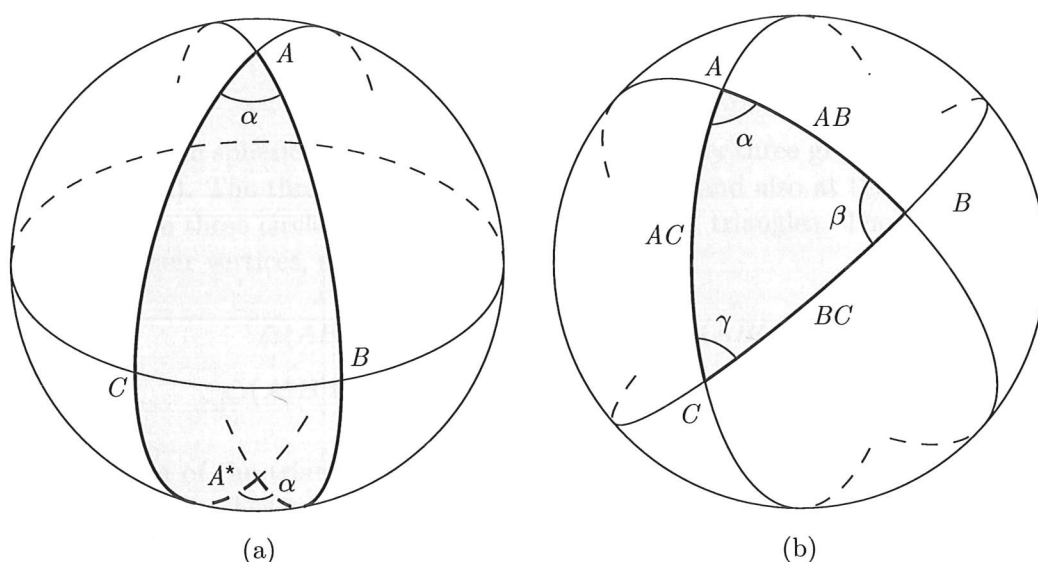


Figure 5.2: Spherical geometry (a) A lune, and (b) A spherical triangle

5.2.1 Spherical Excess

Next it is shown that the sum of the angles of a spherical triangle is not constant, but is equal to π plus the area of the bounded triangle. This is another significant difference from Euclidean geometry for which the sum of angles is always equal to π . The area is therefore often referred to as the *spherical excess*, \mathbf{E} , as it is the amount by which the sum of the angles in the spherical triangle exceeds the sum of the angles in a plane triangle.

To find the area of a spherical triangle consider first the area of the lune AA^* in Figure 5.2(a). From first principles the proportion of the total area of the sphere covered by the lune is identical to the vertex angle α divided by 2π . Hence the area of the lune is $\mathbf{A}(\text{lune}) = \mathbf{A}(\text{sphere}) \times \alpha/2\pi = 4\pi \times \alpha/2\pi = 2\alpha$.

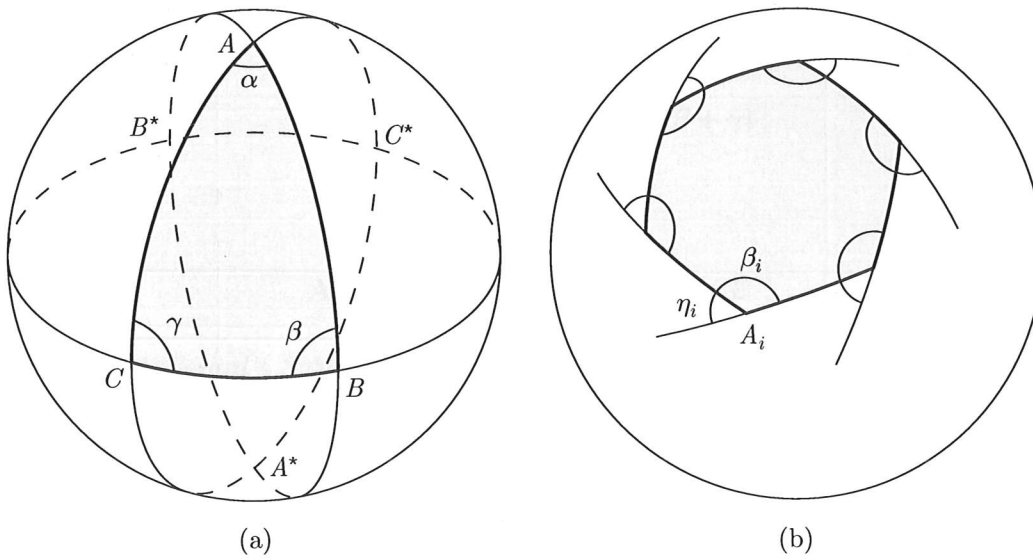


Figure 5.3: Spherical geometry (a) Area of a triangle, and (b) Area of a polygon

Now consider the spherical triangle $\Delta(ABC)$, bounded by three great circles as shown in Figure 5.3(a). The three circles intersect at A, B, C and also at the antipodals A^*, B^*, C^* . Hence these circles divide the sphere into *eight* triangles. These triangles are denoted by their vertices, so they are

$$\begin{aligned} &\Delta(ABC), \Delta(A^*BC), \Delta(AB^*C), \Delta(ABC^*), \\ &\Delta(A^*B^*C), \Delta(AB^*C^*), \Delta(A^*BC^*), \Delta(A^*B^*C^*) \end{aligned}$$

Note, the area of the triangle $\mathbf{A}(\Delta(ABC))$ is identical to $\mathbf{A}(\Delta(A^*B^*C^*))$. Similarly the areas of the other triangles are equal in pairs. Hence only the area of a single hemisphere, 2π , need be considered

$$\mathbf{A}(\Delta(ABC)) + \mathbf{A}(\Delta(A^*BC)) + \mathbf{A}(\Delta(AB^*C)) + \mathbf{A}(\Delta(ABC^*)) = 2\pi \quad (5.1)$$

The two triangles $\Delta(ABC)$ and $\Delta(A^*BC)$ form a lune with the area

$$\mathbf{A}(\Delta(ABC)) + \mathbf{A}(\Delta(A^*BC)) = 2\alpha \quad (5.2)$$

Similarly,

$$\mathbf{A}(\Delta(ABC)) + \mathbf{A}(\Delta(AB^*C)) = 2\beta \quad (5.3)$$

$$\mathbf{A}(\Delta(ABC)) + \mathbf{A}(\Delta(ABC^*)) = 2\gamma \quad (5.4)$$

Adding these together

$$3\mathbf{A}(\Delta(ABC)) + \mathbf{A}(\Delta(A^*BC)) + \mathbf{A}(\Delta(AB^*C)) + \mathbf{A}(\Delta(ABC^*)) = 2(\alpha + \beta + \gamma) \quad (5.5)$$

From Equation 5.1 it is hence found

$$2\mathbf{A}(\Delta(ABC)) + 2\pi = 2(\alpha + \beta + \gamma) \quad (5.6)$$

giving

$$\mathbf{A}(\Delta(ABC)) = \alpha + \beta + \gamma - \pi = \mathbf{E} \quad (5.7)$$

This is called *Gerard's Spherical Excess Formula* after the French mathematician and engineer Albert Girard and, considering a triangle lying on a sphere of radius R , Equation 5.7 gives

$$\alpha + \beta + \gamma = \pi + \mathbf{A}(\Delta(ABC))/R^2 \quad (5.8)$$

This more clearly shows that the sum of angles is equal to π plus the area of the triangle and the well-known $\alpha + \beta + \gamma = \pi$ is obtained for the plane Euclidean triangle.

Angular Defect

More generally the area of an n -sided spherical polygon $\mathbf{A}(\text{poly})$, Figure 5.3(b), can be determined from the sum of its vertex angles β_i

$$\frac{\mathbf{A}(\text{poly})}{R^2} = \sum_{i=1}^n \beta_i - (n-2)\pi \quad (5.9)$$

The area of the polygon is also known as the *angular defect*, δ . From Figure 5.3(b) the *external angle* is defined as $\eta_i = \pi - \beta_i$. The angular defect can then be written, from Equation 5.9, as

$$\frac{\delta}{R^2} = 2\pi - \sum_{i=1}^n \eta_i \quad (5.10)$$

5.2.2 Spherical Trigonometry

Similarly to the trigonometric rules for a triangle in Euclidean geometry, a number of rules can be derived for the spherical triangle. Proofs are not given here but can be found in Carne (2002) and Clough-Smith (1978). Consider the spherical triangle ΔABC shown in Figure 5.2.

The Spherical Cosine Rule I is

$$\cos(\angle BOC) = \cos(\angle AOC) \cos(\angle AOB) + \sin(\angle AOC) \sin(\angle AOB) \cos \alpha \quad (5.11)$$

The Spherical Cosine Rule II is

$$\cos \alpha = -\cos \beta \cos \gamma + \sin \beta \sin \gamma \cos(\angle BOC) \quad (5.12)$$

The Spherical Sine Rule is

$$\frac{\sin(\angle BOC)}{\sin \alpha} = \frac{\sin(\angle AOC)}{\sin \beta} = \frac{\sin(\angle AOB)}{\sin \gamma} \quad (5.13)$$

The Four-part Rule is

$$\cot(\angle BOC) \sin(\angle AOC) = \cot \alpha \sin \gamma + \cos(\angle AOC) \cos \gamma \quad (5.14)$$

If one or more of the six angles defining the spherical triangle, three at the vertices and three arc lengths, is a right-angle then given any two angles, any third can be found using what is known as Napier's Rules (Clough-Smith, 1978). These allow the relationship between the two given angles and the third unknown angle to be written directly without the use of the above equations.

5.3 Pantographic Elements on a Spherical Surface

Consider the spherical pantographic element shown in Figure 5.4. The element consists of the two identical angulated elements AEB and $A'EB'$. Each element is comprised of two identical curved bars defined as great arcs, e.g. AE and BE . These two curved angulated elements are the spherical analogues of Hoberman's angulated elements presented in Section 2.4.2 for Euclidean geometry. The hinges are defined with axes of rotation normal to the sphere and hence all intersecting at the centre of the sphere. This allows the pantographic element to rotate about hinge E while maintaining all hinges on the sphere. Similarly to the planar lazy-tong a number of these spherical pantographic elements can be connected while preserving the single internal mechanism of the pantograph.

To form a closed loop ring structure from n identical spherical pantographic elements, each pantographic element must subtend the constant angle α defined by the two meridians PA and PB . The intersection point P of the meridians is hence the centre of the structure and $\alpha = 2\pi/n$. A third meridian intersects the first two meridians at P and is defined such that it passes through hinge E . For the closed loop structure formed by these n pantographic elements to have an internal mechanism α must be constant when the angulated elements are rotated. Following symmetry the angles $\angle APE$ and $\angle BPE$ must also remain constant. By considering the spherical triangles defined in Figure 5.4, next it will be shown that a ring structure formed by identical curved bars is rigid, and hence does not form a mechanism, as angle $\angle BPE$ does not remain constant when the hinges A and B are moved along meridians subtending the constant angle α .

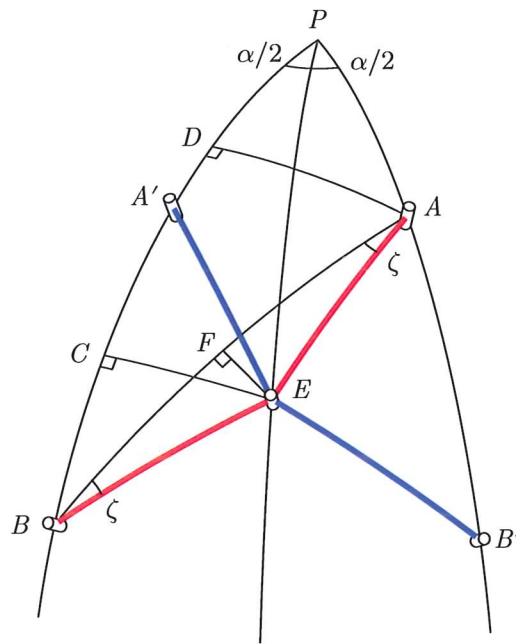


Figure 5.4: Pantographic element on a spherical surface

The angulated element consists of identical bars AE and BE , here recall that $\angle AOE$ is the angular arc length of AE . The angles $\angle EAB$ and $\angle EBA$ are identical and denoted by ζ . By considering the closed configuration of the pantographic element, where A coincides with P , it can readily be seen that $\zeta = \alpha/2$. Using Napier's Rules, the constant angular length of AB can be written from $\triangle AEF$ and $\triangle BEF$ as

$$\tan(\angle AOB/2) = \tan(\angle AOE) \cos \zeta = \tan(\angle BOE) \cos \zeta \quad (5.15)$$

Consider $\triangle PAB$. As $\angle AOB$ and α are constant a change in $\angle POA$ will cause a change in $\angle POB$. By considering $\triangle PAD$ and $\triangle BAD$ this change can be found as follows. From $\triangle PAD$

$$\tan(\angle POD) = \tan(\angle POA) \cos \alpha \quad (5.16)$$

$$\sin(\angle AOD) = \sin(\angle POA) \sin \alpha \quad (5.17)$$

and from $\triangle BAD$

$$\sin(\angle ABD) = \frac{\sin(\angle AOD)}{\sin(\angle AOB)} \quad (5.18)$$

$$\cos(\angle DOB) = \frac{\cos(\angle AOB)}{\cos(\angle AOD)} \quad (5.19)$$

The length of PB , $\angle POB$, can hence be found by adding together $\angle POD$ and $\angle DOB$. The angle $\angle BPE$ can then be found by considering $\triangle BEC$ and $\triangle PEC$. Note, $\angle EBC = \angle ABD + \zeta$ and hence for $\triangle BEC$

$$\tan(\angle BOC) = \tan(\angle BOE) \cos(\angle ABD + \zeta) \quad (5.20)$$

$$\sin(\angle COE) = \sin(\angle BOE) \sin(\angle ABD + \zeta) \quad (5.21)$$

From $\angle POC = \angle POB - \angle BOC$ the following expression is obtained for $\triangle PEC$

$$\tan(\angle BPE) = \frac{\tan(\angle COE)}{\sin(\angle POB - \angle BOC)} \quad (5.22)$$

Hence it is possible to determine if $\angle BPE = \alpha/2$, and therefore constant for varying $\angle POA$.

The limits for $\angle POA$ corresponding to the open and closed configurations of a closed loop structure are found as follows. In the closed configuration A coincides with P and hence $\angle POA$ is zero. In the open configuration AB is perpendicular to PE , since $\angle POA = \angle POB$, and hence

$$\sin(\angle POA) = \frac{\sin(\angle AOB/2)}{\sin(\alpha/2)} \quad (5.23)$$

The length of AB gives the length of bars AE and BE and hence the size of the pantographic element. The length of the bars is then following Equation 5.15

$$\cot(\angle AOE) = \cot(\angle BOE) = \cot(\angle AOB/2) \cos(\alpha/2) \quad (5.24)$$

In Figure 5.5 the angle $\angle BPE$ is plotted, using Equations 5.16–5.22, as a function of $\angle POA$ for a number of particular designs given by n and five different lengths of AB ranging from $\alpha/5$ to α . The figure shows that $\angle BPE$ is not constant and only equal to $\alpha/2$ at the limits of $\angle POA$, i.e. in the fully opened or closed configurations. Hence, a closed loop structure formed by spherical pantographic elements is rigid and does not therefore form a mechanism.

If ζ is not equal to $\alpha/2$, but still constant, then $\angle BPE = \alpha/2$ can be satisfied in the open and one other configuration. If ζ is not required to be constant, i.e. the two bars of each angulated element are allowed to rotate relative to each other, then $\angle BPE = \alpha/2$ can be satisfied in all configurations. Of course, this structure is no longer a pantograph, but a series of spherical four-bar linkages.

Another approach is to allow the hinge E to move away from the surface of the sphere, for example by rotating the angulated element about an axis through A and B . Thus, hinge E can be positioned so that it lies in a plane that is at an angle $\alpha/2$ to the planes OPA and OPB . As the pantograph element is opened or closed, hinge E will thus move away from and then back to the spherical surface. To allow this motion as well as a rotation about the normal, the hinges must allow additional rotations. For a closed loop structure all hinges have to allow rotations about all three axes, i.e. they are spherical joints, which would result in a system with additional internal degrees-of-freedom.

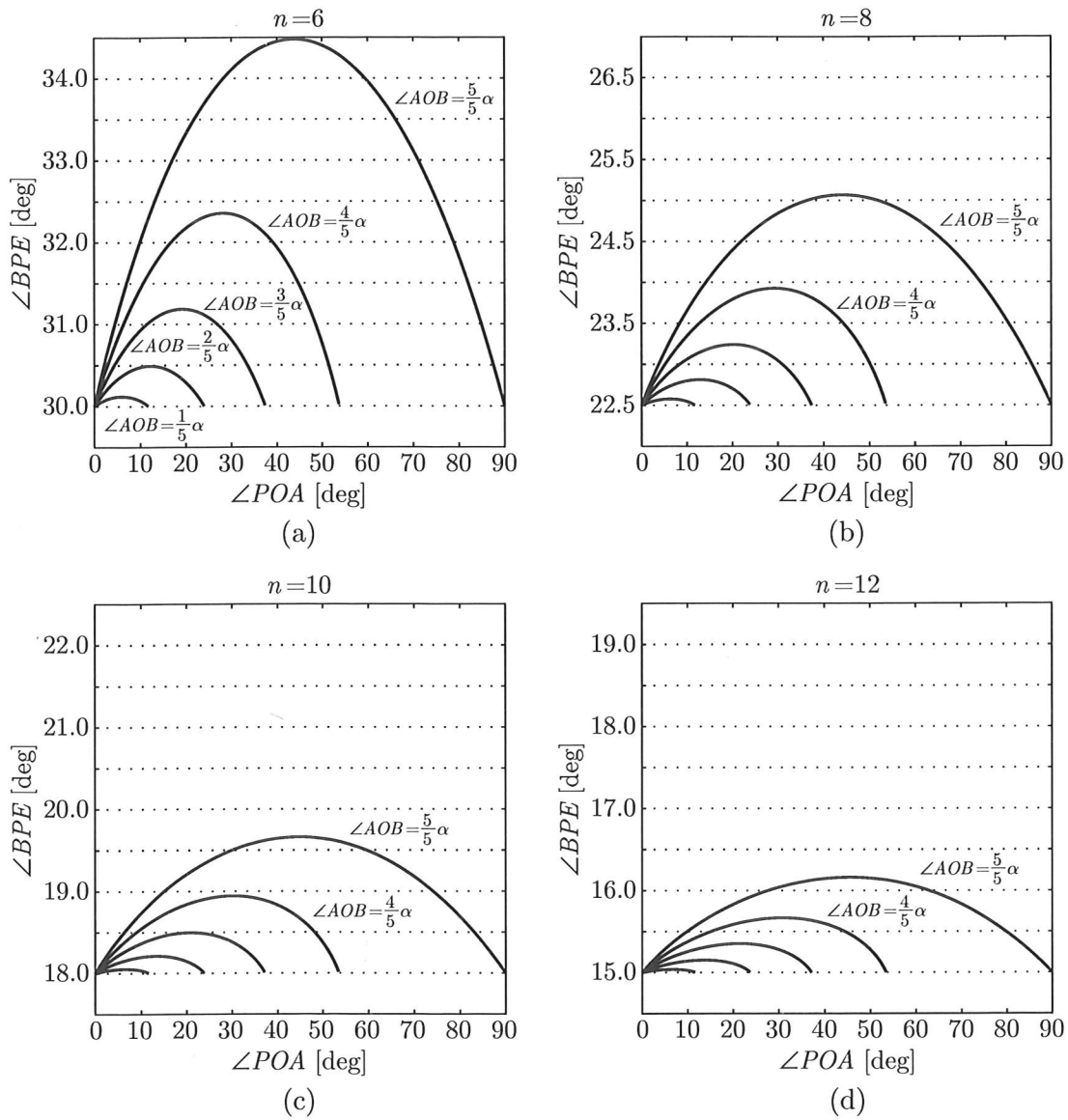


Figure 5.5: Plots of $\angle BPE$ for different n and lengths of AB

Instead of only allowing hinge E to move away from the spherical surface, hinges A and A' could also be allowed to move away from the surface. If the hinges A and A' are also allowed to move away from each other it is possible to arrange all five hinges of the pantographic element on a spherical surface of higher curvature such that it subtends the angle α as before. Hence, when the pantographic element is opened, changes in angular defect and internal angles can be made compatible by changing the curvature of the sphere. This, however, still requires the hinges to allow rotation about all three axes.

Because the three hinges A , B and E always lie on a spherical surface, it then becomes possible to use multi-angulated elements. The additional hinges of the multi-angulated element lie in the same plane as the original three hinges of the simple angulated element. The intersection of this plane and the sphere defines a circle of constant radius on which the hinges are then located similarly to the planar solution, regardless of the changes in curvature. Kokawa (2000, 2001) has shown it to be possible to construct such structures with only a single internal mechanism, as the additional connections made by the multi-angulated elements limit the number of internal degrees-of-freedom. One such structure is shown in Figure 5.6, and the change in curvature is clearly visible as it opens. Note, the lowest set of triangles form a supporting structure for the bottom edge. Kokawa's structure has also been covered with rigid cover elements which form a gap and overlap free surface in the closed configuration. In the open configuration there are considerable gaps and small overlaps of the cover plates, partly caused by the change in curvature between the two extreme configurations.

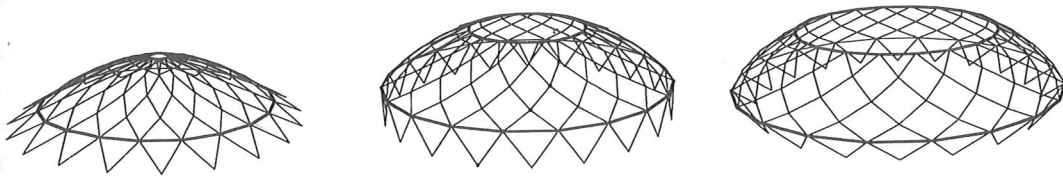


Figure 5.6: Spherical structure formed by multi-angulated elements (Kokawa, 2000)

5.4 Plate Shape

Though it has been shown that spherical retractable structures cannot be formed by pantograph elements it is still of interest to investigate if a series of wedge-shaped curved plate elements would be capable of forming a gap and overlap free surface in two different configurations, open and closed, on the sphere.

Consider a spherical cap on a unit sphere. If the cap is cut into n pieces by an equal number of meridians, the result is n identical spherical wedge-shaped plates as shown in Figure 5.7(a). Each plate subtends at its *apex* the constant angle α and the apexes of all plates coincide at the pole of the sphere in this *closed* configuration. Note that the two boundaries between adjacent plates, formed by the meridians, are great arcs while the third boundary is formed by a small circle.

Instead of only allowing hinge E to move away from the spherical surface, hinges A and A' could also be allowed to move away from the surface. If the hinges A and A' are also allowed to move away from each other it is possible to arrange all five hinges of the pantographic element on a spherical surface of higher curvature such that it subtends the angle α as before. Hence, when the pantographic element is opened, changes in angular defect and internal angles can be made compatible by changing the curvature of the sphere. This, however, still requires the hinges to allow rotation about all three axes.

Because the three hinges A , B and E always lie on a spherical surface, it then becomes possible to use multi-angulated elements. The additional hinges of the multi-angulated element lie in the same plane as the original three hinges of the simple angulated element. The intersection of this plane and the sphere defines a circle of constant radius on which the hinges are then located similarly to the planar solution, regardless of the changes in curvature. Kokawa (2000, 2001) has shown it to be possible to construct such structures with only a single internal mechanism, as the additional connections made by the multi-angulated elements limit the number of internal degrees-of-freedom. One such structure is shown in Figure 5.6, and the change in curvature is clearly visible as it opens. Note, the lowest set of triangles form a supporting structure for the bottom edge. Kokawa's structure has also been covered with rigid cover elements which form a gap and overlap free surface in the closed configuration. In the open configuration there are considerable gaps and small overlaps of the cover plates, partly caused by the change in curvature between the two extreme configurations.

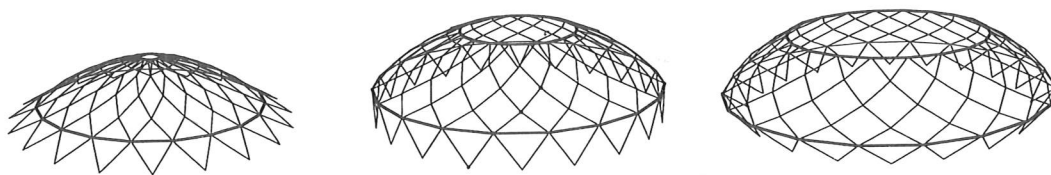


Figure 5.6: Spherical structure formed by multi-angulated elements (Kokawa, 2000)

5.4 Plate Shape

Though it has been shown that spherical retractable structures cannot be formed by pantograph elements it is still of interest to investigate if a series of wedge-shaped curved plate elements would be capable of forming a gap and overlap free surface in two different configurations, open and closed, on the sphere.

Consider a spherical cap on a unit sphere. If the cap is cut into n pieces by an equal number of meridians, the result is n identical spherical wedge-shaped plates as shown in Figure 5.7(a). Each plate subtends at its *apex* the constant angle α and the apexes of all plates coincide at the pole of the sphere in this *closed* configuration. Note that the two boundaries between adjacent plates, formed by the meridians, are great arcs while the third boundary is formed by a small circle.

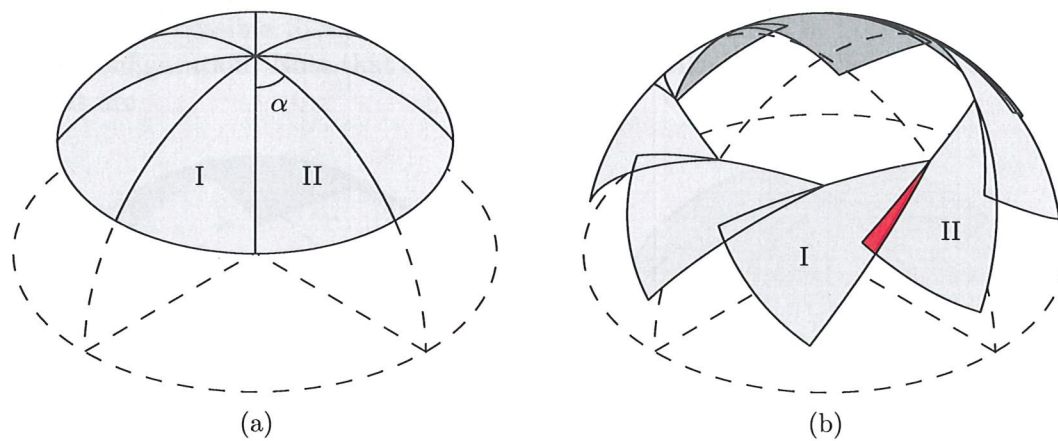


Figure 5.7: Spherical plates with straight boundaries in (a) Overlap free closed configuration, and (b) Overlapping open configuration

An *open* configuration is found by rearranging the plates such that parts of their left boundaries form the central symmetric opening shown in Figure 5.7(b). The opening is shaped as an equal, n sided polygon. Note how the plates are now overlapped in the region highlighted in red for plates I and II in the figure. To prove that this is always the case, and that simple wedge-shaped plates cannot form an overlap free open configuration, the angular defect of the opening is considered.

First the open configuration is defined as a configuration where a central and symmetric opening is created by a continuous boundary formed by the plates. The apex of each plate must therefore be located on the boundary of the neighbouring plate, as is the case in Figure 5.7(b). The opening will hence be a symmetric n -sided spherical polygon with vertices located at the apexes of the plates. The area of this polygon is identical to the angular defect and hence $\delta = \mathbf{A}(\text{poly})$ following Section 5.2.1.

For no gap or overlap to occur between the plates, they must be arranged such that the left and right boundaries of two neighbouring plates coincide. Hence the polygon external angle η must be equal to the angle subtended by each plate, α . The total sum of external angles must then always be 2π , as $\alpha = 2\pi/n$. Following Equation 5.10 the angular defect must then be equal to *zero*. This is only the case in the closed configuration as the area of the central polygon is larger than *zero* for all open configurations. Hence it is not possible to form an open configuration without overlaps using simple wedge-shaped plates where the boundaries are formed by straight arcs.

The overlap can be eliminated by removing the overlapping part of plate II. Thus no overlap would occur in the open configuration and the left boundary of plate II would have a kink at the location of plate I's apex. Moving the plates to the closed configuration the structure now has a gap where the previously overlapping part of plate II has been removed. To close this gap, the right boundary of plate I must also be kinked such that it again fully coincides with the boundary of plate II. This is shown in Figure 5.8(b). Returning the plates to the open configuration, Figure 5.8(a), it is found that neither gaps or overlaps are present in this configuration also. It has thus been discovered that by making identical kinks in the two boundaries of a plate

element it is possible to form a gap and overlap free surface in both an open and a closed configuration. Note that each piece of these kinked boundaries is still formed by a great arc.

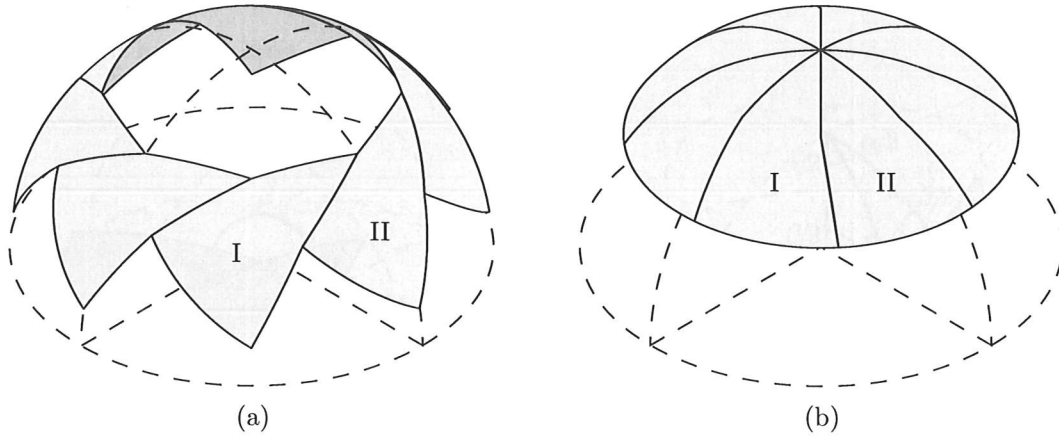


Figure 5.8: Spherical plates with kinked boundaries in (a) Overlap free open configuration, and (b) Overlap free closed configuration

To determine the size of the necessary kink consider Figure 5.9(a). The *kink* angle, κ , is defined as

$$\kappa = \alpha - \eta \quad (5.25)$$

using the previous definition $\eta = \pi - \beta$

$$\kappa = \alpha - \pi + \beta = \frac{2\pi}{n} - \pi + \beta \quad (5.26)$$

or, from symmetry

$$\kappa = \frac{\delta}{n} = \frac{2\pi}{n} - \pi + \beta \quad (5.27)$$

The vertex angle β can be found by considering the spherical triangle $\triangle PAB$ in Figure 5.9(b). Note that the boundary part AC is always perpendicular to a meridian PB at its midpoint B . Letting a minimum radius of the opening PB be the governing size and $\alpha/2 = \pi/n$, then

$$\cos(\beta/2) = \cos(\angle POB) \sin(\pi/n) \quad (5.28)$$

and the location of the kink is found from $\angle AOC = 2(\angle AOB)$ and

$$\tan(\angle AOB) = \sin(\angle POB) \tan(\pi/n) \quad (5.29)$$

The same triangle also produces the relationship

$$\cot(\angle POA) = \cot(\angle POB) \cos(\pi/n) \quad (5.30)$$

which will be used later on.

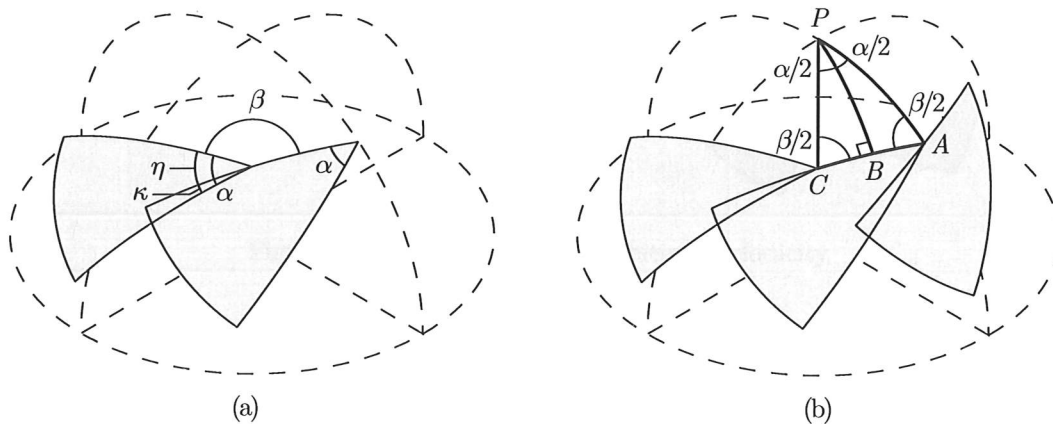


Figure 5.9: Determining (a) Kink angle κ , and (b) Vertex angle α

Hence it is possible to determine the shape of a kinked plate element capable of forming a gap and overlap free surface in an open and a closed configuration from only the number of plates in the structure and the minimum radius of the wanted opening. Interestingly, the area $A(\triangle(PAC)) = \delta/n = \kappa$, from symmetry.

5.4.1 Periodicity of Boundaries

Though no specific motion path has yet been considered it can be seen that two adjacent plates must translate a distance L , equal to $\angle AOC$, and rotate through κ relative to one another when moving between the two extreme, i.e. open and closed, configurations. Hence, if a boundary length is longer than L , additional kinks must be introduced to prevent overlap from occurring. From Figure 5.10 it can be seen that the kinks must then occur periodically and this kinked boundary exhibits similar characteristics to those found for the straight boundaries of planar plate elements, in Section 3.3.4.

A common characteristic is the possibility of the boundary shape deviating from the original straight, or kinked form. Without a specific motion path only a single condition must be satisfied by the boundary of the spherical plate element — the rule of periodicity. All shape features must repeat with a period of L and be rotated by κ relative to the last period.

Two other examples of periodic boundaries are shown in Figures 5.11 and 5.12. The first example is generated by observing that in both Euclidean and non-Euclidean geometry three points define both a plane and a circle. Thus, using the point of the apex and two other points along the boundary of a plate element, all with an internal spacing of L , and using these points as standard “kink points”, a small circle can be defined.

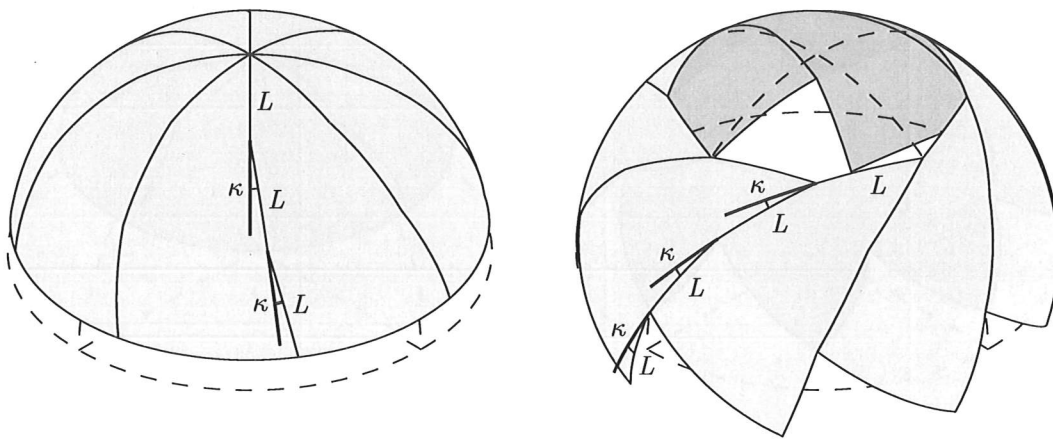


Figure 5.10: Plate elements exhibiting periodicity

as shown in Figure 5.11. Using this small circle to define the periodic shape of the boundary a smooth continuous boundary is created. The radius r_1 of this small circle can be determined by considering the plane defined by the small circle.

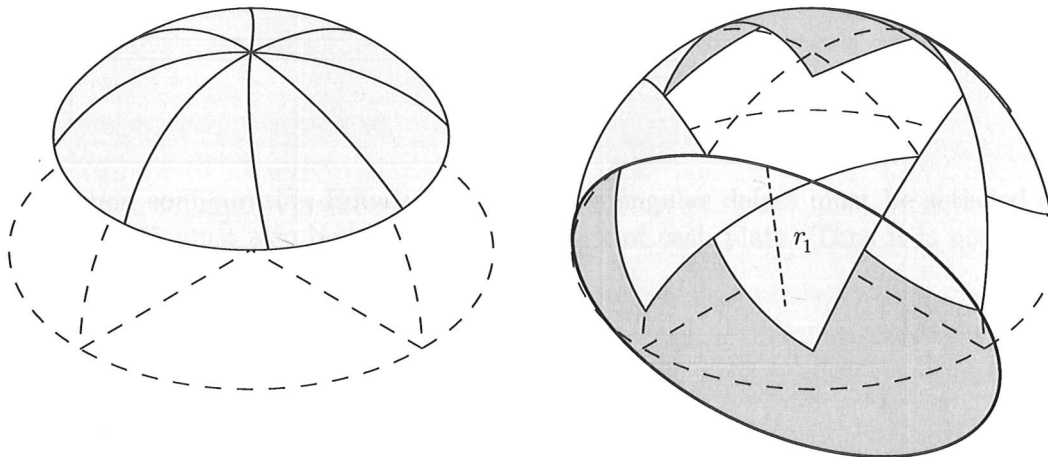


Figure 5.11: Plate elements with periodic boundary formed by a small circle

The second example also uses a small circle. The small circle is defined by the apexes of the plates in the open position. Using this circle to define a periodic boundary formed by small arcs, a perfect circular opening is created, see Figure 5.12. The radius of the opening is found by considering the plane passing through apex A , pole P and the centre of the sphere O . Hence,

$$r_2 = R \sin(\angle POA) \quad (5.31)$$

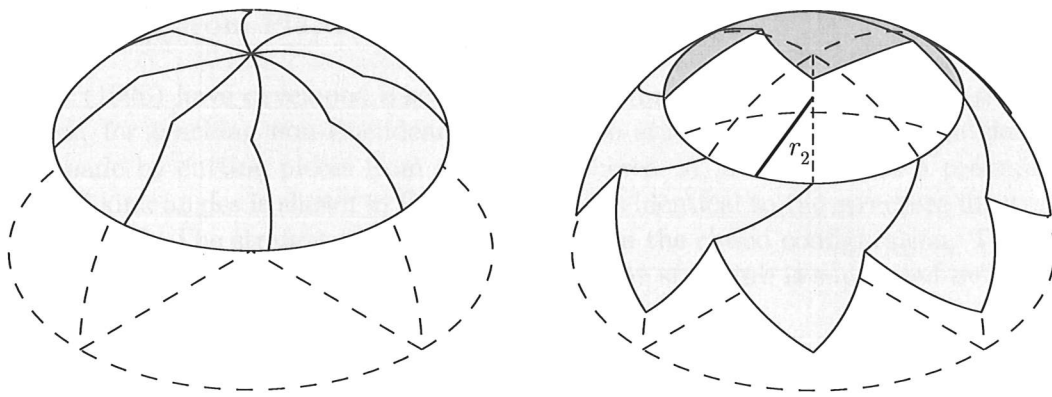


Figure 5.12: Plate elements with periodic boundary forming a perfect circular opening

5.4.2 Non-Symmetric Structures

Non-symmetrical structures can also be formed if certain conditions are satisfied. To prevent gaps or overlaps in the closed configuration, clearly the following condition must be satisfied at the pole

$$\sum_{i=1}^n \alpha_i = 2\pi \quad (5.32)$$

In the open configuration Equation 5.10 for the angular defect must be satisfied and Equation 5.25 must also be satisfied at the apex of each plate. Thus it is possible to write

$$\sum_{i=1}^n \kappa_i = \sum_{i=1}^n \alpha_i - \sum_{i=1}^n \eta_i = \delta \quad (5.33)$$

This equation shows that there are an infinite number of possible solutions to this problem. As for the boundary period L for the symmetric structure the period for any particular boundary, L_i in a non-symmetric structure is always equal to the length of AC for that particular boundary, i.e. the length of the opening polygon's side formed by that particular boundary.

5.4.3 Physical Models

The double-curvature of the spherical plate elements makes it more difficult to fabricate physical models of these structures. Since it is impossible to use flat sheets of material, as in Section 3.3.3, new methods for making physical models had to be developed.

Models Cut From Plastic Hemispheres

Lénárt (1996) have developed a set of tools, including thin, transparent plastic hemispheres, for teaching non-Euclidean geometry to students. Spherical plate elements were made by cutting pieces from such hemispheres. A model used for a preliminary study of kink angles is shown in Figure 5.13 and is identical to the structure illustrated in Figure 5.8. The straight meridians are visible in the closed configuration. The individual elements are held together with tape and the structure is supported by another plastic hemisphere.

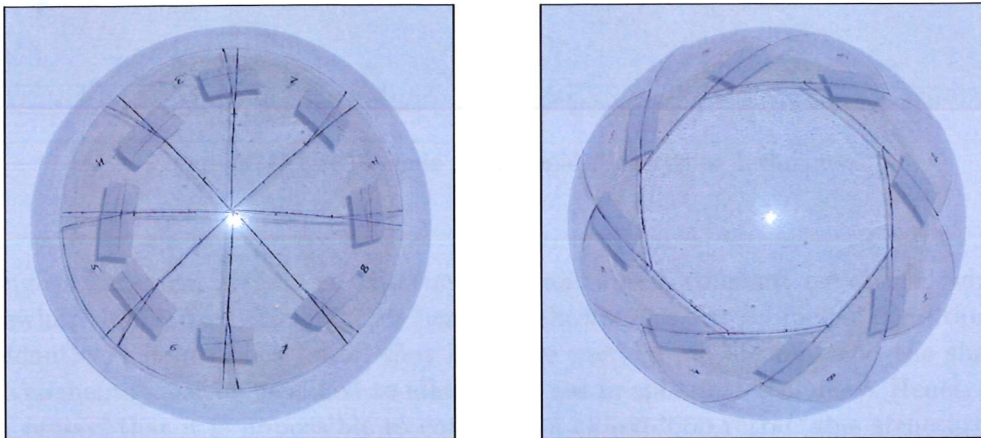


Figure 5.13: Model made from plastic hemispheres

Rapid Prototyping

For geometrically more detailed models, which were difficult to draw and cut manually, a rapid prototyping technique was used. From three-dimensional computer models physical models were produced using Fused Deposition Modelling (FDM) (Stratasys, 1999). This is a layered manufacturing method that extrudes a thin bead of plastic, one layer at a time. A thread of plastic is fed into an extrusion head, where it is heated into a semi-liquid state and extruded through a very small hole onto the previous layer of material. Support material is also laid down in a similar manner. The plastic used is a high strength ABS and hence the finished model is of high strength and high accuracy.

The plates were produced individually and then mounted on a plastic hemisphere. Figure 5.14 shows a model with plate boundaries formed from small circles to provide continuous, smooth boundaries. To allow the plates, which have finite thickness, to fit together all boundaries are normal to the sphere.

5.5 Discussion

Since it has been shown in Chapter 3 that it is possible to create covered retractable bar structures with planar geometry, this chapter has investigated the possibility of adapting to spherical geometry both the simple pantographic element and the wedge-shaped cover plates.

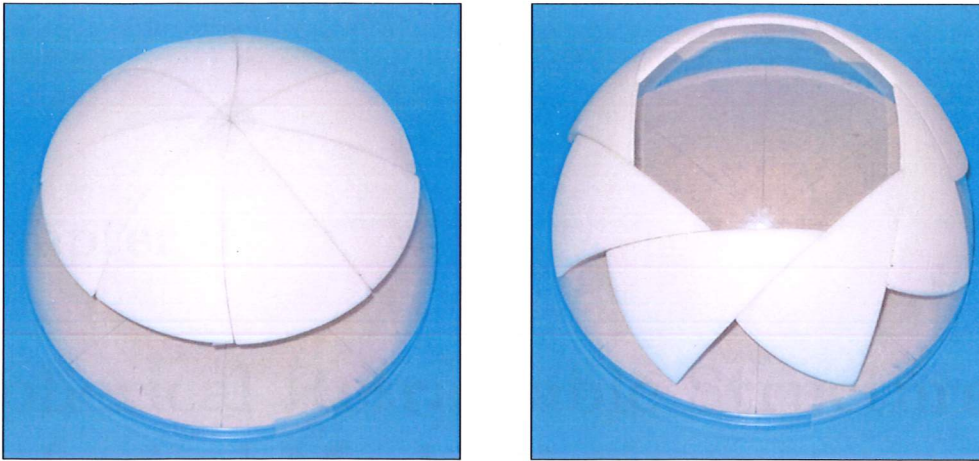


Figure 5.14: Model made using rapid prototyping techniques

Though a spherical surface is axi-symmetric and has a constant curvature, which is somewhat similar to a flat plane, it has been shown that the geometric conditions are not identical. It has been found that both the pantograph element and the shape of plate elements must be modified to allow their use in spherical geometry. Hence, it has been proved that it is impossible to construct a closed-loop retractable structure on a sphere using pantographic elements connected through simple scissor hinges. As the angle subtended by such an element is not constant during the transformation, it has been shown that it is necessary to allow additional rotations in the hinges to preserve its mechanism.

Considering only the extreme configurations of a spherical, retractable plate structure it has been shown that simple wedge-shaped plate elements cannot form an overlap-free surface in any other configuration than the initial closed configuration. It has, however, been found possible to modify the shape of such spherical plate elements by forming kinks along the boundaries of the elements. This allows spherical structures consisting of such kinked plates to create gap- and overlap-free surfaces both in an open and a closed configuration. It has been determined that the size and location of these kinks are, for symmetrical structures, only a function of the number of plates used and the size of the central opening created.

Furthermore, it has been shown that this modified plate element, with kinked boundaries, exhibits similar periodic characteristics like those found for the two-dimensional plate elements derived in Section 3.3.4. However, as no motion paths have been prescribed, no conditions have been defined for the range of possible periodic features. Further variations have been shown to be possible, as non-symmetric structures can also be formed.

Finally, note that the plate structures studied in this chapter have only been considered in two extreme configurations. The next two chapters are concerned with mechanisms that will allow the plate elements presented in this chapter to form retractable roof structures.

Chapter 6

Spherical Retractable Structures: Spherical Mechanisms

6.1 Introduction

Chapter 5 has presented a study of the shape of spherical plate elements that fit together on a spherical surface, in two different configurations. The present chapter is concerned with developing a spherical mechanism that will allow structures composed of such elements to open and close while moving on the spherical surface.

In Euclidean geometry the motion of structures can be described in terms of translations and rotations. In non-Euclidean geometry, however, every motion can be described as a pure rotation and the work presented in this chapter is based on this concept. The first part of the chapter is concerned with this concept and how it can be used to derive a simple method for opening and closing a spherical retractable roof where each plate element is simply rotated about a fixed point.

The second part investigates the parameters that govern the position of this fixed point. It is found that a geometric relationship between the two extreme configurations for a plate element governs the location of its fixed point. Thus, it is shown to be possible to design structures where the fixed points are suitably located within the boundaries of the plate elements, hence simplifying the structural design of the structure.

The final part of this chapter describes the relative motion between neighbouring plates as they are rotated about their fixed points. Through the study of this relative motion it is shown that it is not possible to interconnect two neighbouring elements using only rigid bars and cylindrical hinges with only one axis of rotation. Hence an alternative system of constraints, which includes sliding mechanisms is developed. The ability of this system to form a self-supporting structure with only a single internal mechanism is proven by the construction of a half metre span physical model.

6.2 Euler Pole

When deriving the spherical plate elements in Chapter 5, only the two extreme configurations were considered. To use these plates to form a spherical retractable structure it is necessary to consider also all intermediate configurations of these structures, in order to determine a suitable motion for the plate elements. Here, a suitable motion will be defined as a motion such that; (i) there is no overlap of the plates; (ii) the plates remain on the spherical surface at all times; and (iii) any hinges are required to have only a single axis of rotation. Initially, no structural requirements will be set and also no restrictions will be posed on the number of internal mechanisms of the structure; hence allowing also a structure consisting of a number of "free" plate elements to be considered initially.

Consider the plate elements shown in Figure 6.1(a). In the closed configuration, labelled with the subscript 0 in the figure, it can be seen that the apex A of the element coincides with the pole of the sphere, P . It can also be seen that the first piece of the plate's left boundary AC coincide with the meridian PP' in this configuration. In Section 5.4 it was found in the open configuration AC is perpendicular to a meridian at the midpoint B , Figure 6.1(a). Let this meridian be PP' also. Hence the relative location of the closed and open configurations has been defined. Following this, it is possible to describe a single motion or a set of motion increments that will move the plate from one extreme position to the other. In previous chapters only the extreme configurations were considered and hence denoted as *open* and *closed*. Here, however, intermediate configurations must also be identified and hence the points A , B and C will be denoted as A_0 , B_0 , C_0 and A_m , B_m , C_m for the closed and open configurations respectively, while intermediate positions will be denoted by A_1, A_2, \dots, A_{m-1} and similarly for B and C . Hence, m is the number of rotations undergone between the two extreme configurations.

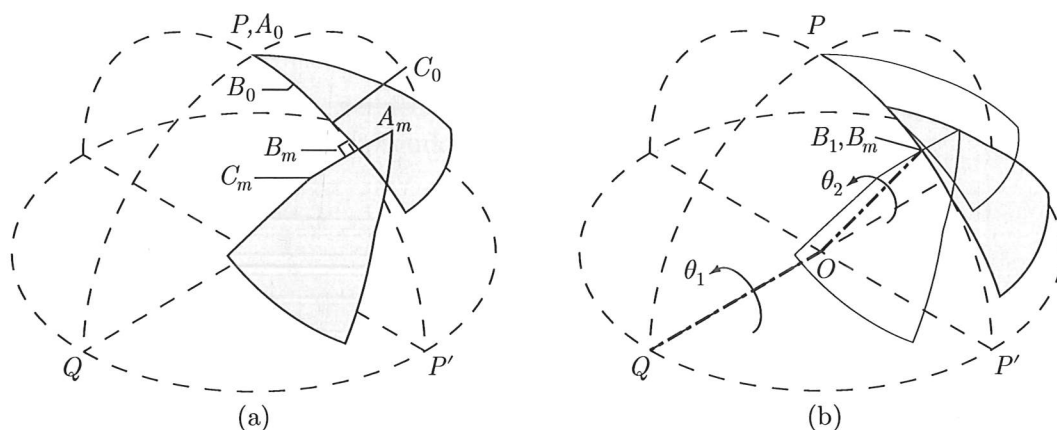


Figure 6.1: Rotated plate element in (a) Two extreme configurations, labelled 0 and m , and (b) Intermediate configuration

Consider a motion composed of two parts: first, a rotation of the plate element along PP' so that B_1 coincides with B_m , as shown in Figure 6.1(b), and secondly

a rotation about the axis OB_1 which aligns the element with its final configuration. The first rotation about the axis OQ perpendicular to the plane of the meridian is $\theta_1 = -(\angle POB_m - \angle POB_0)$ and following Section 5.4 then $\theta_1 = \angle AOB - \angle POB_m$. Note, in Section 5.4 no subscripts were used when deriving the spherical plate elements. The second part of the motion is clearly a rotation of $\pi/2$ about the axis OB_1 . Hence, it is possible to determine a motion for the plate element from the closed to the open position by dividing the motion into two separate parts.

However, this incremental motion can be simplified using *Euler's Theorem* which states that: "The general displacement of a rigid body with one point fixed is a rotation about some axis which passes through that point" (Felippa, 2001). Hence, if the centre of a sphere is fixed, then any movement of a rigid body between any two positions or orientations on the sphere's surface can be described by a single rotation about a specific axis passing through the centre of the sphere.

Therefore, following Euler's Theorem, the plate element does not need to undergo two separate rotations to move from the closed to the open position, as proposed above. Instead, the element can be moved between the two extreme positions by a simple rotation about an axis or an *Euler pole* as it is also known. As a single rotation is the simplest way of moving the plate element on the sphere, this is of particular interest. The location of the Euler pole, P_E , and the rotation undergone by the plate element about this pole, θ_E , can be found using either compound rotations or spherical trigonometry. Both methods are used later and hence presented below.

6.2.1 Compound Rotations

The order in which large rotations are applied to a rigid body influences the final outcome as illustrated in Figure 6.2 and hence the addition of rotations cannot be analysed using simple vectors. A method to determine the combined or *compound* rotation is to use pseudo-vectors $\vec{\theta}$ and *Rodrigues Formula*. This method is outlined below and further information can be found in Crisfield (1997) and Felippa (2001).

In Figure 6.3, point $A(\vec{v}_0)$, defined by the vector \vec{v}_0 , is rotated to $A(\vec{v}_1)$ by the rotation θ about the unit-axis \vec{e} . The pseudo-vector for this rotation is defined as

$$\vec{\theta} = \theta \vec{e} = \theta \begin{bmatrix} e_x \\ e_y \\ e_z \end{bmatrix} \quad (6.1)$$

For compound rotations it is useful to modify the pseudo-vector such that

$$\vec{\omega} = \omega \vec{e} = 2 \tan(\theta/2) \vec{e} \quad (6.2)$$

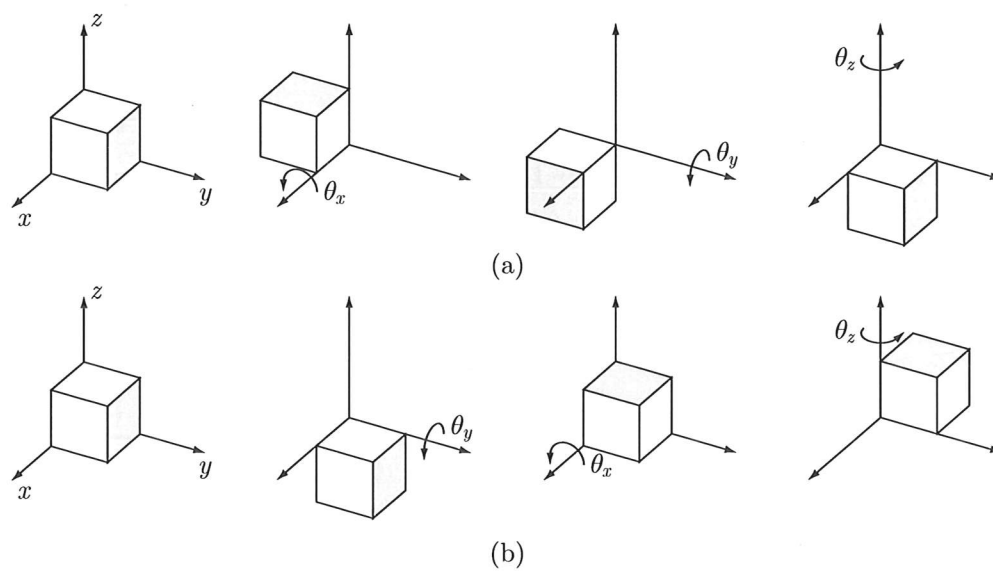


Figure 6.2: The non-commutativity of vector rotations (a) $\theta_x, \theta_y, \theta_z$, and (b) $\theta_y, \theta_x, \theta_z$

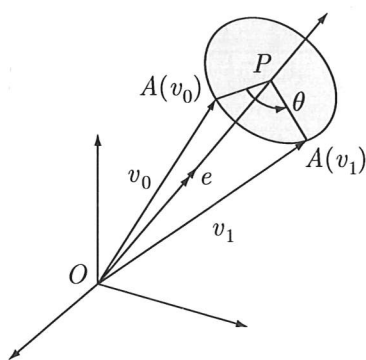


Figure 6.3: Large three-dimensional rotation about OP

The rotation can then be written using the three-by-three rotation matrix $\mathbf{R}(\vec{\omega})$

$$\vec{v}_1 = \mathbf{R}(\vec{\omega})\vec{v}_0 \quad (6.3)$$

where

$$\mathbf{R}(\vec{\omega}) = \mathbf{I} + \frac{\mathbf{S}(\vec{\omega}) + \frac{1}{2}\mathbf{S}(\vec{\omega})^2}{1 + \frac{1}{4}\vec{\omega}^T\vec{\omega}} \quad (6.4)$$

and

$$\mathbf{S}(\vec{\omega}) = \omega \begin{bmatrix} 0 & -e_z & e_y \\ e_z & 0 & -e_x \\ -e_y & e_x & 0 \end{bmatrix} \quad (6.5)$$

If the point $A(v_0)$ undergoes two rotations θ_1 and θ_2 about \vec{e}_1 and \vec{e}_2 respectively, then

$$\vec{v}_1 = \mathbf{R}_1(\vec{\omega}_1)\vec{v}_0 \quad \text{and} \quad \vec{v}_2 = \mathbf{R}_2(\vec{\omega}_2)\vec{v}_1 \quad (6.6)$$

hence

$$\vec{v}_2 = (\mathbf{R}_2(\vec{\omega}_2)\mathbf{R}_1(\vec{\omega}_1))\vec{v}_0 = \mathbf{R}_{12}(\vec{\omega}_{12})\vec{v}_0 \quad (6.7)$$

where $\vec{\omega}_{12}$ is the pseudo-vector for the rotation about the Euler pole for $A(v_0)$ to $A(v_2)$ and is given by

$$\vec{\omega}_{12} = \frac{\vec{\omega}_1 + \vec{\omega}_2 - \frac{1}{2}\vec{\omega}_1\vec{\omega}_2}{1 - \frac{1}{4}\vec{\omega}_1^T\vec{\omega}_2} \quad (6.8)$$

The unit-axis of the Euler pole is found through normalisation of $\vec{\omega}_{12}$, using Equation 6.2

$$\vec{e}_{12} = \frac{\vec{\omega}_{12}}{\omega_{12}} = \frac{\vec{\omega}_{12}}{|\vec{\omega}_{12}|} = \frac{\vec{\omega}_{12}}{\sqrt{\omega_{12,1}^2 + \omega_{12,2}^2 + \omega_{12,3}^2}} \quad (6.9)$$

The rotation angle can then be obtained through

$$1 + 2 \cos \theta_{12} = \text{trace}(\mathbf{R}(\vec{\omega}_{12})) = \text{trace}(\mathbf{R}(\vec{\omega}_2)\mathbf{R}(\vec{\omega}_1)) \quad (6.10)$$

Hence, if the motion of a plate element can be defined as a series of individual rotations, then the Euler pole P_E and its associated rotation θ_E can be determined using the equations above. For the two part motion described in Section 6.2, the Euler pole

and its associated rotation are thus found from Figure 6.1 using the right hand rule: $\vec{e}_1 = \vec{OQ}$, $\theta_1 = \angle AOB - \angle POB_m$ and $\vec{e}_2 = \vec{OB}_m$, $\theta_2 = -\pi/2$. The resulting Euler pole and rotation are shown in Figure 6.4.

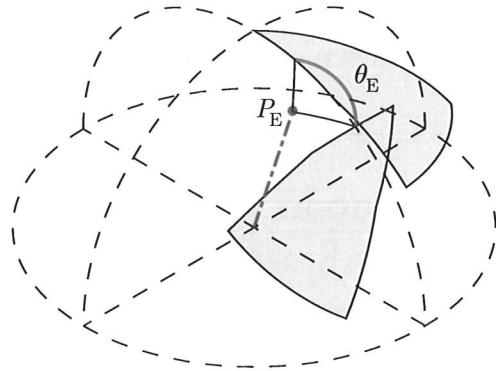


Figure 6.4: A single rotation θ_E about P_E moves the plate element from its closed to its open configuration

6.2.2 Spherical Trigonometry

Using the trigonometric functions provided in Section 5.2.2, the location of the Euler pole P_E and rotation θ_E can also be determined from $\triangle P_E B_0 B_m$, shown in Figure 6.5.

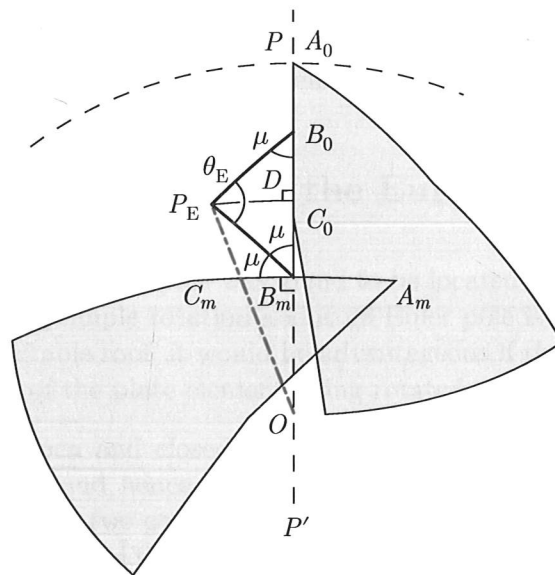


Figure 6.5: Determining the Euler pole P_E and rotation θ_E from $\triangle P_E B_0 B_m$

As the plate element undergoes a rigid body rotation θ_E about the axis OP_E , the distance from any point on the plate to the axis must remain constant, i.e. $\angle P_E O A_0 = \angle P_E O A_m$, $\angle P_E O B_0 = \angle P_E O B_m$ and so forth. Hence the angle $\angle P_E B C$ is also constant, giving $\angle P_E B_0 C_0 = \angle P_E B_m C_m = \mu$. From the isosceles triangle $\triangle P_E B_0 B_m$ it can be shown that $\angle P_E B_0 B_m = \angle P_E B_m B_0 = \mu$.

In the closed position $A_0B_0C_0$ is parallel to the meridian PP' and in the open position $A_mB_mC_m$ is perpendicular to the meridian. The angle μ can therefore be determined directly from the sum of angles at B_m

$$\pi = \pi/2 + 2\mu \Rightarrow \mu = \pi/4 \quad (6.11)$$

The rotation θ_E can then be found from $\triangle P_E B_0 B_m$

$$\cos(\theta_E/2) = \cos\left(\frac{\angle B_0 O B_m}{2}\right) \sin \mu \quad (6.12)$$

where $\angle B_0 O B_m$ is the angular length of the great arc $B_0 B_m$ and

$$\angle B_0 O B_m = \angle P O B_m - \angle A O B \quad (6.13)$$

Both $\angle P O B_m$ and $\angle A O B$ were determined when the plate shape was found in Section 5.4. The location of P_E is then determined from

$$\cot(\angle P_E O B_0) = \cot(\angle P_E O B_m) = \cot\left(\frac{\angle B_0 O B_m}{2}\right) \sin \mu \quad (6.14)$$

Using spherical trigonometry it is therefore possible to determine the position of P_E without defining intermediate steps for the motion. This method is therefore simpler than that proposed in Section 6.2.1 using compound rotations where it is necessary to determine a possible motion for the plate before the Euler pole can be determined.

6.3 Varying the Location of the Euler Pole

In the previous section the Euler pole was found to be located outside the rotated plate element, Figure 6.4. If a simple rotation about an Euler pole is to be used as part of a mechanism for a retractable roof, it would be advantageous if the pole could be located within the boundaries of the plate element being rotated.

Considering only the open and closed configurations of the plate element, the Euler pole can be determined and hence its position must be a function of the geometric relationship between those two configurations only. Therefore, to alter the position of the pole the relative position of the two configurations must be changed. However, there are a number of constraints that must be observed, which follow from the definition of the plate shape. In the closed configuration the apex A must coincide with P , thus making ABC parallel to a meridian PP' . In the open configuration the length $\angle POB$ is defined and ABC must be perpendicular at B to a meridian PP'' . Hence only the angle λ subtended by the meridians PP' and PP'' can be varied. In Section 6.2 the two meridians, PP' and PP'' , were assumed to coincide and hence λ was equal to zero.

Figure 6.6 is identical to Figure 6.5, except that the two meridians PP' and PP'' are no longer coincident. From $\triangle P B_0 B_m$

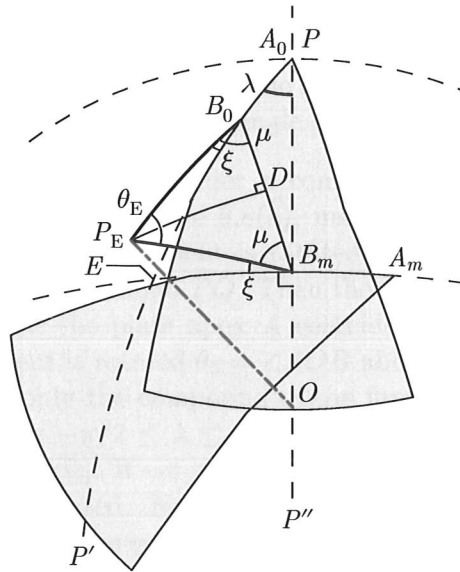


Figure 6.6: Determining P_E and θ_E from $\triangle P_E B_0 B_m$ and the initial position given by λ

$$\cos(\angle B_0 O B_m) = \cos(\angle P O B_m) \cos(\angle P O B_0) + \sin(\angle P O B_m) \sin(\angle P O B_0) \cos \lambda \quad (6.15)$$

The point E is defined as the intersection of meridian PP' and the great circle passing through A_m and B_m , and is hence similar to point B_m which defines the intersection of the same great circle and the meridian PP'' . From E the triangles $\triangle EPB_m$ and $\triangle EB_0 B_m$ can be defined. For $\triangle EPB_m$ the following can be found

$$\cos(\angle PEB_m) = \sin \lambda \cos(\angle POB_m) \quad (6.16)$$

$$\sin(\angle EOB_m) = \frac{\sin \lambda \sin(\angle POB_m)}{\sin(\angle PEB_m)} \quad (6.17)$$

$$\sin(\angle POE) = \frac{\sin(\angle POB_m)}{\sin(\angle PEB_m)} \quad (6.18)$$

And from $\triangle EB_0 B_m$, μ can be determined as follows

$$\sin(\mu - \xi) = \sin(\angle EB_0 B_m) = \frac{\sin(\angle PEB_m) \sin(\angle EOB_m)}{\sin(\angle B_0 O B_m)} \quad (6.19)$$

$$\sin(\mu + \xi) = \sin(\angle EB_m B_0) = \frac{\sin(\angle PEB_m) \sin(\angle POE - \angle POB_0)}{\sin(\angle B_0 O B_m)} \quad (6.20)$$

$$\mu = \angle P_E B_0 B_m = \angle P_E B_m B_0 = \frac{(\mu - \xi) + (\mu + \xi)}{2} \quad (6.21)$$

Using Equations 6.14 and 6.12, respectively, can P_E and θ_E now be found.

In Figure 6.7(a–e) the location of the Euler pole is shown for different values of λ . Interestingly, the poles are all found to lie on a single great circle, as shown in Figure 6.7(f).

To understand this latent result, consider a compound rotation composed of three separate rotations, illustrated in Figure 6.8(a), instead of two rotations as described in Section 6.2.1. First the plate element is rotated $\theta_1 = \lambda$ about the axis OP such that ABC coincides with the meridian PQ . Then the element is rotated $\theta_2 = \angle POB_m$ about the axis OQ so that the plate apex A coincides with the final position of B , i.e. B_m . Finally, the element is rotated $\theta_3 = \angle AOB$ about an axis normal to the plane of OA_mB_m . Considering only the compound of the first two rotations, it can be seen from Figure 6.8(b) that for $-\pi/2 \leq \lambda \leq \pi/2$ the solutions for \vec{e}_{12} define a great arc from Q to the midpoint of PB_m . If $-\pi \leq \lambda \leq \pi$ and the antipodal of \vec{e}_{12} is also plotted, a complete great circle is created. Now plotting \vec{e}_{13} , also in Figure 6.8(b), it can be seen that the third rotation in the compound has only rotated the previous solution for \vec{e}_{12} and hence these solutions must also lie on a great arc.

6.3.1 Selection of Euler Pole

For each point on the great circle defined by \vec{e}_{13} in Figure 6.8(b) there is a corresponding value of λ . Hence it is possible to choose on the great circle a suitable location for the Euler pole, and thus find the corresponding closed position of the plate element in terms of λ .

In Figure 6.9 four different plate shapes, each with a different opening size, have been plotted together with their possible locations of P_E for $-\pi/2 \leq \lambda \leq \pi/2$. All have $n = 8$ plates, while the minimum size of the opening $\angle POB_m$ is increased from $\pi/16$ to $\pi/4$. For an increase in the opening size the length of each boundary period L is increased and so is the kink angle κ . For $\angle POB_m = \pi/4$ it is not possible to find any location of P_E inside the element. It is, however, possible to find a suitable Euler pole inside the plate elements if the opening size is reduced. It has therefore been shown that it is possible to move a plate element from its closed to its open position by rotating the element about a fixed point that lies within its own boundaries.

6.3.2 Physical Models

So far only a single plate element has been considered. To investigate the possibility of using this method for opening and closing a complete structure several physical models were built. One such model is shown in Figure 6.10. The model is a modification of that shown in Figure 5.14. Thin steel rods have been added to provide the fixed points of rotation for each plate. These rods are held in place by holes in the supporting plastic hemisphere and, similarly, at the centre of the sphere by holes in the cardboard base. Hence, these rods fix the axes of rotation normal to the sphere.

Using this and other models it was found that the plates do not interfere with each other if their rotations are synchronised. When the structure is opened, a gap appears between the plates, as can be seen in the sequence in Figure 6.11. The relative motion

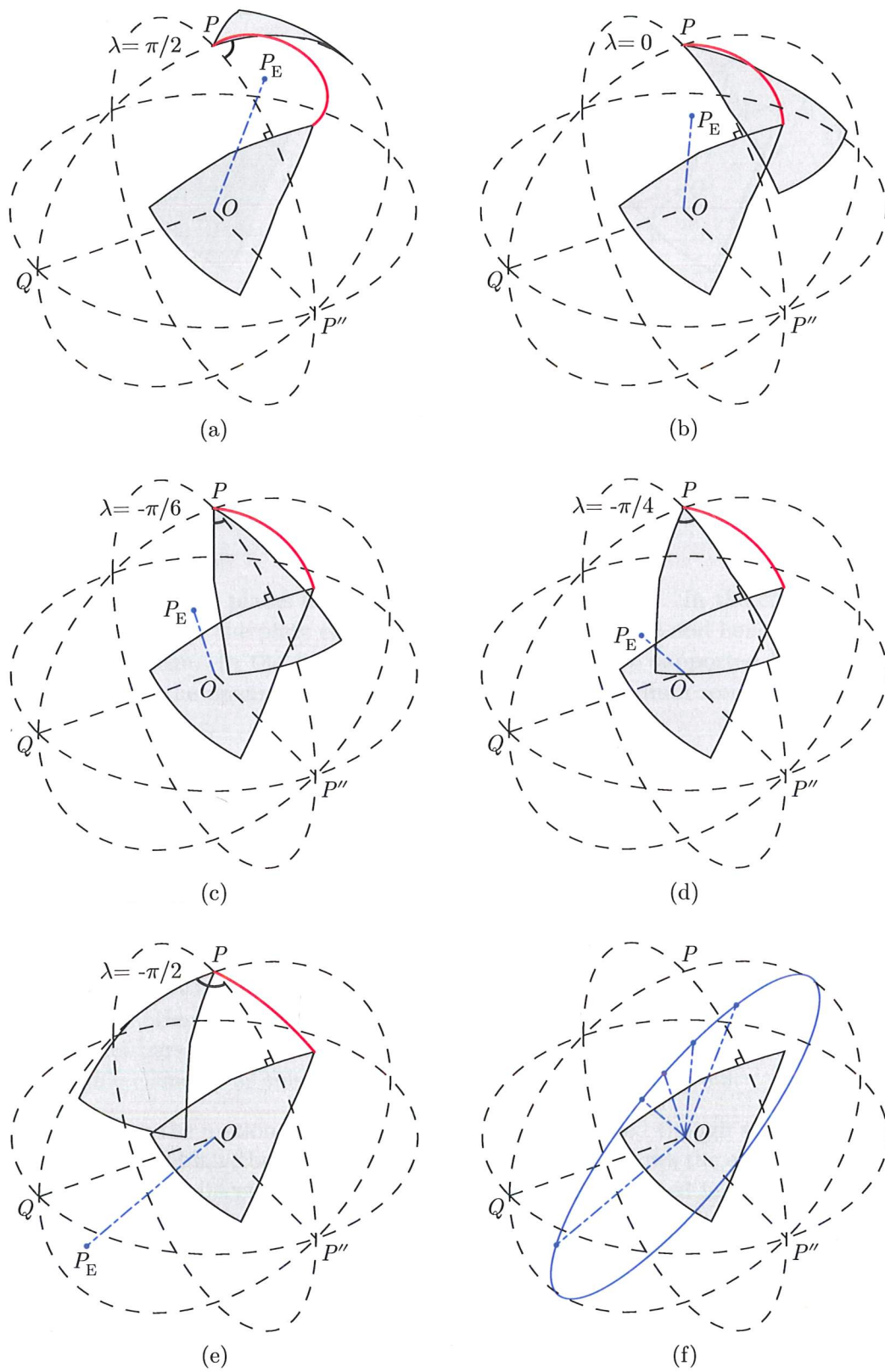


Figure 6.7: Location of the Euler pole, P_E , for varying positions λ of the plate in the closed configuration

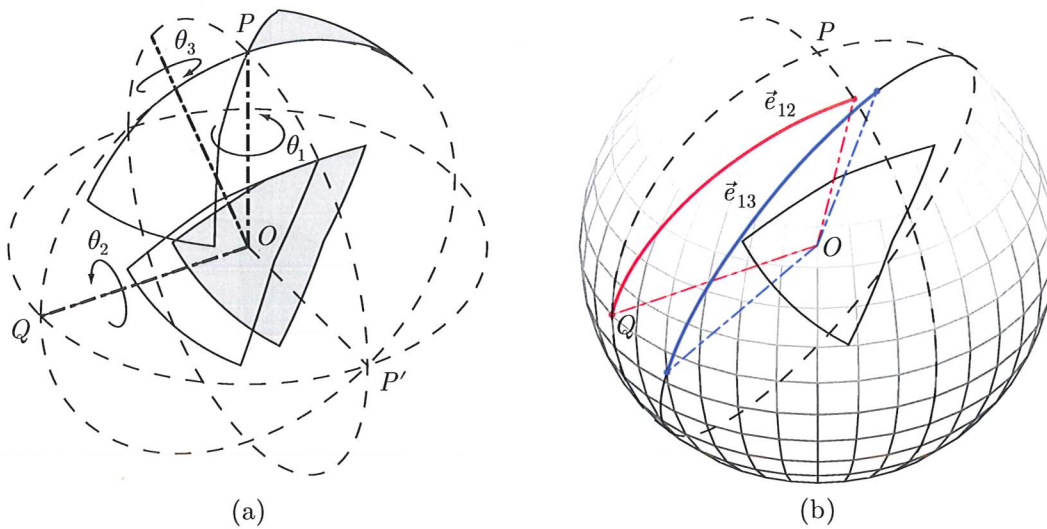


Figure 6.8: Compound rotations for $-\pi/2 \leq \lambda \leq \pi/2$ (a) Individual rotations, and (b) Solutions for \vec{e}_{12} and \vec{e}_{13}

between neighbouring plates is described below in Section 6.4. In the concept model shown in Figure 6.11 the plate elements are not interconnected and hence do not form a single mechanism. In the figure, the individual plates are supported by a series of arches spanning the opening, as is the case for the Oita Stadium retractable roof, see Figure 2.7.

6.4 Relative Motion of Parts

The relative motion of two neighbouring spherical plate elements is similar to that of two adjacent planar plate elements that are connected through parallel bars as described in Section 3.3.1. Both types of plates move between extreme positions where the adjacent plates are in contact. In the intermediate positions there is a gap between the plates, in both cases. Hence, it might be possible to connect two adjacent spherical plates using parallel bars similarly to the planar structure, though they cannot form simple pantographic elements as this possibility was ruled out in Section 5.3.

In the following the motion of the apexes has been considered though any other points on the plates could have been used instead. Figure 6.12(a) shows the circular motion of the apexes of two adjacent plates, A_I and A_{II} , as they are rotated incrementally about their fixed points. Denoting the fixed points \vec{e}_I and \vec{e}_{II} , and their identical rotations θ_E , the pseudo-vectors for the rotation of the apexes can be obtained from Equation 6.2

$$\vec{\omega}_I = 2 \tan(\theta_E/2) \vec{e}_I \quad \text{and} \quad \vec{\omega}_{II} = 2 \tan(\theta_E/2) \vec{e}_{II} \quad (6.22)$$

Consider the same rotations if plate I is fixed and plate II is allowed to move relative to this by releasing \vec{e}_{II} . Figure 6.12(b) shows how \vec{e}_{II} then moves along a circular arc about

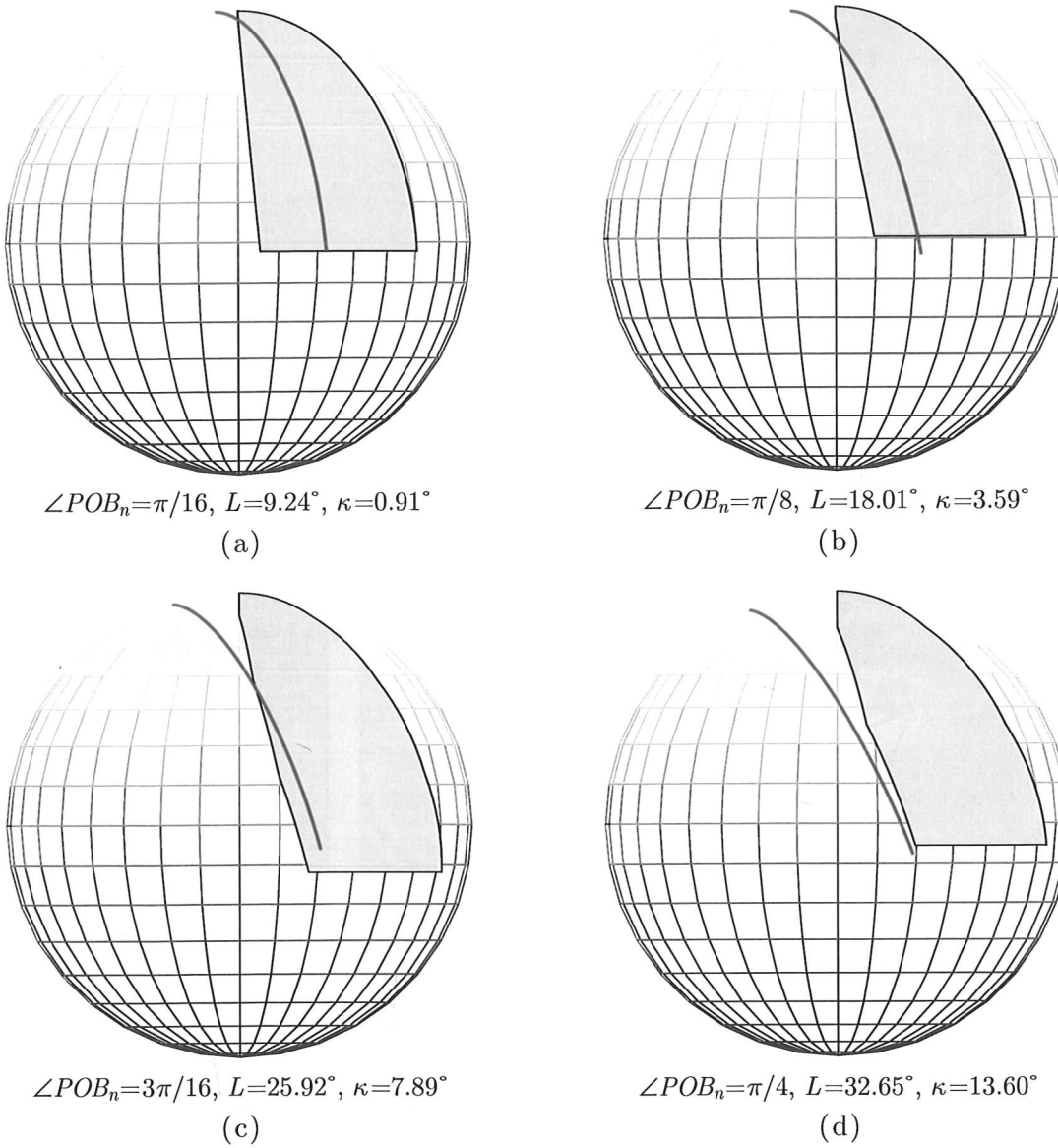


Figure 6.9: Possible locations of P_E for structures with $n = 8$ plates and increasing opening size $\angle POB_m$

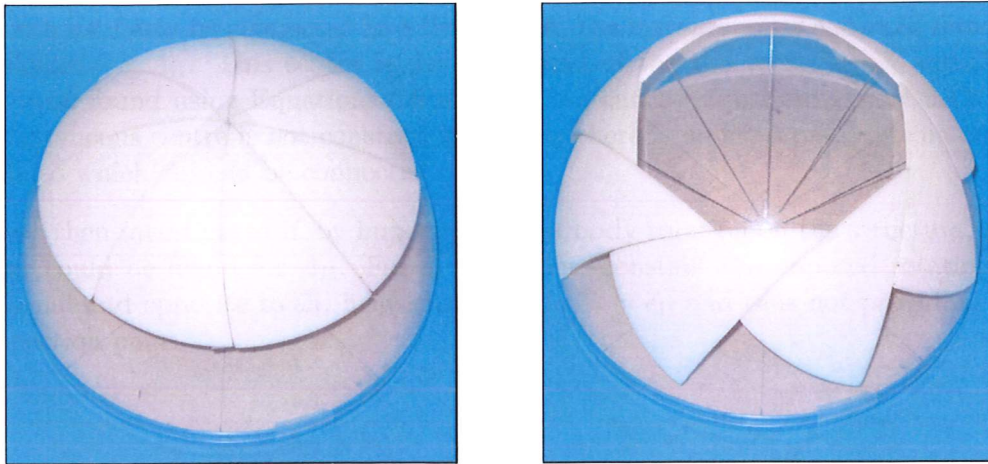


Figure 6.10: Physical model with fixed points of rotation

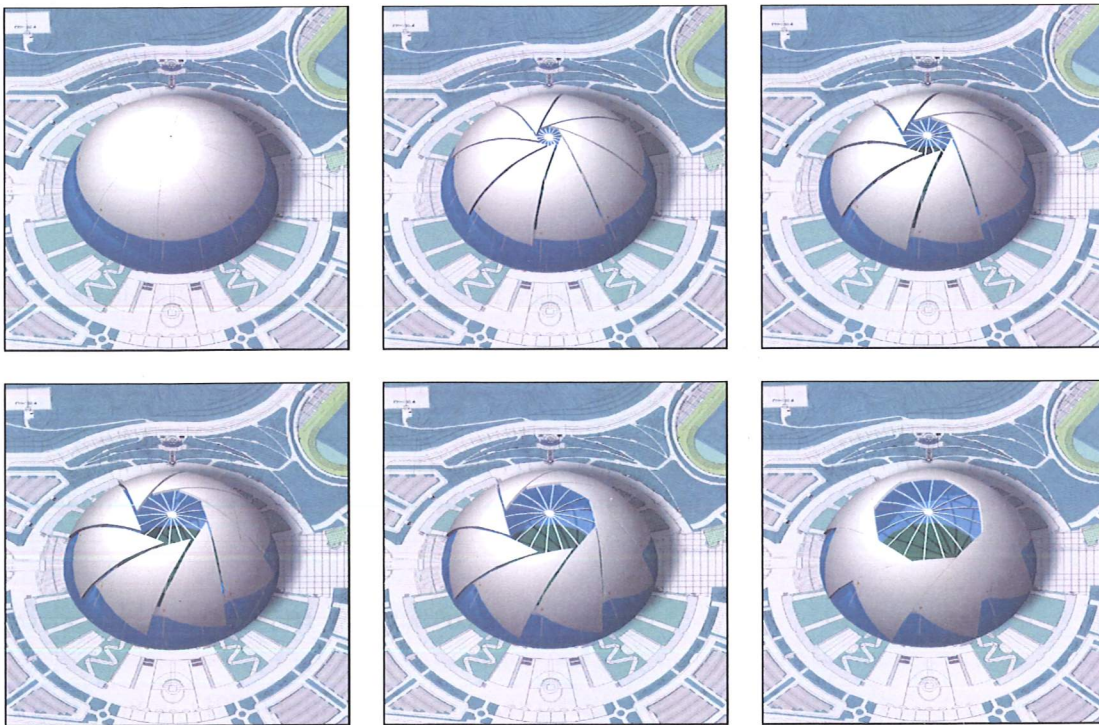


Figure 6.11: Computer generated images of how a retractable roof could be constructed from spherical plates with fixed points of rotation

\vec{e}_I hence keeping a constant length between the two points. This allows these points to be connected by a rigid bar through cylindrical hinges, as shown. To determine if A_{II} can similarly be connected to a fixed point, the instantaneous centre of rotation \vec{e}_i is plotted for A_{II} . This centre is the compound of the two rotations $\vec{\omega}_I$ and $\vec{\omega}_{II}$ and has been found using Equations 6.8 and 6.9. As can be seen from Figure 6.12(b) the instantaneous centre is not constant and hence there is no fixed point on the adjacent plate to which A_{II} can be connected.

It was then investigated if, by imposing a rigid body rotation on the structure, a fixed point could be found for A_{II} . For \vec{e}_i to become constant the imposed rotation must be equal and opposite to $\vec{\omega}_I$, hence resulting in $\vec{e}_i = \vec{e}_{II}$ and thus not providing a new connection point.

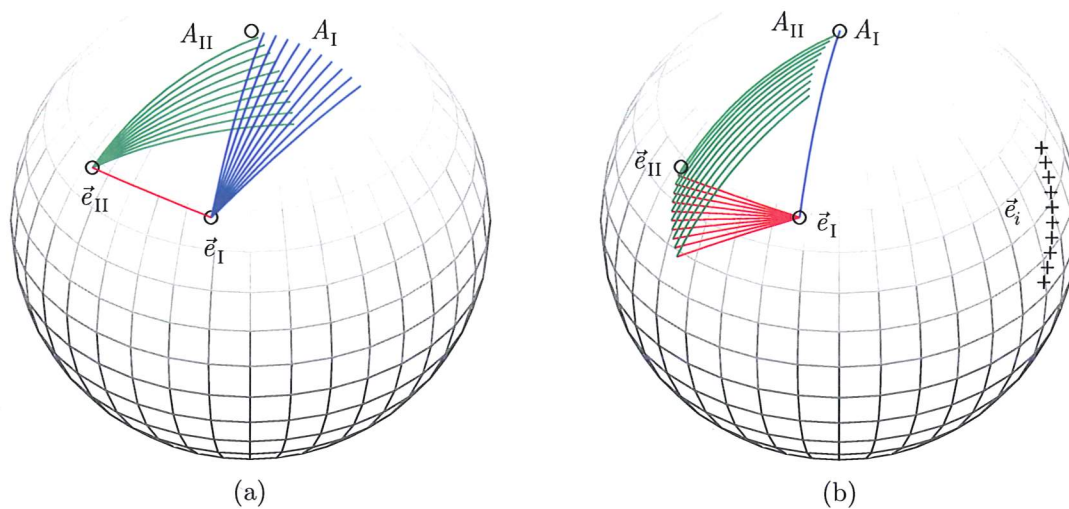


Figure 6.12: Incremental rotations of apex A_I and A_{II} (a) Absolute, and (b) Relative

Though only the motion of the apexes has been considered here, the same result can be found for any other point. It has thus been found that it is not possible to interconnect any point on plate I to plate II, other than the two fixed points. Therefore, other methods for interconnecting the plates are considered.

6.5 Reciprocal Mechanism

Chilton *et al.* (1998) proposed the planar retractable structure based on a transformable “reciprocal” frame, shown in Figure 6.13(a). A reciprocal framework consists of a three-dimensional beam grillage in which the beams mutually support each other. Each beam is only supported externally at its outer end, while the inner end is supported on the adjacent beam in the closed-loop structure. As all beams rest on each other, the structure formed is structurally stable. By allowing the inner beam ends to slide along the length of the adjacent beam a retractable system can be formed.

Allowing the beams to rotate relative to each other by means of simple scissor hinges and letting the inner end of the beam slide along its supporting beam is not enough to form a retractable mechanism. Consider the structure shown in Figure 6.5(a). If the structure is to have only a single internal degree-of-freedom the rotations of all beams must be identical. However, simple trigonometry shows that if the distance between the external supports A and C is constant and $\angle BAC = \angle DCE$ then both AB and BC must change lengths for $\triangle ABC$ to maintain the constant sum of angles π . Hence two sliding connections and two hinges are needed for each beam in the structure. The sliding connection that allow changes in length of AB can be positioned at either A or B (Chilton *et al.*, 1998).

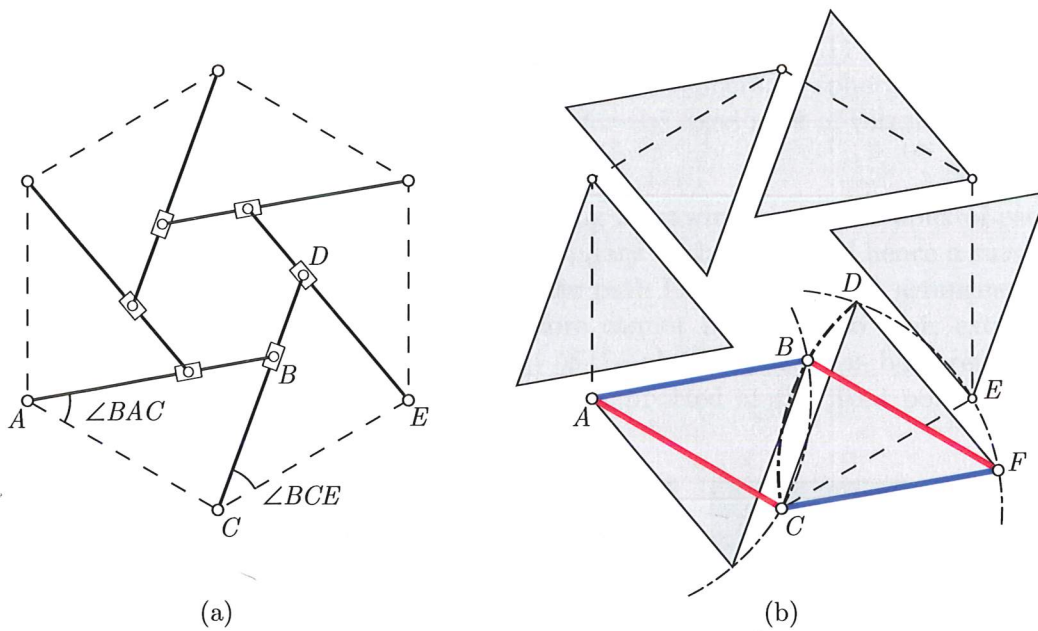


Figure 6.13: Reciprocal retractable structures (a) Beam grillage, and (b) Swivel Diaphragm

A similar mechanism is proposed for the spherical plate structure. As for the planar mechanism, Figure 6.12(b) shows that the length of arc $\vec{e}_{II}A_{II}$ must be increased if A_{II} is to lie on the arc $\vec{e}_I A_I$ as the two apexes are rotated synchronically. The solution for the beam structure has been to add an additional sliding connection. This is however not necessary for the spherical plate structure.

In the beam structure, the use of beam elements required hinge B to follow the straight beam CD , which on the sphere corresponds to the arc $\vec{e}_I A_I$. This is not the case for a plate element, where non-straight paths can be accommodated within the boundaries of the plate. Hence it is possible for apex A_{II} to slide along its non-straight path shown in Figure 6.12(b), thus allowing the spherical plate elements to form a reciprocal retractable structure without a second sliding connection.

The shape of the non-straight path is identical for all plates. Therefore, the motion of all plate apexes will occur synchronously along identical paths, following a rotation of each plate about its fixed point. Two smaller models have been constructed to show

the principles of such a reciprocal spherical structure.

Note, for a planar structure consisting of plate elements where the length of AB is constant, the instantaneous centre of rotation for hinge B lies on the circular arc DEF , as shown in Figure 6.13(b). Points D and F on the neighbouring plate element follow the same path as the plate is rotated about C . It can be shown that the length of BF is constant and these two points can hence be connected, thus forming the four-bar linkage $ABCF$. This solution is that of Rodriguez & Chilton (2003), see Section 2.4.3.

6.5.1 Small Physical Model

The first smaller model is based on the design shown in Figures 6.11 and 6.12. The model, Figure 6.14, consists of a supporting plastic hemisphere, of spherical plate elements fabricated using FDM, of steel rods used for the fixed axes of rotation, and of sliding connections realised as follows.

The sliding mechanism was modelled by attaching a drawing pin at the apex of each plate. The path of the apex lies outside the boundary of the plate and hence a curved slot in a piece of thin, clear plastic provided the path for the pin. This arrangement limits the motion of the plates, which therefore cannot be moved to their extreme positions, Figure 6.14. In this model, the top of the plastic sphere has been removed and the structure thus spans the gap; it is only supported at the fixed points, thus proving the concept of the reciprocal structure.

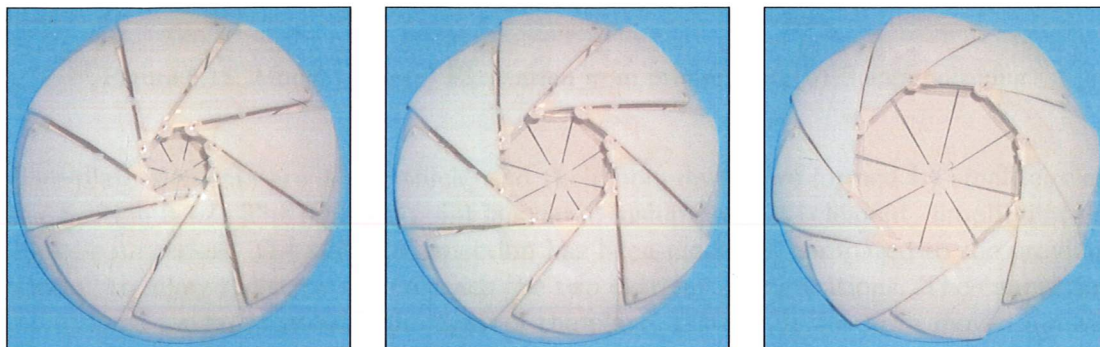


Figure 6.14: Smaller model interconnected by pins running along curved paths

6.5.2 Large Physical Model

A larger and more detailed model was also fabricated but using a different prototyping technique. This 400 mm span model consists of eight spherical plate elements, eight curved columns and four curved beam elements, Figure 6.15(b). All parts were fabricated in a single *nine* hour printing process at the Faculty of Architecture, University of Delft.

The fabrication process used is based on 3D Ink-Jet printing of binder fluid which

fuse the elements formed from a plaster-based powder (Z Corporation, 2001). First, the printer spreads a thin layer of powder on top of a piston. Second, a layer of the part being created is then printed with a binder from an ink-jet print head. Next, the piston is lowered to make room for the next layer of powder and the process is repeated. As the part is taking shape it is surrounded and supported by loose powder. This is removed from the finished part using a vacuum cleaner and compressed air, Figure 6.15(a). After a twenty-four hour curing period the parts were infiltrated with a cyanoacrylate adhesive to increase strength and durability. This also allows the surface of the parts to be polished.

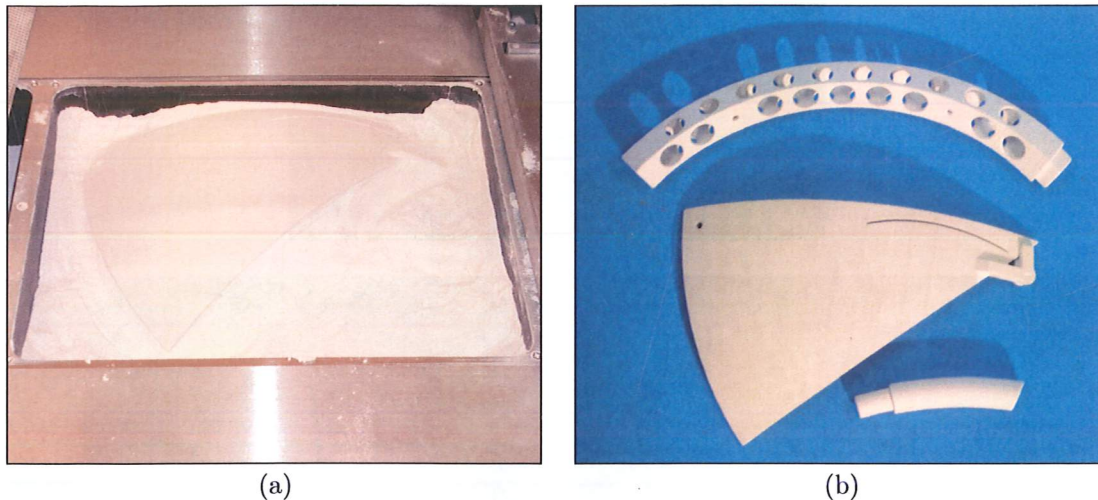


Figure 6.15: Model parts (a) Excavation from printer, and (b) Before polishing

The plate elements are 4 mm thick, and their boundaries are formed by small circles, see Section 5.4.1. The rotation point is located inside the plate element, simplifying the hinge connection. The sliding connection has been modified, compared to the previous model, to allow the structure to reach the two extreme configurations. The connection point is no longer located at the apex of the plate. Instead, it has been moved outside the element using four short beams. This allows the path of the connection point to lie within the boundaries of the neighbouring plate. The four beams were integrated into the plate shape and hence fabricated as a single part. The beams are arranged in pairs on the inside and the outside of the plate, to allow the neighbouring plate to slide between them. The four beams are used to hold a 2 mm diameter aluminium pin which connects the two plates through a curved slot. The slot was included in the 3D computer model, allowing it to be printed directly, which resulted in higher accuracy than if the slot had been cut after fabrication.

The larger size of the model prevented the use of the smaller plastic hemispheres for support. The supporting structure was therefore made using the same fabrication method as for the plate elements, as this allowed a spherical support surface to be formed. The support structure is formed by four curved beam elements which when slotted together form a circular ring beam. The ring is carried by eight columns slotted into the beam elements. The ring was prestressed using rubber bands to eliminate any



Figure 6.16: 400 mm span model fabricated using 3D Ink-Jet printing

loss of stiffness due to the opening of any gaps. The connections between the spherical plates and the supporting structure was made with 5 mm diameter pins machined from a polytetrafluoroethylene (PTFE) rod. To reduce friction the contact surfaces were polished with fine sand paper and spraycoated with PTFE.

The fabrication time and costs were governed by several factors: volume, surface area and orientation during printing. The parts of the model were designed to minimise the costs of the model. Without quantitative knowledge of the material properties, a thickness of 4 mm was decided upon for the plates. To provide sufficient stiffness to the structure while minimising material use the ring beam was formed as a hollow section. Further reductions in material use were achieved by introducing circular holes in the walls.

Though the structure is relatively small, it exhibits some interesting structural properties. In the open and closed configurations the plates come in contact along their adjoining boundaries. Hence the structure performs more like a continuous shell in these configurations than a three-dimensionally connected series of plates. If this could be implemented on a larger scale, the structural efficiency of such a structure would be increased considerably as a retractable roof would be required to carry the ultimate loadings only in these extreme configurations.

Another interesting feature of the model is that it normally tends to move toward the open configuration as in the closed configuration the potential energy is at its maximum. This enabled a very simple actuation system to be implemented on the model. By mounting a cable loop near the apexes of the plates it was found possible to control both the opening and the closing of the structure. As the model always wants to open itself the cable loop remains in tension. Therefore, by varying the length of the cable loop the model can be opened or closed. For a larger structure the required tension force and hence actuator effect could be lowered by running the cable around the opening a number of times, thus providing an efficient gearing.

6.6 Discussion

Based on the shape of spherical plate elements described in Chapter 5 this chapter has presented two simple mechanisms that allow the uninhibited movement of the plates between their extreme configurations.

Using the theorem of Euler it has been found possible to determine a fixed point of rotation about which a spherical plate element can be moved between its two extreme configurations through a simple rotation on a spherical surface. The location of the fixed point has been found to be governed only by the relative position of the extreme configurations with respect to the central axis of the structure, see Section 6.3. Furthermore, a single great arc has been shown to define all possible locations for the fixed point, as shown in Figure 6.9. The figure also shows that for some structures it is possible to choose the location of the fixed point such that it is located within the boundary of the rotated element thereby simplifying the structure. Based on this discovery a novel type of retractable roof system has been proposed, where each individual spherical plate element is rotated about a fixed point.

A geometric study of the relative motion of two adjacent plate elements rotated about fixed points has found that it is not possible to interconnect the plate elements using a rigid member and cylindrical hinges only. Instead, a single degree-of-freedom mechanism based on a three-dimensional reciprocal system has been proposed. The mechanism connects the individual plate elements to each other through sliding connections, thus forming a self-supporting structure. Both novel concepts have been proved using physical models.

This chapter has only been concerned with identifying possible mechanisms for which the motion occurs on a spherical surface as this permits the use of simple hinges with only a single axis of rotation. Since it has been shown that it is not possible to connect neighbouring plates using rigid bars if the motion is to occur on the spherical surface, the next chapter investigates the possibility of interconnecting the plates with rigid bars when the motion is not constrained to a spherical surface.

Chapter 7

Spherical Retractable Structures: Spatial Mechanism

7.1 Introduction

In this chapter a third mechanism for spherical plate elements is presented. The mechanisms presented in the previous chapter were based on the use of cylindrical and sliding connections. The mechanism presented in this chapter uses spherical hinges only, i.e. hinges that allow rotation about all three axes. The motion is hence no longer constrained to the surface of the sphere and can thus be described as spatial.

The first part of this chapter shows that a particular symmetric structure formed by spherical plate elements and interconnected by rigid bars through spherical hinges has *zero* internal degrees-of-freedom and is hence kinematically a “rigid” structure. This is shown to cause internal strains in the structure if it is forced open or closed, using a simple geometric model.

The second part describes the optimisation process used to minimise the magnitude of the peak strain that occurs in the structure as it is forced to move. Modelling the opening of the structure through a number of identical steps the current spatial orientation of the plate elements is optimised such that the strain energy in the mechanism is minimised. Using the same model the position of the connecting hinges is also optimised. The result of this optimisation process is that it is possible to form a hinged structure which has negligible internal strains during opening and closing, though it is overconstrained.

The third part of this chapter presents the kinematic computer simulation carried out in order to verify the concept. The symmetry constraint imposed in the previous geometrical study is removed and using non-symmetric actuation it is found that the structure still exhibits a symmetric transformation. This shows that the structure has no other competing modes of deformation, which might allow it to start moving along an unexpected path.

7.2 Spatial Mechanism

As shown in Chapters 5 and 6, the angular defect of the sphere does not allow a spherical mechanism based on simple cylindrical hinges to be formed from either spherical plate or pantographic elements. Kokawa (2000, 2001) overcame the problem, for pantographic elements, by introducing additional rotational freedoms in the connections, as described in Section 5.3. For the spherical plate elements presented in Chapter 5 to form a gap and overlap free surface in both extreme configurations, the plates must necessarily lie on the same spherical surface in these two configurations. This is not the case for the mechanism proposed by Kokawa and hence a different mechanism is proposed for the spherical plate elements.

Consider the closed structure shown in Figure 7.1(a). This structure is composed of eight identical spherical plate elements, each fixed against translation through a spherical joint at point A . Each plate is hence capable of freely rotating about the three axes A_1 , A_2 and A_3 . The axis A_1 is normal to the sphere and the point A is chosen so that it coincides with P_E and hence a rotation θ_E about the axis A_1 will move the plate from its closed configuration to the open configuration as described in Chapter 5. The axis A_2 is tangential to the sphere and horizontal in the closed configuration, while A_3 is perpendicular to the plane defined by A_1 and A_2 . The three axes are local and defined relative to the plate element. Following Section 6.2.1 any orientation in space of the plate element can be described by rotations about A_1 , A_2 and A_3 . For the rotations about A_2 and A_3 equal to *zero* and that about A_1 also equal to *zero* the closed configuration is obtained while for the rotation about A_1 equal to θ_E and the rotations about A_2 and A_3 equal to *zero* the open configuration is obtained.

7.2.1 Mobility Count

A rigid body such as a plate element has six degrees-of-freedom in space. The three translational restraints of the spherical joint at A leave each plate element with three degrees-of-freedom, i.e. the ability to rotate freely about the fixed point. From this it is possible to determine how many connections must be made between adjacent plates in order for the structure to have only a single internal degree-of-freedom. This is done by determining the *mobility* of the structure.

The number of relative degrees-of-freedom between the bodies in a structure or mechanism, M , is equal to number of rigid bodies, each with six degrees-of-freedom, minus the number of independent constraints in the system. As explained above a spherical joint imposes three constraints, while a simple cylindrical hinge imposes five. The number M is generally referred to as the *relative mobility* of a mechanism. For a structure consisting of n plate elements connected by j joints, where joint i imposes u_i constraints the mobility relative to an origin O is equal to (McCarthy, 1990)

$$M = 6n - \sum_{i=1}^j u_i \quad (7.1)$$

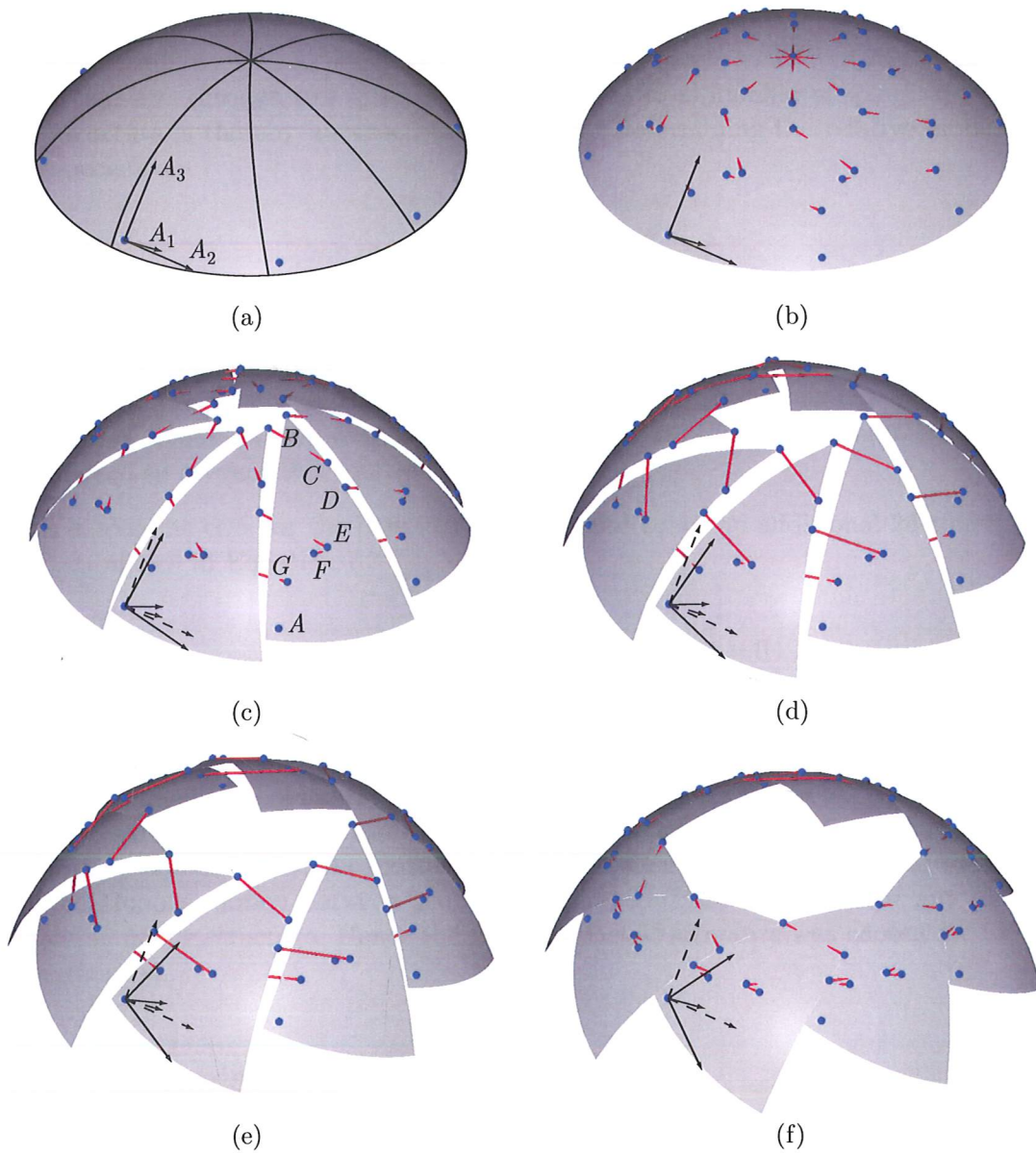


Figure 7.1: Spatial motion of $n = 8$ plate structure (a) Axes of rotation, and (b)–(f) Opening of structure

For the structure shown in Figure 7.1(a) the relative mobility is hence

$$M = 6 \times 8 - 3 \times 8 = 24 \quad (7.2)$$

To produce a structure with only a single internal degree-of-freedom it is therefore necessary to introduce a further 23 constraints. In Figure 7.1(b-f) the plate elements have been interconnected using 24 rigid bars. Each bar is connected to two adjacent plate elements through two spherical joints and the total number of spherical joints in the structure is thereby increased from 8 to 56. Determining the relative mobility of this mechanism

$$M = 6(8 + 24) - 3 \times 56 = 24 \quad (7.3)$$

Hence, introducing the bars has apparently been without effect. Consider a single bar fixed in space by two spherical joints. The bar should have zero degrees-of-freedom as $M = 6 - 3 \times 2 = 0$. It has however a single degree-of-freedom as the bar is capable of rotating about its own axis, i.e. $M = 1$. Hence an additional constraint must be introduced to prevent this rotation.

This is also the case for the bars in Figure 7.1 and hence an additional 24 constraints are introduced in Equation 7.3

$$M = 6(8 + 8 \times 3) - 3(8 \times 7) - 24 = 0 \quad (7.4)$$

Therefore, either this structure is not a mechanism, i.e. it is "rigid", or it is both statically indeterminate and kinematically indeterminate, in which case the mechanism is overconstrained (Pellegrino & Calladine, 1986). Removing a single bar should therefore give the structure a single degree-of-freedom but it would also remove the structural symmetry. Furthermore, the existence of a mechanism does not guarantee that there is a continuous motion between the two extreme configurations without any internal straining of the structure. Hence the fully symmetric structure was chosen for further investigation.

7.3 Optimisation

For both "rigid" and overconstrained mechanisms, internal strains occur in the structure if it forced to move. Therefore, an approach of minimising the peak strains occurring in a particular structure as it is forced to move, is valid for both the structure's mechanism being rigid or overconstrained. Thus, it is not necessary to determine whether the structure is rigid or overconstrained for the purpose of forming a hinged structure which develops only negligible internal strains when moved.

The magnitude of the strains developed in the structure as it is forced to move is determined by the overall shape of the structure and hence by altering the design of the structure, the strains can be influenced. It is therefore possible to minimise the

strains in the structure to prevent material failure and lower the energy required for opening and closing the structure. The technique used below is similar to that used for a solid surface deployable antenna by Guest & Pellegrino (1996a,b).

To optimise the design the strains must be determined. These can be found using a variety of methods, and a non-linear finite element analysis would provide the most accurate results. However, instead of this complex analysis a simpler approach based on geometry is proposed. If the plate elements are modelled as rigid, all straining will occur in the connecting bars and the strains can then be found by considering the position of the connection points. By imposing perfect symmetry on the structure, and hence additional constraints, the problem is further simplified as only a single plate element and its connection points need be considered.

The initial closed configuration is defined as unstrained and hence the strains for all other configurations can be found from the current distance between the connection points. The strain to be minimised, Δ , is defined as the sum of the squares of the strains in the three bars connecting two adjacent plates, ε_{BC} , ε_{DE} and ε_{FG} . Hence

$$\Delta = \sqrt{\varepsilon_{BC}^2 + \varepsilon_{DE}^2 + \varepsilon_{FG}^2} \quad (7.5)$$

7.3.1 Element Orientation

To find the current location of connection points B , C , D , E , F and G for any particular configuration let the orientation of the plate element be defined by rotations about the three axes A_1 , A_2 and A_3 . Then given, in the closed configuration, the position of connection point $B(\vec{v}_0)$ the current position $B(\vec{v}_3)$ for another configuration can be found using compound rotations as described in Section 6.2.1

$$\vec{v}_3 = (\mathbf{R}_3\mathbf{R}_2\mathbf{R}_1)\vec{v}_0 \quad (7.6)$$

where the three rotation matrices correspond to rotations θ_1 , θ_2 and θ_3 about the axes A_1 , A_2 and A_3 respectively. Note that the axes are local to the plate element and hence are also rotated, as can be seen in Figure 7.1(b-f). A fourth rotation of $2\pi/n$ about the central, vertical axis of the structure produces the location of the connection points on the adjacent plate, allowing Δ to be determined for the current configuration. The strain is hence a function of the three rotations $\Delta(\theta_1, \theta_2, \theta_3)$ if the locations of the connection points on the plate element are given.

Because the fixed point A coincides with the Euler pole P_E the rotation about A_1 can be used to drive the opening of the structure using $0 \leq \theta_1 \leq \theta_E$. This range of rotation is subdivided into s identical steps, defining the total number of configurations for which Δ is to be evaluated. As θ_1 is predetermined for all configurations the optimisation problem then becomes a function of θ_2 and θ_3 only.

The optimisation of $\Delta(\theta_2, \theta_3)$ has been solved using the MATLAB function *fminunc* from the optimisation toolbox (The MathWorks, Inc., 2002, 2003). This function finds a minimum using unconstrained nonlinear optimisation based on a Quasi-Newton

method. Gradients were not provided and hence MATLAB used its medium-scale algorithm, which uses finite-difference to find the gradients. Convergence was achieved in approximately five iterations, and hence the formulation was found computationally efficient. The number of steps was found to have negligible effects on the convergence.

To allow faster convergence, the values of θ_2 and θ_3 obtained from the previous step were fed into a higher level optimisation loop. As the motion path of the plate elements is continuous the results from the previous step are in the vicinity of the results for the current step, and hence the last set of results provides a good initial estimate for the optimisation algorithm. For the first step the initial estimates were all set to zero.

For a chosen particular design, it is thus possible to determine the spatial motion of the plate elements which minimises the strain in the bars at each opening step. The motion is given in terms of rotation about A_1 , A_2 and A_3 and allows the peak strain in the structure to be determined.

Figure 7.2 shows the results for a simulation of the structure shown in Figure 7.1. This trial design was found using heuristic methods and with the AutoCAD drawing package (Autodesk, Inc., 2002). Figure 7.2(a) shows the results for the strains in all three bars and the strain function Δ when the simulation is carried out in 50 steps. The peak strain was determined as $\varepsilon_{FG} = -0.069\%$, i.e. close to the yield strain of steel. From the figure it can be seen that strains are not equal in all bars and they vary as the structure is opened. Figure 7.2(b) shows the optimised rotations θ_2 and θ_3 . As the rotations are not small they represent a significant deviation from the surface of the sphere. This is clearly visible in Figure 7.1 also. Note that both the strains and the rotations are equal to *zero* at both extremes, showing that these two configurations are unstrained and coincide with the surface of the sphere.

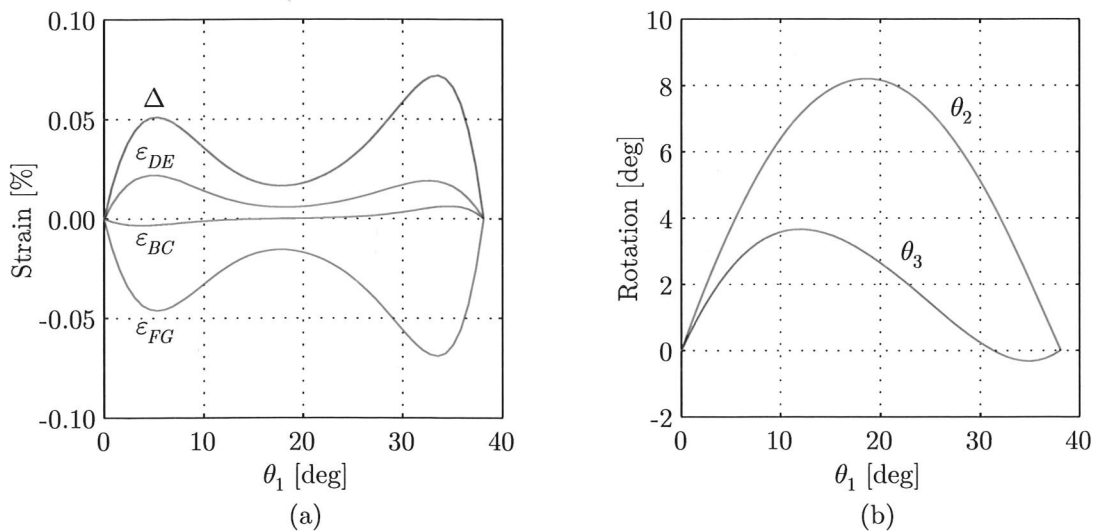


Figure 7.2: Simulation results for (a) Internal strains, and (b) Rotations

7.3.2 Connection Points

In the previous section a particular design was considered. This section is concerned with optimising the design of the structure and hence the location of the connection points B, \dots, G . The overall plate shape, location of the fixed point and its associated rotation are not included in the following optimisation and are hence held constant.

Consider the structure in Figure 7.1. In the closed configuration the connection points lie on the surface of a unit sphere and hence each point is defined by only two spherical coordinates, longitude and latitude. Thus for the six connection points a total of *twelve* variables are to be optimised. However, by defining both the initial closed and the final open configuration as unstrained, it is possible to reduce this number.

Consider Figure 7.3. In Section 5.4.1 it was found that two neighbouring plates move by a distance L and rotate by an angle κ relative to one another when moved from the closed to the open configuration, see Figure 5.10. Therefore, if plate II is fixed, plate I and hence point B must move by a distance L as shown. If bar BC is to be unstrained in the two extreme positions, then C must lie on a great arc which is perpendicular to the great arc B_0B_m , defined by the extreme positions. Hence, if B is defined then C can be determined from the *connection angle* ϕ_C as shown. The total number of variables for the optimisation problem is thus reduced to *nine* as the same applies for connection points E and G .

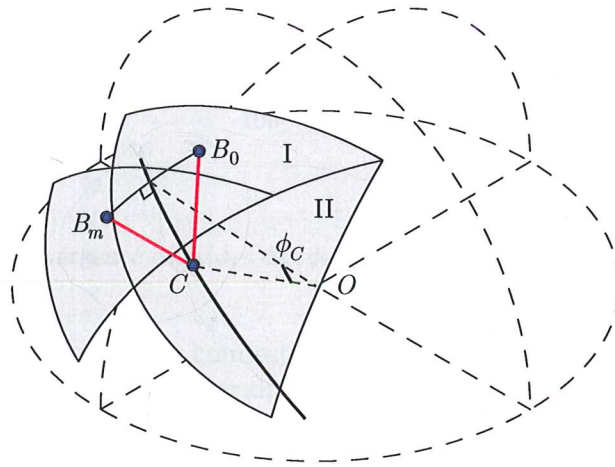


Figure 7.3: Defining the location of point C using point B and angle ϕ

Optimisation Using Connection Angles Only

Before attempting to solve the full optimisation problem a smaller problem was solved. By only optimising the location of the points C, E and G the design optimisation problem is limited to *three* variables and the strain function is thus $\Delta(\phi_C, \phi_E, \phi_G)$.

For a particular design given by ϕ_C, ϕ_E and ϕ_G , the peak strain occurring in the structure as it is moved is found by optimising the problem $\Delta(\theta_2, \theta_3)$ as described in Sec-

tion 7.3.1. Thus, for each loop of $\Delta(\phi_C, \phi_E, \phi_G)$ the problem $\Delta(\theta_2, \theta_3)$ is solved to allow the peak strain to be minimised for that particular design.

To solve $\Delta(\phi_C, \phi_E, \phi_G)$ MATLAB was used. Two different functions were tested for best performance, *fminunc* and *fminsearch*, both from the optimisation toolbox. From Figure 7.1(c) it can be seen that point *C* is located on the boundary of the plate and hence ϕ_C should be constrained to prevent the point lying outside the boundary of the element. As both MATLAB functions use unconstrained algorithms, the constraints were imposed within the strain function itself. For the current problem it was found necessary to constrain ϕ_C only. Figure 7.4 shows the convergence of the two functions. Using 54 iterations and 302 function evaluations *fminunc* found a minimum of 0.03866%, while *fminsearch* used 64 iterations and only 118 function evaluations to find the same minimum. Hence it was, in general, found for the current formulation that, although generally less efficient, the direct search method of *fminsearch* was superior to *fminunc* if given identical initial estimates for the variables.

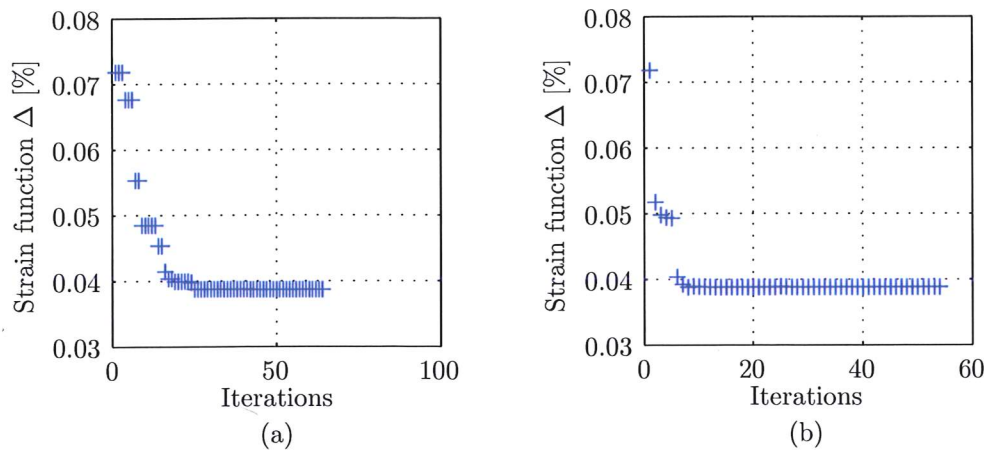


Figure 7.4: Convergence of $\Delta(\phi_C, \phi_E, \phi_G)$ using (a) *fminsearch*, or (b) *fminunc*

The optimised locations for the connections were $\phi_{BC} = 10.5^\circ$, $\phi_{DE} = 12.6387^\circ$ and $\phi_{FG} = 20.1186^\circ$ and the resulting strains and rotations are shown in Figure 7.5. When compared with the original results shown in Figure 7.5 for $\phi_{BC} = 10.5^\circ$, $\phi_{DE} = 12.5006^\circ$ and $\phi_{FG} = 19.8793^\circ$ it can be seen that Δ has been correctly optimised as the peaks of Δ are now of the same magnitude. The location of the connection points has not been significantly changed, although the peak strain in bar *FG* has been lowered from $\varepsilon_{FG} = 0.069\%$ to $\varepsilon_{FG} = 0.037\%$, i.e. almost halved. This has been achieved by finding a solution where the strain in the bars varies between tension and compression. Note that there are four configurations in which there are no strains in either bars and an additional configuration for which *BC* is unstrained. This indicates that in practice the structure will have some sort of snap-through behaviour.

Parametric Study

It was found through a limited parametric study that the length of bar *BC* governs the rotations about A_2 . As the bar is located the furthest away from the fixed point *A*, it

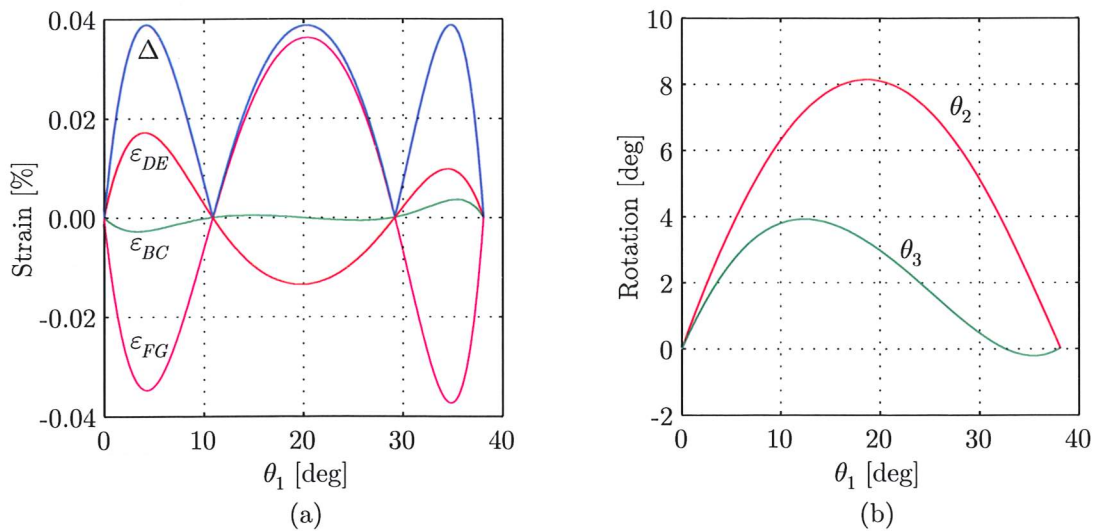


Figure 7.5: Simulation results for optimised values of ϕ (a) Internal strains, and (b) Rotations

governs the extent of the deviation away from the spherical surface. It was observed that if the bar was shortened the plates would have to be rotated further away from the sphere in order to accommodate the length of the bar. This was found to be caused by the length of the bar being determined by both ϕ_C and L . If ϕ_C is set equal to zero the bar has a length of approximately L (it is a straight line and not a great arc hence the approximation to L) and hence the gap between adjacent plates is approximately L when the structure is opened halfway. As ϕ_C is increased the gap is reduced as this is approximately equal to the length of the bar minus the arc length subtended by ϕ_C . It was also found that the strains in all bars are generally reduced as ϕ_C is increased and hence ϕ_C was found to be constrained by the boundary of the plate element.

Similarly it was observed that bars DE and FG governed the rotation about A_3 . From Figure 7.5 it can be seen that the strains in these two bars are of opposite signs, though they were not of identical magnitude. It can also be seen that the strains decrease with an increased distance between a bar and the fixed point.

Optimisation of All Points

The optimisation of all or selected connection points is an optimisation problem of higher order than that for ϕ only. Convergence and solutions of the two MATLAB functions *fminunc* and *fminsearch* were therefore compared again. For a fifth order problem, i.e. five variables, convergence plots are shown in Figure 7.6. For this and other problems it was found that from identical initial estimates that *fminsearch* produced superior results in terms of the minimum found, here $\Delta = 0.0029\%$ compared with $\Delta = 0.0157\%$. The difference was found to be large enough to justify the higher number of function evaluations required, 855 compared to 501, and hence *fminsearch* was used for subsequent simulations. Though this algorithm produced good results, restarting the algorithm at a previously found minimum would sometimes produce

another lower minimum hence suggesting that there exist local minima in the solution space.

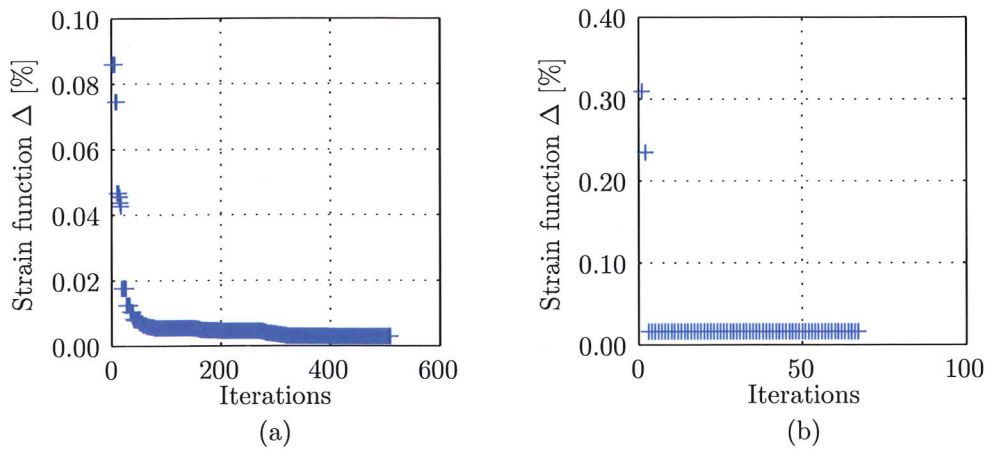


Figure 7.6: Convergence of Δ using (a) *fminsearch*, or (b) *fminunc*

Instead of solving the problem with nine variables, it was found that it could be advantageous to only release a few points at a time and hence iterate towards a better solution by restarting the algorithm. Using this technique two issues were discovered. The problem had been formulated such that the strain function would become *zero* if two bars were to coincide, i.e. effectively reducing the number of bars to only two and resulting in the mechanism being no longer overconstrained. Based on this, constraints were introduced on the latitude of points B , D and E . Similarly, it was also found that point B would tend to move away from the constrained point C and hence lie outside the boundaries of the plate element. Constraints were thus imposed also on the longitudes of points B , D and F .

By releasing the location of points B , D and F it was found necessary to update continuously the constraints for ϕ_C , ϕ_E and ϕ_G , using spherical trigonometry.

Connections of Finite Size

With the aim of designing a physical model it was decided to introduce constraints that would represent spherical joints of finite size. Figure 7.7 shows two designs where the extent of the connections is shown as circular holes in the plate elements. The radius of the joints is equal to 10% of the radius for the spherical surface. The size of the joints were chosen with the aim of constructing a small scale model, hence the relatively large size of joints. Inspection of the figure shows if joints interfere with each other or lie outside the boundary of the plate. In Figure 7.1 it was found that the bars would conflict with the plate elements and hence it is thought that a physical model would have plate elements defined on a larger spherical surface and attached to the connection points using rigid links normal to the surface.

The solutions presented in Figure 7.7 were found by fixing the points B and D , resulting in an optimisation problem with five variables. As can be seen, B was located as close

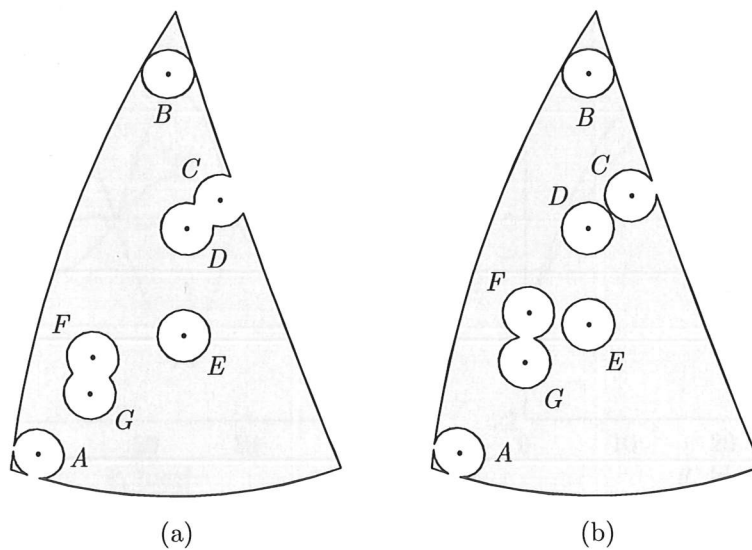


Figure 7.7: Two designs with finite sized spherical joints

to the apex as possible so this would be properly supported. D was located such as to avoid interference with point C . As the location of D and the constraints for F were defined iteratively, early designs showed some interference, Figure 7.7(a).

The peak strains for the design presented in Figure 7.7(a) were found to be $\Delta = 0.00068\%$, Figure 7.8(a). For all practical purposes these strains are negligible and hence justify the use of the simple geometric model presented, instead of a more complex finite-element model. From Figure 7.8(b) it can be seen that the rotation about A_2 has also been reduced, compared with Figure 7.5(b), as a result of an increased length of bar BC .

Figure 7.7(b) shows a design where there is little interference between the spherical joints. This was achieved at a small increase in strains, though they were still negligible as shown in Figure 7.9. The larger strains were found to be caused by the increased distance of points F and G from the fixed point A . If no constraints were imposed on these points they would tend to coincide with A , hence eliminating the strain in bar FG and subsequently the mechanism.

Figure 7.12 shows a design which is a compromise between the two shown in Figure 7.7. Unlike any of the results presented above, the strain function Δ has *four* peaks for this design, Figure 7.10. Though the first peak does not have the same height as the three others it shows that three peaks are not an inherent feature of this type of mechanism.

7.4 Kinematic Model

To verify the results presented above, a kinematic model was built using ProEngineer and its kinematic analysis package. The parts of the model, plate elements and bars were defined as rigid bodies. A fixed, rigid ring beam was used as a support. The

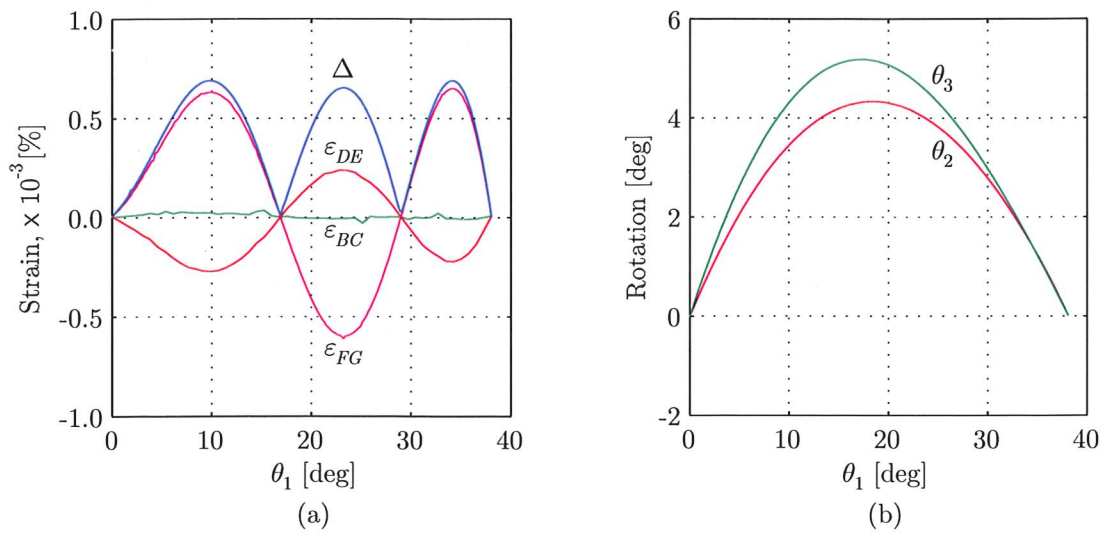


Figure 7.8: Simulation results with lowest achieved strains (a) Internal strains, and (b) Rotations

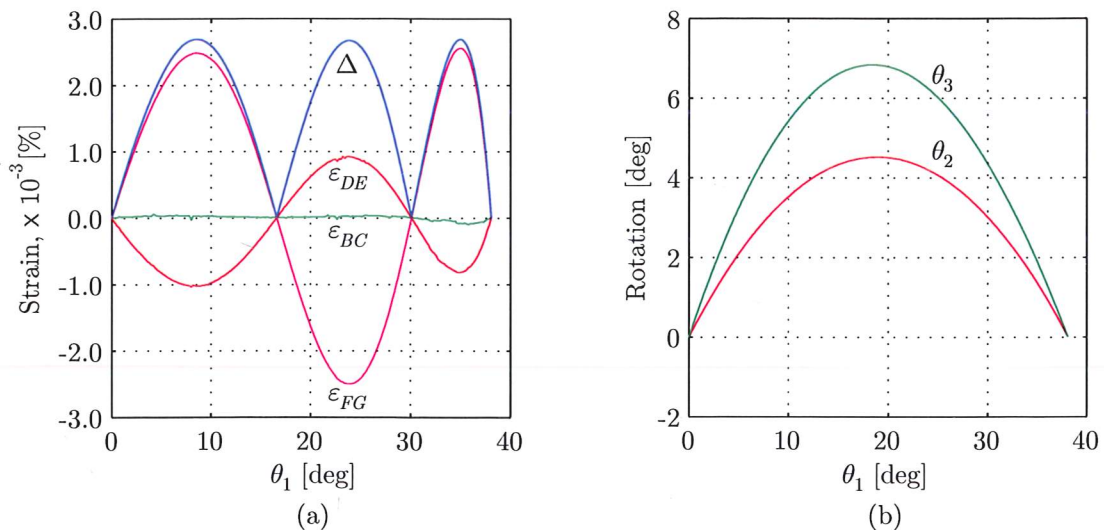


Figure 7.9: Simulation results for design with finite sized joints (a) Internal strains, and (b) Rotations

plate elements were connected to this ring via spherical joints. Similarly the bars were connected to the plate elements through spherical joints.

The design used was that optimised for ϕ only and hence with a peak strain of 0.037%. However, the kinematic simulation module available in ProEngineer is based on rigid bodies and hence no elastic deformation is modelled. This issue is solved in ProEngineer by allowing a definable misfit at the connections, i.e. the connection between two parts is modelled as a deformable element with a predefined maximum *tolerance*. Hence,

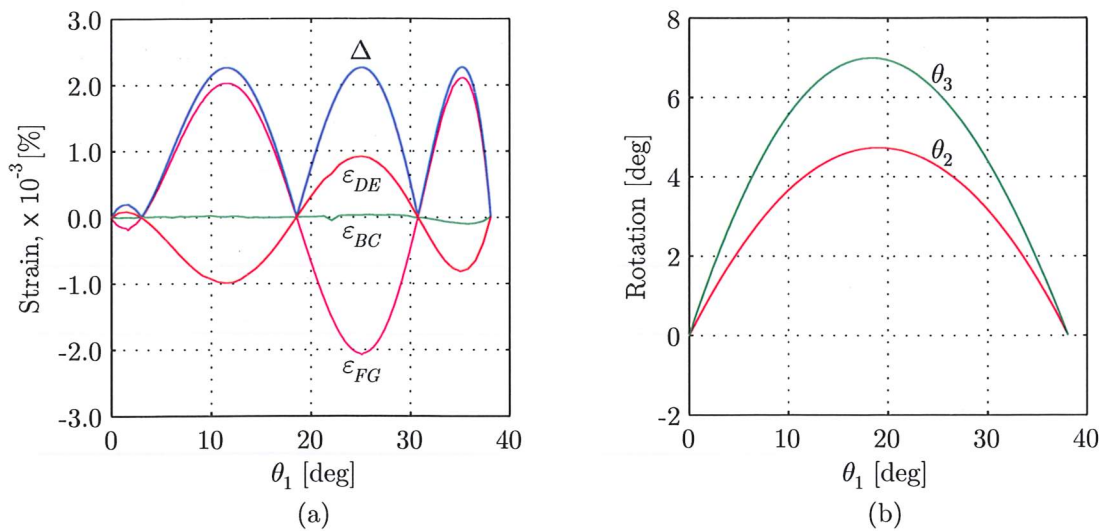


Figure 7.10: Simulation results with four peaks in the strain function Δ (a) Internal strains, and (b) Rotations

to assemble the parts of the model, the program solves a numerical problem which may not necessarily result in a perfectly symmetric solution. Furthermore, for each configuration or step of the motion the program had to solve this numerical problem, i.e. reassembling the structure at each step. It was found that the program would have problems in obtaining solutions if the step size was too large, and hence s was set at 500 though a high tolerance was still required to obtain convergence for all configurations. The original, non-optimised solution of Figure 7.2 could not successfully be modelled for all steps of opening.

The geometry was based on a unit sphere and hence the length of bar FG was 0.398. For the kinematic analysis package a *typical length* of *one* was defined to allow the tolerance to be defined also. To obtain convergence in all configurations the tolerance was increased until the full motion could be modelled. This required the tolerance to be set at 0.010. For the bar FG this corresponded to a peak strain of $2 \times 0.010/0.398 = 5.0\%$. Comparing this with the expected strain of 0.037% it is clear that the solution obtained by ProEngineer is less accurate than that found above. However, from the image sequence in Figure 7.11 it can be seen that the opening process is correctly modelled and the structure preserves symmetry throughout the opening, though symmetry is not imposed.

In the geometric analysis of Section 7.3 symmetry was assumed and hence the structure was effectively actuated at eight locations thereby imposing additional constraints. The kinematic model was used to investigate if the removal of these additional constraints would result in additional degrees-of-freedom. This was done by using a single asymmetrically placed actuator. To excite any additional mechanisms the actuation was not imposed as a rotation about an axis. Instead, the model was actuated by imposing an outward, horizontal translation of the apex of a single plate element. In Figure 7.11 the apex of the nearest plate element is moved horizontally in a direction perpendicular to

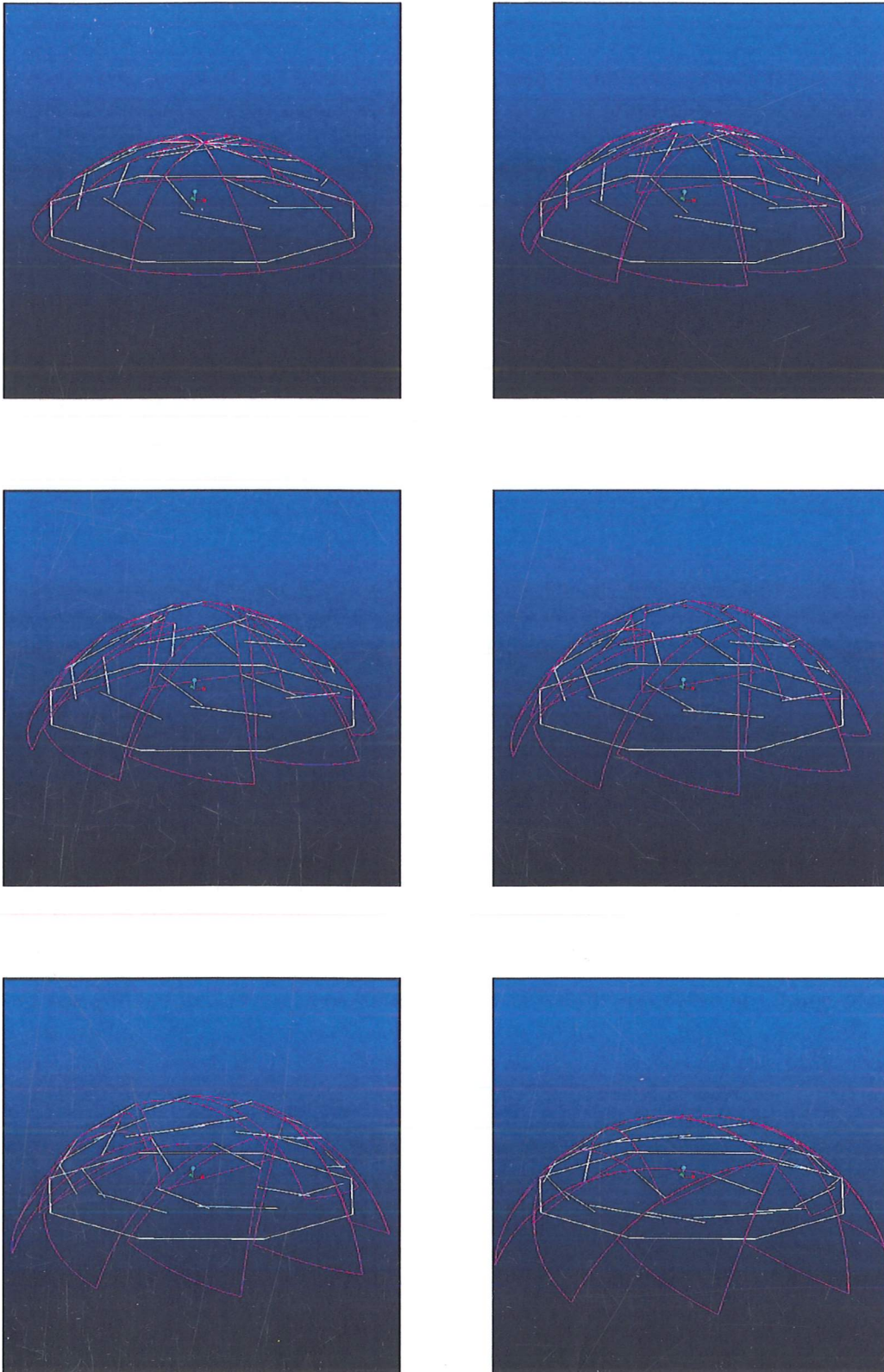


Figure 7.11: ProEngineer kinematic model

that defined by the nearest side of the octagonal ring beam.

As the motion was only imposed at a single point and in a single constant direction no symmetry was imposed on the structure. With non-symmetric actuation and the high tolerances allowed, it was expected that some type of non-symmetric motion would occur. This did not happen, as shown in Figure 7.11, hence proving that the structure only possesses a single internal mechanism. This was confirmed by altering the direction of the imposed motion as these only achieved small motions before the maximum tolerance was reached at the connections and convergence failure occurred.

7.5 Discussion

Based on the spherical plate elements derived in Chapter 5, this chapter has developed a spatial mechanism that allows the plate elements to be interconnected through fixed connection points only, hence omitting the need for sliding connections. To allow the resulting spatial motion, connections between plate elements were made through spherical joints.

The mechanism formed by the structure was found to be overconstrained by determining its mobility. Using a simple geometric model of the mechanism the magnitude of the internal strains occurring during a forced motion was determined. A limited parametric study based on the same geometrical model was used to determine the causes for these strains. The model was then used first to optimise the motion of the structure and then the location of the connection points on the plate elements. The optimisation process allowed the strains to be effectively eliminated, thereby creating a single degree-of-freedom for the structure.

This result was verified using a numerical kinematic analysis. Unlike the geometric model, this analysis did not impose symmetry on the structure or additional constraints in the form of synchronous actuation. The kinematic model showed that the structure only possesses a single internal degree-of-freedom and hence forms a true mechanism.

From the geometric study of the structure it was found that there are many possible designs with negligible small strains. It was also found to be possible to create such designs when joints of finite size were considered. However, the designs proposed can be further improved as collisions occur between the connecting bars as the structure opens and closes. This problem can be viewed in Figures 7.1 and 7.12. In the latter figure bar BC conflicts with DE in the final step shown, while DE collides with FG in the second step. Only limited attempts were made at resolving this issue and hence a satisfactory solution is still to be found. This might involve changes to the parameters excluded from the present study such as the number of plates, opening size and location of the fixed point.

Compared to the mechanisms presented in Sections 2.4.4 and 6.5 the current structure has a number of advantages. Though the structure has been formed on a spherical surface the method of geometrically minimising the internal strain can be used for structures of other shapes as shown by Guest & Pellegrino (1996a,b) hence allowing greater freedom in the choice of shape. Compared to the flat solution, the main struc-

tural elements, the plate elements, are fixed directly with a more direct load path as a result. Though spherical joints are more complex than simple cylindrical hinges the use of these avoids the sliding connections employed in the previous chapter. The limited rotations about the two axes A_2 and A_3 allow spherical joints with limited rotations to be used. Furthermore, the use of spherical joints will allow the connecting bars to act in tension or compression only and hence increase their effectiveness, though friction in the connections will be considerable and might cause bending in the bars. The main structural members are the plate elements which can be sized accordingly. The current design is thus structurally simpler than that proposed and constructed by Kokawa (2000, 2001) which also uses spherical joints. Importantly, the proposed structure also creates continuous, gap free surfaces in both the extreme configurations.

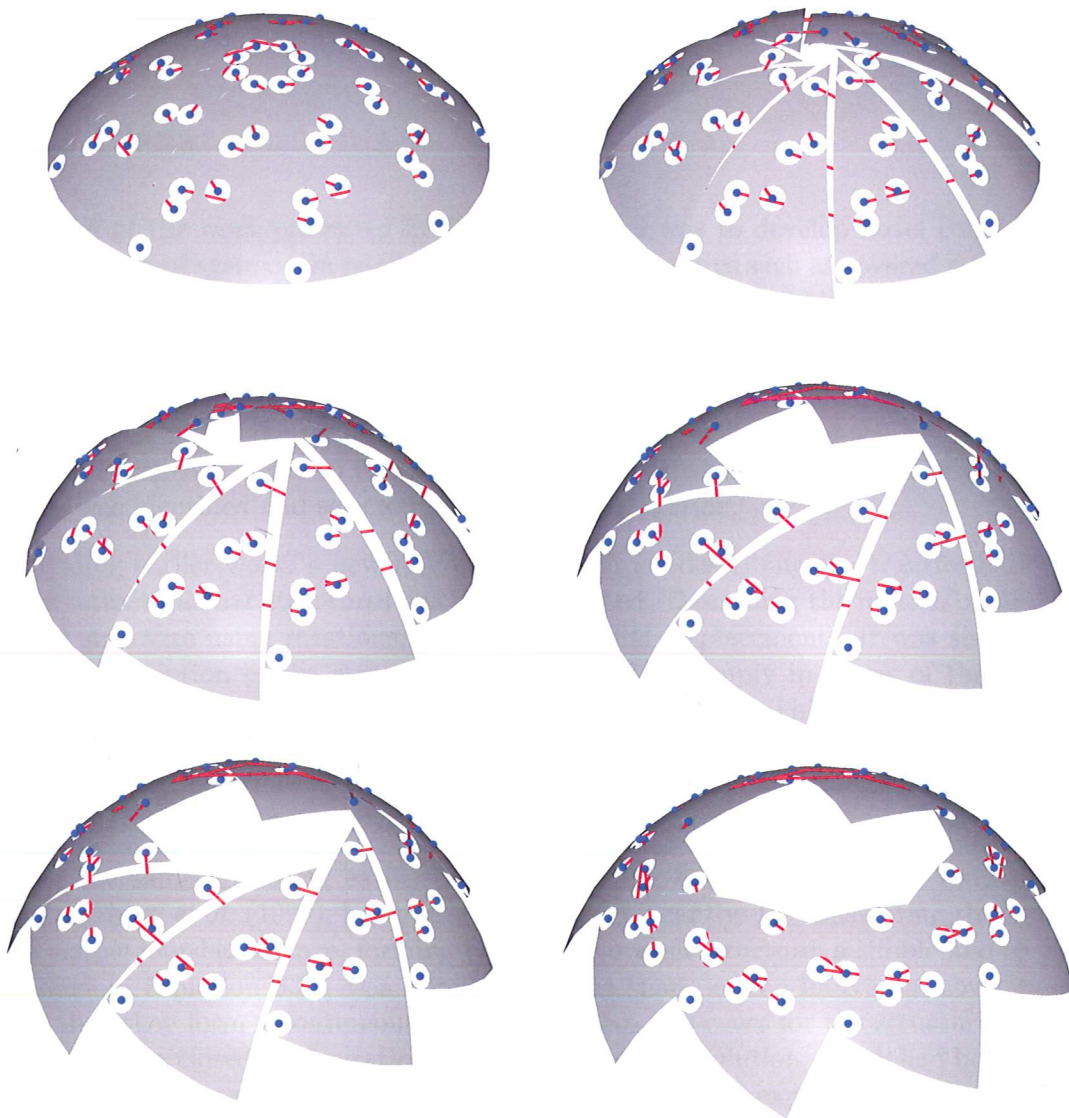


Figure 7.12: Motion revealing conflicts between bars

Chapter 8

Conclusions

8.1 Planar Structures

The aim of the work presented in this dissertation was to develop novel concepts for retractable roof systems, in particular large span structures such as covered stadia. The understanding of several previously known solutions for retractable structures has been advanced, and also a series of novel concepts for retractable roof structures has been proposed.

Based on an initial review of both existing and proposed state-of-the-art concepts, a promising concept based on two layers of interconnected bar elements covered by rigid plates was identified and selected for further investigation.

Extending earlier work, a new uniform approach for describing the transformation of these retractable bar structures has been developed. Describing the motion of all parts of the structure using rotations, rather than radial displacements, it was shown that the overall motion of the structure can be expressed simply in terms of the relative rotations undergone at each of the hinges in the structure. This, importantly, allows the constraints on the motion associated with members and hinges of finite size to be easily determined while also allowing structures of any planar shape to be designed much more easily than previously.

Using the same approach, earlier work on covering bar structures with rigid plates, by Kassabian *et al.* (1999), has been extended significantly. By considering the motion of a simple four-bar linkage, forming part of the overall structure, a simple and elegant expression, Equation 3.31, was obtained for the shape of the individual cover plates such that they form a continuous, gap and overlap free cover for the structure in both an open and a closed configuration. Unlike the previous solution, which had been found for particular plan shapes by heuristic methods, this general expression allows solutions to be found for retractable plate structures of any plan shape.

It has been shown that if certain constraints are satisfied the basic triangular wedge-shaped solution for the cover plates can be modified to have non-straight boundaries of nearly any shape. Hence, a great degree of freedom in the design of both the overall plan shape and the shape of the individual cover plates has been shown to exist and

demonstrated through a number of physical models.

A further advance that has been made is the design of plate elements that cover all the hinges of the underlying angulated elements to which they are attached. This allows the bar structure itself to be removed and two layers of plates to be connected directly, by means of hinges, hence forming a hinged plate structure. As the plates are connected at exactly the same locations as the original bar structure the kinematic behaviour of this hinged plate structure is identical to that of the original bar structure.

To evaluate the structural properties of such a plate structure, a 1.3 m proof-of-concept model has been designed and constructed. Using finite element analysis the required thickness of the plates and the location and number of supports was determined for the model. With the model suspended horizontally the analysis showed that the optimal arrangement of the supports is that all plates are supported directly, thereby significantly shortening the load paths in the structure. Comparing the analysis results with the physical model it was found that out-of-plane rotations in the bearings caused the maximum deflections of the physical model to be four to six times those predicted. However, the model did prove the concept of a retractable roof structure formed by hinged plates as the structure was, when held both horizontally and vertically, capable of supporting itself while opening and closing.

8.2 Spherical Structures

To increase their structural efficiency for longer spans, retractable structures of curved shape have been investigated. First, it was investigated whether the planar geometry of the plates could be adapted to a spherical surface. It was found that a structure composed of wedge-shaped spherical plates, with boundaries formed by great arcs would overlap in the extreme open configuration due to a change in the angular defect of the central opening. However, it has been discovered that by kinking or curving the boundaries of the spherical plates overlap can be avoided and a structure capable of forming a continuous gap and overlap free spherical surface, in both an open and a closed configuration, can be formed. Previous solutions for spherical retractable structures have all, as shown in Section 2.4.4, had some degree of overlap between their plates and hence this finding represents a significant improvement over existing solutions. It has been shown that it is possible to modify the basic shape of the spherical plates in a similar manner to the planar plates, if certain conditions are satisfied. This allows some freedom in the design of their final shape.

By considering the motion of pantographic elements adapted to a spherical surface, i.e. by letting all rotation axes be normal to the spherical surface, it has been proved that a circular closed loop mechanism could not be formed by such pantographic elements. Hence, alternative mechanisms had to be considered for a spherical retractable plate structure and a total of three mechanisms have been developed, allowing structures formed by spherical plates to open and close. The motion of the first two mechanisms occur on the surface of the sphere while the third is spatial.

When geologists model tectonic drift of the earth's continents, they describe the motion in terms of simple rotations about fixed axes running through the centre of the earth.

Using the same technique to describe the motion of the spherical plates that make up the retractable structure, it has been investigated how the spherical plates could be made to move from the closed configuration to the open configuration without interfering with one another. A simple solution where each plate rotates by equal amounts about symmetrically located fixed points was obtained. Based on this solution an original type of retractable dome structure was proposed.

With the aim of generating a single degree-of-freedom mechanism for the structure, thus eliminating the need for external synchronisation of the rotation, compound rotations were used to determine if neighbouring plates could be interconnected. It was shown not to be possible to use interconnecting bars and simple cylindrical hinges, but instead a self-supporting reciprocal mechanism, similar to that proposed by Piñero, was used for the structure (Escrig, 1993). Unlike the concept proposed by Piñero, shown in Figure 2.25, the current structure does not have any overlaps, and hence friction between neighbouring plates is removed. This makes it better suited for large scale applications. Other advantages are the possibilities of modifying the plate boundaries and the location of the fixed points about which the plates rotate. Small proof-of-concept models were constructed to demonstrate the ability of such a structure to open and close while supporting itself.

Unlike any previous retractable roof structures, the third mechanism is based on the use of spherical joints, i.e. hinges which allow rotation about three axes. Interconnecting the spherical plates through bars and spherical joints, the plates are no longer constrained to a spherical surface, hence giving this new self-supporting structure a spatial motion. By initially forming an overconstrained mechanism, effectively a single degree-of-freedom mechanism was obtained through geometric design optimisation. This was achieved by minimising the internal strains occurring in the structure as it opens and closes. Connecting the plates through spherical joints increases the complexity of the structure but it also generates a unique mechanism which, unlike a spherical motion, might allow non-symmetric structures, capable of moving in three dimensions, to be formed.

8.3 Further Work

It has been shown that planar plate structures have limited efficiency as a cover for large horizontal spans. Hence, to further develop this type of retractable structure smaller scale applications should be sought. Many such applications have been proposed in the form of table tops, shading devices and small scale retractable roofs. For the planar plate structure to become a viable solution for these applications more detailed design studies are needed. This work should include determining viable methods for structural redundancy and tolerances depending on the application. This work might reveal the need for further expanding the geometric studies presented in this dissertation though it is likely that the requirements of most applications are already covered.

Limited work has been carried out on arrays of interconnected, individually retractable plate structures. To develop these geometric shapes into practical applications further studies of the external support requirements, stiffness and actuation is needed.

No structural analysis has been carried out for the proposed spherical retractable structures. Though proof-of-concept models have showed that the concepts are realisable on a small scale, they did not provide any data on the structural efficiency of these structures when applied on a much larger scale. Therefore the next step in the development of these types of retractable roof systems should be the detailed analysis and verification of the structural efficiency of these doubly-curved structures. Specific areas of interest should be the forces in the connections and the exploitation of in-plane forces in order to reduce the out-of-plane bending of the spherical plates, especially in the two extreme configurations where load requirements are usually the highest and where adjacent plate elements are in direct contact. Structural redundancy, tolerances, thermal and non-symmetric loading should also be investigated.

Further geometric studies are also needed for the proposed concept, using spherical joints in order to eliminate the collision of the bars during opening and closing. Alternative applications for spherical retractable structures should also be investigated together with the possibility of applying a similar spatial mechanism to non-symmetrical structures.

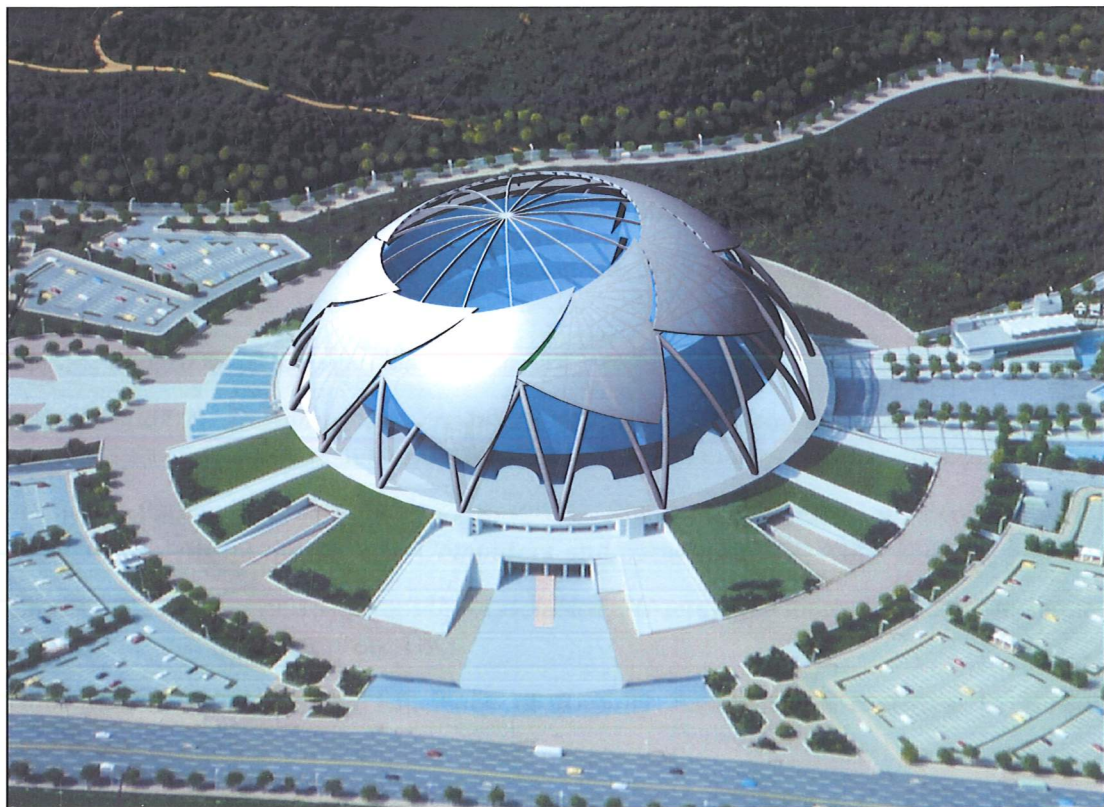


Figure 8.1: Rendering of novel concept retractable roof

Bibliography

- Allen, C.M. & Robbie, R.G. (1994). Stadium building. United States Patent No. 5,351,449.
- Autodesk, Inc. (2002). *AutoCAD 2002 User's Guide*. San Rafael, CA, USA, <http://www.autodesk.com>.
- Balz, M. (2003). Interview, 06/03/03. Schlaich Bergermann und Partners, Stuttgart, Germany.
- Barker, M.J. (2000). Development of the new Wembley Stadium Roof. In Barnes & Dickson (2000), 241–246.
- Barnes, M. & Dickson, M., eds. (2000). *Widespan Roof Structures*, Thomas Telford Publishing, London, UK.
- Beijing Municipal Commission of Urban Planning (2003). Presentation of Competition for the Architecture Design of National Stadium (2008 Olympic Main Stadium). <http://www.bjghw.gov.cn/NationalStadiumE/index.asp>.
- Belda, E.P. (1996). Constructive problems in the deployable structures of Emilio Pérez Pinero. In Escrig & Brebbia (1996), 23–34.
- Bisson, M. (2003). Tuft agendas. *Stadia*, **22**, 18–24.
- Buhl, T. (2002). *Design of non-linear mechanisms - Topology and shape optimization*. PhD dissertation, Danish Center for Applied Mathematics and Mechanics.
- Buhl, T., Jensen, F.V. & Pellegrino, S. (2004). Shape Optimization of Cover Plates for Retractable Roof Structures. *Computers and Structures*, **82**, 1227–1236.
- Bulson, P.S., ed. (1991a). *Rapidly Assembled Structures*, Computational Mechanics Publications, Southampton, UK.
- Bulson, P.S. (1991b). The Efficiency of Rapidly Assembled Structures. In Bulson (1991a), 3–14.
- Candela, F., Piñero, E.P., Calatrava, S., Escrig, F. & Valcárcel, J.P. (1993). *Arquitectura Transformable*. Publication de la Escuela Tecnica Superior de Arquitectura de Sevilla, Sevilla, Spain.
- Carne, T.K. (2002). Geometry. Lecture Notes Easter Term 2002, University of Cambridge, Department of Pure Mathematics and Mathematical Statistics, <http://www.dpmms.cam.ac.uk/~tkc/Geometry/Notes.pdf>.

- Chilton, J.C., Choo, B.S. & Wilkinson, D. (1998). A parametric analysis of the geometry of retractable reciprocal frame structures. In *Proceedings of the LSA98 Conference "Lightweight Structures in Architecture Engineering and Construction"*, vol. 1, 547–555, Sydney, Australia.
- Clough-Smith, J.H. (1978). *Spherical Trigonometry*. Brown, Son & Ferguson Ltd, Glasgow, UK, Second edn.
- Crisfield, M.A. (1997). *Non-linear Finite Element Analysis of Solids and Structures*, chap. 16, 188–197. John Wiley & Sons, Chichester, UK.
- Dean, B.K., Wagner, C. & Morley, S. (1998). Victoria Docklands Stadium, Melbourne. In *Proceedings of the LSA98 Conference "Lightweight Structures in Architecture Engineering and Construction"*, vol. 1, 556–563, Sydney, Australia.
- Escrig, F. (1993). *Las estructuras de Emilio Pérez Piñero*, 11–32. In Candela *et al.* (1993).
- Escrig, F. (1996). General survey of deployability in architecture. In Escrig & Brebbia (1996), 3–22.
- Escrig, F. & Brebbia, C.A., eds. (1996). *Mobile and Rapidly Assembled Structures II*, Computational Mechanics Publications, Southampton, UK.
- Escrig, F. & Valcarcel, J.P. (1993). Geometry of Expandable Space Structures. *International Journal of Space Structures*, **8**, 127–134.
- Escrig, F., Sanchez, J. & Valcárcel, J.P. (1996). Two-way deployable spherical grids. *International Journal of Space Structures*, **11**, 257–274.
- Farrugia, P. (2002). Spatial Foldable Structures. In Parke & Disney (2002), 613–624.
- Felippa, C. (2001). Mathematics of Finite Rotations. Lecture Notes Fall 2002, University of Colorado at Boulder, Department of Aerospace Engineering Sciences, <http://caswww.colorado.edu/courses.d/NFEM.d/NFEM.AppR.d/NFEM.AppR.pdf>.
- Fuller, R.B. (1962). Tensile-integrity structures. United States Patent No. 3,063,521.
- Gantes, C.J. (2001). *Deployable Structures: Analysis and Design*. WIT Press, Southampton, UK.
- Gee, D. (2002). Making progress: Advances in mechanical roof systems. *Stadia*, **17**, 32–34.
- Geraint, J. & Sheard, R. (2001). *Stadia: a design and development guide*. Architectural Press, Oxford, UK, Third edn.
- Griffins, L.G. (2003). Reliant Stadium, Houston, Texas. *Structural Engineering International*, **13**, 103–106.
- Guest, S.D. & Pellegrino, S. (1996a). Design optimization of a solid surface deployable antenna. In D. Bestle & W. Schielen, eds., *IUTAM Symposium on Optimization of Mechanical Systems*, 105–112, Kluwer Academic Publishers, Southampton, UK.

- Guest, S.D. & Pellegrino, S. (1996b). A new concept for solid surface deployable antennas. *Acta Astronautica*, **38**, 103–113.
- Hernandez, M., Carlos, H. & Zalewski, W. (1991). Deployable Structures. In Bulson (1991a), 237–248.
- Hewitt, J., Roberts, J.T. & Mann, S. (1998). Miller Park Stadium - Design of the Retractable Roof Structure. In *Proceedings of the LSA98 Conference "Lightweight Structures in Architecture Engineering and Construction"*, vol. 1, 564–573, Sydney, Australia.
- Hoberman, C. (1990). Reversibly Expandable Doubly-Curved Truss Structure. United States Patent No. 4,942,700.
- Hoberman, C. (1991). Radial Expansion/Retraction Truss Structures. United States Patent No. 5,024,031.
- HPC Gears Ltd. (2002). Data provided by HPC Gears Ltd. Chesterfield, UK, <http://www.hpc-gears.co.uk>.
- Institute for Lightweight Structures (1971). *IL5 (Convertible Roofs)*. University of Stuttgart, Stuttgart, Germany.
- Ishii, K., ed. (2000). *Structural design of retractable roof structures*. WIT Press, Southampton, UK, First edn.
- Ishii, K. (2001). Retractable roof structures. *Journal of The International Association for Shell and Spatial Structures*, **42**, 27–33.
- Jensen, F.V. (2001). *Cover elements for retractable roof structures*. First-year report, University of Cambridge, Department of Engineering.
- Jensen, F.V. & Pellegrino, S. (2001). Arm Development, Review of Existing Technologies. Cambridge Report CUED/D-STRUCT/TR198, University of Cambridge, Department of Engineering.
- Jensen, F.V. & Pellegrino, S. (2002). Expandable structures formed by hinged plates. In Parke & Disney (2002), 263–272.
- Jensen, F.V. & Pellegrino, S. (2004). Expandable "blob" structures, extended abstract. In Motro (2004), 44–45, paper on CD-ROM.
- Kassabian, P.E. (1997). *Investigation into a type of Deployable Roof Structure*. Masters dissertation, University of Cambridge, Department of Engineering.
- Kassabian, P.E., You, Z. & Pellegrino, S. (1997). Retractable Structures based on Multi-Angulated Elements. IASS Colloquium on Structural Morphology.
- Kassabian, P.E., You, Z. & Pellegrino, S. (1999). Retractable roof structures. *Proceedings of the Institution of Civil Engineers, Structures & Buildings*, **134**, 45–56.
- Kitamura, T., Yamashiro, K., Obata, A. & Natori, M. (1990). Development of a high stiffness and retractable mast "HIMAT" for space applications. In *Proceedings of 31st AIAA/ASME/ASCE/AHS/ASC Structures, Structural Dynamics and Materials Conference, Long Beach, CA*.

- Kokawa, T. (2000). Structural idea of retractable loop-dome. *Journal of the IASS*, **41**, 111–116.
- Kokawa, T. (2001). Proposal of retractable loop-dome. In Kunieda (2001), 1–8, paper on CD-ROM.
- Kovács, F. (2000). Foldable bar structures on a sphere. In Pellegrino & Guest (2000), 221–228.
- Kovács, F. & Tarnai, T. (2000). An expanable dodecahedron. In *Bridge between civil engineering and architecture*, 227–234, IASS Working Group No 15 'Structural Morphology'.
- Kronenburg, R. (2000). *Portable Architecture*. Architectural Press, Oxford, UK, First edn.
- Kunieda, H., ed. (2001). *International Symposium on Theory, Design and Realization of Shell and Spatial Structures*, IASS.
- Lénárt, I. (1996). *Non-Euclidean Adventures on the Lénárt Sphere*. Key Curriculum Press, Berkeley, CA.
- Lenczner, E.A.R. (1998). Making a new stadium special. In Thompson *et al.* (1998), 15–21.
- Manica, D. (2003). Taking cover: Evolving roof options. *Stadia*, **20**, 26–30.
- McCarthy, J.M. (1990). *An introduction to theoretical kinematics*. MIT Press, London, UK.
- Mellon Arena (2004). Arena History. <http://www.mellonarena.com/>.
- Miura, K. & Pellegrino, S. (2002). Structural Concepts, unpublished.
- Mollaert, M. (1996). Retractable membrane roofs. In Escrig & Brebbia (1996), 407–417.
- Mollaert, M., Temmerman, N.D., Daerden, F., Block, P. & Mele, T.V. (2003). Adaptable tensioned coverings, extended abstract. In Yang *et al.* (2003), paper on CD-ROM.
- Monjo, J., Gámes, R. & Tejera, J. (2002). Some problems in the refurbishing of the Zaragoza bullring retractable roof. In Obrębski (2002), 91–93.
- Motro, R. (1992). Tensegrity systems: the state of the art. *International Journal of Space Structures*, **7**, 75–83.
- Motro, R., ed. (2004). *International Symposium on Shell and Spatial Structures from Models to Realization*, IASS.
- Murray, C. (1995). *Stadium Roofs*. The Sports Council, London, UK, 1995th edn.
- Nijsse, R. & van Vliet, H. (2003). Interview, 01/05/03. ABT Consulting Engineers, Arnhem, The Netherlands.

- Obrębski, J.B., ed. (2002). *Proceedings of the International IASS Symposium on Lightweight Structures in Engineering*, Micro-Publisher, Warsaw, Poland.
- Otto, F., Rasch, B., Pfafferoth, G., Schönborn, A. & Schanz, S. (1995). *Finding Form*. Deutscher Werkbund Bayern, Germany.
- Parametric Technology Corporation (2001). *Pro/Engineer, Pro/Mechanica Release 2001*. Needham, MA, USA, <http://www.ptc.com>.
- Parke, G.A.R. & Disney, P., eds. (2002). *Space Structures 5*, Thomas Telford Publishing, London, UK.
- Parrish, J. (2003). Interview, 17/09/03. Arup Sport, London, UK.
- Pellegrino, S. (1995). Large retractable appendages in spacecraft. *Journal of Spacecraft and Rockets*, **32**, 1006–1014.
- Pellegrino, S. & Calladine, C.R. (1986). Matrix analysis of statically and kinematically indeterminate frameworks. *International Journal of Solids and Structures*, **22**, 409–422.
- Pellegrino, S. & Guest, S.D., eds. (2000). *IUTAM-IASS Symposium on Deployable Structures: Theory and Applications*, Kluwer Academic Publishers, Southampton, UK.
- Pellegrino, S. & You, Z. (1993). Foldable ring structures. In G.A.R. Parke & C.M. Howard, eds., *Space Structures 4*, vol. 1, 783–792, Thomas Telford Publishing, London.
- Post, N.M. (2000). Houston's retractable roof is in league of its own. *Engineering News-Record*, 31/01/2000.
- Riberich, B. (2003). Making the turf move: Field system design. *Stadia*, **22**, 33–34.
- Roberts, P. & Dickson, M. (1998). Stadium planning in today's townscapes. In Thompson *et al.* (1998), 3–14.
- Rodriguez, C. & Chilton, J.C. (2003). Swivel Diaphragm – A New Alternative for Retractable Ring Structures. *Journal of The International Association for Shell and Spatial Structures*, **44**, 181–188.
- Rodriguez, C., Chilton, J. & Wilson, R. (2004). Kinetic grids with swivel diaphragm, extended abstract. In Motro (2004), 316–317, paper on CD-ROM.
- Sanchez, J., Valcárcel, J.P. & Escrig, F. (1996). The adventure of covering a swimming-pool with an x-frame structure. In Escrig & Brebbia (1996), 113–122.
- Schlaich, J. (2000). Lightweight structures. In Barnes & Dickson (2000), 178–188.
- Sheard, R.K. (1998). Stadia and arena through the ages. In Thompson *et al.* (1998), xvii–xxi.
- Sheldon, M.L. & Dean, B.K. (2002). Colonial Stadium, Melbourne. *Structural Engineering International*, **12**, 4–7.

- Shibata, I. (2003). Toyota Stadium, Toyota City, Japan. *Structural Engineering International*, **13**, 153–154.
- SMB Bearings Ltd. (2002). Data provided by SMB Bearings Ltd. Brize Norton, Oxon, UK, <http://www.smb-bearings.co.uk>.
- Stratasys (1999). *FDM 3000 User's Guide*. Eden Prairie, MN, USA, <http://www.stratasys.com>.
- Teall, M.J. (1996). *Deployable Roof Structure*. Masters dissertation, University of Cambridge, Department of Engineering.
- The MathWorks, Inc. (2002). *Learning MATLAB 6.5, Release 13*. Natick, MA, USA, <http://www.mathworks.com>.
- The MathWorks, Inc. (2003). *Optimization Toolbox User's Guide, Version 2.3*. Natick, MA, USA, <http://www.mathworks.com>.
- Thompson, P., Tolloczko, J.J.A. & Clarke, J.N., eds. (1998). *Stadia, Arenas & Grandstands*, E & FN Spon, London, UK.
- Tibert, G. (2002). *Deployable Tensegrity Structures for Space Applications*. PhD dissertation, Royal Institute of Technology, Stockholm.
- Tzonis, A. (1999). *Santiago Calatrava, The Poetics of Movement*. Thames & Hudson, London, UK.
- UEFA (2003). UEFA diary: August. <http://www.uefa.com/uefa/news/>.
- Valcárcel, J.P. & Escrig, F. (1996). Recent advances in the analysis of expandable structures. In Escrig & Brebbia (1996), 45–54.
- Verheyen, H.F. (1993). A single die-cut element for transformable structures. *International Journal of Space Structures*, **8**, 127–134.
- Wembley Stadium (2004). Images of new stadium. <http://www.wembleystadium.com/>.
- WG16 IASS (2001). Recent examples of space structures in Japan. *Journal of The International Association for Shell and Spatial Structures*, **42**, 34–94.
- Wohlhart, K. (2000). Double-chain mechanisms. In Pellegrino & Guest (2000), 457–466.
- Wolfram Research (2004). MathWorld – Spherical Trigonometry. <http://mathworld.wolfram.com/SphericalTrigonometry.html>.
- Yang, Y.B., Leu, L.J., Chen, C.S., Hsieh, S.H. & Leei, Y.S., eds. (2003). *International Symposium on New Perspectives for Shell and Spatial Structures*, IASS.
- You, Z. (2000). A new approach to design of retractable roofs. In Pellegrino & Guest (2000), 477–483.
- You, Z. & Pellegrino, S. (1996). New solutions for foldable roof structures. In Escrig & Brebbia (1996), 35–44.

- You, Z. & Pellegrino, S. (1997). Foldable bar structures. *International Journal of Solids and Structures*, **34**, 1825–1847.
- Z Corporation (2001). *Z406 User's Guide*. Burlington, MA, USA, <http://www.zcorp.com>.
- Zablocki, W. (2002). Mobility in sport architecture. In Obrębski (2002), 99–106.
- Zanardo, A. (1986). Two-dimensional articulated systems developable on a single or double curvature. *Mecanica*, **21**, 106–111.
- Zeigler, T.R. (1981). Collapsible self-supporting structures and panels and hub therefor. United States Patent No. 4,290,244.
- Zeigler, T.R. (1984). Collapsible self-supporting structures. United States Patent No. 4,437,275.
- Zeigler, T.R. (1987). Portable shelter assemblies. United States Patent No. 4,689,932.
- Zeigler, T.R. (1993). Polyhedron building system. United States Patent No. 5,230,196.